General Disclaimer

One or more of the Following Statements may affect this Document

- This document has been reproduced from the best copy furnished by the organizational source. It is being released in the interest of making available as much information as possible.

- This document may contain data, which exceeds the sheet parameters. It was furnished in this condition by the organizational source and is the best copy available.

- This document may contain tone-on-tone or color graphs, charts and/or pictures, which have been reproduced in black and white.

- This document is paginated as submitted by the original source.

- Portions of this document are not fully legible due to the historical nature of some of the material. However, it is the best reproduction available from the original submission.

Produced by the NASA Center for Aerospace Information (CASI)

(NASA-CR-144183) APPLICATIONS STUDY OF AERO-MANEUVERING ORBIT-TO-ORBIT SHUTTLE (AMOOS) Final Report (Lockheed Missiles and Space Co.) 224 p HC $7.75 CSCL 22B

N76-18210

Unclas
G3/18 14320

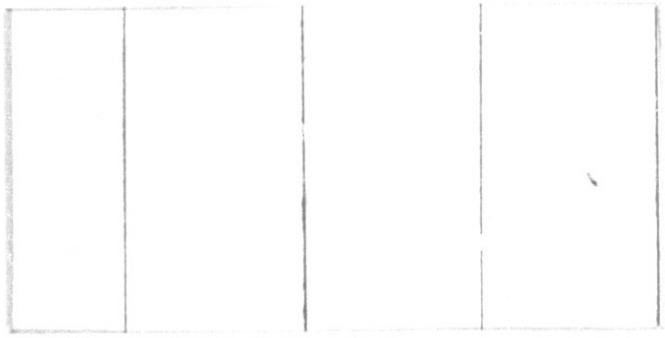

Lockheed

HUNTSVILLE RESEARCH & ENGINEERING CENTER

LOCKHEED MISSILES & SPACE COMPANY, INC.
A SUBSIDIARY OF LOCKHEED AIRCRAFT CORPORATION

HUNTSVILLE, ALABAMA

Lockheed

Missiles & Space Company, Inc.

HUNTSVILLE RESEARCH & ENGINEERING CENTER

Cummings Research Park
4800 Bradford Drive,
Huntsville, Alabama

APPLICATIONS STUDY OF AERO-MANEUVERING ORBIT-TO-ORBIT SHUTTLE (AMOOS)

FINAL REPORT

January 1976

Contract NAS8-31452

Prepared for National Aeronautics and Space Administration
Marshall Space Flight Center, Alabama 35812

by

John White

APPROVED: C. Donald Andrews

C. Donald Andrews, Lead Engineer
Flight Mechanics Group

B. Hobson Shirley

B. Hobson Shirley, Supervisor
Engineering Sciences Section

J. S. Farrior

J.S. Farrior
Resident Director

FOREWORD

The work reported herein was performed by the Lockheed-Huntsville Research & Engineering Center for the Payload Studies Office of Program Development, Marshall Space Flight Center, under Contract NAS8-31452. The MSFC technical monitor for this study is Mr. J.P. Hethcoat, PS04.

ACKNOWLEDGMENTS

The author thanks Messrs. L.B. Brandon, B.A. Neighbors and A.C. Young of Program Development, MSFC, for their suggestions and discussions of the AMOOS and AMRS concepts and applications. The author is also grateful for the technical support and contributions during the analysis effort by the following Lockheed-Huntsville personnel: D.A. Love, W.G. Dean, Dr. A. Wernli, W.E. Jones and Z.S. Karu.

SUMMARY

The results of the Applications Study of the Aeromaneuvering Orbit-to-Orbit Shuttle (AMOOS) and the Aeromaneuvering Recovery System (AMRS) are reported. Preliminary designs and the supporting analysis for both AMOOS and AMRS are presented. The AMOOS design is shown to yield from twice to almost three times the round-trip payloads as a purely propulsive vehicle of the same all up weight. Typically AMOOS can perform a crew rotation mission to equatorial geosynchronous orbit in one Space Shuttle launch. The weight of the manned module designed for this mission is 6800 lb, which is approximately 300 lb below the AMOOS round-trip payload capability. AMOOS can also place the 11,250 lb (12,000 lb with crew) AMRS on station in equatorial geosynchronous orbit. This represents a 40% increase in payload delivery capability over the Baseline Space Tug.

The model flight test program analysis has yielded a 10 ft long, 1500 lb vehicle that can demonstrate the feasibility of aeromaneuvering. The major parameters, such as maximum dynamic pressure, heating rates, guidance, stability and recovery, can be modeled or demonstrated as is appropriate. Two model flight schedules were developed, one consisting of four flights and the other of two flights. The former is considered a very low risk, high information return program whereas the latter is a minimal cost program consistent with reasonable data returns and chance of success.

The AMOOS and AMRS guidance scheme developed using linear regulator theory proved a precise and accurate guidance scheme. Both it and a classical linear systems based scheme were evaluated using 65 simulated trajectories in which the position in the entry corridor and the atmospheric density were varied randomly. The latter was varied randomly at each

integration time step with due allowance made for correlation in density from point to point. The linear regulator approach also proved adequate for the AMRS ground recovery guidance.

Two areas are recommended for further study. These are: (1) navigation and guidance, and (2) alternate configurations. The objective of the first task would be to match navigation hardware against AMOOS and AMRS requirements and evaluate the alternatives using the AMOOS and AMRS guidance simulation. Under the second task, the alternate configurations for AMOOS would be considered. These may include such items as AMOOS payload performance using a hybrid engine, changes in external geometry, and heavy lift vehicles.

CONTENTS

Section 1
INTRODUCTION

In the AMOOS studies, the term aeromaneuvering is used to cover all uses of aerodynamic forces to assist in an orbit transfer maneuver. This would, then, include aeromaneuvering on the ascent as well as on the descent phases of the n ission. So that work would not be duplicated, a literature survey was performed at the beginning of the first AMOOS contract (Ref. 1). As a result of this survey, aeromaneuvering orbit transfer was divided into three classes:

- Synergetic Plane Change Maneuvering (plane change using lift with propulsive forces used to compensate for the effects of drag)
- Aerobraking (use of drag forces only)
- Other Aeromaneuvering (use of drag and lift forces)

At that time, the literature was sufficiently extensive on the first and second classes to be able to identify the bounds of applicability and associated problem areas. A discussion of the first and second classes is given in Ref. 1. Since the above classes were so well covered in the literature, the Lockheed studies were confined to the third class and to the large deployable drag device such as the ballute.

The third class of maneuvers is that which uses both lift and drag forces to maneuver from the return transfer trajectory to the low earth orbit used for phasing with the Space Shuttle Orbiter. Excluded from the previous Lockheed studies (Ref. 1) were the reentry maneuvers of vehicles such as the Apollo command module and the Space Shuttle Orbiter because the aerodynamic forces were not used to transfer from one orbit to another but to land on the earth's surface. However, upon the advent of the Aeromaneuvering Recovery System (AMRS) maneuvers to a ground recovery are applicable and were considered in this study.

The basic concept that distinguishes the Lockheed AMOOS studies from previous orbit-to-orbit transfer studies is that the prime use of the lift force is for trajectory control. Other systems use the lift force to control the environment of the vehicle or to change an orbital parameter directly, e.g., the Shuttle Orbiter reentry or the synergetic plane change. On the other hand, the aerodynamic drag force is used primarily to change the orbital parameters in the AMOOS concept. Lift forces are used to ensure that the desired effects of drag are realized. That a small plane change can also be accomplished by AMOOS is an outcome of the optimum means of modulating the vertical component of the lift force rather than a necessary use.

The AMRS can operate in the AMOOS mode to rendezvous with the Space Shuttle orbiter or maneuver to a recovery on the earth's surface. This latter mode will be referred to as the AMRS maneuver. This maneuver is similar to other recovery modes and, as such, lies between the Apollo and the Space Shuttle Orbiter for maneuverability.

The feasibility studies of earlier AMOOS contracts were directed toward establishing the sufficiency of the aerodynamic forces to effect the desired energy loss, trajectory control and plane change requirements. Based on the flight environment, including the ascent and descent in the Shuttle Orbiter's cargo bay, a vehicle was designed capable of performing a round trip equatorial geosynchronous mission. Furthermore, this vehicle demonstrated a payload capability well in excess of any other vehicle capable of being transported in the Shuttle Orbiter's cargo bay (Fig. 1).

In the previous Lockheed aeromaneuvering studies, Refs. 1 and 2, the navigation, guidance and control requirements for AMOOS were not analyzed. However, the static stability was considered, and only those configurations displaying such were considered for further study. Past studies (Ref. 3) of navigational accuracy required for multi-pass aerobraking and inspection of the specifications of current navigational hardware is sufficient to eliminate the navigation requirements from immediate study. For this reason, guidance was considered the most important technology area and so was included in the current contract.

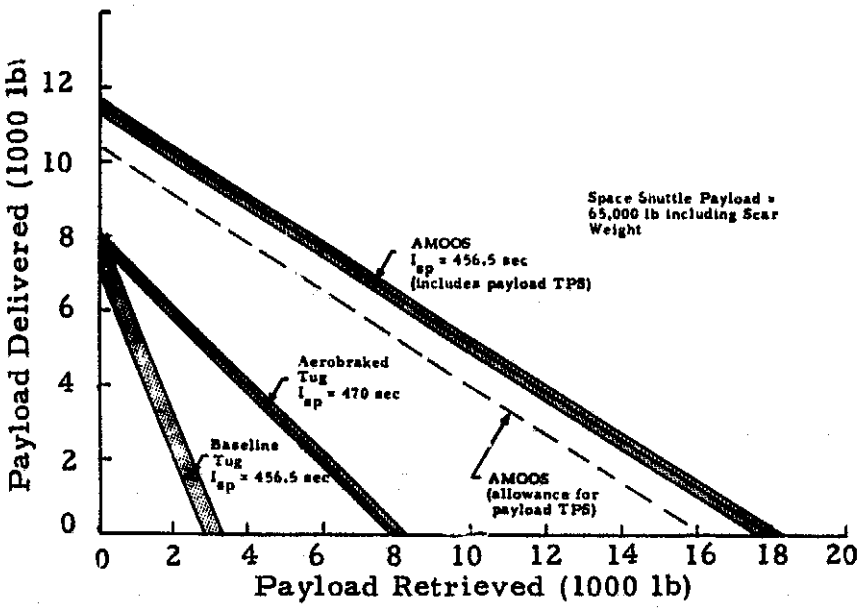

Fig. 1 - Comparison of Payload Capabilities for Several Recoverable Upper Stage Alternatives

These guidance studies include both the pass through the atmosphere to Space Shuttle orbiter rendezvous type guidance (AMOOS and AMRS) and ground recovery type guidance (AMRS). A very simple guidance scheme had already been suggested for AMOOS and a preliminary evaluation completed (Ref. 4). Further development of this scheme was to be considered as well as more conventional approaches such as the linear regulator and classical linear systems.

During the studies reported in Refs. 1 through 3, AMOOS and the aerobraked tug were considered as general transport vehicles and unmanned. Payloads were defined in general terms of mass and dimension. However, by the end of the feasibility studies (Ref. 2), manned missions, in particular to geosynchronous orbit, had become of prime importance. For this reason, study of the application of the aeromaneuvering concept to particular manned roles was included in the contract. The four to six man geosynchronous crew rotation was considered baseline. However, lunar orbital and earth orbital

missions were to be considered as well as geosynchronous. Furthermore, the use of multiple Shuttle launches and the mating of AMOOS vehicles and payloads in low earth orbit to form a two-stage vehicle was to be included.

A second application of aeromaneuvering to be considered was the use of the aeromaneuvering concept in the design of an emergency vehicle. This application, called the Aeromaneuvering Recovery System (AMRS), is to provide emergency recovery of a four-to-six man crew from geosynchronous altitude. The requirements for return from a lunar orbit were also considered.

Finally, the feasibility of demonstrating the aeromaneuvering concept using a flight test model was to be studied briefly. This model flight test plan was to demonstrate the basic feasibility of the concept and to provide design data for the full-scale vehicle. The model testing must reduce the flight testing of the full-scale vehicle.

For these studies, the favored external geometry of vehicles studied in Refs. 1 and 2 was selected as the basic configuration since it is considered the more adaptable to the modular configuration. This vehicle will be described in the following section.

- Background

The first class of aeromaneuvering, as listed previously, is the synergetic plane change maneuver. The basic concept behind such a maneuver is that the lift vector can be used to produce a plane change. This plane change, if performed propulsively, can require a velocity increment larger than the velocity lost due to drag. In such a maneuver the vehicle starts from low earth orbit, slows propulsively to enter the atmosphere, changes orbital inclination using lift and then acquires its mission altitude propulsively. The literature (reviewed in Ref. 1) shows that the region of application is restricted to plane changes of 30 deg or more, to vehicles with moderate to high L/D, about 1 or greater, and to mission altitudes below 1000 n.mi. With such restrictions, it has no practical application to AMOOS or AMRS in the ascent phase of a mission and so was not studied.

Dropping synergetic plane change from the studies left only the applications of aeromaneuvering on the return transfer phase of a mission. Such applications are considered in the second and third classes listed previously. Aerobraking, which entails the use of aerodynamic drag forces to dissipate energy without the use of lift forces, is studied extensively in Ref.3. The use of drag and drag augmenting devices are extensively studied therein. The studies in Ref.3 were directed at kit modifications to the Baseline Tug. This is not considered restrictive since the propellant volume requirements needed for a geosynchronous mission and the cylindrical shape of the cargo bay of the Shuttle Orbiter allows practically no deviation from a circular shape. Two basic types of kits were proposed. The first was a deployable metal skirt, short relative to the length of the Baseline Space Tug and mounted near the front end of the Tug. The engine nozzle was protected by a cap and the vehicle flew in the atmosphere engine first. The second method consisted of a very large deployable device such as a ballute or a fabric flare.

The strategy in these kit concepts was to reduce the heating rates to the point where reradiative materials may be used for the protective cap, etc. In the case of the small skirt, many (30) passes through the atmosphere are used to reduce the heating rate whereas for the very large skirt or deployable device two passes are used and the device made sufficiently large so that a high altitude trajectory is flown.

For this technique, trajectory control is by small corrective Δv's at each apogee between atmospheric passes. The flight through the atmosphere is unguided after an initial targeting immediately prior to atmospheric entry. The flight path angle at atmospheric entry (600,000 ft (180 km) altitude in Ref.3) is closely controlled so that off nominal target vacuum perigee errors have small effects compared to variations in atmospheric density. The navigation system required a landmark tracker and furthermore assumed that the full theoretical accuracy of the Kalman filter could be realized. The accuracy required of the navigation system is approximately 0.35 n.mi. (0.7 km) along the radius vector.

The large deployable drag device was an attempt to reduce the number of passes to two and so not violate the on orbit lifetimes of both the Baseline Space Tug and the Space Shuttle Orbiter. When unpredictable atmospheric density variations and navigation errors are considered the guidance problem becomes difficult and would probably need some form of drag modulation. The large deployable drag device has been studied in both Refs. 2 and 3. The conclusion in Ref. 2 is that the ballute is not practical since it yields negligible payload. The analysis of Ref. 3 yields a favorable payload for the large AIRMAT flare. However, the stability of this device has not been established. Presumably, fiber B (Ref. 2) could be substituted for AIRMAT which is no longer available.

The AMOOS studies signalled a new start to the aeromaneuvering approach to orbit transfer. These studies were founded on a broad base covering all uses of aeromaneuvering. Existing literature was to be used wherever possible. The existing literature, discussed briefly above, revealed extensive studies in the first and second classes of aeromaneuvering. In general, no further work was considered necessary on these classes since the areas of feasibility could be readily ascertained from the existing literature.

This left, therefore, the aeromaneuvering aspects of the maneuver from return transfer orbit to the phasing orbit with the Shuttle Orbiter. These studies were intended to be comprehensive and therefore included lifting and non-lifting nominal trajectories, single and multiple pass maneuvers, plane change requirements, insulative, reradiative and ablative TPS and hybrid modes of operation in which the maneuver is performed part propulsively and part aerodynamically. Extremes of the atmospheric flight environment were simulated by combinations of lift vector modulation, maximum atmospheric density variations, estimates of the exoatmospheric navigation accuracy and effects of non-continuum aerodynamics.

These studies lead to several very important conclusions which governed the basic external geometry and mode of operation of AMOOS and later AMRS. The first conclusion was that AMOOS must be basically a cylindrical lifting body vehicle in order to meet the volume requirements of fuel and payload to

geosynchronous orbit and fit in the Shuttle Orbiter's cargo bay. Such a vehicle, consisting essentially of a cylindrical body and a somewhat blunt nose (Fig. 2) will yield only a moderate lift-to-drag (L/D) ratio, about 0.5 to 1.0, at hypersonic speeds.

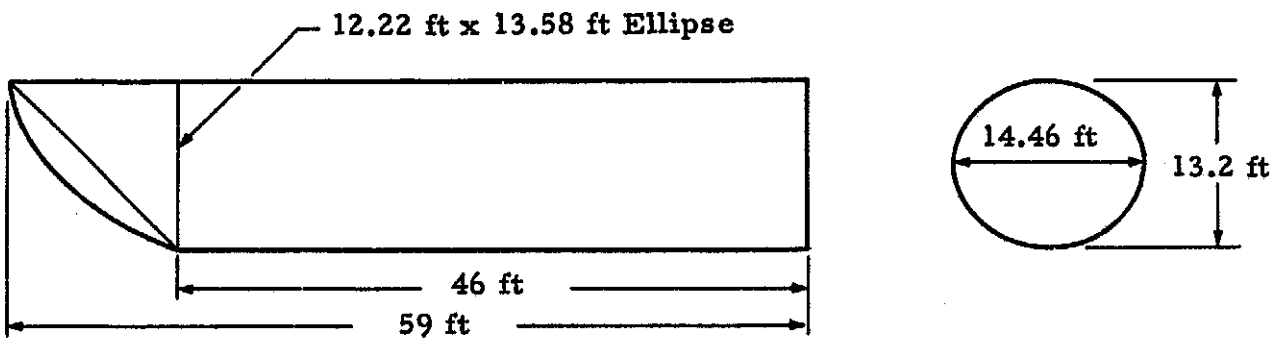

Fig. 2 - AMOOS External Geometry (maximum length vehicle)

The plane change studies showed that, with such an L/D, a vehicle could only perform a small (5 to 10 deg) plane change during atmospheric flight. The basic operation of AMOOS would, therefore, need to include a propulsive plane change maneuver on return from an equatorial geosynchronous mission orbit. Furthermore, aeromaneuvering plane change capability decreases rapidly with decreasing mission altitude. However, trade studies showed that the lift vector could be used for both moderate plane change, about 7 deg on return from geosynchronous altitude, and trajectory control during atmospheric flight without significant deleterious effects on either use. This

result led to the selection of a nominal 90 deg bank angle (lift vector horizontal) with modulation of bank angle to provide modulation of the vertical component of the lift vector.

The third fundamental result has more far reaching effects and applies equally well to aerobraking as well as aeromaneuvering. It is that the product ρ_{max} n C_D is a slowly varying function of each of the three variables for a successful ballistic maneuver to phasing orbit. In this product, ρ_{max} is the maximum value of the atmospheric density encountered, n is the number of passes through the atmosphere to complete the orbit transfer maneuver and C_D is the drag coefficient of the vehicle based on some fixed area, e.g., cross-sectional area of the Shuttle Orbiter cargo bay. The implications of this relationship upon atmospheric flight and vehicle design, etc., will now be discussed.

First, apply this relationship to the task of reducing heating rate and hence heat load. For current purposes, the relationship that heating rate, $\dot{Q}$, is proportional to $\rho^{1/2}$ is sufficiently accurate. This means that relatively large reductions in ρ are required to decrease the heating rate significantly, e.g., if the heating rate needs to be reduced to one-half its present value then ρ_{max} must be reduced to one quarter of its present value. Using the invariance of the product ρ_{max} n C_D shows that the product n C_D must be increased four-fold, hence the relative insensitivity of heating rate to the number of passes per maneuver and the drag coefficient.

It should be recalled here that temperature varies as the fourth root of the heating rate. Therefore to reduce the temperature significantly requires massive changes in ρ and hence in the product n C_D.

Next consider the navigation and guidance requirements. Select n sufficiently large so that, regardless of the atmospheric density variation and navigation errors, the vehicle will not reenter but will skip through the atmosphere in the required manner. The value of n required is dependent upon the navigation accuracy and, as will be shown, must be larger than 2 for a ballistic trajectory for currently attainable navigational accuracies.

The unpredictable variation in the four-dimensional world atmosphere at aeromaneuvering perigee is about $\pm 12\%$ (Ref. 5). Dimensions of this atmospheric model are: altitude, longitude, latitude and time (month). This must be combined with the effects of the entry corridor which is ± 2 n.mi. (± 3.5 km) about the nominal trajectory (Ref. 1) if neither a landmark tracker nor navigational equipment of comparable accurary is used. Superimposing these effects, neither of which is linear, yields a ρ_{max} along the trajectory of about one-half to two times the nominal value, ρ_N. This variation in ρ_{max} will now be discussed in relation to the three guidance options available to a ballistic vehicle. These options are: (1) modulate n, the number of passes; (2) modulate C_D; and (3) make corrections to the trajectory by small velocity increments at apogee as in Ref. 3.

The first pass in options (1) and (3) are uncorrected during atmospheric flight. In the case of the maximum atmospheric density being $2\rho_N$, this means that the first pass is equivalent to the first pass of an n/2 pass maneuver. Since n/2 cannot be smaller than one, then the smallest nominal number of passes is two for guidance options (1) and (3) of the ballistic maneuver. In the case of option (2) it means that the drag coefficient must be reduced to half of its nominal value. In each case, the heating rate is increased approximately to $\sqrt{2}$ times the nominal value. This does not take into consideration decreases in radius to modulate the drag coefficients in the case of the second option. The maximum aerodynamic load increases similarly.

Now TPS studies (Ref. 1) have shown that n must be at least 5 to reduce the surface temperatures to acceptable levels where C_D for AMOOS has a typical value, about 3 based on Shuttle Orbiter cargo bay cross-sectional area. As examples of the effect of the foregoing discussion on the operation of an aerobraked vehicle, it means that the nominal number of passes must be at least 10 or that for a large deployable using drag modulation the drag area must be 10 times that for the basic vehicle.

On the other hand, if the experienced value of ρ_{max} is half the value of ρ_N, the nominal maximum value, then the nominal values of nC_D must

be multiplied by 2. This means that if guidance is by modulation of n, the number of passes may increase to 20 or, equivalently, in the case of C_D modulation, the drag area must be 20 times the vehicle alone value. In summary, then, if n or C_D are modulated then the appropriate parameter must be modulated from one-half to two times the nominal value. Such modulation is rather difficult to achieve. In the case of the third guidance option, in which small velocity increments are added at apogee between atmospheric passes, the vehicle must be designed to withstand an environment corresponding to one-half the nominal number of passes to complete the maneuver. For this reason, and because according to Ref. 1 n must be at least 5, the minimum number of passes must be 10 unless carbon-carbon is used for the TPS.

The above discussions are predicated upon two tenets, one is that ablators are not recyclable and so not usable for multiple pass maneuvers, and the other that the minimum achievable entry corridor is ± 2 n.mi. (3.5 km). If ablators are recyclable then the nominal number of passes may be reduced to 2. Recently, limited data on recycling of ablators has become available (Ref. 6).

In summary, therefore, a ballistic trajectory using aerobraking alone requires at least one of the following: (1) a large increase, about twentyfold, in drag area over the basic vehicle and a means of modulating this drag area to one-quarter of this value; (2) an extension of the on-orbit lifetime of the Tug to accomodate a large number (about 20) of passes per maneuver; and (3) a lightweight, recyclable, high temperature TPS for which, currently, only ablators can meet the weight and temperature limitations. Upon consideration of these above requirements the only potentially successful alternative is the one-pass maneuver using aerodynamic lift to control the trajectory during atmospheric flight and an ablative TPS to protect the vehicle from the thermal environment. The study of this alternative is the heart of the Lockheed contribution.

The previous Lockheed studies (Refs. 1 and 2), have considered the use of several structural materials for the primary structure. These materials were based on the selection of a 600F (589K) bondline temperature. The bondline temperature is the maximum temperature reached at the bond material between the ablator and the primary structure skin supporting the ablator. The value of 600F (589K) is considered a practical maximum for current technology. The primary structure must also be able to withstand the bondline temperature. This reduces the usable materials for the primary structure; in particular it eliminates the popular aluminum alloys and epoxy-based composites. Four materials were selected for evaluation: (1) titanium, (2) beryllium-aluminum, (3) magnesium, and (4) graphite-polyimide. The steel-based alloys were eliminated because they would yield a higher structural weight than titanium at the 600F (589K) operating temperature.

Of the materials considered, beryllium-aluminum yielded the lightest structure, followed closely by magnesium. The difference between the two weights was considered insignificant so that magnesium was selected for further study since it is lower priced. The magnesium weight is considered representative of the weight of beryllium-aluminum structure at the 600F (589K) bondline temperature.

Section 2
RESULTS AND DISCUSSION

The studies resulted in a vehicle that can perform a round trip mission to equatorial geosynchronous orbit with a payload in excess of the all up weight of a four-man, 30-day capsule. The round trip payload capability is approximately 7100 lb (3221 kg) and the all up weight of the manned capsule is 6800 lb (3084 kg). The design mission for the vehicle and capsule is to an equatorial geosynchronous orbit and is independent of longitude of the sub-vehicle point. The AMOOS vehicle and its payload may be placed in low earth orbit in one Space Shuttle launch. The all up weight of AMOOS and its payload is 63,100 lb (28,622 kg), thus allowing 1900 lb (862 kg) tare weight for adaption of the Shuttle Orbiter. An I_{sp} of 456.5 sec was used for these consumables and performance analyses.

The analyses showed significant increases in the round trip payloads for increases in the Space Shuttle's payload capability to 80,000 lb and 100,000 lb. Payloads were also estimated for two stage and 1 stage and one-half AMOOS vehicles transported to low earth orbit in one, two or three Space Shuttle launches.

The structural materials selected for the primary structure were either magnesium HM 21A-T8 or beryllium-aluminum (Be-38Aℓ). The structural analysis was performed with magnesium since it is expected to give a significantly cheaper cost for the primary structure at only a slightly higher weight than Be-38Aℓ. Other structural materials, e.g., titanium, are expected to yield a significantly higher weight (Ref. 2) or a significantly higher TPS weight to reduce the bondline temperature below the 600F (589K) selected for use in Refs. 1 and 2. The primary structure is a computer optimized ring-stringer stiffened shell with due allowance made for solid ring attachment points, mating points, etc. The ablative TPS uses the Martin Marietta SLA-561 flight rated material.

Similar analysis for the AMRS vehicle yielded an all up weight of 12,000 lb (5443 kg) including a crew of four. Approximately one-half of the total weight is space storable propellant and consumables.

The model flight test program studies showed that the essential subsystems, except the life support, could be checked out in four flights, each of which could share a Space Shuttle launch with another payload.

The linear regulator guidance technique is recommended since it proved accurate and readily adaptable to both AMOOS and AMRS. The classical linear system approach yielded considerably more scatter in the target parameters, some unacceptably large. In each case the trajectory was controlled to a nominal.

2.1 CONFIGURATION AND PERFORMANCE ANALYSIS

The design and performance of the AMOOS vehicle is refined and extended from the studies of Refs. 1 and 2 to yield a more complete picture of the overall AMOOS performance. The analysis is also extended to cover AMRS.

The details of the methods used in the above analysis are given in Appendixes A, B and C.

2.1.1 AMOOS/AMRS Requirements and Mission Analysis

The requirements and mission analysis performed herein was toward establishing the overall mission capability of AMOOS and AMRS. Design criteria were selected from the possible mission and performance capabilites. After the preliminary design of the vehicle was performed, the analysis was used to establish the performance spectrum of the specific vehicles.

2.1.1.1 Consumables Analysis

A comprehensive consumables analysis was performed for AMOOS for equatorial orbits about the earth from 5000 n.mi. altitude to geosynchronous.

An analysis was also performed for orbits about the moon. The analysis for AMRS was confined to equatorial geosynchronous orbits and lunar orbits. For AMOOS an I_{sp} = 456.5 sec was chosen. The sensitivity of payload to I_{sp} was determined in the feasibility studies (Ref. 2) about an I_{sp} = 470 sec which is considered sufficiently close to 456.5 sec to remain applicable. The range of I_{sp} = 260 through 350 sec was used for AMRS.

The consumables analysis was performed using impulsive Δv's with an allowance for gravity and purge losses. Chilldown was computed on assuming maximum chilldown time of 91 sec. During the chilldown an I_{sp} of 377 sec was assumed. The Δv imparted for the full 91 sec was computed and checked against the Δv required. If the chilldown Δv is greater than the required Δv, then the propellant usage is computed using the chilldown I_{sp}; if it is less, then the propellant usage is computed by combining that for the chilldown with that for the remaining Δv. Two engine burn modes are recognized beside the chilldown mode, these are: (1) full thrust burn with I_{sp} = 456.5 sec and (2) pump idle mode with I_{sp} = 434 sec. The chilldown mode may also be referred to as tank head idle mode. Very small Δv's are performed with the RCS which has an I_{sp} = 230 sec. These RCS usages are recognized by the low I_{sp} which causes the chilldown calculations to be bypassed. All other uses of consumables must be input as an event. Use of inerts, payload retrieved, residuals, etc. must also be input as events. The delivered payload is computed for a mission involving one delivery payload. If the mission involves two payload deliveries, one payload must be input as an event, the other will be computed. Typical results will now be presented and discussed.

The payload is, of course, a function of vehicle dry weight and all up weight among others. Also, payload delivered is a function of payload retrieved. Payloads have been computed as a function of these three parameters, namely, all up weight (or net delivered weight to low earth orbit), dry weight and payload retrieved.

The first case considered is the single stage vehicle delivered to low earth orbit by one Shuttle launch. The net weight delivered by the Shuttle is 63,100 lb (28,622 kg) which, when combined with an estimated 1900 lb (862 kg) tare weight on the Orbiter, gives a total of 65,000 lb (29,484 kg), the maximum baseline Shuttle payload. The results are presented as a carpet plot of payload delivered versus dry weight and payload retrieved in Fig. 3.

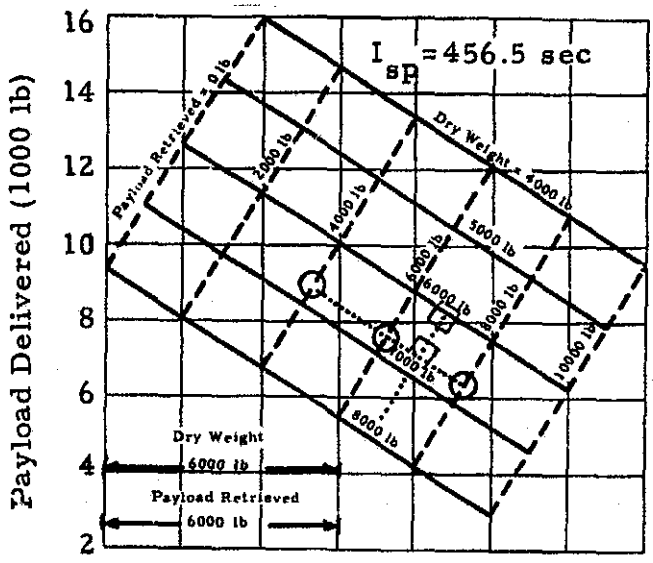

Fig. 3 - Modular AMOOS Payload Capabilities to Equatorial Geosynchronous Orbit for a Single Stage Vehicle Using One 65,000 lb Shuttle Launch

This figure represents all the possible design points for AMOOS for dry weights from 4000 lb to 8000 lb (1814 to 3629 kg) and retrieved payloads from 0 to 10,000 lb (0 to 4500 kg). The corresponding range of delivered payloads is 2900 lb to 15,900 lb (1315 kg to 7212 kg). Some of these design points may not be practical; currently, in particular, a dry weight of 4000 lb (1814 kg) is probably not achievable with current technology. As an example, consider the following case: the expected dry weight of AMOOS is 6700 lb (3039 kg) and the weight, including TPS, of a manned capsule, fully loaded with crew is 6800 lb (3084 kg). The question to be answered is: What is the up payload and is

it greater than 6800 lb (3084 kg) thus allowing AMOOS to perform a manned mission to equatorial geosynchronous orbit?

An inspection of any constant payload retrieved line reveals that traversing one grid unit horizontally represents 2000 lb (908 kg) of vehicle dry weight (one solid line to the next). The 6700 lb (3039 kg) dry weight found on each broken line is therefore the intersection of a vertical line 7/20 of the way from the 6000 lb (2722 kg) dry weight line toward the 7000 lb (3175 kg) point. The points on the 4000 (1814 kg), 6000 (2722 kg) and 8000 lb (3629 kg) retrieved payload points are shown by circles. Joining these points gives the curve for 6700 lb (3039 kg) dry weight. The next step is to construct the 6800 lb (3084 kg) return payload curve. This is performed in an analogous manner. One grid unit horizontally also represents 2000 lb (908 kg) of payload retrieved, therefore, the 6800 lb (3084 kg) return payload points are the intersection of a vertical line 4/10 of a grid unit from the 6000 lb (2722 kg) payload retrieved line and the dry weight lines each taken in turn. These points are enclosed in square symbols. Joining these two points gives the line for 6800 lb (3084 kg) retrieved payload. The intersection of these two lines just constructed is the point fulfiling the aforementioned requirements. Reading horizontally (7200 lb or 3266 kg) gives the payload delivery capability. The value, 7200 lb (3266 kg) is greater than 6800 lb (3084 kg), the weight of the flight ready manned capsule and crew, therefore, AMOOS can perform this mission.

Now, the main engine consumables varies with the payloads and the dry weight. This variation may be seen in Fig. 4 where main engine consumables is plotted against payload retrieved and vehicle dry weight. In an analogous manner to determining delivered payload, it is possible to determine main engine consumables. Repeating the construction of the 6700 lb (3039 kg) dry weight and 6800 lb (3084 kg) retrieved payload lines yields the required main engine consumables of 48,500 lb (22,000 kg). Now if the tanks are designed to perform the above mission, then any mission requiring more than 48,500 lb (22,000 kg) of propellants cannot be performed. For this particular design, then, the mission profile for geosynchronous equatorial missions follows the

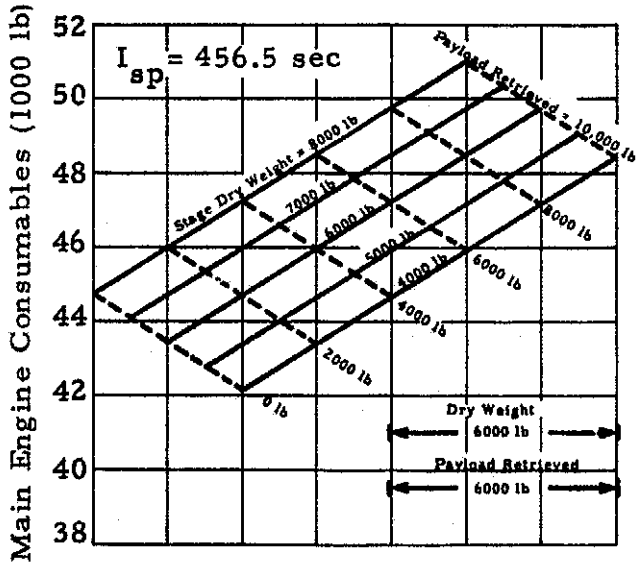

Fig. 4 - Modular AMOOS Main Engine Consumables for Equatorial Geosynchronous Orbit for a Single Stage Vehicle Using One 65,000 lb Shuttle Launch

6700 lb (3039 kg) dry weight line from zero to 6800 lb (3084 kg) retrieved payload and then falls more rapidly. The reason for this is that an all up weight less than 63,100 lb (28,622 kg) is being delivered to low earth orbit because the payload to be delivered is less than 7100 lb (3221 kg) and the tanks are full. When the up payload is greater than 7100 lb (3221 kg) then propellant must be off-loaded to keep the all up weight to 63,100 (28,622 kg). This is so that the Shuttle payload will not exceed 65,000 lb (29,484 kg) including the tare remaining in the orbiter. This aspect of performance will be demonstrated more completely in Section 2.1.1.2.

Analysis similar to the foregoing was also performed for two-stage and stage and one-half vehicles, each delivered to low earth orbit by one 65,000 lb (29,484 kg) payload Shuttle launch. These studies are reported in detail in Appendix A. The dry weights of such vehicles had to be reduced to unrealistically low values to be competitive with the single stage vehicle if completely recoverable. The stage and one-half concept offers advantages provided the tank half stage is expendable. Also, payload performance to 15,000, 10,000 and 5,000 n.mi. (27,795, 18,530 and 9,265 km) circular equatorial orbits was computed. These results are also given in Appendix A.

The two-stage and stage and one-half vehicle analysis was also performed for vehicles and payloads requiring two and three shuttle launches for delivery to low earth orbit. These vehicles must be mated in low earth orbit. The analysis of these multi-staged vehicles was for stages carrying equal weights of propellant. A typical two-stage vehicle is shown in Fig. 5.

As an example of the multi-stage vehicle consumables analysis, the two-stage, two-shuttle launch vehicle payload capability is given in Fig. 6. Each propulsion module is essentially a single stage AMOOS with suitable adapters and docking devices. The total payload and consumables per stage are obtained from Figs. 6 and 7, respectively. As an example, consider a two-stage vehicle, each stage weighing 7000 lb (3175 kg). The required return payload is also 7000 lb (3175 kg) representing a four-man capsule suitable for crew transportation on a geosynchronous sortie mission. The delivered payload is 25,700 lb

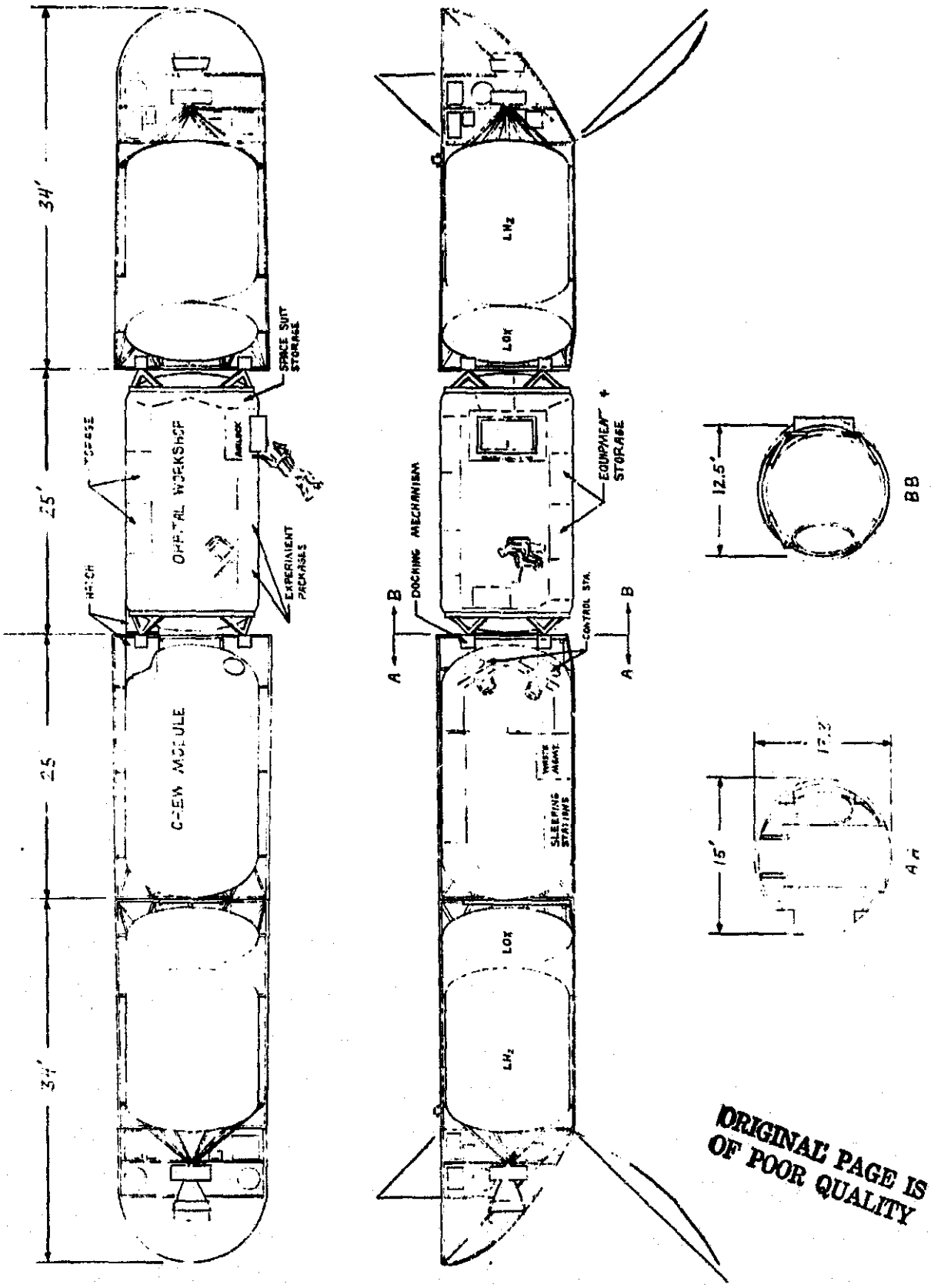

Fig. 5 - Typical Two-Stage AMOOS Configuration Requiring Two 65,000 lb Space Shuttle Launches

ORIGINAL PAGE IS OF POOR QUALITY

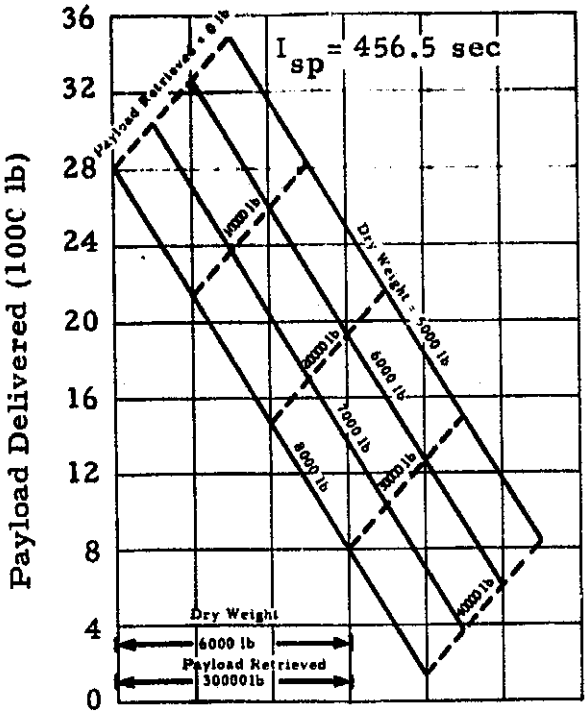

Fig. 6 - Modular AMOOS Payload Capabilities to Equatorial Geosynchronous Orbit for a Two-Stage Vehicle Using Two 65,000 lb Shuttle Launches

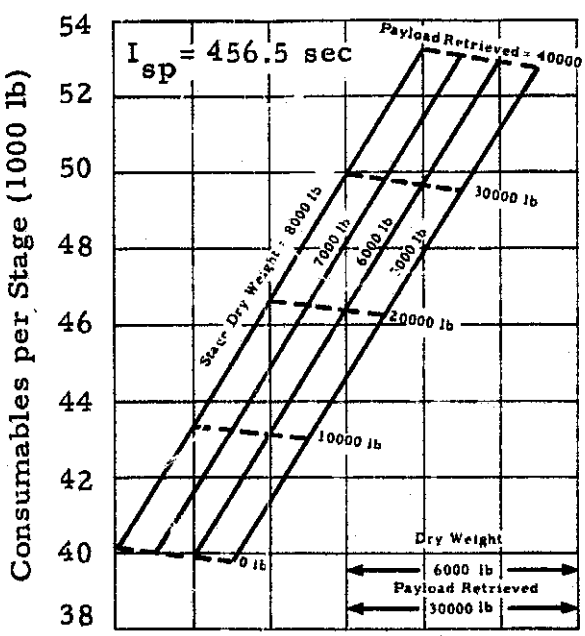

Fig. 7 - Modular AMOOS Main Engine Consumables for Equatorial Geosynchronous Orbit for a Two-Stage Vehicle Using Two 65,000 lb Shuttle Launches

(11,678 kg) which yields 18,700 lb (8482 kg) that may be consumed or left in geosynchronous orbit. Both AMOOS propulsion units are, of course, recovered.

Similar analyses were performed for missions to lunar orbit. The Δv budget included a 30-deg plane change in the vicinity of the moon in order to yield reasonable launch opportunities and stay times to selected lunar orbits. The 72 hr transfer orbit was chosen for the AMOOS lunar mission. The results for the single stage vehicle delivered to low earth orbit in one shuttle launch and the two-stage two-shuttle launch vehicle are presented here as examples of the lunar mission analyses.

The payloads to these lunar orbits are larger because the total Δv requirement is smaller than for the equatorial geosynchronous mission. In fact, for AMOOS missions the geosynchronous Δv requirement is very close to the maximum (Ref. 2). The mission involving a lunar landing requires a considerable increase in Δv. The capability of AMOOS to perform a lunar landing was not considered.

Figure 8 gives the payload delivered as a function of vehicle dry weight and payload returned. The payload delivered may be obtained as for the geosynchronous case given in Fig. 3. As an example consider a 6700 lb (3039 kg) AMOOS propulsion module and a 7300 lb (3311 kg) return payload. The total up payload is 10,500 lb (4763 kg) or net 3,200 lb (1452 kg). Recall that the comparable weights for the equatorial geosynchronous mission are total up payload of 7200 lb (3266 kg) (net 400 lb (182 kg)) and 6800 lb (3084 kg) down. The main engine consumables, Fig. 9, are 44,500 lb (20,185 kg) for the lunar missions reflecting the smaller total Δv requirements for the lunar mission over the equatorial geosynchronous.

The two-stage, two EOS AMOOS vehicle performing a lunar mission shows a corresponding increase in payload capability over the equatorial geosynchronous. As an example, consider again the 6700 lb (3039 kg) stage with a return payload of 7300 lb (3311 kg). The total delivered payload (from

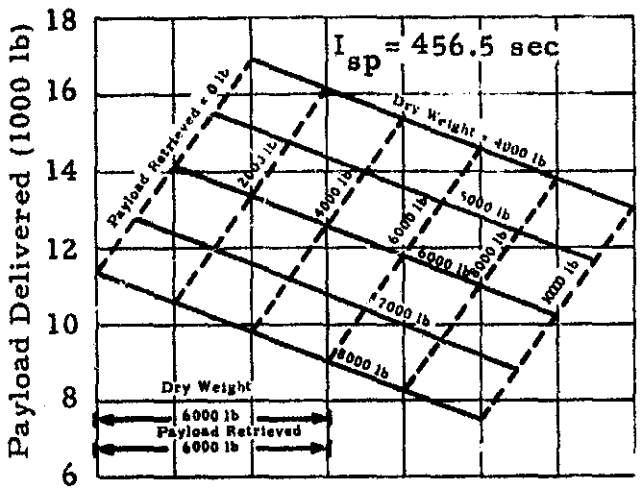

Fig. 8 - Modular AMOOS Payload Capabilities to Lunar Orbit for a Single-Stage Vehicle Using One 65,000 lb Shuttle Launch

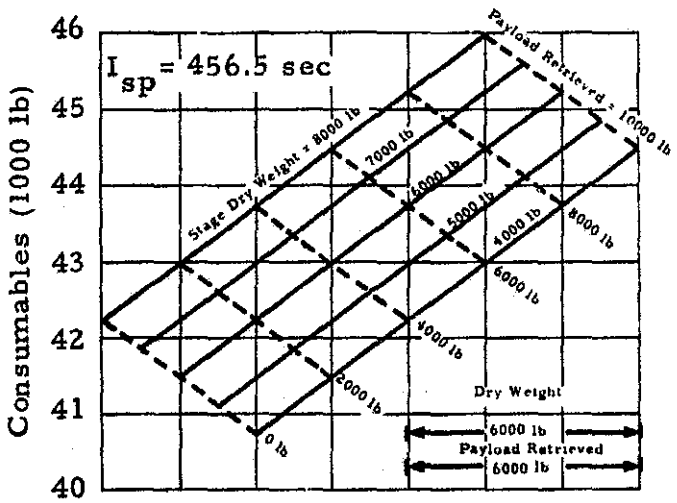

Fig. 9 - Modular AMOOS Main Engine Consumables for Lunar Orbit for a Single-Stage Vehicle Using One 65,000 lb Shuttle Launch

Fig. 10) is 29,000 lb (13,154 kg) or 21,700 lb (9843 kg) net if the 7300 lb (3311 kg) is round tripped. The corresponding main engine consumables are approximately 40,000 lb (18,144 kg) per stage from Fig. 11. On such a mission, the 21,700 lb (9843 kg) net payload is placed in lunar orbit by the AMOOS vehicle and not returned to low earth orbit.

Consumables analysis was also performed for the uprated shuttles of 80,000 and 100,000 lb (36,288 and 45,360 kg) payload capability to low earth orbit. Only geosynchronous equatorial missions were considered for one stage vehicles delivered by one EOS launch and two-stage vehicles delivered by two and three EOS vehicles. These analyses are reported in detail in Appendix A.

A separate consumables analysis was performed for the AMRS vehicle. The concept of the AMRS vehicle is that it is available on-station for an emergency crew transfer either to low earth orbit or to the earth's surface. The external geometry of the AMRS is similar to AMOOS and is depicted in Fig. 12. The on-orbit lifetime of such a vehicle should be compatible with space station lifetime; therefore, a long term space storable propellant is required. From these two considerations, the variables chosen for an AMRS mission were recovered weight and I_{sp} so that a wide range of possible designs could be covered. The dependent variable was on-orbit weight. Both on-orbit weight and recovered weight include the weight of a four-man crew. Therefore, the weight of the crew must be subtracted to give the AMRS unmanned weight that must be delivered to a station orbit. The first mission considered was a return from equatorial geosynchronous orbit. The on-orbit weight immediately prior to separation from the space station is given in Fig. 13 as a function of recovered weight for I_{sp} = 260, 290, 320 and 350 sec. As an example, consider a vehicle with a recovered weight, including crew, of 6000 lb (2722 kg) and I_{sp} = 300 sec. The required on-station weight is approximately 12,500 lb (5670 kg), again including crew. Subtracting the crew weight of 750 lb (340 kg) yields an on-station net weight of 11,750 lb (5330 kg). Referring to Fig. 3, the up payload for AMOOS is 11,500 lb (5216 kg). Increasing the AMRS I_{sp} to 320 sec yields an on-station weight of 12,000 lb (5443 kg) and hence a net

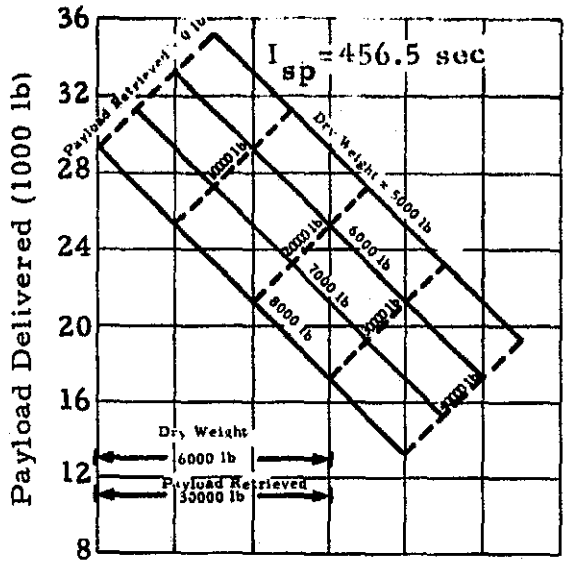

Fig. 10 - Modular AMOOS Payload Capabilities to Lunar Orbit for a Two-Stage Vehicle Using Two 65,000 lb Shuttle Launches

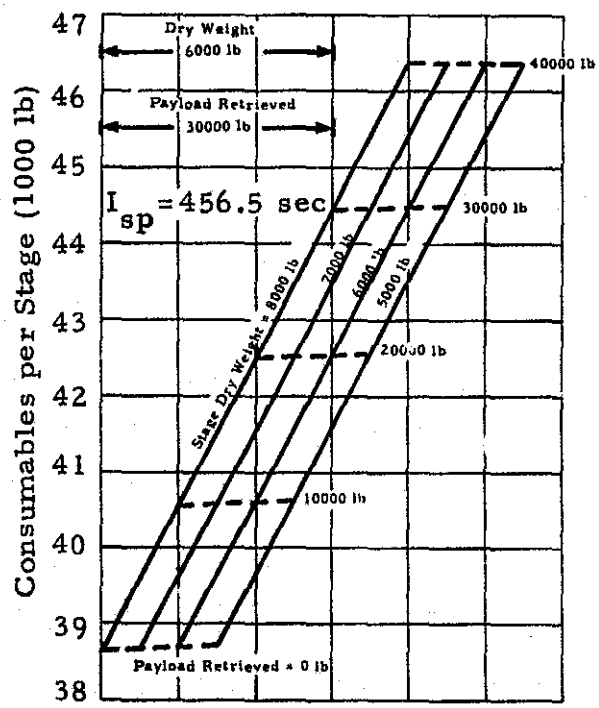

Fig. 11 - Modular AMOOS Main Engine Consumables for Lunar Orbit for a Two-Stage Vehicle Using Two 65,000 lb Shuttle Launches

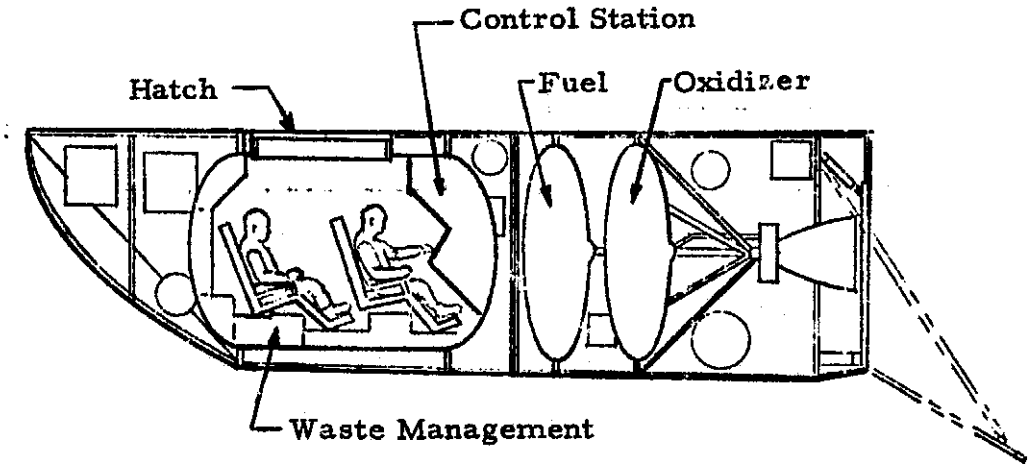

Fig. 12 - Typical AMRS Layout

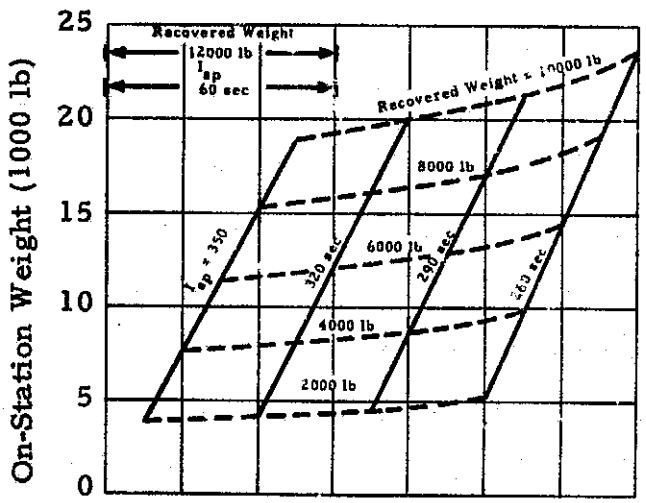

Fig. 13 - AMRS Equatorial Geosynchronous On-Station Weight, Including Crew

weight without crew of 11,250 lb (5103 kg). The design I_{sp} for AMRS should, therefore, be about 320 sec if the recovered weight is 6000 lb (2722 kg). The main engine consumables (from Fig. 14) for the return from geosynchronous orbit is approximately 5850 lb (2654 kg). The remainder of the weight to 12,000 lb (5443 kg) namely 150 lb (68 kg) are the consumables for the RCS, etc.

The other AMRS mission considered was return from a lunar orbit. A 30 deg plane change in the vicinity of the moon is allowed which is combined with phasing in lunar orbit. A 72 hr transfer orbit is used to return to the vicinity of the earth. A required on-orbit weight of 10,000 lb (4536 kg) (net 9250 lb (4196 kg)) is required (Fig. 15) to recover 6000 lb (2722 kg) with an I_{sp} = 300 sec. Such a payload, 9250 lb (4196 kg), is well within the capability of AMOOS which (from Fig. 8), is 13,250 lb (6010 kg). Such an AMRS vehicle could, then, be delivered by a single stage AMOOS which in turn is delivered to low earth orbit by a single Space Shuttle launch. The AMRS consumables for this mission are given in Fig. 16.

2.1.1.2 AMOOS Performance Spectrum

The AMOOS consumables analysis for the single stage vehicle delivered by one Shuttle launch has been analyzed to give the AMOOS performance spectrum. The results are plotted in Fig. 17 for equatorial missions to geosynchronous, 15,000 (27,795), 10,000 (18,530) and 5000 n.mi (9265 km) circular orbits. The current maximum length of an AMOOS payload is approximately 25 ft (7.62 m). The maximum diameter is 14.67 ft (4.47m) but this includes the structure necessary to support the TPS for the return trip. The net diameter is approximately 12 ft (3.66 m) for the recovered payload. If no payload TPS is required, e.g., a delivery only mission, then the full 14.67 ft (4.47 m) diameter may be realized. On a manned mission these dimensions are not restrictive since a typical manned capsule is some 11 ft (3.35 m) long with an internal diameter of approximately 10 ft (3.05 m). This is a practical maximum volume for a manned spacecraft with an all up weight of 7000 lb (3175 kg) or less.

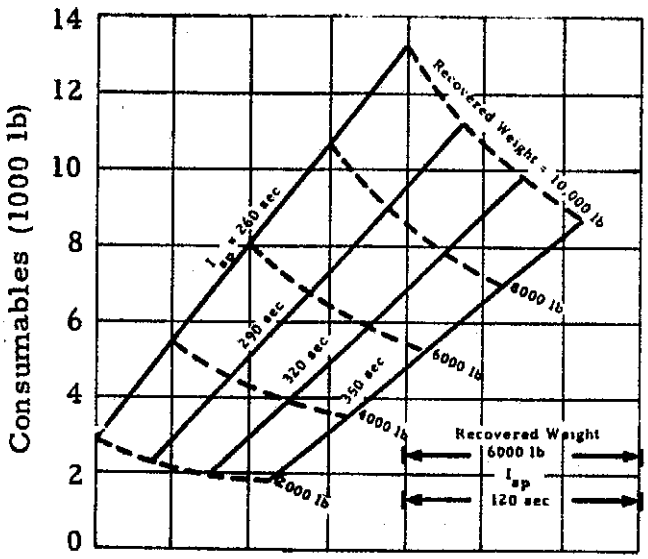

Fig. 14 - AMRS Main Engine Consumables for Recovery from an Equatorial Geosynchronous Orbit

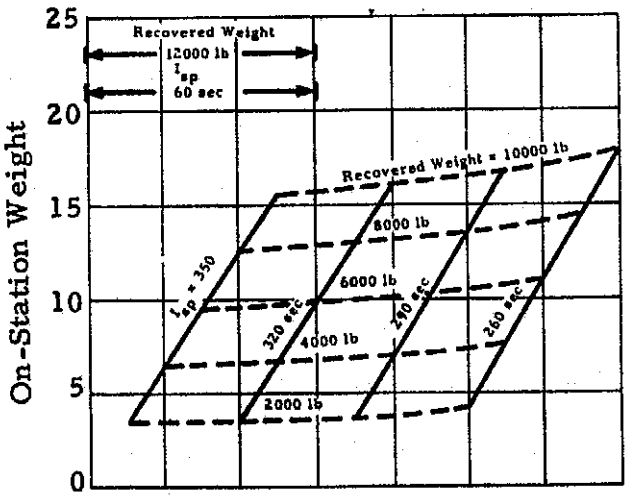

Fig. 15 - AMRS Lunar Orbit On-Station Weight

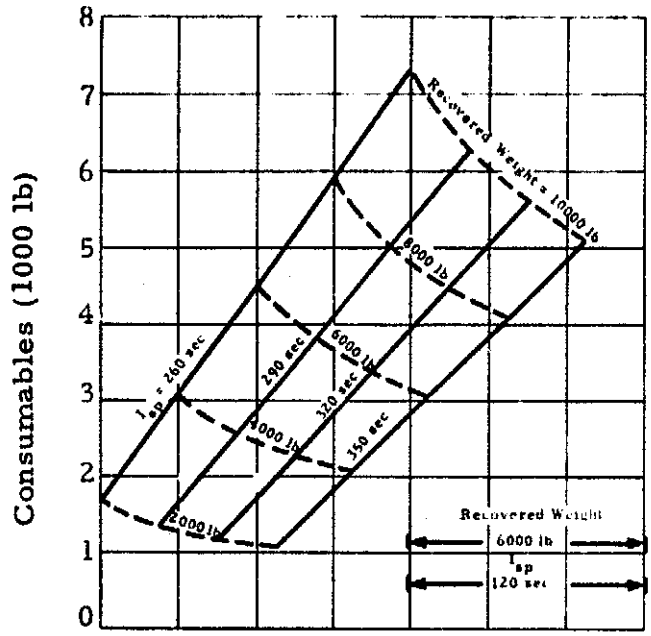

Fig. 16 - AMRS Main Engine Consumables for Recovery from Lunar Orbit

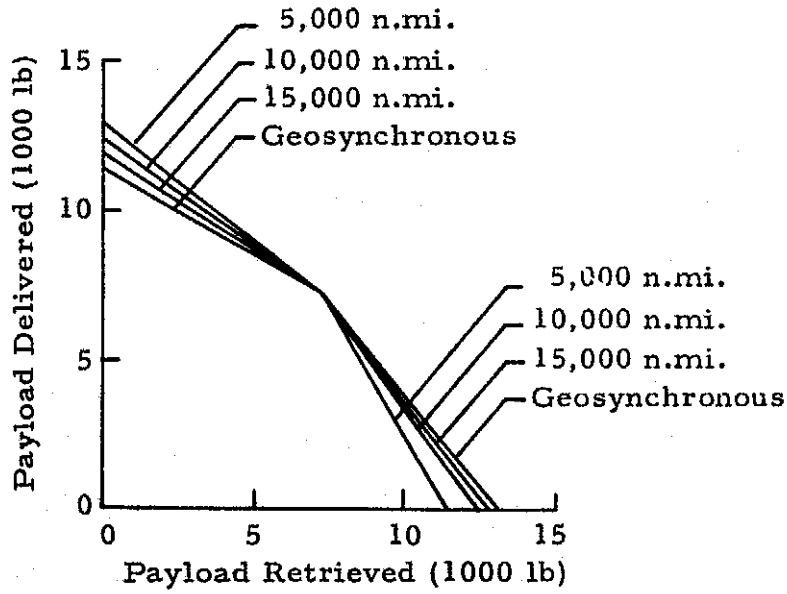

Fig. 17 - AMOOS Payload Capabilities for 6700 lb Dry Weight and 48,500 lb Propellant Capacity

The payload weight capabilities of AMOOS are summarized in Fig. 17. This summary is for the single stage AMOOS placed in low earth orbit by one space shuttle launch. The mission orbits covered are circular equatorial geosynchronous, 15,000 (27,795), 10,000 (18,530) and 5000 n.mi. (9265 km). The round trip payloads showed little sensitivity to mission altitude. This is caused by the total Δv requirements being essentially identical. The increase in Δv required to circularize and change plane at lower mission altitudes is offset by the decrease in Δv required for the maneuver to ascent transfer orbit.

The effects of different weights at the various burns are shown as the delivered payload differs from the retrieved payload. As the mission altitude decreases the delivered payload increases slightly for retrieved payloads below the round trip payload. The reverse is true for retrieved payloads above the round trip value. In this region the delivered payload decreases with decreasing mission altitude.

The break in the curves at the round trip payload value is due to the maximum propellant volume being reached at that point. For delivery payloads below 7100 lb (3221 kg) approximately, AMOOS, in its launch condition, weighs less than the maximum 63,100 lb (28,622 kg) allowable. The difference in the all up weight from the maximum is just the difference between the delivered payload and the round trip payload. If the delivered payload is increased above the round trip payload then propellant must, of course, be off loaded to keep the all up weight at 63,100 lb (28,622 kg).

The AMOOS vehicle may also be operated in the purely propulsive mode. In this mode the TPS and the nose cap are not required thus saving approximately 1300 lb (590 kg) of dry weight. In this mode, AMOOS has a performance very close to the Baseline Space Tug performance.

2.1.1.3 Vehicle Environment

The environment of both AMOOS and AMRS may be divided into three distinct phases. The first is transportation in the Shuttle cargo bay, the second is flight in space, and the third is the flight within the atmosphere. Of these, the environment of the shuttle cargo bay and that during atmospheric flight may be important in the design of the primary structure. This is due to the thrust to weight ratio of approximately 2 for both the AMOOS and AMRS vehicles being well below the number of g's acceleration experienced within the other two phases. The atmospheric flight phase, of course, governs the design of the TPS. The environment in the Shuttle cargo bay is given in Ref. 7 so only the environment during atmospheric flight will be given in detail herein.

In Fig. 18, the dynamic pressure, q, is plotted as a function of time from atmospheric entry for a typical trajectory. The maximum dynamic pressure was analyzed for 65 guidance validation runs. The average maximum q was 75.42 lb/ft^2 (3613 N/m^2) with a standard deviation of 1.870 lb/ft^2 (89.55 N/m^2). The $\pm 3\sigma$ variations in q are shown as broken lines on Fig. 18. The $+3\sigma$ value of 81.03 lb/ft^2 (3881 N/m) is, by coincidence, just equal to the upper limit of the range of q for the 65 trajectories. This figure is well below the value of approximately 104.39 lb/ft^2 (5000 N/m^2) obtained for the worst case, unguided trajectories in the earlier studies. The mean q_{max} of 75.42 lb/ft^2 (3613 N/m^2) is close to the nominal q_{max} of 74.76 lb/ft^2 (3581 N/m^2), the difference being $.36\sigma$. The above discussions are for a W/C_DA = 35.5 lb/ft^2 (1700 N/m^2), which corresponds to the upper limit of the W/C_DA range for AMOOS and AMRS.

The maximum dynamic pressure encountered is both a function of energy to be dissipated and number of passes constituting the aeromaneuver. The maximum dynamic pressure encountered for non-lifting trajectories* is presented in Fig. 19 as a function of atmospheric entry velocity. The sensible atmosphere is assumed to begin at an altitude of approximately 400,000 ft (120 km). The maximum q experienced increases rapidly with increasing entry velocity. These maximum values may be reduced considerably, in fact,

*No vertical component.

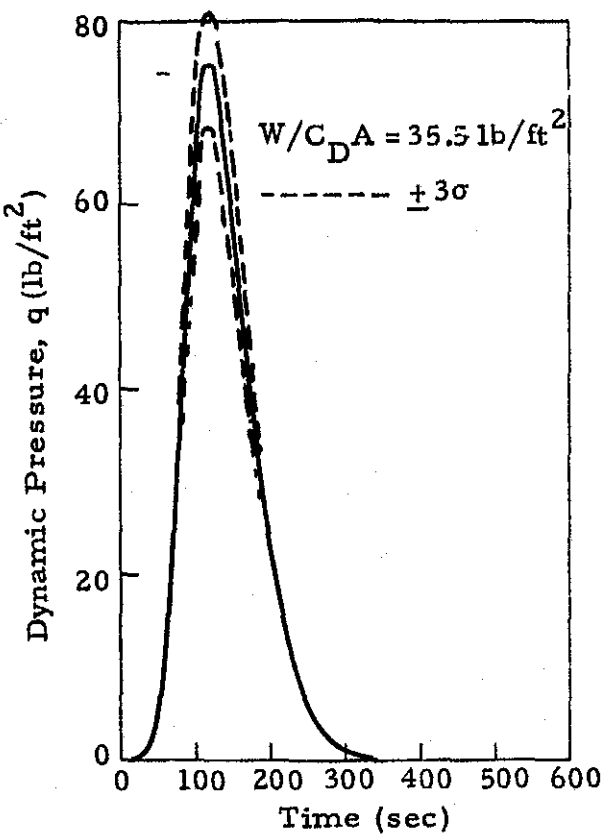

Fig. 18 - Dynamic Pressure vs Time from Atmospheric Entry (400,000 ft)

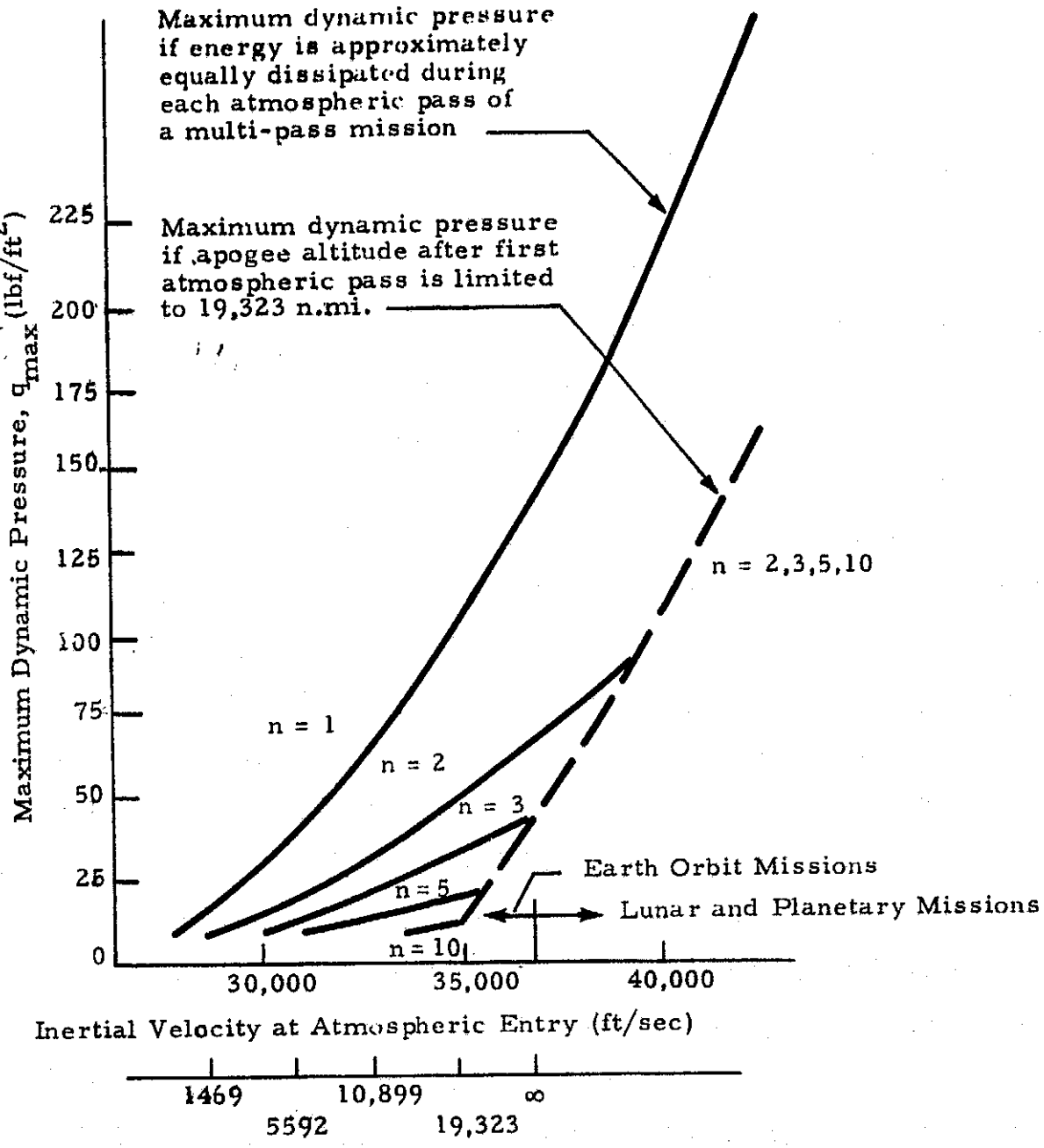

Fig. 19 - Effect of Velocity and Number of Passes on Maximum Dynamic Pressure

to about 0.75 of the no-lift value, by choosing a lift downward (Refs. 1 and 2) trajectory. Such a trajectory would use about one-third or less of the total available lift for q_{max} reduction and about one-half for trajectory control.

Maximum atmospheric density encountered follows a trend similar to the maximum dynamic pressure. The density peaks later than the dynamic pressure, which is seen in the example given in Fig. 20. The peak values are, of course, only a few seconds apart.

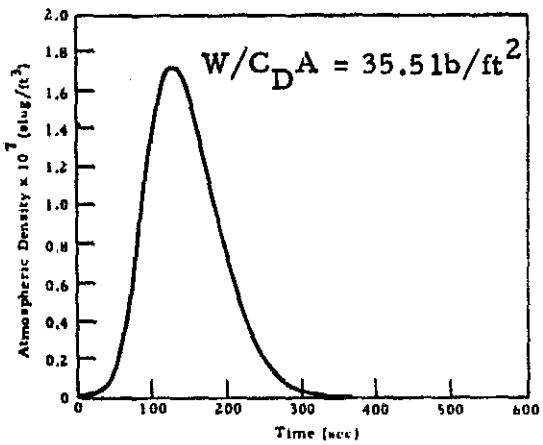

Fig. 20 - Atmospheric Density vs Time from Atmospheric Entry (400,000 ft)

The effect of number of passes on maximum density encountered is shown in Fig. 21. Again the peak value can be reduced by flying a downward lift nominal trajectory. The reduction in ρ_{max} would be approximately the same as for q_{max}, namely to about 0.75 of the no-lift value.

In both Figs. 19 and 21 there is a minimum value of the respective variables for entry velocities above earth escape velocity for 400,000 ft (120 km). The logic behind this is that the vehicle must be captured by the earth on the first pass through the atmosphere. From the two-body point of view, the first pass must put the vehicle into a parabolic orbit, but from a practical point of view an elliptical orbit with a relatively low apogee must be obtained. Quite arbitrarily geosynchronous altitude, 19,000 n.mi. (34,500 km) approximately, has been chosen as the maximum permissible apogee altitude after one atmospheric pass. The broken line reflects this upper limit to the first pass apogee.

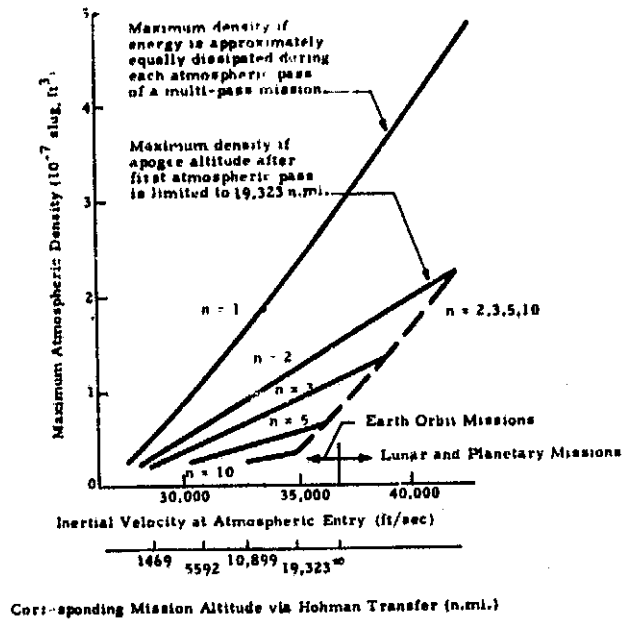

Fig. 21 - Effect of Entry Velocity and Number of Passes on Maximum Atmospheric Density

A typical relative velocity-time history is given in Fig. 22. The exit velocity is, for practical purposes, a function of desired apogee altitude, and hence, for AMOOS, almost constant. The effects of guidance on the nominal velocity are small since the guidance tends to negate off-nominal conditions rapidly. This appears to be due to the fact that as the drag force increases then so does the lift force, thus allowing corrections to accompany the accumulation of velocity errors due to off-nominal conditions.

Since the ballistic coefficient, W/C_DA, for AMRS is approximately the same as for AMOOS, the above data on the return from geosynchronous altitude apply equally well to each. However, AMRS must have the capability of ground recovery. The flight environment applicable for ground recovery will now be discussed.

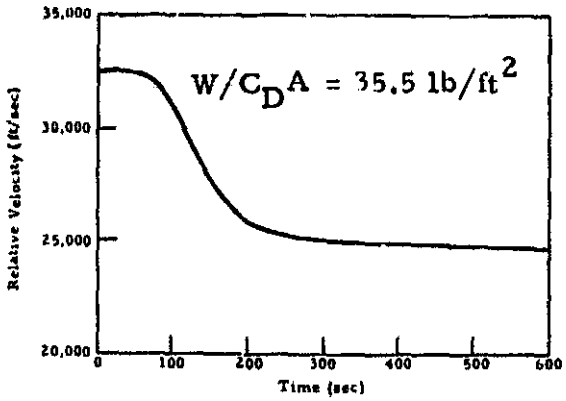

Fig. 22 - Relative Velocity vs Time from Atmospheric Entry (400,000 ft) for a Skip Type Trajectory

Since the relative velocity is eventually reduced to zero, there is no longer the need to target for a velocity loss. Instead of accepting the environment necessary to effect the fixed velocity loss, the environment may be ameliorated by suitable modulation of the lift vector. To this end, a bank angle time history has been chosen that modifies the dynamic pressure from the ballistic reentry values. The first 300 sec of atmospheric flight are plotted in Fig. 23. The bank angle is modulated to reduce the peak values to 100 lb/ft^2 (4788 N/m^2). The value of q remains below 55 lb/ft^2 (2635 N/m^2) from 300 sec to the termination of the simulated trajectory at approximately 20,000 ft (6000 m). Atmospheric density is also plotted on Fig. 23. As before, its maxima and minima lag those of q. Since this AMRS environment is for ground recovery, the density eventually tends steadily to that at sea level.

The double peak in q shown is due to the particular bank angle time history used. To eliminate such a double peak, if desired, a guidance scheme controlling on acceleration would be desired.

The heating rate on a 1 ft (0.3048 m) radius sphere is used as a measure of the thermal environment. Three thermal regimes are recognized, namely, free molecular, where $M_\infty/\sqrt{Re} > 3$, continuum, where $M_\infty/\sqrt{Re} < 0.05$, and transitional where $0.05 \leq M_\infty/\sqrt{Re} \leq 3$. Reynolds number (Re) is based on

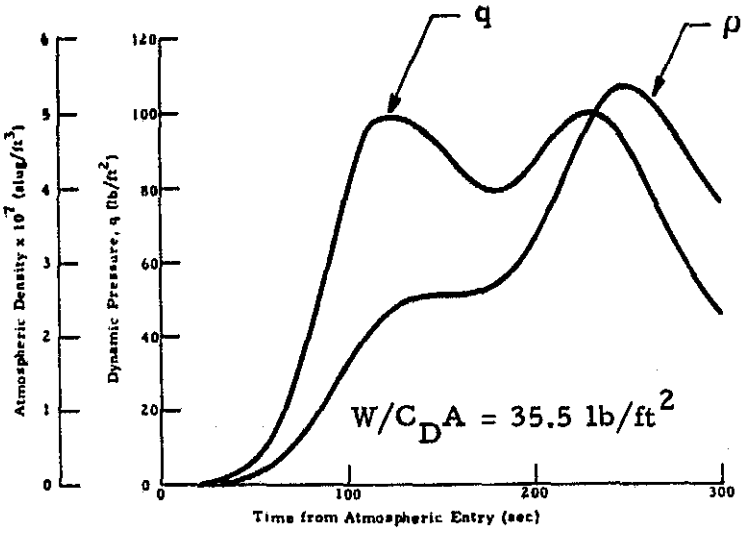

Fig. 23 - Maximum Dynamic Pressure and Atmospheric Density vs Time from Atmospheric Entry for the AMRS Ground Recovery Mode

body radius for these classifications. The transitional heating rates and the values of $M_\infty/\sqrt{Re}$ based on a 1 ft radius sphere are given in Fig. 24 for the AMOOS and AMRS rendezvous type trajectory. The transitional heating rate only is plotted in Fig. 24 since the values of $M_\infty/\sqrt{Re}$ for both AMOOS and AMRS are in the range $0.05 \leq M_\infty/\sqrt{Re} \leq 3$ for all except the very high altitude, low heating rate portion of the trajectory.

The AMRS vehicle is also in the transitional heating rate regime during the peak heating period of the ground recovery trajectory. The first 300 sec of this heating rate time-history is given in Fig. 25.

2.1.1.4 Design Parameters

The foregoing data represent the capabilities available to an AMOOS or AMRS vehicle and the possible environments it may meet. In order to design a vehicle, some set of capabilities and environment must be extracted.

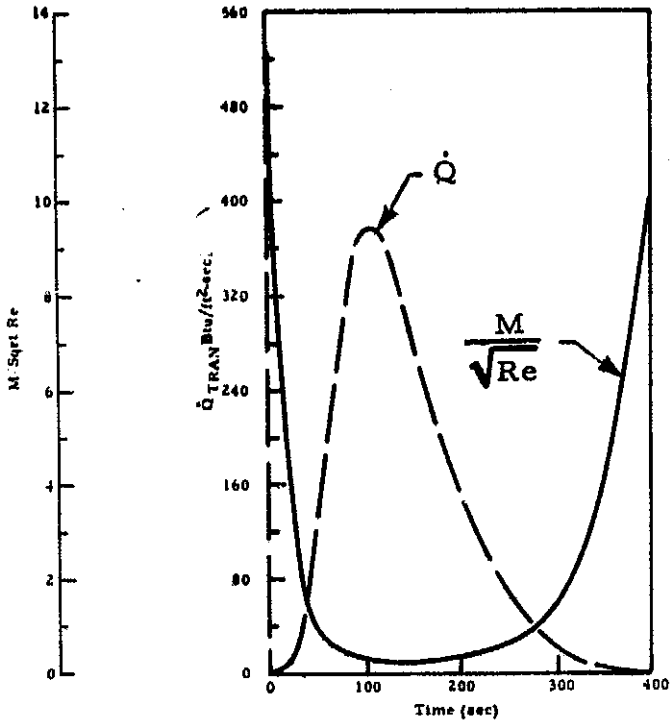

Fig. 24 - Heating Rates to a 1 ft Radius Sphere Along the AMOOS Design Trajectory (Stagnation Point)

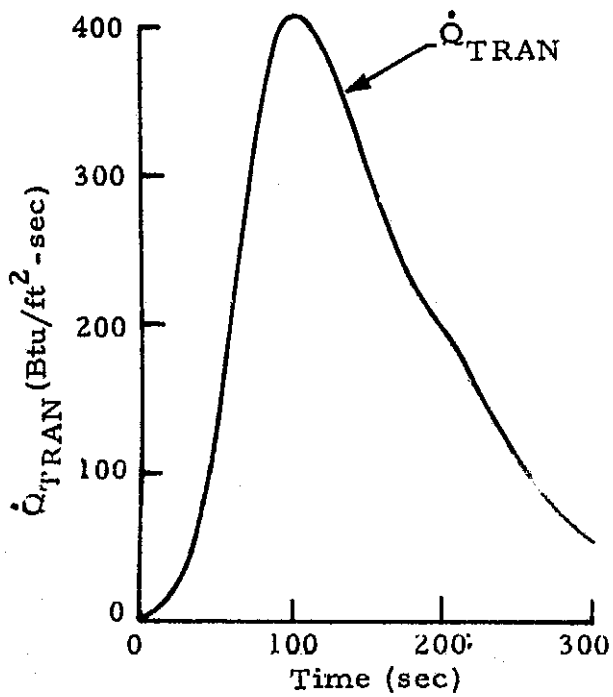

Fig. 25 - Heating Rates on a 1 ft Radius Sphere Along the AMRS Design Trajectory (Stagnation Point)

These need not represent an actual performance capability and in general will not since the best practical overall performance is probably a compromise among several possible performance capabilities. For example, consider an AMOOS vehicle required to be able to round trip 7100 lb (3221 kg). Such a vehicle could perform a one way retrieval of some 14,000 lb (6350 kg). It is most unlikely that such a large return payload will be required for a single stage, one EOS launch AMOOS, therefore the design maximum reentry weight for such an AMOOS could be set at 15,000 lb (6804 kg), which represents approximately a 7500 lb (3402 kg) return payload. Setting such a return payload allows some margin for variation in payloads but does not unduly penalize the vehicle by designing for an unusable capability.

The structural design conditions may be separated into two classes. These are:

1. The fully loaded vehicle in the Shuttle Orbiter cargo bay. In this condition the AMOOS/AMRS structure is cold.
2. The lightly loaded vehicle during the aeromaneuver. In this condition the AMOOS/AMRS structure is hot.

The AMOOS engine burn condition can be quickly eliminated since the engine thrust is only 15,000 lb (66,723 N). A 5000 lb (22,241 N) thrust engine will suffice for AMRS. It must, of course, be considered when designing the thrust structure.

In selecting the design conditions, experience was called upon to reduce the number of conditions. During transportation in the Shuttle cargo bay, the most highly stressed section of AMOOS or AMRS is near the propellant tanks where a large fraction of the total mass is concentrated. Note that, in the case of AMOOS, the mass concentration is particularly pronounced at the LOX tank. These large localized masses produce the highest internal loads in the structure. Off-loading propellant, in order to carry a large delivery payload,

results in a lower stressed structure since the weight in the critical section is reduced and the increased payload weight is carried into the orbiter structure at relatively lightly loaded AMOOS sections. For these reasons only the tanks full case need be used for structural design. On the other hand, during the aeromaneuver, the configuration with the highest W/C_DA experiences the highest loads. For this case, therefore, the heaviest practical recovery weight is used in combination with the appropriate shortest length to determine the design trajectory.

For use in designing the structure, the aerodynamic loads are specified as a distribution and a design dynamic pressure. This allows the design loads to be readily changed by changing the dynamic pressure. The load distribution remains essentially unchanged at the high Mach numbers at which maximum dynamic pressure occurs. The properties of materials are also temperature dependent so that, in this application, a structural temperature must be specified. This design temperature is chosen upon the consideration of several parameters. Taken into consideration are the structural materials themselves, the ablator or other TPS material and the bonder used to bond the TPS to the structure. Brief optimization studies (Appendix C) have shown that 600F (589K) is a reasonable bondline temperature.

The design data for the one stage AMOOS placed in low earth orbit in one EOS launch is given in Table 1.

Table 1
SINGLE STAGE AMOOS DESIGN DATA

Total (all up) Weight: 63,100 lb (28,622 kg)
Payload: Up 7100 lb (3221 kg); Down 7100 lb (3221 kg)
Main Engine Consumables: 48,500 lb (22,000 kg)
Design Reentry Weight: 15,000 lb (6804 kg)
Bond Line Temperature: 600 F (589 K)
Design Dynamic Pressure: 100 lb/ft^2 (5000 N/m^2)

With the expected dry weight of 6700 lb (3039 kg) for AMOOS, propellant will have to be off-loaded to deliver more than 7100 lb (3221 kg). Designing the AMOOS vehicle for a reentry weight of 15,000 lb (6804 kg) represents what is believed to be a practical upper limit to the AMOOS single EOS launch round-trip payload capability. A round-trip capability of 7500 lb (3402 kg) corresponds to a dry weight of 6300 lb (2858 kg). Such a dry weight is feasible with moderate advances in technology. As stated previously, prior experience has shown that the maximum propellant case yields the design loads. A minimum skin gage is specified upon consideration of it supporting the ablator. This results in a very lightly stressed structure at the aft end where the payload is attached. Because of this lightly loaded condition a 59 ft (17.98 m) long vehicle of 25,000 lb (11,340 kg) reentry weight could also be used without appreciable penalty.

Similarly, design data have been chosen for the AMRS and are given in Table 2.

Table 2
AMRS DESIGN DATA

Total (all up) Weight: 12,500 lb (5670 kg)
Payload, Up Zero, Down: 748 lb (339 kg) (4 men)
Main Engine Consumables: 6,500 lb (2948 kg)
Design Reentry Weight: 7,000 lb (3175 kg)
Bondline Temperature: 600 F (589K)
Design Dynamic Pressure: 140 lb/ft^2 (7,000 N/m^2)

The aeromaneuvering loads design data are completed by the load distribution given in Fig. 26. The distribution is given as a function of body diameters. It is plotted in this manner so that it applies to both AMOOS and AMRS. Furthermore, recall that the Mach number is in the hypersonic regime

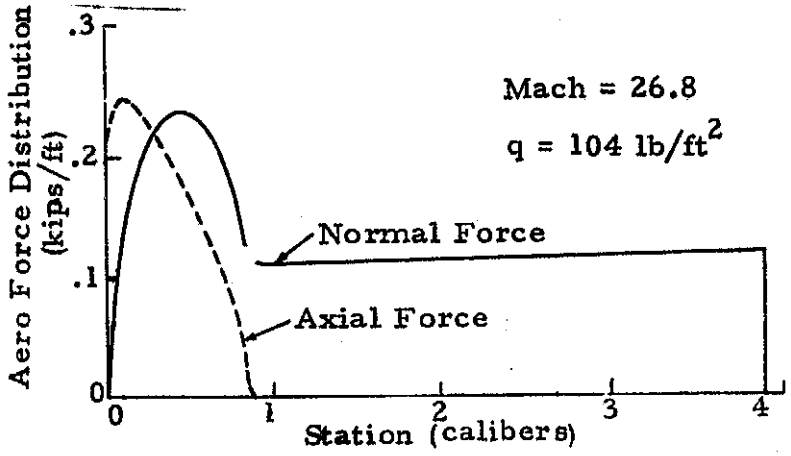

Fig. 26 - Normal and Axial Force Distribution Along the AMOOS Configuration

so that the distribution for the shorter, truncated bodies may be obtained by using the fore part of the curve up to the number of body diameters equal to the fineness ratio of the vehicle considered. For example, suppose the vehicle length is 45.6 ft (13.9m) and the body diameter is 14.7 ft (4.48 m), then the load distribution for this configuration would be that part of the curve of Fig. 26 from 0 to 3.10 body diameters (calibers).

The above design data are also used to determine a design trajectory and hence a design heating rate time history. Since the ballistic coefficients for the four-man crew module AMOOS and AMRS are approximately the same, the same design trajectory may be used for both in the Shuttle Orbiter recovery rendezvous mode. However, AMRS must also have ground recovery capability, therefore a reentry design trajectory and corresponding heating rates must be developed. The selected trajectories are, of course, those given in Figs. 18 through 23. The corresponding stagnation heating rates on a 1 ft radius sphere are given in Figs. 24 and 25.

For completeness, the Shuttle Orbiter cargo bay loads are given. Experience has shown that these loads do, in fact, design much of the AMOOS and AMRS vehicles, These loads are given in Table 3 and are taken from Ref. 7.

Table 3

SHUTTLE PAYLOAD BAY LIMIT LOAD FACTORS

Condition*	Linear - g		
	X	Y	Z
Lift-Off	-0.1 -2.9	+1.0 -1.0	+1.5 -1.5
High-Q Boost	-1.6 -2.0	+0.5 -0.5	+0.6 -0.6
Boost-Max. LP (Stack)	-2.7 -3.3	+0.2 -0.2	-0.3 -0.3
Boost-Max. LP (Orb Alone)	-2.7 -3.3	+0.2 -0.2	-0.75 -0.75
Entry and Descent Pitch Up	+1.06 -0.02	0 0	+2.5 -1.0
Entry and Descent Yaw	+0.75 +0.75	+1.25 -1.25	+1.0 +1.0
Landing	+1.0 -0.8	+0.5 -0.5	+2.8 +2.2
Crash**	+9.00 -1.5	+1.50 -1.50	+4.5 -2.0
Crash (Crew Compartment Interior)	+20.0 -3.3	+3.3 -3.3	+10.0 -4.4

*Positive X, Y, Z directions equal aft, right and up. Load factor carries the sign of the externally applied load.

**Crash load factors are ultimate and only used to design payload support fittings and payload attachment fasteners. Crash load factors for the nominal payload of 65,000 lb (29,485 kg). Longitudinal load factors are directed in the forward azimuth within 20 deg of the orbiter longitudinal axis. The specified load factors will operate separately.

2.1.2 AMOOS/AMRS Concepts and Applications

A modular AMOOS concept was developed initially in Ref. 2 and is further developed herein. A typical modular layout is shown in Fig. 27.

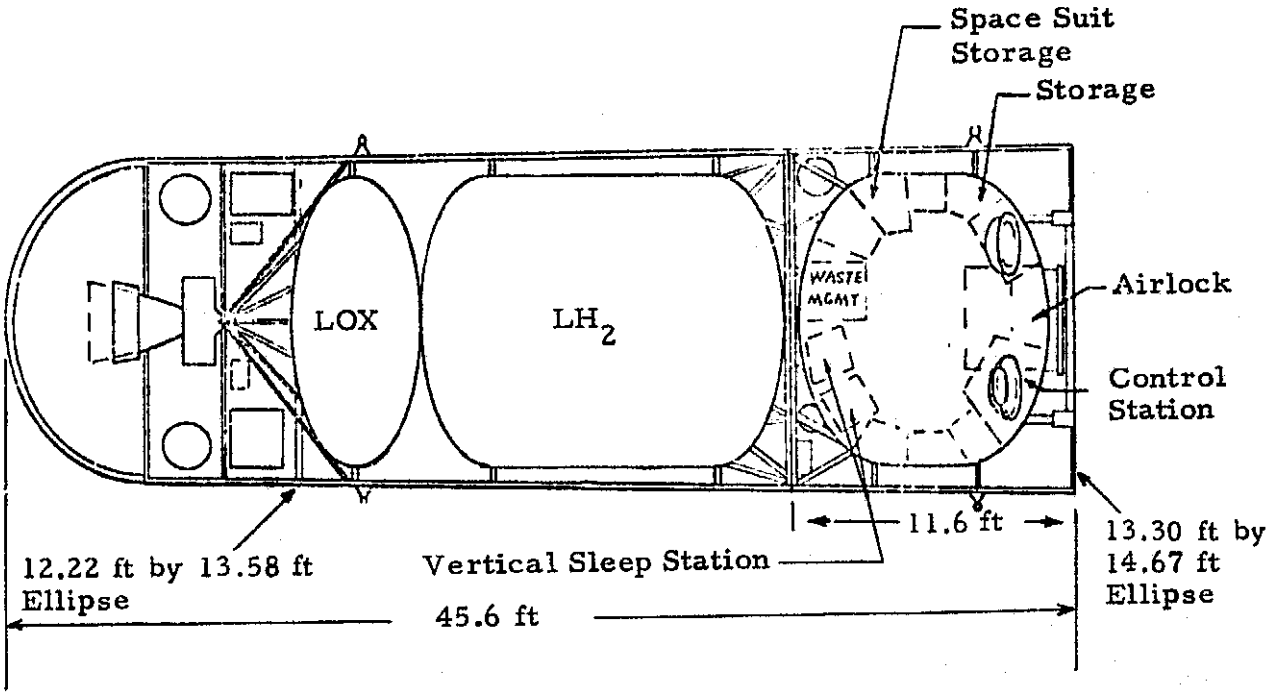

Fig. 27 - Typical AMOOS and Manned Module Layout

Basically, the vehicle consists of a tapered elliptical body, raked off at approximately 45 deg at the nose. The nose consists of a complexly curved cap designed to give a high drag coefficient. The lengths of the propulsion module and crew module are 34 ft (10.4 m) and 11.6 ft (3.54), respectively. The elliptical cylinder section tapers from a 12.22 ft (3.72 m) x 13.58 ft (4.14 m) ellipse at the forward most point of the LOX tank to a 13.30 ft (4.05 m) by 14.67 ft (4.47 m) ellipse at the aft end of the crew module.

The application of AMOOS to the manned geosynchronous sortie mission was also considered. This application is for two AMOOS stages delivered by two Shuttle launches. The structural design and weight analysis was not performed to the same degree of detail as for the crew rotation application.

The complete vehicle is shown in Fig. 28 and consists of two AMOOS propulsion modules, a crew quarters module and a workshop module. The crew quarters module and both AMOOS propulsion modules would be recovered. The smaller crew module of Fig. 27 could be substituted for the large crew module of Fig. 28. Typical total weights for the crew module of Fig. 28 would be 10,000 lb (4536 kg). The corresponding weight of the workshop would be 8000 lb (3629 kg) approximately. If the smaller, 6800 lb (3084 kg) crew module of Fig. 27 is used then the workshop, as left in orbit, may weigh as much as 18,000 lb (8165 kg). The AMRS external geometry was obtained by scaling the AMOOS configuration. The design of the Fig. 27 vehicle and AMRS will now be discussed.

2.1.2.1 Design of the AMOOS Propulsion Module

In previous AMOOS studies, a non-optimized ring-stringer stiffened skin primary structure has been used. In this contract it was decided to use a structural design computer program that will optimize the structure. This is accomplished partially by user input and partially within the program so that several cases must be run before the minimum weight structure is obtained.

The ring-stringer stiffened skin structure is considered optimum for AMOOS and AMRS applications since the skin must give rigid support to the ablator. This type of structure gives a good compromise between structural weight and skin thickness. The thickness of the skin is also considered important in the refurbishment of the TPS.

The choice of structure material was based on the experience gained from previous contracts. Although Be-38Al Beryllium-Aluminum yielded the lightest structure, HM21A-T8 Magnesium gave a comparable weight. The other materials considered, namely titanium and graphite/polyimide, yielded much heavier weights. Stainless steel was eliminated since it would give a heavier structure than titanium at 600F (589K). For these reasons,

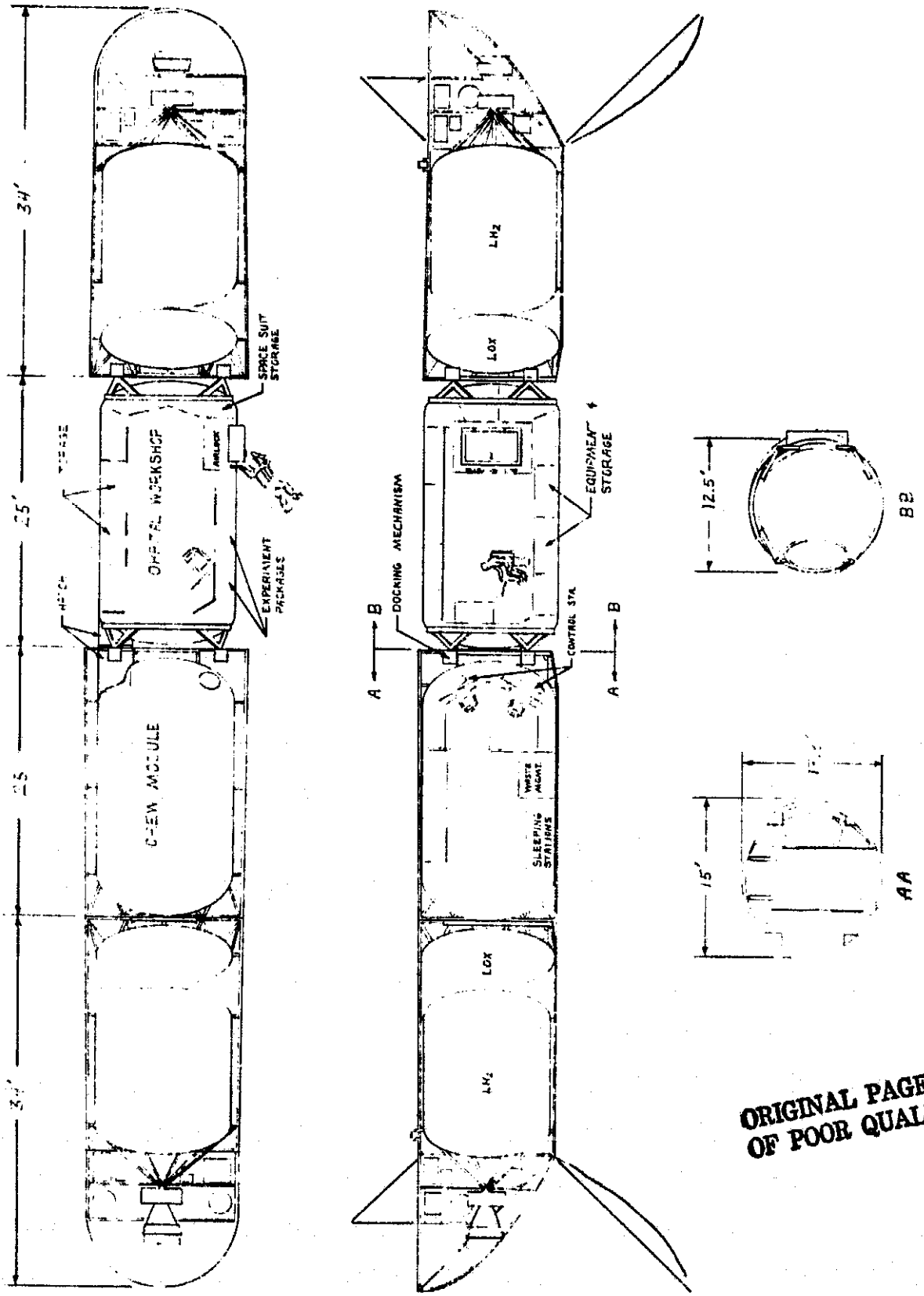

Fig. 28 - Schematic of AMOOS Sortie

ORIGINAL PAGE IS OF POOR QUALITY

and its relatively low cost, magnesium HM21A-T8, has been chosen for the current designs. The expected weight of the primary structure using Be-38Al would be slightly lighter and for other materials somewhat heavier.

The primary structure weight for HM21A-T8 magnesium is given in Table 4.

Table 4

AMOOS PROPULSION MODULE PRIMARY STRUCTURE WEIGHTS

Section	Station (in)	Design Condition	Length (in)	Weight (lb)
Nose	0-114	Orbiter	114	301
Fwd Body	114-240	Orbiter	126	321
Aft Body	240-408	Aero	168	391
10% Contingency				101
Total				1114

A typical segment of this structure is shown in Fig. 29. The structural weights also include solid circumferential rings placed at appropriate locations to allow for splice areas and major component attachment points. Nine such rings are included, each four inches wide and 0.5 in. thick.

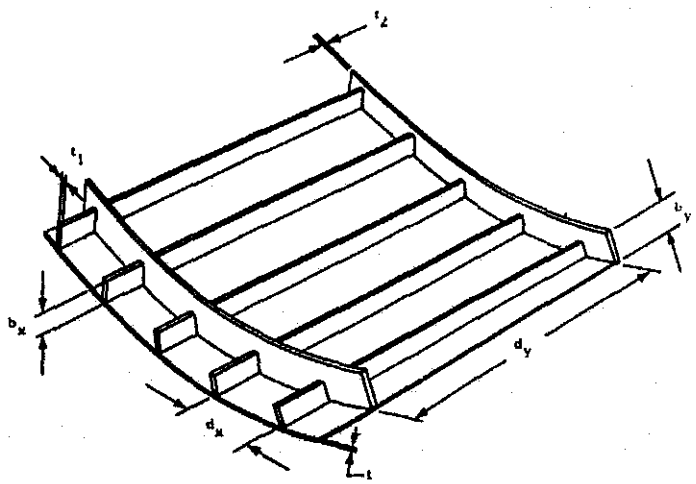

Fig. 29 - Typical Segment of AMOOS and AMRS Primary Structure

In all, four design cases were considered. These are: (1) the fully loaded AMOOS vehicle in the Shuttle Orbiter cargo bay during ascent; (2) the propulsion unit alone; (3) the propulsion unit with the crew module; and (4) the maximum length, maximum reentry weight vehicle. The last three cases are during the atmospheric pass. The vehicle was designed to withstand each case by using the critical load to design each section.

Except for the primary structure and TPS, AMOOS subsystems are either identical to those of the Baseline Space Tug (Ref. 8) or similar. The weights of these subsystems were either taken or estimated from Ref. 8. The following subsystems or components of AMOOS are identical to the Baseline Tug of Ref. 8; engine, gimbal, thrust structure, mounting structure, feed, fill drain and vent, pneumatic and pressure, hydraulic (except nose actuator), propellant loading and measuring, tank insulation, purge and thermal control system and rendezvous and docking. The weights of the above systems were taken from Ref. 8. The APS system for AMOOS must be operative in the atmosphere and hence more powerful thrusters are needed at least in pitch and yaw. An APS weight of 500 lb, excluding consumables was allowed against 301 lb for the Baseline Space Tug. The navigation studies of Ref. 3 were used to determine that the Baseline Space Tug avionics would be adequate for AMOOS. Since the manned capsule would not be detached from the propulsion module in space, the payload and umbilical interface was omitted for the manned AMOOS. If a detachable payload is carried, then this weight must be taken from the AMOOS payload capability. A scar weight of 30 lb was allowed for this capability and called the aft ring interface.

The Martin Marietta SLA 561 ablator was chosen as the TPS material for the AMOOS vehicle and the payload protection structure. This material was chosen since it is flight rated and the heating rates are within its range. It is also expected to yield a relatively light weight TPS because of its good insulative and ablative properties and its low density of 15 lb/ft^3 (240.28 kg/m^3).

The heating rates on the vehicle were computed for the trajectory given in Section 2.1.1.3. These heating rates were then used to compute

the required ablator thickness over the vehicle using the STAB II computer program. The TPS weight given in the weight breakdown (Table 5) was selected from consideration of bondline temperature, angle-of-attack and off-nominal conditions. The method is explained fully in Appendix C.

An overall weight contingency of 10% was allowed on dry weight. On top of this, an unbudgeted contingency of 200 lb was added since it was considered that further study of the navigation, guidance and control system was required to describe the system adequately.

2.1.2.2 Design of AMRS

The same approach was taken to the AMRS vehicle as to AMOOS. In the case of AMRS there is essentially only one vehicle configuration so that there was only one atmospheric flight case to consider. The ascent in the Shuttle Orbiter's cargo bay was also considered in the primary structure design.

The AMRS primary structure weight was optimized in a manner similar to that described for AMOOS. The subsystems and components weights were obtained from Refs. 8, 9 and 10. The avionics weights were obtained from Ref. 8 (Baseline Tug) upon consideration of the minimal system required for AMRS. The crew, life support and related systems volumes and weights were taken from Ref. 9. The estimate of the engine, tank and plumbing weights were obtained from Ref. 10. The avionics weight was checked against the estimate using Ref. 10. The AMRS vehicle was designed to support a crew of 4 for 24 hours with 100% reserves. (Recall that the time to transfer from geosynchronous to a perigee within the sensible atmosphere is less than six hours.) The resulting AMRS weight breakdown is given in Table 6.

The design of the TPS followed closely that for the AMOOS propulsion module. The details are given in Appendix C.

Table 5

AMOOS PROPULSION UNIT WEIGHT BREAKDOWN

Components	Weight, lb	(kg)
Gimbal	30	(14)
Fuel Tank and Supports	417	(189)
Oxidizer Tank and Supports	238	(108)
Thrust Structure	29	(13)
Mounting Structure	100	(45)
Nose Actuator	100	(45)
Engine	442	(200)
Feed, Fill, Drain and Vent	256	(116)
Pneumatic and Pressure	234	(106)
Hydraulic	63	(29)
Propellant Loading and Measuring	50	(23)
APS	500	(227)
Tank Insulation	130	(59)
Purge and Thermal Control System	311	(141)
Navigation Guidance and Control	154	(70)
Data Management	158	(72)
Communications	72	(33)
Measuring System	92	(42)
Electrical Power and Distribution	410	(186)
Rendezvous and Docking	35	(16)
Aft Ring Interface	30	(14)
	3851	(1747)
Thermal Protection System	1036	(470)
Shell Structure	1013	(459)
Contingency 10%	590	(268)
Unbudgeted Contigency	210	(95)
Total Dry Weight	6700	(3039)

Table 6

AMRS WEIGHT AND VOLUME BREAKDOWN

	Vol. ft^3	(m^3)	Wt, lb	(kg)
Crew, Four @ 56 ft^3	224	(6.34)	748	(334)
Food 8 lb/ft^3	2	(0.057)	16	(7)
Furnishings 2 lb/ft^3	43	(1.22)	86	(39)
Medical 10 lb/ft^3	2	(0.057)	20	(9)
Personnel Effects	10	(0.283)	56	(25)
EC/LSS			738	(335)
Atmosphere	2	(0.057)		
Water 62 lb/ft^3	1	(0.028)		
Wastes Management	4	(0.113)		
Hardware	10	(0.283)		
Electronics	4	(0.113)	130	(59)
Communications and Data System	10	(0.283)	327	(148)
Instrumentation	16	(0.453)	188	(85)
Miscellaneous Equipment	10	(0.382)	20	(9)
Expendables	3	(0.085)		
Crew Capsule			507	(230)
Engine and Thrust Structure			185	(84)
Tanks and Support Structures			375	(170)
Astrionics			400	(181)
Plumbing Weight			132	(60)
Flap			50	(23)
TPS			500	(227)
APS and Structure			500	(227)
Shell Structure			469	(213)
Contingency 10%	34	(0.963)	473	(215)
Total Dry Weight	375	(10.62)	5920	(2685)

2.1.3 Integrated Crew Module/AMOOS Analysis

The AMOOS crew module was designed to provide life support for a crew of four for 30 days. Negligible weight changes could also result in a six man, 20-day configuration. The capsule is designed to accomodate the crew but not to provide working area. The primary structure and TPS for the module was designed in conjunction with the propulsion module and so the same trades and optimization were performed. The crew requirements were determined from Ref. 9. The AMRS crew compartment was designed for a four-man, one day occupancy in space. The vehicle is designed for emergency use. The life support subsystems comsumables do, however, include the recommended contingencies, usually 100% of the required value.

The weights of the AMOOS crew module are given in Table 7. The AMRS crew compartment weights are given in Table 6 of the preceeding section with the dry weight, including crew, since an integral vehicle is chosen for AMRS.

2.1.4 AMOOS/AMRS Flight Test Program Analysis

The purpose of this analysis is to determine the requirements of a model flight test program applicable to both AMOOS and AMRS. The flight test program must provide design data for AMOOS and AMRS and concurrently check out common subsystems of these vehicles. It is envisioned that such model testing will significantly reduce the flight testing of the full-scale vehicles and hence result in a lower overall flight test program cost.

Two test programs have been identified: (1) the first is designed to provide data for AMOOS and AMRS design and concurrently check out the concepts and subsystems basic to AMOOS and AMRS, and (2) the second is considered the minimal program to demonstrate the feasibility of the use of aeromaneuvering.

A preliminary design of a test vehicle was performed in order to determine the approximate weight of the model and the subsystems required. The weights of the subsystems reflects IUS technology. The primary structure was designed from the point of view of simplicity of construction, hence a

Table 7

AMOOS MANNED UNIT WEIGHT AND VOLUME BREAKDOWN

	Vol. ft^3	(m^3)	Wt, lb	(kg)
Crew: Two @ 75 ft^3/man	150	(4.25)	748	(339)
Two @ 56 ft^3/man	112	(3.17)		
Food 8 lb/ft^3	6	(0.170)	50	(23)
Furnishings	93	(2.63)	185	(64)
Bunks 3 @ 15 lb				
Seats 4 @ 20 lb				
Misc. 4 @ 15 lb				
Medical 5.5 lb	2	(0.057)	22	(10)
Personal Effects	11	(0.312)	213	(97)
Clothing 4 @ 35 lb				
Hygiene 28 lb				
Personal 10 lb/man				
EVA	25	(0.708)	372	(169)
Suits 2 @ 62 lb				
PLSS 2 @ 62 lb				
Equip 2 @ 62 lb				
Interior Space Suit 4 @31 lb (14)	8	(0.227)	124	(56)
EC/LSS	21	(0.595)	1531	(694)
Cabin Pressurization 55 lb (25)				
O_2/N_2 Leak (5 lb/day + 100%) 300 lb (136)				
O_2 Consumption (2 lb/day + 100%) 120 lb (54)				
Water (6.2 lb/man/day) 152 lb (69) (reclamation)				
Hardware 904 lb (410)				
Electrical Power	4	(0.113)	130	(59)
Communication and Data System	10	(0.283)	327	(148)
Instrumentation	16	(0.453)	188	(85)
Miscellaneous	10	(0.283)	80	(36)
Maintenance Equipment			40	(18)
Flap			225	(102)
Docking Mechanism			120	(54)
Capsule			1225	(556)
TPS			335	(152)
Shell Structure			326	(148)
Contingency 10%	48	(1.36)	624	(283)
Total	516	(14.61)	6820	(3094)

0.1 in. thick load bearing aluminum skin was selected. The TPS weight was estimated from the AMOOS TPS studies for a bondline temperature of 200F (366.3K). The vehicle layout is shown in Fig. 30.

The parameters and subsystems to be tested in this way are the vehicle environment, ablation rates, skin temperatures, and the navigation, guidance and control subsystem. The return from an equatorial geosynchronous mission will be considered baseline. Each of the above will now be discussed individually.

The vehicle environment consists of dynamic pressure, atmospheric density, aerodynamic loads, heating rates and heating loads. The dynamic pressure and atmospheric density may be obtained by flying a nominal trajectory. However, this would mean boosting the vehicle to about 8000 ft/sec (2300 m/sec) above the Shuttle Orbiter velocity and also have active guidance of the vehicle to attain the desired entry conditions. It is considered desirable to fly as simple a system as possible on the first flight. To preserve the simplicity it is suggested that the model be deorbited from the Shuttle orbit. This will also require that a ground recovery trajectory be flown. Both the peak dynamic pressure and the peak heating rate increase with decreasing (larger negative) flight path angle at entry. The lower entry velocity can, therefore, be partially or even totally compensated for by increasing this flight path angle.

As an example of this modeling, consider the modeling of air loads and heating rates in the continuous flow regime. The air loads are proportional to $q = 1/2\ \rho\ V_r^2$ and the heating rates, $\dot{Q}$, to $(\rho/r)^{1/2}\ V_r^{3.15}$ where ρ is the density, r is the body radius and V_r is the relative velocity. Now, along the trajectory, these air loads and heating rates have maximum values. Since V_r is a function of ρ along the trajectory, the maximum values of each may be modeled. However, for the design of the ablative TPS, the heat load, Q, is more important. It may or may not be possible to fly a low energy reentry trajectory that has the same heat load as the skip type maneuver used for rendezvous.

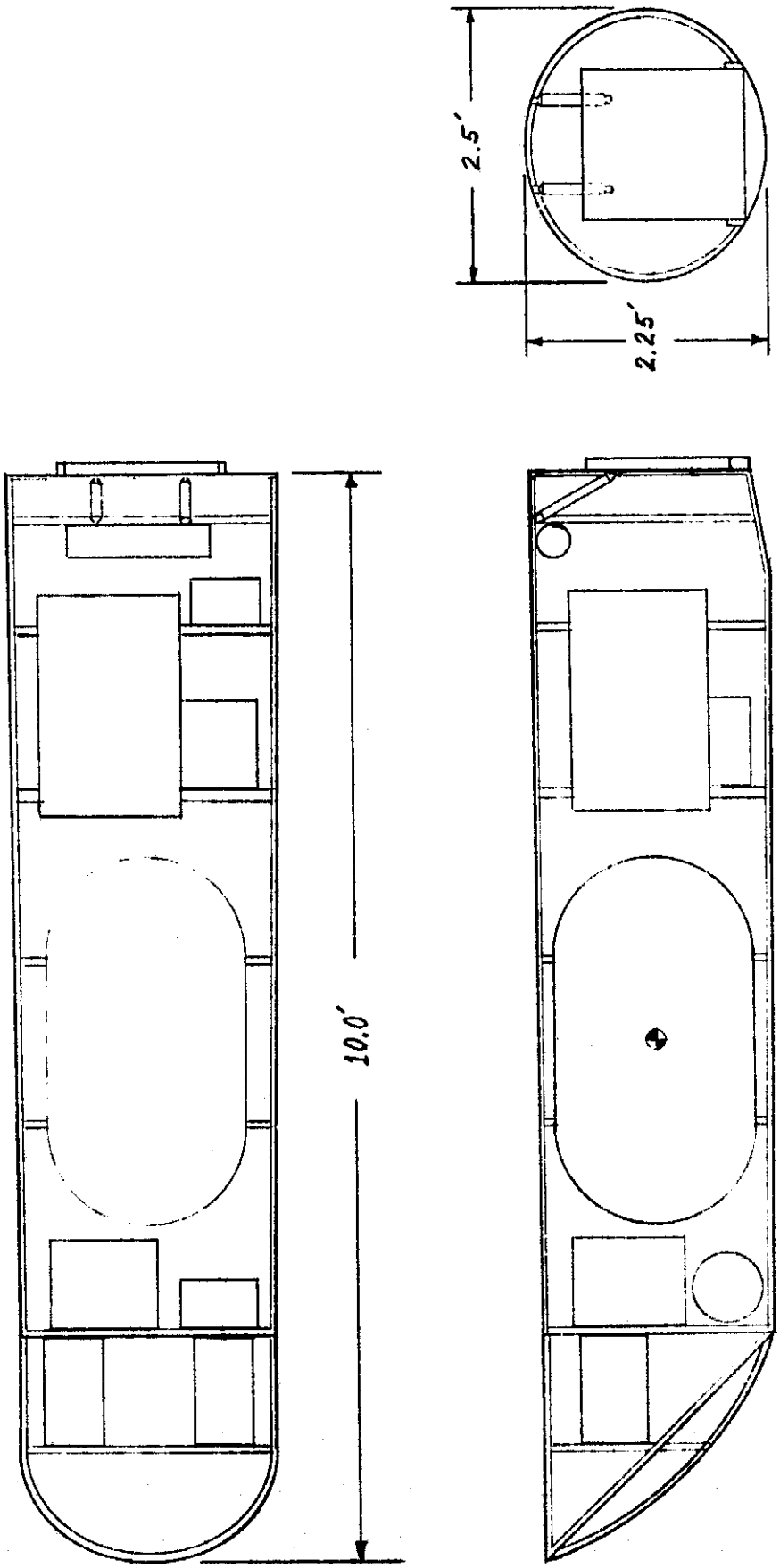

Fig. 30 - Schematic of Flight Test Model

Several computer runs have been made to investigate the extent of modeling heating rate and heat load that can be achieved.

An unguided trajectory, such as envisioned for the first model flight, cannot be used to model air loads and thermal environment accurately. However, if the vehicle is designed conservatively and recovered, then overall effects of the thermal environment may be obtained. Embedding thermocouples in the ablator may also be used to obtain data on conditions within the ablator, or at least until exposed.

The stability of the vehicle is independent of the air loads and thermal environment provided that the ablation does not appreciably change the shape of the vehicle.

Each model flight test program will now be discussed, beginning with the more comprehensive plan. One model can, therefore, be used to perform the initial tests of stability, thermal environment, air loads and a parachute recovery system. This is shown as the first flight of the flight test schedule, Chart 1.

The second test flight would be of heating rate, air load measured as acceleration on the vehicle and vehicle controllability. A high energy orbit would be proposed since the attitude control system would be active. The appropriate entry velocity may be obtained in one of several ways. The minimum Δv method is a two burn method with the first burn at perigee to raise the apogee to the mission altitude to be simulated. A small burn at apogee lowers the vacuum perigee to within the sensible atmosphere. Since the attitude control system is active, programmed bank angle and angle-of-attack time histories may be input. In this way the acceleration and the heating rate may be approximately controlled. The controllability, heating rates and accelerations on the vehicle may be performed in one flight. These tests are recommended for the second test flight in Chart 1.

Number of Shuttle Launches	Target Perigee	Orbit Energy	Test	1980	1981
S*	Low	Low	Vehicle Stability, TPS Ablative Rate and Ground Recovery Test	Δ	
S	Low	High	Vehicle Controllability, Heating Rate, Acceleration Test	Δ	
S	High	High	Vehicle Guidance, Heat Load and Phasing with Space Shuttle Test		Δ
S	Low	High	Simulated Manual Guidance and Backup Systems Test		Δ

*S denotes a shared Space Shuttle flight.

Chart 1 - Flight Test Plan

The next objective of the model flight test program is to check out the guidance of the vehicle. The skip through the atmosphere to a rendezvous with the Shuttle Orbiter is considered the more demanding maneuver for the AMOOS/AMRS guidance. Considerable data are available on reentry to surface recovery guidance from past space flights. More data will become available with the Space Shuttle Orbiter flights. With the vehicle guidance system active, which requires the control system active, a complete check out of the automatic operation of the aeromaneuver may be performed. This is flight 3 of Chart 1.

The prime systems have been checked out in flight 3. There remains then, the requirement to check out the backup systems. The flight will be unmanned so that the actions that a crew may take in guiding and controlling the vehicle will need be simulated. This is flight 4 of Chart 1.

The minimal model flight test program consists of two flight tests designed to demonstrate the feasibility of the AMOOS and AMRS concepts. The first flight is identical to the first flight of the four test series. The second flight is also a low energy flight. It is designed to test the vehicle controllability and guidance. The hardware will include an inertial platform, attitude rate sensors, reaction control system and a guidance computer. The trajectory will be controlled to a nominal as in a high energy pass thus demonstrating the feasibility of the guidance scheme. The minimal model flight test program is given in Chart 2.

Number of Shuttle Launches	Target Perigee	Orbit Energy	Test	1980	1981
S*	Low	Low	Vehicle Stability, TPS Ablative Rate and Ground Recovery Test	Δ	
S	Low	Low	Vehicle Controllability and Guidance Test		Δ

*S denotes shared Space Shuttle flight.

Chart 2 - Minimal Model Flight Test Plan

2.1.4.1 Phased Plan

To accomplish the design and development of a flight test model and the flight test plan a phased development plan will be used. However, prior to this phased plan, it is considered necessary that certain studies be performed to determine: (1) the specific trajectories that should be flown to obtain particular modeling and test parameters; (2) the off-nominal conditions that may be experienced; (3) design parameters for the structure and TPS; and (4) the design parameters for the parachute recovery system.

- Phase A

  Objective: Establish the feasibility of modeling the design parameters of AMOOS and ARMS using models.

  Tasks: Determine parameter values required and scaling factors affecting these parameters. Determine model trajectory as a function of model scale to obtain the desired values. Develop vehicle preliminary designs and perform trades among the alternative configurations. Select best configurations for further studies.

- Phase B

  Objective: Determine full potential of alternative configurations to increase confidence in its design parameters.

  Tasks: Analyze mission spectrum for each test flight. Determine values of parameters to be modeled. Compute the effects of off-nominal conditions. Define flight test data analysis methods. Estimate accuracy of results. Establish vehicle design methods based on these data. Refine design of each configuration. Perform weights estimates. Establish method of operation. Identify launch conditions and recovery areas and methods.

- Phases C-D

  Objective: Develop operational vehicles.

  Tasks: Design, build and test vehicles. Model, build and test vehicles. Model, build and test subsystems. Develop ground check out. Establish data recovery system. Analyze data to show desired values of design parameters. Verify design methods and criteria.

2.2 SIMULATION TECHNIQUES

The linear regulator approach to the guidance task of AMOOS and AMRS is recommended. A set of 65 randomly generated test cases showed the scheme to be accurate and precise. In this application, the scheme is used to control to a nominal trajectory. A combination of systematic errors and randomly generated atmospheres were also used to search for bias in the guidance law. Approximately 200 cases have been run to evaluate this guidance scheme.

The classical linear systems approach was also applied to the AMOOS/AMRS guidance. This method proved less adaptable than the linear regulator. The histogram of the 65 test cases for both techniques is given in Fig. 31. This histogram clearly shows the greater spread of apogee altitude for the classical linear approach as compared with the linear regulator approach.

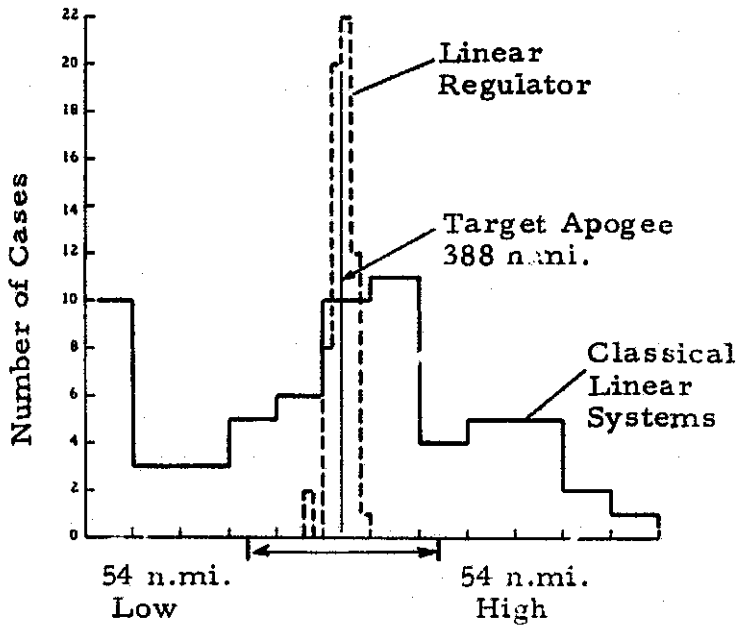

Fig. 31 - Histograms of Apogee Altitude for the Linear Regulator and the Classical Linear Systems Guidance Applied to the AMOOS Type Maneuver

The velocity lost approach of Ref. 4 was also considered. However, this approach does not appear amenable to development without considerable change in the fundamentals of this approach.

The linear regulator approach was also proved adequate for the ground recovery guidance requirement for AMRS. Again, control was to a nominal trajectory. Since the linear regulator had already been selected for the rendezvous type guidance, no other schemes were evaluated for the ground recovery guidance.

2.2.1 AMOOS/AMRS Conceptual Guidance Schemes

The AMOOS/AMRS guidance scheme should be applicable to both the pass through the atmosphere and surface recovery type aeromaneuver. The guidance for the surface recovery maneuver has many similarities with the Space Shuttle Orbiter, Apollo, Gemini and Mercury reentry guidance. The AMRS L/D places it between the Shuttle Orbiter and Apollo for maneuverability. Present and future data will assist significantly in the ground recovery type guidance.

On the other hand, the AMOOS type guidance, in which one pass or more is made through the atmosphere, has several unique features. The requirements of guidance for this type aeromaneuver will now be compared with those of ground recovery and synergetic plane change maneuvers.

AMOOS must be guided through the atmosphere so that it has just sufficient energy to reach a predetermined apogee. This required energy will fluctuate slightly since it is a function of flight path angle at exit, or, equivalently, the hypothetical vacuum perigee of the motion at egress. These fluctuations in vacuum perigees must be small when compared with the radius of the earth because the actual perigee altitude is small when compared with an earth radius and, furthermore, AMOOS has limited maneuverability so that possible fluctuations are considerably less than the 400,000 ft (120 km) depth of the sensible atmosphere. The practical result of this is that it is sufficient for AMOOS to leave the atmosphere with a given velocity. This velocity is

close to low earth orbital velocity. During atmospheric flight it is always greater, of course, than the local in-vacuum orbital velocity. For gaining insight into AMOOS guidance it is convenient to consider that a fixed velocity reduction must be achieved. This reduction is, of course, a function of the entry velocity and desired apogee altitude. On the other hand, ground recovery aeromaneuvers require the relative velocity be reduced to or below terminal, with the use of parachutes or lifting flight if necessary. This condition may readily be achieved so that guidance emphasis is on other parameters such as air loads, thermal environment and recovery point. The guidance and design of such recoverable vehicles reflects the use of these parameters, e.g., heating rate limitations on the trajectory. The differences in time at which the recovery point is reached is of little importance. AMOOS, on the other hand, has just the opposite conditions and requirements, in particular, velocity loss and time of arrival are important to ensure proper phasing with the Shuttle Orbiter requirements. The air loads and thermal environment entailed must be accepted. This does not mean that a technique minimizing them may not be chosen but that during an actual flight these variables are essentially uncontrolled or only indirectly controlled, e.g., by limiting velocity excursions from nominal. However, maintaining vehicle integrity is of prime importance so that air loads and thermal environment become non-violable boundaries. However, they are chosen and the vehicle designed so that achieving these boundaries does, in fact, signify a failure or condition far from nominal, e.g., the design dynamic pressure is 100 lb/ft^2 (5000 N/m^2),* the ultimate without safety factor, is 150 lb/ft^2 (7500 N/m^2) and the nominal maximum is 75 lb/ft^2 (3600 N/m^2). The standard deviation, σ_q, is 2 lb/ft^2 (90 N/m^2) so that the safety margin extends some $12\sigma_q$ or more above the nominal. The likelihood of violating this boundary is therefore very small, usually a 3σ margin is considered sufficient.

Synergetic maneuvering guidance minimizes the velocity to be added while achieving an accurate value of some other parameter which, in all applications to date, is plane change with or without a change in mission altitude. As a comparison, the AMOOS desired energy loss is a large fraction of the total energy and when off-nominal conditions are met, the guidance law would minimize energy deviations about this large desired loss. In the case of

*These conversions are rounded to yield convenient numbers.

synergetic plane change the desired energy loss is zero but the best that can be achieved is the loss of a large fraction of the total energy. Off-nominal conditions will, in general, cause a further loss of energy since such conditions are deviations from the optimum. As in the case of surface recovery guidance, air loads and thermal environment represent barriers that must be flown closely for efficiency and may be somewhat arbitrarily chosen.

Another significant difference is that AMOOS is at all times during atmospheric flight above the local circular orbital velocity. This is not so for synergetic plane change where the velocity is sub-orbital. The tasks are therefore reversed in that AMOOS must be retained within the atmosphere for a sufficient period of time to make the necessary energy adjustment whereas for the synergetic plane change the vehicle must be held out of the more dense atmosphere to limit air loads and thermal environment. Furthermore, the investigations of synergetic plane change are more of the nature of targeting in which an optimum nominal trajectory is determined. In the synergetic maneuvering studies to date, off-nominal conditions are not considered. On the other hand, the AMOOS guidance includes the compensation of both off-nominal entry conditions and unpredictable atmospheric density variations.

In the AMOOS guidance, lift is used for trajectory control. Two basically different ways of lift vector modulation were studied to evaluate the guidance schemes. The selected way was to modulate bank angle about 90 deg in order to produce a vertical component of lift. Using a nominal bank angle of 90 deg with an angle of attack of about 35 deg gives AMOOS a small plane change capability which is decreased by the use of lift for trajectory control. Fortunately, the changes in plane change capability proved very small, thus allowing bank angle modulation to be used. The other method considered was to modulate lift using angle of attack. The vehicle would be flown at a bank angle of 180 deg, i.e., upside down. This method has the advantage that drag increases with increasing angle of attack and so has an additive effect on control effectiveness. Unfortunately, the propulsion module alone had insufficient variation of lift coefficient with angle of attack to make this method usable. It was, therefore, dropped, since the bank angle modulation technique worked so well.

The objective of the AMOOS type guidance is to achieve an acceptable phasing orbit. The nominal phasing orbit has a 10 min period difference from the Shuttle Orbiter. It was considered that 8 to 12 min period difference was acceptable. These times were then translated into apogee altitudes to yield variations of ±54 n.mi. (±100 km) about the nominal of 388 n.mi. (720 km). This reduction of the guidance objective to an allowable variation in target apogee is shown in Fig. 32.

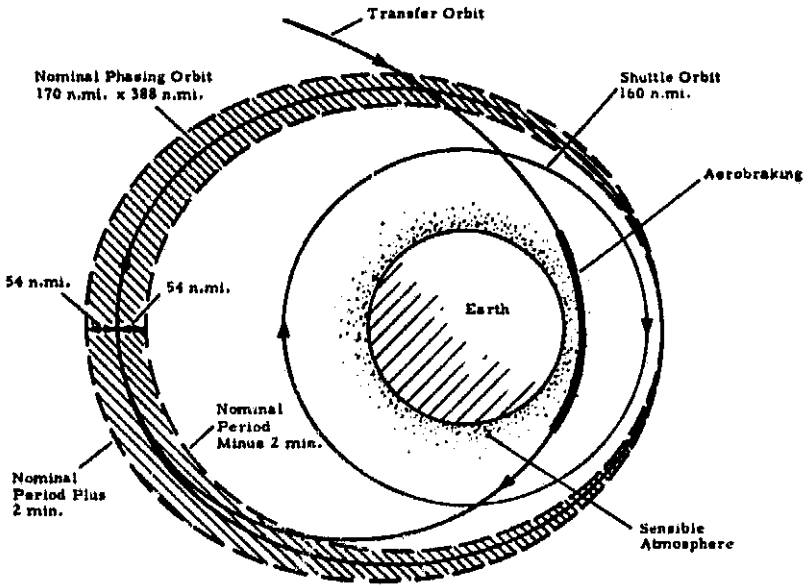

Fig. 32 - Diagramatic Representation of the Guidance Objective for the AMOOS Type Aeromaneuver

The AMRS surface recovery guidance requirements are comparable to Apollo and Space Shuttle Orbiter requirements. Guidance techniques based on existing schemes could be developed. However, AMRS may be used in either mode, namely surface recovery or Orbiter rendezvous, therefore, the AMOOS type guidance, i.e., linear regulator is desirable for surface recovery since it will minimize the onboard changes to the guidance scheme. The main objective of the AMRS guidance is to ensure the integrity of the vehicle during atmospheric flight without incurring excessive landing position errors.

2.2.1.1 Linear Regulator Approach

In the linear regulator approach a trajectory control and an index of performance must be chosen. Optimum control techniques are then employed to obtain the control function which minimizes the index of performance. Both angle of attack, α, and bank angle, β, were considered as the trajectory control parameters. The angle of attack method resulted in insufficient vehicle controllability and was therefore not further pursued. The bank angle method employs variations of β from its nominal 90 deg position to produce a positive or negative lift component. This method was used with this guidance approach. The index of performance was chosen to minimize the error in phasing orbit apogee. Specifically, it consists of the square of the apogee error plus the integral of the square of the control variable over the flight time. The integral portion of the index of performance is considered a measure of the consumables used in controlling the trajectory. The minimization of the index of performance based on the linearized equations of motion along a nominal trajectory results in a linear time-varying guidance law. The guidance law is expressed in terms of the deviations of the parameters velocity, flight path angle and density altitude from their nominal trajectory values. Implementation of the guidance law therefore requires a set of time-varying gain factors and a nominal trajectory.

The details of the formulation are given in Appendix D and the results are given in Section 2.2.2.1.

2.2.1.2 Classical Linear Systems Approach

In this method, the trajectory control parameter is written as a linear function of the deviations of selected trajectory parameters from nominal. Only bank angle was used as a trajectory control parameter since angle of attack had failed to yield sufficient lift modulation for the linear regulator approach applied to the propulsion unit alone case. In this classical linear systems approach, the trajectory control parameter, namely the bank angle, was chosen to be a function of the error in velocity and acceleration. Later the time differential of acceleration, jerk, had to be included to improve the scheme. The gains were obtained by trial and error using a small number of randomly generated entry conditions and atmospheric densities.

2.2.1.3 Test Cases

In order to evaluate the schemes, 65 test cases were generated. Each case was commenced at geosynchronous altitude with a randomly generated velocity designed to yield a $\pm 3\sigma$ entry corridor of 3.89 n.mi. (7.2 km). The atmospheric density was varied in a random manner about the 1962 U.S. Standard Atmosphere as mean. The correlation in time and space was also incorporated. The randomness and correlation were obtained from Ref. 5. The reasoning behind this choice is as follows. Provided the atmospheric density is predictable as a function of altitude, then a nominal trajectory can be computed. This predictable density along the trajectory has negligible effect upon the guidance because it is predictable and can, therefore, be negated by targeting. Any nominal atmosphere that yields a reasonable solution to the targeting can be used as a base for evaluating a guidance scheme. The guidance scheme is to correct the effects of unpredictable variations. Therefore, the best estimate of possible conditions must be made and for this reason the 4D world atmosphere (Ref. 5) is used. The 1962 U.S. Standard Atmosphere is used for the nominal since it is both realistic and readily available as a subroutine in a manner suited for use in trajectory programs.

Also incorporated in the test cases is the effect that navigation and targeting errors have on the trajectory. These errors manifest themselves as position in an entry corridor. To simulate these errors, the velocity at geosynchronous altitude was varied randomly.

Tests of the variables generated randomly showed that the error of the mean and standard deviation were small for the sample used.

As an evaluation criterion, the precision with which the guidance schemes achieve target apogee was used. The nominal phasing orbit has a period of approximately 10 min longer than that of the Shuttle Orbiter. Based on this, a phasing orbit with a period difference of from 8 to 12 min would be adequate. This in turn gave an apogee variation of ± 54 n.mi. (± 100 km) as being acceptable. This guidance objective is diagrammed in Fig. 32, page 63.

2.2.2 Computer Coding, Checkout and Demonstration

The guidance techniques were coded and incorporated in a three-dimensional point mass computer program. This modified program was then used to evaluate the guidance schemes. The modified computer program is described in Ref. 11.

2.2.2.1 Results of Test Cases

The linear regulator guidance was more precise than the classical linear approach. Although the latter system always achieved an apogee above the sensible atmosphere, the achieved apogees were occasionally too low or too high. An apogee was considered not acceptable if below 170 n.mi. (315 km) since more than one burn was required to achieve a 170 x 388 n.mi. (315 x 720 km) phasing orbit. Also some apogee altitudes for the classical linear systems were above 442 n.mi. (820 km) again requiring two burns to achieve acceptable phasing, and so were considered unacceptable.

The linear regulator guidance scheme was first inspected for bias and range of application. This was achieved by systematically changing parameters instead of random variation. Both target vacuum perigee and atmospheric density were changed systematically. The effects on apogee altitude and on maximum dynamic pressure were inspected for bias and to determine range of applicability. The effects of the maximum permissible change in bank angle, $\Delta\beta_{max}$, and the absolute value of angular acceleration of the bank angle, $\ddot{\beta}$, were also investigated.

The effect of target perigee on apogee altitude is given in Fig. 33. The guidance scheme appears to be able to compensate with negligible error for target perigees from approximately 2 n.mi. (4 km) below nominal to 1.5 n.mi. (3 km) above nominal. From these points the apogee altitude deviates noticeably from the nominal with a definite bias toward the low side. Only the 3 n.mi. (6 km) high target perigee gives a definitely unacceptable apogee altitude. At the 2.5 n.mi (5 km) high target perigee, an unexpected value of apogee altitude is obtained if the smooth curve through the remaining points is constructed. This phenomenon appears to be associated with a combination of guidance cycle time

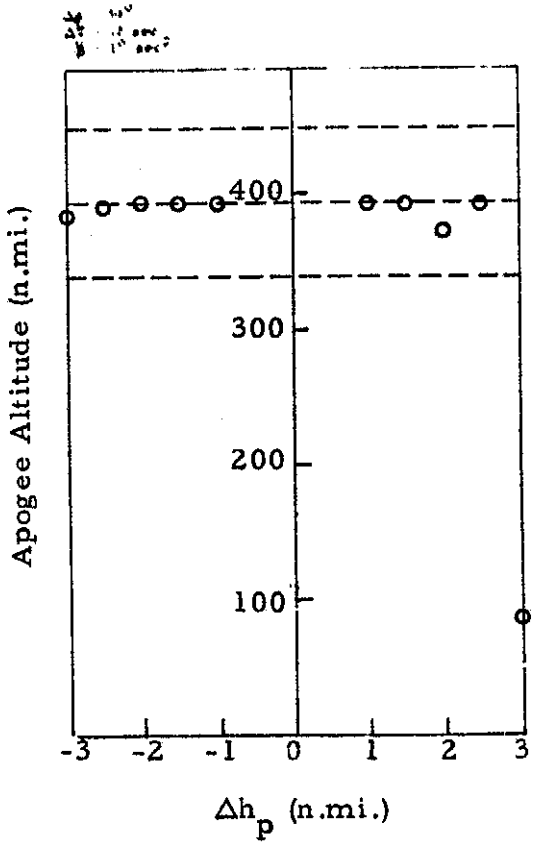

Fig. 33 - Effects of Systematic Errors in Target Perigee on Apogee

and the fact that the maximum value of the control variable, $\Delta\beta_{max}$, is achieved during a considerable length of time due to the large errors in perigee. This, in turn, introduces a nonlinearity not accounted for in the derivation of the linear guidance law. The region of applicability of the guidance scheme appears to be from 2.5 n.mi. (5 km) high to at least 3 n.mi. (6 km) low which includes the design range of $\pm$1.8 n.mi. ($\pm$3.5 km) about the target perigee. Changes in the gains of the guidance law could be used to extend the range of applicability.

The maximum dynamic pressure, q_{max} encountered has a marked bias, Fig. 34, with low perigees giving in general low q_{max} and high perigees giving

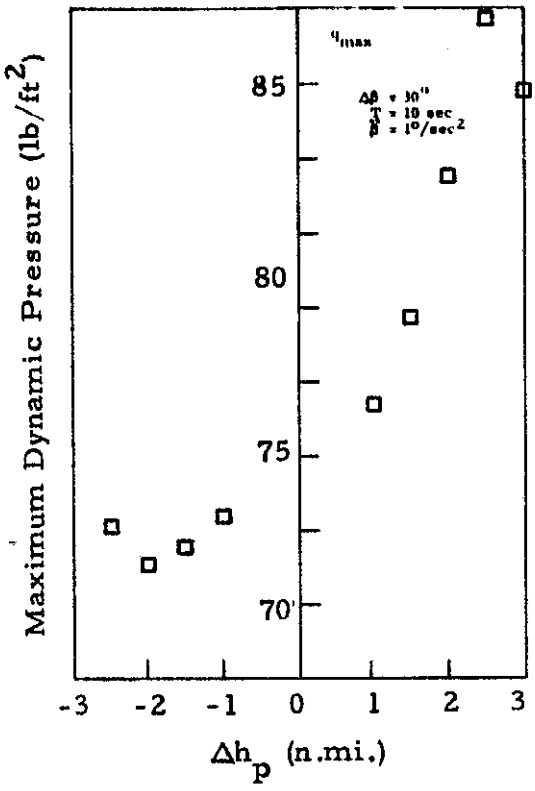

Fig. 34 - Effects of Systematic Errors in Target Perigee on Maximum Dynamic Pressure

high q_{max}. This is opposite to the unguided ballistic flight and so may be attributed to the guidance scheme. All values of q_{max} obtained are well below the design value of 100 lb/ft^2 (5000 N/m^2).

The effects of $\Delta\beta_{max}$, $\ddot{\beta}$ and guidance cycle time, ΔT, are now considered. The range of $\Delta\beta_{max}$ is from 15 deg to 60 deg and $\ddot{\beta}$ is from 0.5 deg/sec^2 to 2 deg/sec^2. Each value of $\ddot{\beta}$ is plotted separately. Figure 35 shows that for non-zero values of ΔT, the apogee is biased toward the high side. There is no obvious bias or trend with $\Delta\beta_{max}$ over the range investigated. Increasing $\ddot{\beta}$ to 1°/sec^2, Fig. 36, changes the scatter but produces no

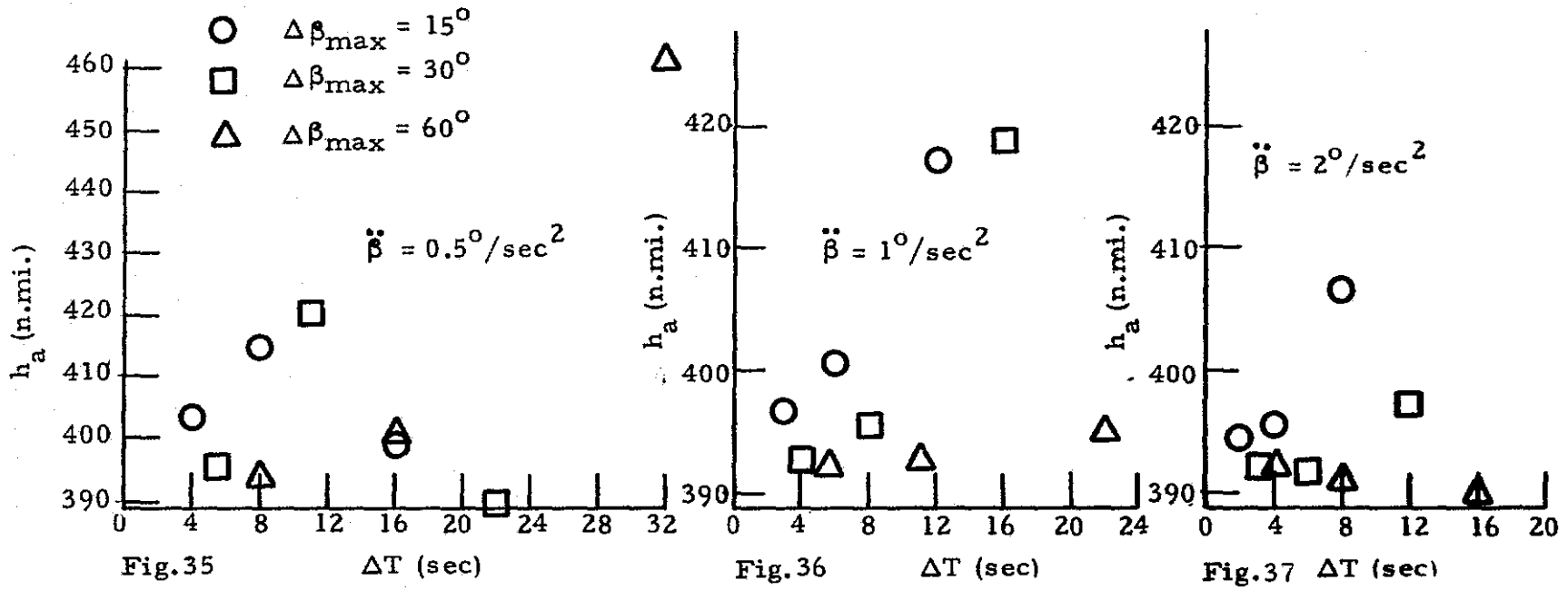

Fig.35 Fig.36 Fig.37

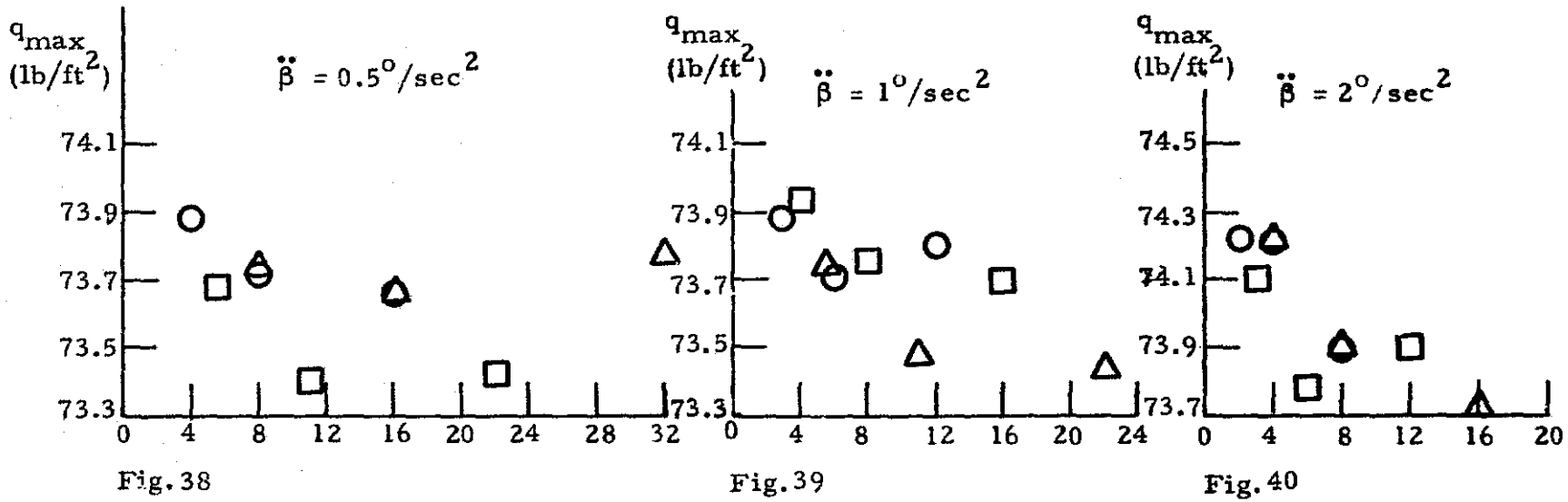

Fig.38 Fig.39 Fig.40

Figs.35,36,37 - Effects of Guidance Parameters on Apogee

Figs.38,39,40 - Effects of Guidance Parameters on Maximum Dynamic Pressure

pattern. Similarly, increasing $\ddot{\beta}$ to 2 deg/sec^2 (Fig. 37) again changes the scatter without producing a well defined pattern. From Figs. 35 through 37 a reasonable control appears to be $\ddot{\beta}$ = 1 deg/sec, $\Delta\beta_{max}$ = 30 deg with $4 < \Delta T < 10$ sec. Quite arbitrarily, ΔT = 10 sec was chosen as the guidance cycle time from this range. However, a 4 sec cycle time would be expected to improve the guidance accuracy and precision as compared to 10 sec.

The maximum dynamic pressure is biased below the nominal of 75 lb/ft^2 (3600 N/m^2), approximately, for all $\Delta\beta_{max}$, $\ddot{\beta}$ and ΔT in the ranges previously defined. The values of q_{max} for $\ddot{\beta}$ = 0.5 deg/sec^2 are given in Fig. 38. The scatter in q_{max} is about 1 lb/ft^2 (50 N/m^2). A possible trend in the data can be seen with the minimum values of q_{max} occurring in the region of $12 \leq \Delta T \leq 16$ sec, approximately. Also $\Delta\beta_{max}$ = 30 deg yields slightly lower q_{max} than $\Delta\beta_{max}$ = 15 deg or $\Delta\beta_{max}$ = 60 deg. The reasons for this latter variation have not been investigated. When $\ddot{\beta}$ is increased to 1 deg/sec^2 (Fig. 39) trends are not so apparent and if there, are altered. In this case, $\Delta\beta_{max}$ = 60 deg gives the lowest values of q_{max}. This is interesting since this value of $\Delta\beta_{max}$ gives the same ratio of $\Delta\beta_{max}/\ddot{\beta}$ as $\ddot{\beta}$ = 0.5 deg/sec case and $\Delta\beta_{max}$ = 30 deg. When $\ddot{\beta}$ is increased to 2 deg/sec^2, Fig. 40, the results yield an increased appearance of scatter about a decreasing mean as ΔT increases. However, no results were obtained for ΔT greater then 16 sec. In all cases the values of ΔT are chosen on consideration of the time taken to change β by $\Delta\beta_{max}$, from rest to rest.

Similar tests for the classical linear systems approach were not run because the results obtained for the 65 random test cases showed the linear regulator approach to be the only acceptable.

The histograms of the 65 random cases have already been displayed in Fig. 31. Visually, the superior precision of the linear regulator guidance over the classical linear approach is obvious. This precision is also presented in Table 8. The important parameters for the evaluation of the guidance schemes are shown in Table 8. Also included are the statistics of the

Table 8

STATISTICS OF LINEAR REGULATOR AND CLASSICAL LINEAR APPROACH
(Sample Size = 65; AMOOS Type Maneuver)

Variable	Linear Regulator		Classical Linear Systems	
	$\bar{x}$	S	$\bar{x}$	S
Apogee Alt., n.mi. (km)	399.9 (720.3)	6.05 (11.2)	359.7 (666.2)	22.4 (226.7)
Inclination, deg	28.62	0.06	28.61	0.19
Longitude, deg	240.40	1.41	239.67	2.90
Time of Exit, sec	19186.55	11.12	19199.68	49.58
q, lb/ft^2 (N/m^2)	75.45 (3612.6)	1.87 (89.55)	76.73 (3663.62)	7.40 (354.49)
Q, Btu/ft^2 (J/cm^2)	17100 (19,400)	115 (130)	17270 (19,600)	969 (1100)
VI, ft/sec (m/sec)	5190.45 (1582.05)	0.46 (0.14)	5190.45 (1582.05)	0.46 (0.14)
Target Perigee, n.mi. (km)	38.16 (70.67)	0.68 (1.26)	38.16 (70.67)	0.68 (1.26)

Table 9

STATISTICS OF LINEAR REGULATOR APPROACH
(Sample Size = 59; AMRS Type Maneuver (Ground Recovery))

Variable	Linear Regulator	
	$\bar{x}$	S
q_{max}, lb/ft^2 (N/m^2)	103.37	3.25
Longitude, deg	-245.81	0.12
Latitude, deg	13.23	1.56
Perigee Altitude, n.mi (km)	36.88 (68.3)	0.686 (1.27)
VI, ft/sec (m/sec)	5189.67	0.459 (0.14)

input variables. These show that the standard deviations of the sample were slightly larger than those of the desired total population. The statistics of the atmosphere were not checked.

The main parameter for evaluation is the apogee altitude and, in particular, its standard deviation. In this, the linear regulator is far superior to the classical linear. With a standard deviation of 6.05 n.mi. (11.2 km), the allowable variation of 54 n.mi (100 km) represents almost $\pm 9\sigma$ limits. Usually $\pm 3\sigma$ is considered sufficient. For phasing with the Shuttle Orbiter the longitude and inclination are important. In the case of both guidance schemes, the 1σ accuracies for the 170 n.mi. x 388 n.mi. (315 km x 720 km) phasing orbit are of the same order as the accuracies required for the 170 n.mi. (315 km) circular rendezvous orbit given in Ref. 8. This means that AMOOS requires less than one revolution in phasing orbit to rendezvous with the Space Shuttle Orbiter. The heat load and dynamic pressure are important in vehicle design. Again the linear regulator gave less scatter than the classical linear systems approach. The 1σ value of less than 1% represents a 3σ variation well within the accuracy of current prediction and design methods.

The linear regulator approach was also applied to the AMRS surface recovery guidance. In this case, 59 test cases were run. The results are given in Table 9.

2.2.2.2 Recommendations and Discussion

The linear regulator approach is recommended for the AMOOS and AMRS guidance. The implementation does not tax current onboard computers since, based on the Univac 1108 simulation, approximately 2000 words of storage are required for both the code, the nominal trajectory and the gains. Furthermore a guidance cycle time as long as 10 sec can be used, which would require a computer cycle time well within current capabilities. Approximately 600 instructions must be executed per guidance cycle which, with Shuttle technology computers, would allow guidance cycle times of much less than one second. At this time no recommendation is made as to guidance cycle time nor the number of points required for the nominal trajectory.

The evaluation of the guidance schemes was based on the schemes being able to correct for navigation errors generated prior to atmospheric entry and unpredictable atmospheric density variations. The navigation errors were assumed unknown but distributed with a standard deviation of approximately 0.65 n.mi. (1.2 km). Choosing this standard deviation effectively simulates the desired entry corridor of $\pm$1.89 n. mi. ($\pm$3.5 km). However, the "real world" situation is less exacting since, at atmospheric entry, the navigation system will give the position within the corridor to the accuracy of the navigation system, which is considerably less than the corridor width. In practice, this knowledge would be used to orient the vehicle immediately prior to entry and so reduce the stress on the guidance. On the other hand, the navigation errors generated and accumulated during the atmospheric flight were not to be included in the simulation. As discussed earlier in Section 2.2, speed at atmospheric exit is most important in determining apogee altitude. However, the error in this parameter is expected to be small since the accelerometers are very accurate and precise instruments for the low-g loads experienced. A realistic estimate of the hardware induced velocity error is 6.6 ft/sec (2 m/sec) which, in turn, generates an error of approximately 3.5 n.mi. (6.6 km) in apogee altitude. On combining this error with the scatter due to the guidance scheme, a standard deviation of approximately 7 n.mi. (13 km) is obtained for the variation in apogee altitude. It should be noted that a 16.5 ft/sec (5 m/sec) hardware induced error in velocity will raise the standard deviation of apogee altitude 11 n.mi. (20 km). These values are well below the allowable variations of $\pm$54 n.mi. ($\pm$100 km). In conclusion, the linear regulator appears well able to guide the vehicles in the Shuttle Orbiter rendezvous (i.e., AMOOS) mode to the required precision.

The surface recovery guidance mode is expected to be less sensitive to such small errors in velocity induced by the navigation hardware during atmospheric flight since the vehicle approaches terminal velocity just prior to parachute deployment. Again, the linear regulator approach limits the variation in flight parameters to acceptable levels (Table 9, page 71).

The velocity lost approach proved intractable to further development. Two areas of extension were considered. The first method was to recycle

the guidance periodically. This proved impractical because of the basic concept of this guidance which restricts it to a single cycle unless considerable modification is allowed. The basic idea behind the velocity lost guidance is as follows. At some time, T_1, after atmospheric entry, the velocity has decreased by Δv_T and the flight path angle, γ, is equatl to $-\gamma_T$. Now, it is supposed that the flight from time T_1, say, when $\gamma = +\gamma_T$ to atmospheric exit produces a velocity change $k_v \Delta v_T$. The next step is to make approximations about the flight from T to T_1, where, as yet, T_1 is undetermined. Between times t = T and t = T_1 the vehicle is banked from β = 90 deg to β = 60 deg and back to 90 deg to yield an upward component of lift sufficient to turn γ through an angle $2\gamma_T$. The time of the maneuver is computed assuming a constant angular acceleration $\ddot{\beta}$. The velocity lost during the maneuver, Δv_M, is computed assuming a constant value for $\dot{V}$. The total velocity lost, if the maneuver were initialized at time T, is therefore

$$\Delta v = (1 + k_v)\, \Delta v_T + \Delta v_M .$$

When Δv is equal to the required velocity loss, the maneuver is initialized. The constant k_v is obtained empirically either from trajectory analysis or by trial and error until acceptable results are obtained. Basic to the technique, therefore, is the maneuver to change the flight path angle from $-\gamma_T$ to $+\gamma_T$ starting at some time T. Obviously, this maneuver can only be performed once in a flight. This causes the inherent intractability of the method to further development.

The second approach was to develop a better analytical prediction of the expected velocity loss for the remainder of the flight. The general intractability of the flight to analytical solution prevented a sufficiently accurate solution being obtained. Even if such a solution can be obtained then it is doubtful that the velocity lost type guidance will be able to compensate for random atmospheric density variations with sufficient accuracy for use as the primary system.

Section 3
CONCLUSIONS

The more detailed analyses of AMOOS and of AMRS have further established the feasibility of the one-pass, ablative TPS AMOOS concept, and, concurrently, established the feasibility of the comparable AMRS concept.

Specific conclusions from the multi-disciplined study of the AMOOS and AMRS configurations are:

- The modular AMOOS vehicle is practical and is within the state-of-the art technology using magnesium (HM 21A-T8) or beryllium-aluminum (Be-38 Aℓ) material for the primary shell structure.
- Performance analysis has shown that AMOOS has payload capabilities to high energy orbits well in excess of the Baseline Space Tug.
- Weights analysis and a design study of the manned module shows that AMOOS can carry a four-man, 30-day module to geosynchronous orbit and return.
- The aerobraking concept is feasible for both AMRS and the modular AMOOS over a wide range of mission altitudes. These missions include lunar orbit as well as earth orbit up to geosynchronous.
- The Martin Marietta SLA 561 ablative material yielded a more practical TPS than other ablative, reradiative or insulative materials.
- The model flight test studies show that unmanned check out could be performed using four flights over approximately a two year period. These tests would be expected to eliminate four full scale flight tests. Each flight would share a Shuttle launch. Useful data could be obtained from a two-flight test.
- The linear regulator approach to atmospheric guidance proved superior to the classical linear systems approach. The velocity lost approach proved intractable to further development.

- Bank angle modulation proved to be an adequate means of lift vector modulation for trajectory control. Angle-of-attack modulation proved inadequate due to the low value of the lift curve slope in the desired angle-of-attack range.
- AMRS on-station weight is moderately sensitive to I_{sp} in the 260 to 350 sec range. Increasing the I_{sp} of space storable propellants to the 350 sec level or above will yield significant weight savings over the currently available 260 to 290 sec propellants.
- The aeromaneuvering plane change capability of the AMOOS configuration is little changed by the concurrent use of lift for trajectory control. For the AMRS-type aeromaneuver, the recovery point is little changed by the dual use of lift.
- The aeromaneuver appears to create no phasing problem with the Shuttle Orbiter with either the linear regulator or the classical linear systems.
- The linear regulator guidance reduces excursions of the dynamic pressure and heat loads to negligible amounts from the means.

Section 4
RECOMMENDATIONS

The results of this study have shown that the current configuration can be expected to yield practical AMOOS and AMRS vehicles. There is no doubt that AMOOS and AMRS vehicles as studied herein could be developed into operational vehicles. However, these studies have identified further areas which require additional investigation to continue the advancement of AMOOS and AMRS as parts of a future orbital transport system.

All of the current technology studies with an application to the Baseline Space Tug have a corresponding application to AMOOS and possibly to AMRS. The recommendations herein are for studies applicable to a wide band of orbit to orbit vehicles, including AMOOS and AMRS.

- Navigational Accuracy Studies

The objectives of this task are:

a. Determine the effects of navigational accuracy on AMOOS/AMRS targeting and guidance. Both atmospheric and exoatmospheric navigation should be considered.

b. Determine the navigational accuracy required for AMOOS/AMRS to perform the atmospheric flight.

c. Determine the extent to which on-going SR&T studies for the Baseline Space Tug are applicable and define hardware development requirements for AMOOS/AMRS.

d. Determine the navigation accuracy required for AMOOS and AMRS as a function of entry corridor depth.

e. Evaluate existing hardware against requirements for various levels of autonomy.

f. Define required or desirable technology and compare to that required for the Baseline Space Tug.

g. Establish a practical set of navigational accuracies, entry corridor widths, navigation hardware and required or desirable technology.

The AMOOS/AMRS guidance computer program will be used to evaluate the effects of guidance errors. Guidance errors of arbitrary magnitude will be introduced systematically throughout the flight. The effect of these errors on phasing with the Shuttle Orbiter will be determined and evaluated against acceptable phasing orbit variations to yield acceptable navigational errors. These errors will then be compared to the accuracy and precision of baseline Space Tug and existing navigation equipment (including the effects of multiple measurements and filtering) to determine navigational hardware technology requirements.

The accuracy with which position and velocity must be known as a function of position on the return transfer trajectory in order to hit an entry corridor width will be determined. The accuracy of current hardware and hardware under development will be established as functions of quantity of data available and data filtering technique. The accuracy of the required mid-course correction will be incorporated into the navigational accuracy estimate. The required accuracy will be compared with the attainable accuracy and a baseline navigational system selected for each level of autonomy under consideration. These baseline navigational systems will then be compared with the Baseline Space Tug. On-going SR&T directed toward the Baseline Space Tug will be identified. Other desirable or required technology will also be identified.

The output of this study will be a baseline guidance system for each level of autonomy. The desired or required technology will be given for each level and evaluated against existing technology and that under development.

- Guidance Development

  The objectives of this task are:

  a. Incorporate navigational knowledge at atmospheric entry into the guidance scheme.

b. Modify the state model to incorporate variables resulting in the minimization of propellant and control usage.

c. Incorporate the position and velocity at atmospheric exit in the performance index so that phase errors with the Space Shuttle orbiter are minimized.

Navigational measurements made between the mid-course correction and atmospheric entry may be used to determine the position within the corridor depth. This information may be used to give initial values of vehicle attitude and hence a new nominal trajectory closer to the actual than the center of the entry corridor nominal trajectory. In this way the demands of the guidance system on the control subsystem may be reduced.

Currently, the performance index uses, with the final state, the trajectory control variable. This latter is a measure of the control actuator and RCS usage and so tends to reduce propellant usage. The index may be improved upon by incorporating the control variable rate and acceleration. Incorporating these terms in the performance index will yield a better estimate of the RCS propellant and aerodynamic control usage.

One important variable that may be changed by the unpredictable variations in the atmospheric flight is the relative state between the AMOOS or AMRS and the Space Shuttle orbiter. Variations in this relative state will affect the phasing prior to rendezvous. Incorporating the appropriate expression in the performance index will minimize the variations in phasing time and concurrently give appropriate weight to other performance index parameters.

- Manual Guidance Technique

The objective of this task is:

Provide a fail-safe mode for AMOOS and AMRS in case of a massive failure of guidance system hardware.

The velocity lost approach to the guidance offers the opportunity to develop a manual backup guidance with minimal hardware. Since the times involved with the velocity lost approach are several seconds to approximately thirty seconds, manual guidance is feasible provided speed and flight path angle are available. The studies would develop a manual guidance technique based on these parameters and search for techniques requiring even fewer state variables.

- Hybrid Engine Vehicle

  Objectives:

  a. Determine the performance characteristics of a hybrid engine vehicle for it to be competitive with the cryogenic vehicle on a manned geosynchronous mission.
  b. Determine the performance of specific, possible hybrid engine vehicle and staged vehicles and hence evaluate the capability of each to perform a manned geosynchronous mission.

Cryogenics may be stored in space provided sufficient insulation and shielding from solar radiation is used. The storability of cryogenics has been established quantitatively under Contract NAS8-29677. The advantages and penalties of using a non-cryogenic fuel with the hybrid engine will be established so that the trades between the two methods may be made.

- Load Bearing Tanks

  Objectives:

  a. Reduce or eliminate the primary structure.
  b. Determine the TPS required for such tanks.
  c. Establish weights trade between load and non-load bearing tanks.

The possibility of bonding insulation and TPS directly to the propellant tanks will be investigated. Both cryogenic and high density propellants will be considered. The latter is expected to give a relatively short vehicle, thus allowing long payloads.

Several tank materials will be considered together with appropriate propellants, insulation and TPS. The design tasks will include a stress analysis of the tanks including the effects of very cold propellants, analysis of TPS and insulation requirements, analysis of heat soak over relatively long times and propellant boil-off.

- Increased Depth of Design Work of AMOOS and AMRS

The objectives of this task are:

a. Reduce structural weight by optimizing structure.
b. Establish trades among candidate structures.
c. Consider alternate vehicle geometry and perform the preliminary design and weights calculation for each alternate considered.
d. Perform preliminary design of the hybrid engine vehicle.
e. Determine the weight reduction for AMOOS used as purely propulsive or expendable vehicle (kit concept).

Under this task the structural design of candidate AMOOS and AMRS vehicles will be continued.

- Abort Analysis

The objectives of this task are:

a. Develop basic operations and performance requirements following a failure in AMOOS or AMRS after separating from the Space Shuttle.
b. Demonstrate the basic advantages of an aeromaneuvering manned vehicle over a purely propulsive vehicle.

This study consists of listing potential failure modes, analyzing these modes to determine should the mission be aborted and establishing the performance requirements for a safe recovery. The aeromaneuvering concept is expected to show considerable advantages in safety over the Baseline Space Tug (manned application) because it can tolerate a main engine failure

during certain parts of the mission, e.g., during burn to transfer orbit. The APS or RCS may be used at apogee to target to atmospheric entry and hence a safe recovery of the crew.

- Multiple Staged Vehicle Operation

  Objectives:

  a. Determine optimum stage configuration for particular missions.
  b. Establish mission events and timeline for multiple staged vehicles.

Multiple staged vehicles will, in general, require multiple Shuttle launches for delivery to low earth orbit. The potential breadth of the multi-staged aeromaneuvering tug's spectrum results in many possible combinations of Space Shuttle payloads to place it in low orbit. These payload possibilities and the resulting events and timelines will yield an optimum configuration for each AMOOS stage.

- Flight Test Plan

  Objectives:

  a. Preliminary design of flight test model.
  b. Determination of trajectories to simulate the full scale vehicle parameters during atmospheric flight.
  c. Determine method of stowing in Space Shuttle orbiter cargo bay and method of deployment.

In general, the basic AMOOS and AMRS design may be proved using models rather than full-scale vehicles. This model testing would greatly reduce the number of full-scale vehicle tests required. The pertinent parameters, such as heating rate, heat load response to controls, etc., may be modeled provided the appropriate trajectory is flown. This trajectory will not, in general, be an actual mission trajectory; a lower energy trajectory

may be frequently flown but the parameters modeled correctly by deeper or shallower penetration of the atmosphere than for the full-scale vehicle. The values of the parameters to be modeled will be obtained from the results of on-going tasks. Trajectories will then be generated to simulate the conditions described by these parameters. Alternate methods of inserting the test vehicles into these trajectories will be considered. These methods will range from minimum Δv to minimum time. The modeling studies will also consider optimum model size compatible with the parameter modeling and stowage in the cargo bay as well as the equipment to be carried on board. Preliminary design of the vehicle will be performed which will include basic structure, TPS, RCS, navigation, guidance and control hardware and software requirements, etc.

- Alternate Configuration Performance

  Objectives:

  a. Determine the performance of high lift/drag ratio vehicles.
  b. Determine cross-range capability.
  c. Determine the increased performance of the uncoupled recovery system over the horizontal landing system.

Vehicles dedicated to manned flight may be designed to allow sufficient aerodynamic shaping to yield L/D's of about 2 in the hypersonic range. With such a high L/D, considerable crossrange and plane change may be obtained. Such vehicles may be ground recovered as an alternative to Space Shuttle orbiter recovery. Previous studies have shown that uncoupled recovery yields a lighter weight vehicle. The increase in cross-range capability of such an AMRS vehicle will be determined so that it may be evaluated against the increased weight due to the vehicle shape and recovery system.

- High Lift AMOOS

  Objective:

  Determine the implications of using a heavy lift or growth Space Shuttle for the delivery of an aeromaneuvering vehicle.

By suitable design of the TPS and the addition of a ground recovery system, the AMOOS vehicle may be recovered without the use of the Space Shuttle orbiter. Recall that AMRS is to have this capability also. Because of this recovery capability, AMOOS and AMRS may be placed in low earth orbit by the high lift shuttle. Candidate heavy lift Space Shuttle concepts provide payload capability to low earth orbit on the range of 160,000 lb to 180,000 lb. With such a capability, a two stage AMOOS with payload may be delivered in one launch. It also opens up a whole new class of vehicles, vehicle combinations and missions. In particular the geosynchronous sortie mission options are greatly increased and less restrained. This task would be to investigate fully the vehicle geometry options (no longer must it fit in a 60 ft long by 15 ft diameter cylinder) and mission spectrum compatible with the growth or heavy lift shuttle booster concepts.

- Space Station, Space Base, Lunar and Planetary

  Objectives:

  a. Determine the possible roles of AMOOS and AMRS in the more distant future of space flight.
  b. Determine vehicle changes and development that would enhance their capability to participate.

Space flight from the mid-1980's and beyond would be baseline for these studies. These probable missions would be analyzed for performing requirements. How these requirements could be met and the impact they would have on current design will be analyzed.

- Aerodynamic Heating and Tunnel Tests

  The objectives of this task are:

  a. Determine heating rates on the AMOOS configuration over the operational angle of attack range.
  b. Evaluate the predictive methods used to determine the aerodynamic heating.

An existing Stycast model will be used for these tests. The heating rate will be determined using temperature sensitive (Tempilaq) paint. Side and bottom view movies of the model at speeds of 16 frames/sec will be taken. Shadowgraphs will be taken at 10 deg angle-of-attack increments for every run.

- Baseline Space Tug Technology

A guideline for the AMOOS feasibility studies and later for the AMOOS and AMRS applications studies was that Baseline Space Tug systems should be used. Following this guideline the following Baseline Space Tug technology under development was used in the weight analysis of the AMOOS and AMRS vehicles:

- Engine Development
- Navigation, Guidance and Control
- Rendezvous and Docking
- Reusability and Refurbishment
- Thin Wall Tanks

Section 5
REFERENCES

1. Andrews, C.D., "Feasibility and Tradeoff Study of an Aeromaneuvering Orbit-to-Orbit Shuttle (AMOOS)," LMSC-HREC TR D306600, Lockheed Missiles & Space Company, Huntsville, Ala., June 1973.
2. White, J., "Feasibility and Tradeoff Study of an Aeromaneuvering Orbit-to-Orbit Shuttle (AMOOS)," LMSC-HREC TR D390272, Lockheed Missiles & Space Company, Huntsville, Ala., August 1974.
3. Corso, C.J., and C.L. Eyer, "Space Tug Aerobraking Study," D5-17142, The Boeing Company, Huntsville, Ala., 12 April 1972.
4. White, J., and A. Wernli, "Guidance Concepts for the Aeromaneuvering Orbit-to-Orbit Shuttle," LMSC-HREC TM D390356, Lockheed Missiles & Space Company, Huntsville, Ala., August 1974.
5. Justus, C.G. et al., "Four-D Global Reference Atmosphere User's Manual and Programmer's Manual," NASA TM X-64872, George C. Marshall Space Flight Center, September 1974.
6. Strauss, E.L., "Ablative Thermal Protection for the Space Tug Multipass, Aerobraking Entry," Martin Marietta Aerospace, Denver, J. Spacecraft, Vol. 12, No. 6, June 1975.
7. "Space Shuttle System Payload Accommodations," JSC 07700, Volume XIV Revision C, NASA-Johnson Space Center, Houston, Texas, 3 July 1974.
8. "Baseline Space Tug, System Requirements and Guidelines," MSFC 68-M00039-1, 15 July 1974.
9. "Space Tug," Vol. 1 of II, Book 2 of 4, Final Report, The Boeing Company, NASA CR-103004, February 1971.
10. Corning, G., "Weight Prediction Method for the Space Tug," IDA Log No. HQ 74-16219, Institute for Defense Analysis, Arlington, Va., June 1974.
11. Wernli, A., "3D Guidance Program for AMOOS and AMRS," LMSC-HREC TR D496661, Lockheed Missiles & Space Company, Huntsville, Ala., January 1976.

Appendix A
CONSUMABLES ANALYSIS

PRECEDING PAGE BLANK NOT FILMED

Appendix A

A consumables analysis was performed for both AMOOS and AMRS for equatorial geosynchronous and lunar orbital missions. The analysis for AMOOS was extended to include equatorial circular orbits of 5000 (9265), 10,000 (18,530) and 15,000 n.mi. (27,795 km) altitudes. The above AMOOS analysis was performed for one, one-and-one-half and two stage vehicles placed in a low earth orbit of 160 n.mi. by one, two or three 65,000 lb (29,484 kg) payload Space Shuttle launches. The analysis was extended to the uprated Shuttle for the geosynchronous cases only. The AMRS analysis included a specific impulse, I_{sp}, sensitivity analysis over the range of 260 through 350 sec.

To perform the consumables analysis the mission must be divided into events. The events, associated Δv's and other consumables usage are given in Tables 1 through 5 for AMOOS and in Tables 6 and 7 for AMRS.

The propellant usage was computed for each event. The inerts and attitude control APS usage were subtracted from the starting mass for each event before computing the propellant required for the propulsive Δv. The propellant usage was computed using

$$\frac{m_o}{m_f} = e^{-\Delta v/g_o I_{sp}} \qquad (A.1)$$

for each element of the Δv budget. Equation (A.1) had, in general, to be applied twice to each main engine Δv event because of the chilldown mode preceding each burn. This was accomplished by first computing the flow rate during chill-down using

$$T = \dot{m} g_o I_{sp} \qquad (A.2)$$

where T is the thrust and $\dot{m}$ is the flow rate. The mass of propellant, Δm, required for chill-down is then

$$m_o - m_f = \Delta m = \dot{m}t \qquad (A.3)$$

where t is the time taken for chill-down. The value of m_f calculated from Eq. (A.3) is then used in Eq. (A.1) to compute the Δv_c imparted during chill-down. If Δv_c is larger than or equal to the event Δv, then the propellant usage is recomputed using Eq. (A.1) and the chilldown I_{sp}. If Δv_c is less than or equal to the event Δv, then the propellant usage was computed using the main engine I_{sp} as specified for the event and a velocity increment of $\Delta v - \Delta v_c$ after the propellant usage for chill down had been subtracted from m_o.

The delivered payload is computed iteratively for a selected returned payload. If two payloads are delivered, only one is computed iteratively. The other must be input as an inert. The computed payload may be either the first or second delivered.

Two stage or stage-and-one-half vehicles are analyzed by stage. The proportion of propellant in each stage may be chosen by the user and has been selected as one-half for the AMOOS analysis. In this way identical stages are used. The program iterates to obtain the specified ratio of propellant loading.

Results

AMOOS: The results of the analysis are summarized in the following carpet plots of payload delivered and main engine consumables. Payload retrieved and stage dry weight are, in general, the independent variables for the AMOOS analysis.

AMRS: The computer code may also be used to compute the AMRS on orbit weight required to perform a mission with a given recovery (dry)

weight and I_{sp} by considering the consumables required to be a negative payload delivered. The results of the AMRS analysis are also given as carpet plots but as on station weight and main engine consumables. Recovered weight and I_{sp} are the independent variables. Carpet plots are discussed in Section 2.1.1.

The best estimate of the dry weight of a single stage AMOOS is 6700 lb. If a two-stage vehicle is used, except for the single shuttle launch, then it is suggested that a stage dry weight of 7000 lb is used to allow for the increased complexity of the interface with the payloads and between the payloads. In the case of the stage-and-one-half vehicles, again single shuttle launch excepted, a stage weight of 7000 lb and a half-stage weight of 2000 lb is recommended. At this weight, the half stage would not be recovered. Currently, it is considered that only small weight savings per stage could be accomplished in the case of the single Space Shuttle launch. A full-stage dry weight of 5000 lb is recommended for use with the two-stage AMOOS, single shuttle launch data. The reason for so small a change is that the savings per stage over the single stage vehicle is confined to the tanks, primary structure and TPS. In all, these components account for less than one half the total dry weight. The recommended weight of the corresponding half stage is 1200 lb. The relatively large reduction is due to the half stage being primarily tanks and structure.

Table A-1

AMOOS Δv BUDGET AND EVENT PARAMETERS FOR SINGLE STAGE EQUATORIAL GEOSYNCHRONOUS MISSION

Event No.	Δv (ft/sec)	I_{sp} (sec)	Inerts (lb)	Other H_2, O_2 Uses (lb)
1	10.	230.		
1SEPARATE FROM SHUTTLE				
2		230.	-8.6	-10.
2COAST TO SAFE DISTANCE				
3		230.	-21.4	-46.
3PHASE IN SHUTTLE ORBIT				
4	4494.	456.5		
4INSERT INTO PHASING ORBIT				
5		230.	-17.5	-5.
5COAST IN PHASING ORBIT				
6	3672.	456.5		
6INSERT INTO TRANSFER ORBIT				
7		230.	-13.8	-6.
7COAST TO MIDCOURSE				
8	50.	377.		
8MIDCOURSE CORRECTION				
9		230.	-14.	-16.
9COAST TO MISSION ALTITUDE				
10	5828.	456.5		
10INSERT TO MISSION PHASING ORBIT				
11		230.	-8.3	-56.
11COAST IN MISSION PHASING ORBIT				
12	258.	434.7		
12RENDEZVOUS WITH SPACE STATION				
13	40.	230.		-15.
13DOCK WITH SPACE STATION				
14		230.		-56.
14ON ORBIT STAY				
15	10.	230.		
15SEPARATE FROM SPACE STATION				
16		230.	-15.	-10.
16COAST TO SAFE DISTANCE				
17	6040.	456.5		
17INSERT INTO TRANSFER ORBIT				
18		230.	-15.	-6.
18COAST TO MIDCOURSE				
19	35.	377.		
19MIDCOURSE CORRECTION				
20		230.	-6.	-18.

(Continued)

ORIGINAL PAGE IS OF POOR QUALITY

Table A-1 (Concluded)

Event No.	Δv (ft/sec)	I_{sp} (sec)	Inerts (lb)	Other H_2, O_2 Uses (lb)
20COAST TO ATMOSPHERIC ENTRY				
21	100.	230.		
21AEROMANEUVERING				
22		230.	-7.5	-6.
22COAST TO APOGEE				
23	200.	434.7		
23INSERT INTO EOS PHASING ORBIT				
24		230.	-12.	-36.
24PHASE WITH EOS				
25	380.	434.7		
25CIRCULARIZE TO 170 NMI				
26	200.	456.5		-400.
26DUMP PROPELLANT RESERVES				

C.2

Table A-2a

AMOOS Δv BUDGET AND EVENT PARAMETERS FOR A TWO STAGE EQUATORIAL GEOSYNCHRONOUS MISSION, FIRST STAGE

Event No.	Δv (ft/sec)	I_{sp} (sec)	Inerts (lb)	Other H_2, O_2 Uses (lb)
1	10.	230.		
1SEPARATE FROM SPACE SHUTTLE				
2		230.	-8.6	-10.
2COAST TO SAFE DISTANCE				
3	40.	230.	-16.	-20.
3DOCK WITH PAYLOAD AND/OR STAGE				
4		230.	-21.4	-46.
4PHASE IN SHUTTLE ORBIT				
5	4484.	456.5		
5INSERT INTO PHASING ORBIT				
6		230.	-17.5	-10.
6COAST IN PHASING ORBIT				
7	3672.	456.5		
7INSERT INTO TRANSFER ORBIT				
8		230.	-13.8	-6.
8COAST TO MIDCOURSE				
9		230.		
9MIDCOURSE CORRECTION				
10		230.	-14.	-16.
10COAST TO MISSION ALTITUDE				
11		230.		
11INSERT TO MISSION PHASING ORBIT				
12		230.		
12COAST IN MISSION PHASING ORBIT				
13		230.		
13RENDEZVOUS WITH SPACE STATION				
14		230.		
14DOCK WITH SPACE STATION				
15		230.		
15ON ORBIT STAY				
16		230.		
16SEPARATE FROM SPACE STATION				
17		230.		
17COAST TO SAFE DISTANCE				
18	50.	377.		
18INSERT INTO TRANSFER ORBIT				
19		230.	-15.	-12.
19COAST TO MIDCOURSE				
20	30.	377.		

(Continued)

ORIGINAL PAGE IS
OF POOR QUALITY

Table A-2a (Concluded)

Event No.	Δv (ft/sec)	I_{sp} (sec)	Inerts (lb)	Other H_2, O_2 Uses (lb)
20MIDCOURSE CORRECTION				
21		230.	-6.	-18.
21COAST TO ATMOSPHERIC ENTRY				
22	100.	230.		
22AEROMANEUVERING				
23		230.	-7.5	-6.
23COAST TO APOGEE				
24	200.	434.7		
24INSERT INTO EOS PHASING ORBIT				
25		230.	-12.	-36.
25PHASE WITH EOS				
26	380.	434.7		
26CIRCULARIZE TO 170 NMI				
27	200.	456.5		
27DUMP PROPELLANT RESERVES				

Table A-2b

AMOOS Δv BUDGET AND EVENT PARAMETERS FOR A TWO STAGE EQUATORIAL GEOSYNCHRONOUS MISSION, SECOND STAGE

Event No.	Δv (ft/sec)	I_{sp} (sec)	Inerts (lb)	Other H_2, O_2 Uses (lb)
1		230.		
1SEPARATE FROM SPACE SHUTTLE				
2		230.	-8.6	-10.
2COAST TO SAFE DISTANCE				
3		230.	-8.	-20.
3DOCK WITH PAYLOAD AND/OR STAGE				
4		230.		-46.
4PHASE IN SHUTTLE ORBIT				
5		456.5		
5INSERT INTO PHASING ORBIT				
6		230.		-10.
6COAST IN PHASING ORBIT				
7		456.5		
7INSERT INTO TRANSFER ORBIT				
8		230.	-13.6	-6.
8COAST TO MIDCOURSE				
9	50.	434.7		
9MIDCOURSE CORRECTION				
10		230.	-14.	-16.
10COAST TO MISSION ALTITUDE				
11	5826.	456.5		
11INSERT TO MISSION PHASING ORBIT				
12		230.	-8.3	-56.
12COAST IN MISSION PHASING ORBIT				
13	258.	434.7		
13RENDEZVOUS WITH SPACE STATION				
14	40.	230.		-15.
14DOCK WITH SPACE STATION				
15		230.		-56.
15ON ORBIT STAY				
16	10.	230.		
16SEPARATE FROM SPACE STATION				
17		230.	-15.	-12.
17COAST TO SAFE DISTANCE				
18	6040.	456.5		
18INSERT INTO TRANSFER ORBIT				
19		230.	-15.	-12.
19COAST TO MIDCOURSE				
20	30.	434.7		

(Continued)

Table A-2b (Concluded)

Event No.	Δv (ft/sec)	I_{sp} (sec)	Inerts (lb)	Other H_2, O_2 Uses (lb)
20MIDCOURSE CORRECTION				
21		230.	-6.	-18.
21COAST TO ATMOSPHERIC ENTRY				
22	100.	230.		
22AEROMANEUVERING				
23		230.	-7.5	-6.
23COAST TO APOGEE				
24	200.	434.7		
24INSERT INTO EOS PHASING ORBIT				
25		230.	-12.	-36.
25PHASE WITH EOS				
26	380.	434.7		
26CIRCULARIZE TO 170 NMI				
27	250.	456.5		
27DUMP PROPELLANT RESERVES				

ORIGINAL PAGE IS
OF POOR QUALITY

Table A-3

AMOOS Δv AND EVENT PARAMETER CHANGES FOR OTHER EARTH ORBITAL MISSIONS

Event No.	Δv (ft/sec)	I_{sp} (sec)
2CONSUMABLES ANALYSIS FOR AMOOS ON A FIFTEEN K NMI		
4	4000.	456.5
6	3560.	456.5
10	6116.	456.5
17	6359.	456.5
2CONSUMABLES ANALYSIS FOR AMOOS ON A FIFTEEN K NMI		
4	4000.	456.5
6	3560.	456.5
10	6116.	456.5
17	6359.	456.5
2CONSUMABLES ANALYSIS FOR AMOOS ON A FIFTEEN K NMI		
5	4000.	456.5
7	3560.	456.5
11	6116.	456.5
18	6359.	456.5
2CONSUMABLES ANALYSIS FOR AMOOS ON A FIFTEEN K NMI		
2CONSUMABLES ANALYSIS FOR AMOOS ON A TEN K NMI		
4	3500.	456.5
6	3212.	456.5
10	6490.	456.5
17	6945.	456.5
2CONSUMABLES ANALYSIS FOR AMOOS ON A TEN K NMI		
4	3500.	456.5
6	3212.	456.5
10	6490.	456.5
17	6945.	456.5
2CONSUMABLES ANALYSIS FOR AMOOS ON A TEN K NMI		
5	3500.	456.5
7	3212.	456.5
11	6490.	456.5
18	6945.	456.5
2CONSUMABLES ANALYSIS FOR AMOOS ON A TEN K NMI		
2CONSUMABLES ANALYSIS FOR AMOOS ON A FIVE K NMI		
4	2700.	456.5
6	2489.	456.5
10	7077.	456.5
17	8094.	456.5
2CONSUMABLES ANALYSIS FOR AMOOS ON A FIVE K NMI		
4	2700.	456.5
6	2489.	456.5
10	7077.	456.5
17	8094.	456.5
2CONSUMABLES ANALYSIS FOR AMOOS ON A FIVE K NMI		
5	2700.	456.5
7	2489.	456.5
11	7077.	456.5
18	8094.	456.5
2CONSUMABLES ANALYSIS FOR AMOOS ON A FIVE K NMI		

Table A-4

AMOOS Δv BUDGET AND EVENT PARAMETERS FOR A SINGLE STAGE LUNAR ORBIT MISSION

Event No.		Δv (ft/sec)	I_{sp} (sec)	Inerts (lb)	Other H_2, O_2 Uses (lb)
1		10.	230.		
1	SEPARATE FROM SHUTTLE				
2			230.	-8.6	-10.
2	COAST TO SAFE DISTANCE				
3			230.	-21.4	-46.
3	PHASE IN SHUTTLE ORBIT				
4		5000.	456.5		
4	INSERT INTO PHASING ORBIT				
5			230.	-17.5	-5.
5	COAST IN PHASING ORBIT				
6		5454.	456.5		
6	INSERT INTO TRANSFER ORBIT				
7			230.	-65.	-130.
7	COAST TO MIDCOURSE				
8		50.	377.		
8	MIDCOURSE CORRECTION				
9			230.	-65.	-130.
9	COAST TO MISSION ALTITUDE				
10		3460.	456.5		
10	INSERT TO MISSION PHASING ORBIT				
11			230.	-8.3	-56.
11	COAST IN MISSION PHASING ORBIT				
12		150.	434.7		
12	RENDEZVOUS WITH SPACE STATION				
13		40.	230.		-15.
13	DOCK WITH SPACE STATION				
14			230.		-56.
14	ON ORBIT STAY				
15		10.	230.		
15	SEPARATE FROM SPACE STATION				
16			230.	-8.6	-10.
16	COAST TO SAFE DISTANCE				
17		3550.	456.5		
17	INSERT INTO TRANSFER ORBIT				
18			230.	-65.	-130.
18	COAST TO MIDCOURSE				
19		50.	434.7		
19	MIDCOURSE CORRECTION				
20			230.	-65.	-130.
20	COAST TO ATMOSPHERIC ENTRY				

Table A-4 (Concluded)

Event No.	Δv (ft/sec)	I_{sp} (sec)	Inerts (lb)	Other H_2, O_2 Uses (lb)
21	100.	230.		
21AEROMANEUVERING				
22		230.	-7.5	-6.
22COAST TO APOGEE				
23	200.	434.7		
23INSERT INTO EOS PHASING ORBIT				
24		230.	-12.	-36.
24PHASE WITH EOS				
25	380.	434.7		
25CIRCULARIZE TO 170 NMI				
26	200.	456.5		-400.
26DUMP PROPELLANT RESERVES				

ORIGINAL PAGE IS
OF POOR QUALITY

Table A-5

AMOOS Δv BUDGET AND EVENT PARAMTERS FOR A TWO-STAGE LUNAR ORBIT MISSION, FIRST STAGE

Event No.	Δv (ft/sec)	I_{sp} (sec)	Inerts (lb)	Other H_2, O_2 Uses (lb)
1	10.	230.		
1SEPARATE FROM SPACE SHUTTLE				
2		230.	-8.6	-10.
2COAST TO SAFE DISTANCE				
3	40.	230.	-16.	-20.
3DOCK WITH PAYLOAD AND/OR STAGE				
4		230.	-21.4	-46.
4PHASE IN SHUTTLE ORBIT				
5	5000.	456.5		
5INSERT INTO PHASING ORBIT				
6		230.	-17.5	-10.
6COAST IN PHASING ORBIT				
7	5454.	456.5		
7INSERT INTO TRANSFER ORBIT				
8		230.	-65.	-130.
8COAST TO MIDCOURSE				
9		377.		
9MIDCOURSE CORRECTION				
10		230.	-65.	-130.
10COAST TO MISSION ALTITUDE				
11		230.		
11INSERT TO MISSION PHASING ORBIT				
12		230.		
12COAST IN MISSION PHASING ORBIT				
13		230.		
13RENDEZVOUS WITH SPACE STATION				
14		230.		
14DOCK WITH SPACE STATION				
15		230.		
15ON ORBIT STAY				
16		230.		
16SEPARATE FROM SPACE STATION				
17		230.		
17COAST TO SAFE DISTANCE				
18	50.	377.		
18INSERT INTO TRANSFER ORBIT				
19		230.	-65.	-130.
19COAST TO MIDCOURSE				
20	30.	377.		

(Continued)

Table A-5 (Concluded)

Event No.	Δv (ft/sec)	I_{sp} (sec)	Inerts (lb)	Other H_2, O_2 Uses (lb)
20MIDCOURSE CORRECTION				
21		230.	-65.	-130.
21COAST TO ATMOSPHERIC ENTRY				
22	100.	230.		
22AEROMANEUVERING				
23		230.	-7.5	-6.
23COAST TO APOGEE				
24	200.	434.7		
24INSERT INTO EOS PHASING ORBIT				
25		230.	-12.	-36.
25PHASE WITH EOS				
26	380.	434.7		
26CIRCULARIZE TO 170 NMI				
27	200.	456.5		-400.
27DUMP PROPELLANT RESERVES				

Table A-5

AMOOS Δv BUDGET AND EVENT PARAMETERS FOR A TWO STAGE LUNAR ORBIT MISSION, SECOND STAGE

Event No.	Δv (ft/sec)	I_{sp} (sec)	Inerts (lb)	Other H_2, O_2 Uses (lb)
1		230.		
1SEPARATE FROM SPACE SHUTTLE				
2		230.	-8.6	-10.
2COAST TO SAFE DISTANCE				
3		230.	-8.	-20.
3DOCK WITH PAYLOAD AND/OR STAGE				
4		230.		-46.
4PHASE IN SHUTTLE ORBIT				
5		456.5		
5INSERT INTO PHASING ORBIT				
6		[illegible].		-10.
6COAST IN PHASING ORBIT				
7		456.5		
7INSERT INTO TRANSFER ORBIT				
8		230.	-65.	-130.
8COAST TO MIDCOURSE				
9	50.	434.7		
9MIDCOURSE CORRECTION				
10		230.	-65.	-130.
10COAST TO MISSION ALTITUDE				
11	3460.	456.5		
11INSERT TO MISSION PHASING ORBIT				
12		230.	-8.3	-56.
12COAST IN MISSION PHASING ORBIT				
13	150.	434.7		
13RENDEZVOUS WITH SPACE STATION				
14	40.	230.		
14DOCK WITH SPACE STATION				
15		230.		-56.
15ON ORBIT STAY				
16	10.	230.		
16SEPARATE FROM SPACE STATION				
17		230.	-8.6	-10.
17COAST TO SAFE DISTANCE				
18	3550.	456.5		
18INSERT INTO TRANSFER ORBIT				
19		230.	-65.	-130.
19COAST TO MIDCOURSE				
20	50.	434.7		

(Continued)

ORIGINAL PAGE IS OF POOR QUALITY

Table A-5 (Concluded)

Event No.	Δv (ft/sec)	I_{sp} (sec)	Inerts (lb)	Other H_2, O_2 Uses (lb)
20MIDCOURSE CORRECTION				
21		230.	-65.	-130.
21COAST TO ATMOSPHERIC ENTRY				
22	100.	230.		
22AEROMANEUVERING				
23		230.	-7.5	-6.
23COAST TO APOGEE				
24	200.	434.7		
24INSERT INTO EOS PHASING ORBIT				
25		230.	-12.	-36.
25PHASE WITH EOS				
26	380.	434.7		
26CIRCULARIZE TO 170 NMI				
27	200.	456.5		-400.
27DUMP PROPELLANT RESERVES				

Table A-6

AMRS Δv BUDGET AND EVENT PARAMETER FOR RETURN FROM AN EQUATORIAL GEOSYNCHRONOUS ORBIT

Event No.	Δv (ft/sec)	I_{sp} (sec)	Inerts (lb)	Other H_2, O_2 Uses (lb)
1	10.	230.		
1SEPARATE FROM SPACE STATION				
2		230.	-7.5	-6.
2COAST TO SAFE DISTANCE				
3	6040.	260.		
3INSERT INTO TRANSFER ORBIT				
4		230.	-7.5	-6.
4COAST TO MIDCOURSE				
5	30.	230.		
5MIDCOURSE CORRECTION				
6		230.	-3.	-9.
6COAST TO ATMOSPHERIC ENTRY				
7	100.	230.		
7AEROMANEUVERING				
8		230.	-4.	-3.
8COAST TO APOGEE				
9	200.	260.		
9INSERT INTO EOS PHASING ORBIT				
10		230.	-6.	-18.
10PHASE WITH EOS				
11	380.	260.		
11CIRCULARIZE TO 170 NMI				
12	100.	260.		-200.
12DUMP RESUDUALS				

Table A-7

AMRS Δv BUDGET AND EVENT PARAMETERS FOR RETURN FROM A LUNAR ORBIT

Event No.	Δv (ft/sec)	I_{sp} (sec)	Inerts (lb)	Other H_2, O_2 Uses (lb)
1 1	10.	230.		
1SEPARATE FROM SPACE STATION				
2 1		230.	-7.5	-6.
2COAST TO SAFE DISTANCE				
3 1	3550.	260.		
3INSERT INTO TRANSFER ORBIT				
4 1		230.	-150.	-100.
4COAST TO MIDCOURSE				
5 1	50.	230.		
5MIDCOURSE CORRECTION				
6 1		230.	-150.	-100.
6COAST TO ATMOSPHERIC ENTRY				
7 1	100.	230.		
7AEROMANEUVERING				
8 1		230.	-4.	-3.
8COAST TO APOGEE				
9 1	200.	260.		
9INSERT INTO EOS PHASING ORBIT				
10 1		230.	-6.	-18.
10PHASE WITH EOS				
11 1	380.	260.		
11CIRCULARIZE TO 170 NMI				
12 1	100.	260.		-200.
12DUMP RESUDUALS				

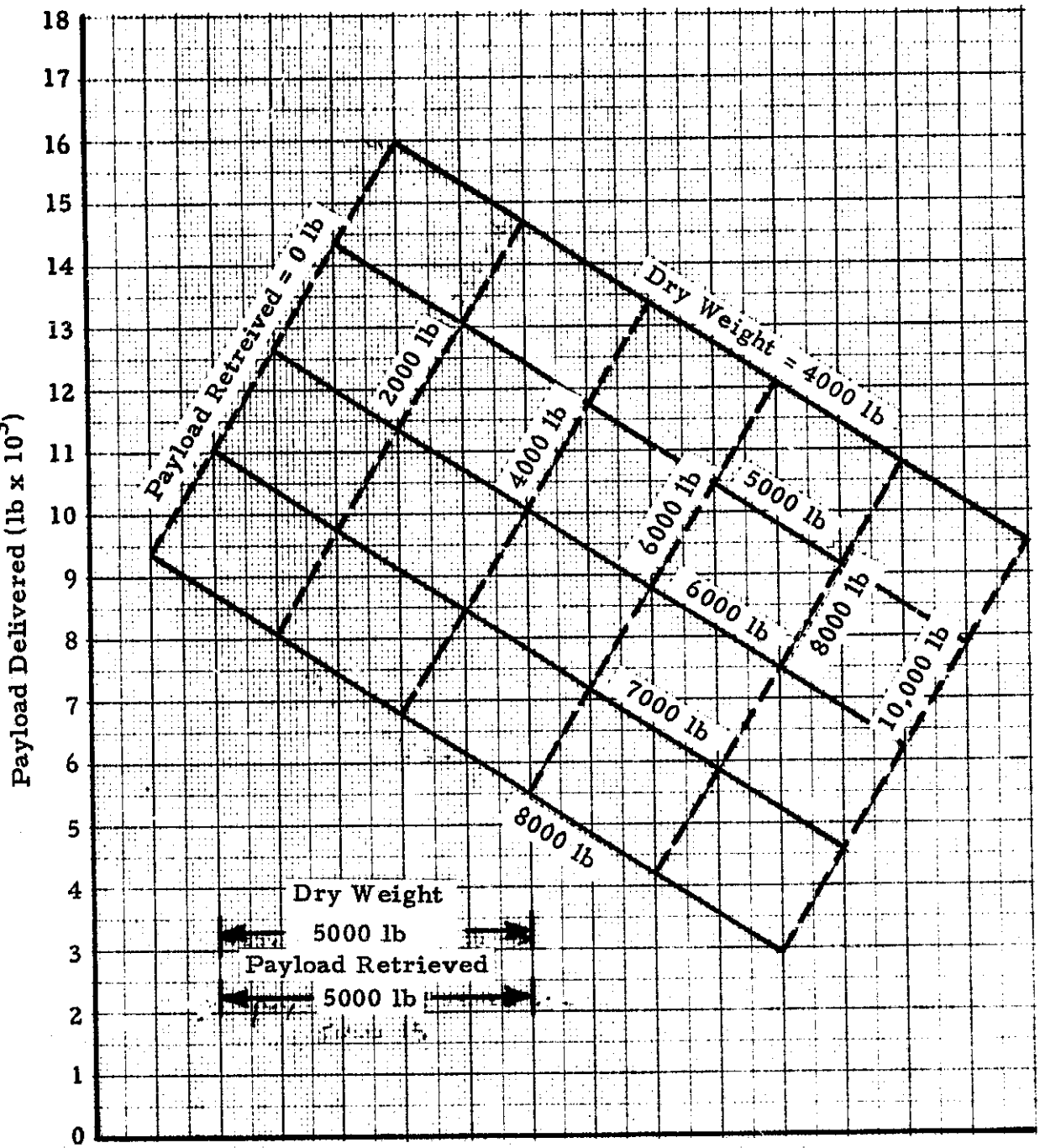

Fig. A-1 - AMOOS Payload and Main Engine Consumables for an Equatorial Geosynchronous Mission, I_{sp} = 456.5 sec and 65,000 lb Payload Shuttle

a. Single Stage AMOOS, One Shuttle Launch

i. Payloads

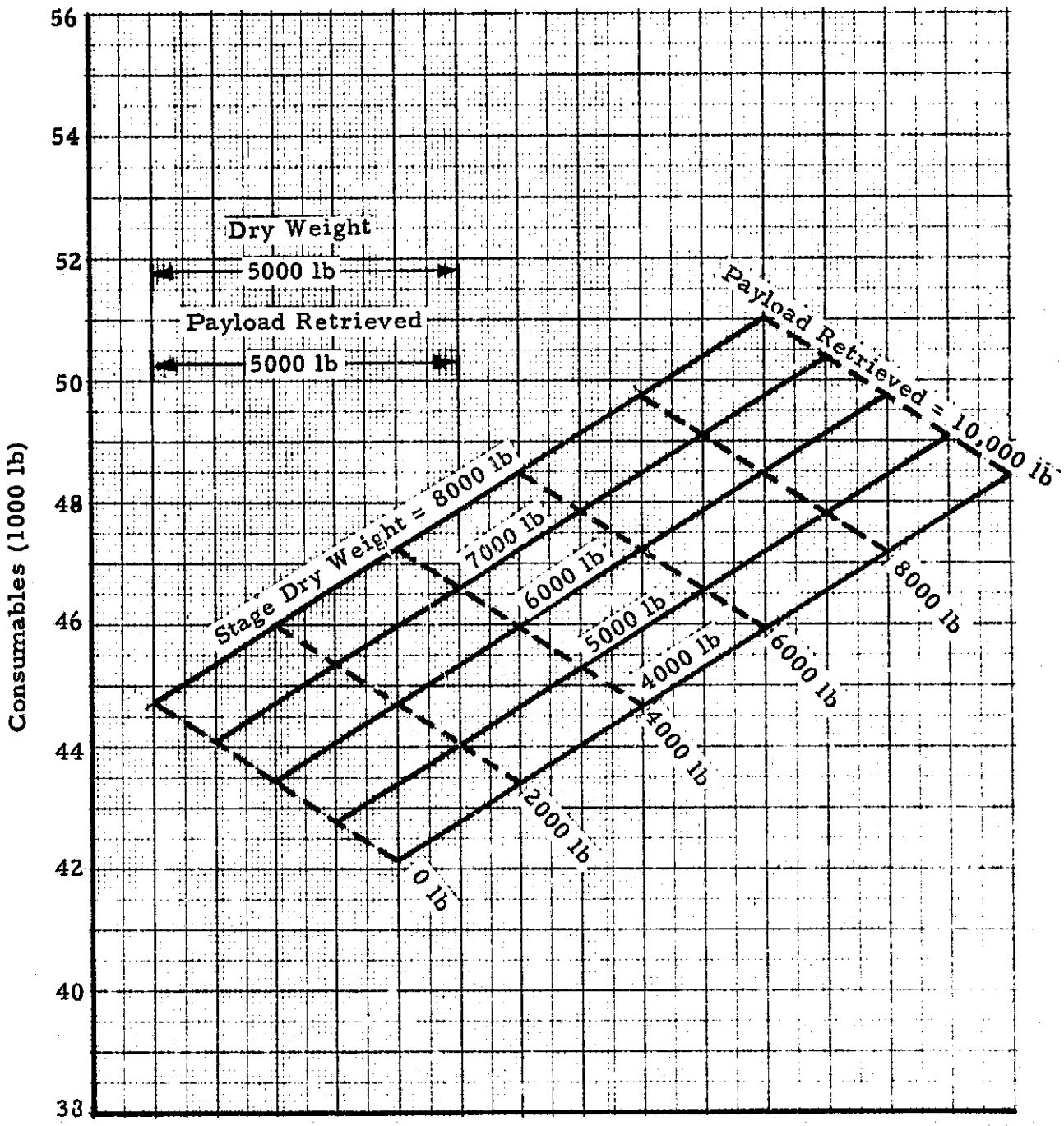

Fig. A-1a (Continued)

ii. Main Engine Consumables

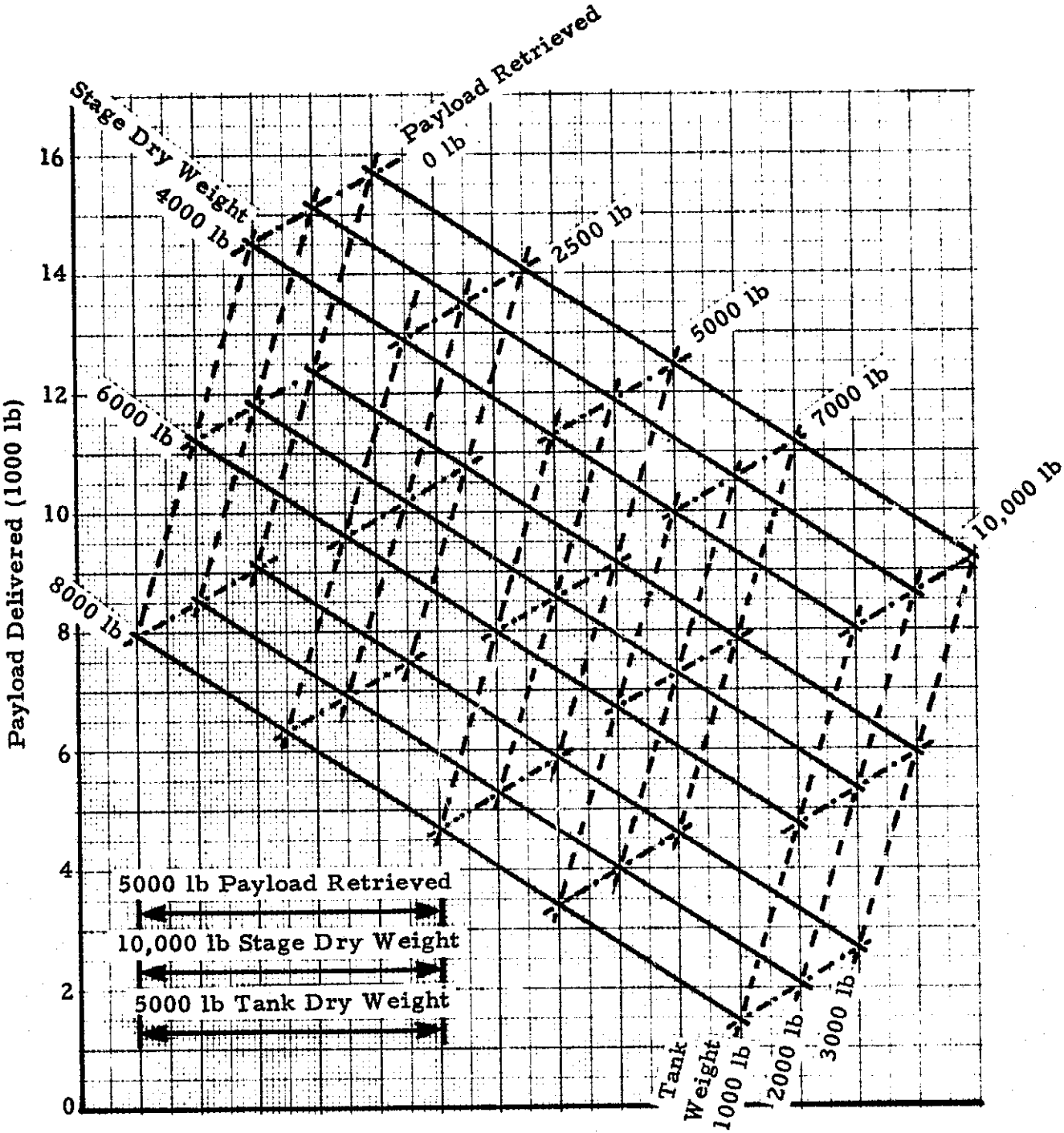

Fig. A-1 (Continued)

b. Stage and One Half AMOOS, One Shuttle Launch

i. Payloads

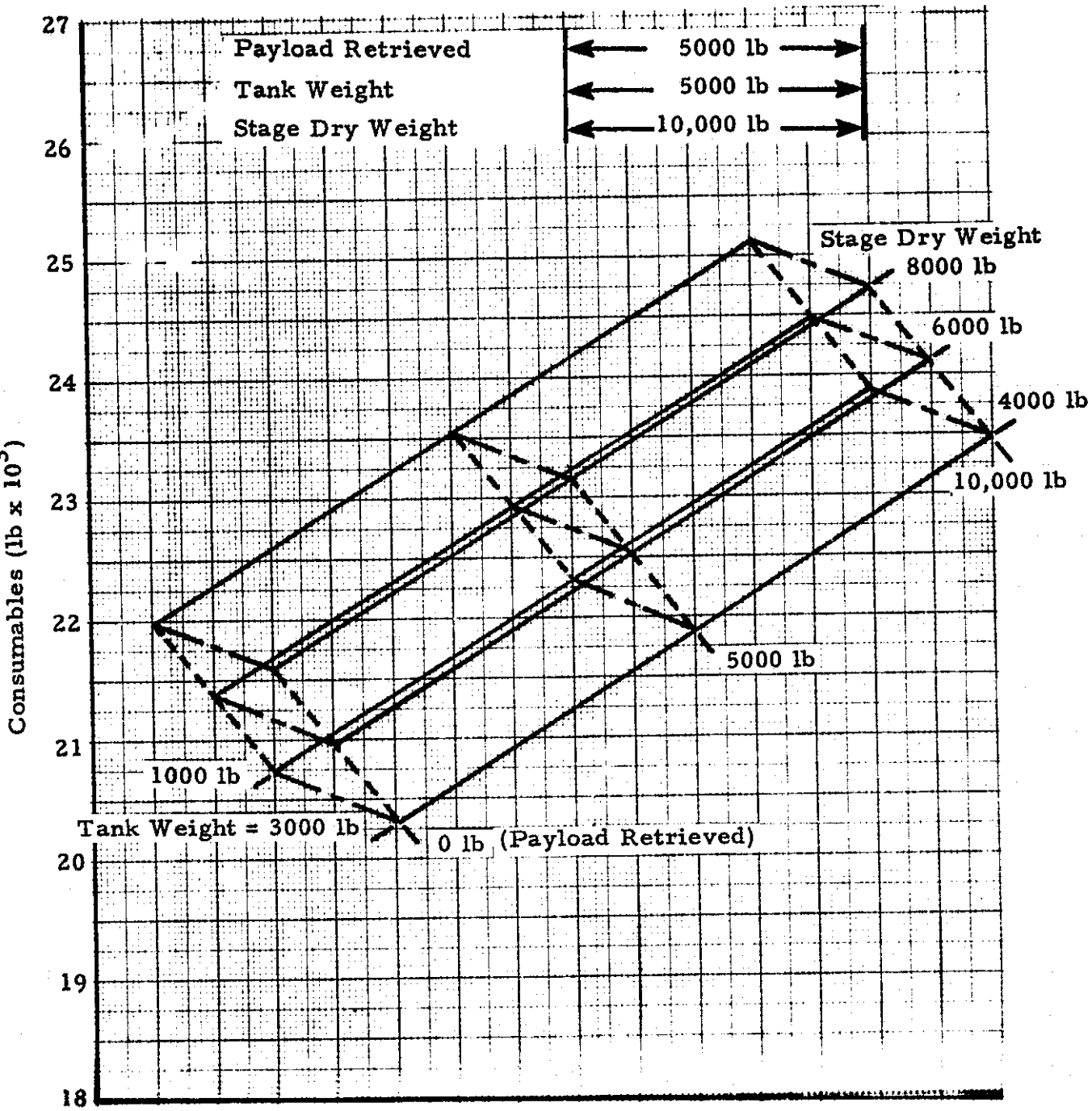

Fig. A-1b (Continued)

ii. Main Engine Consumables

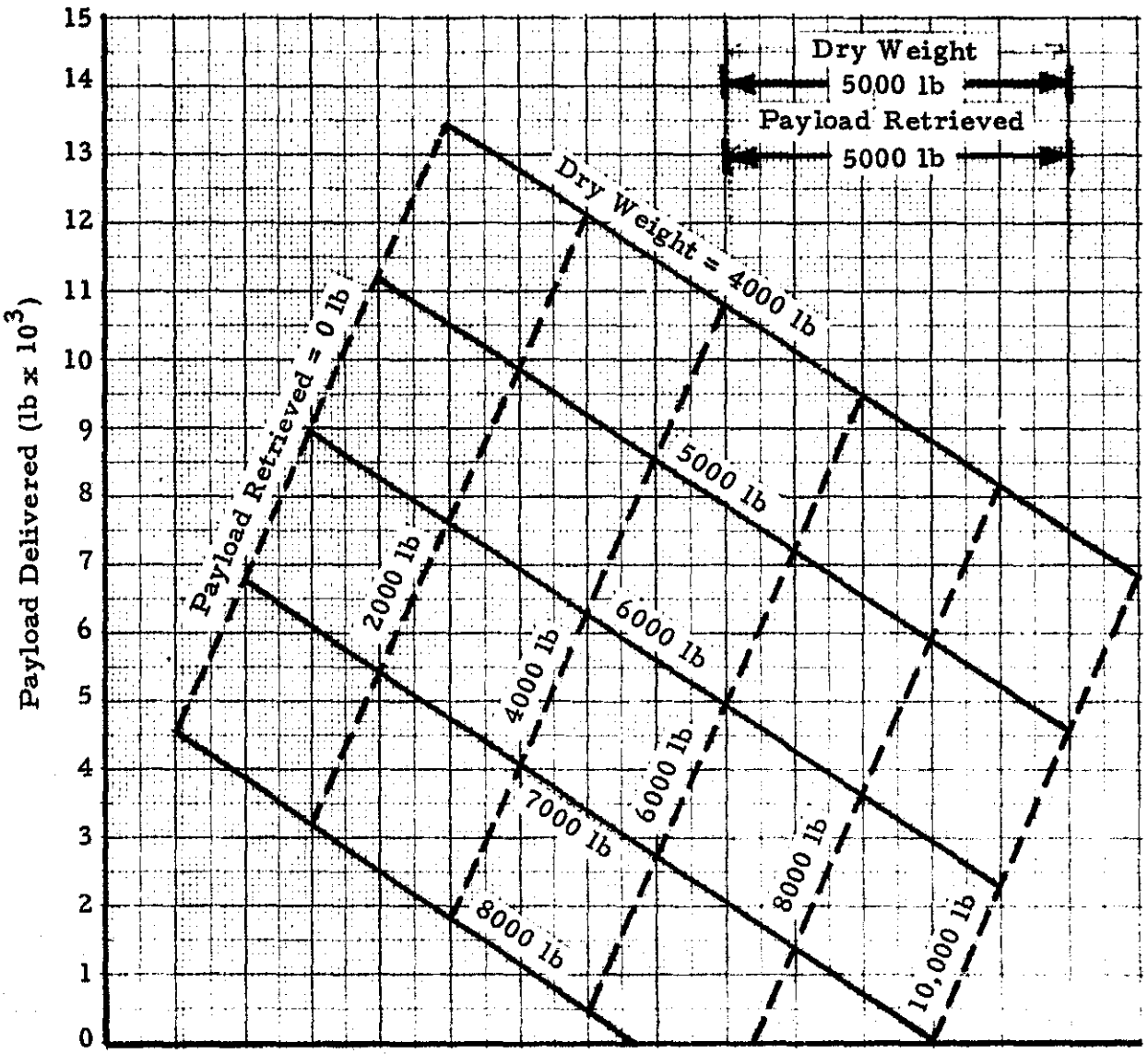

Fig. A-1 (Continued)

c. Two Stage AMOOS,
One Shuttle Launch

i. Payloads

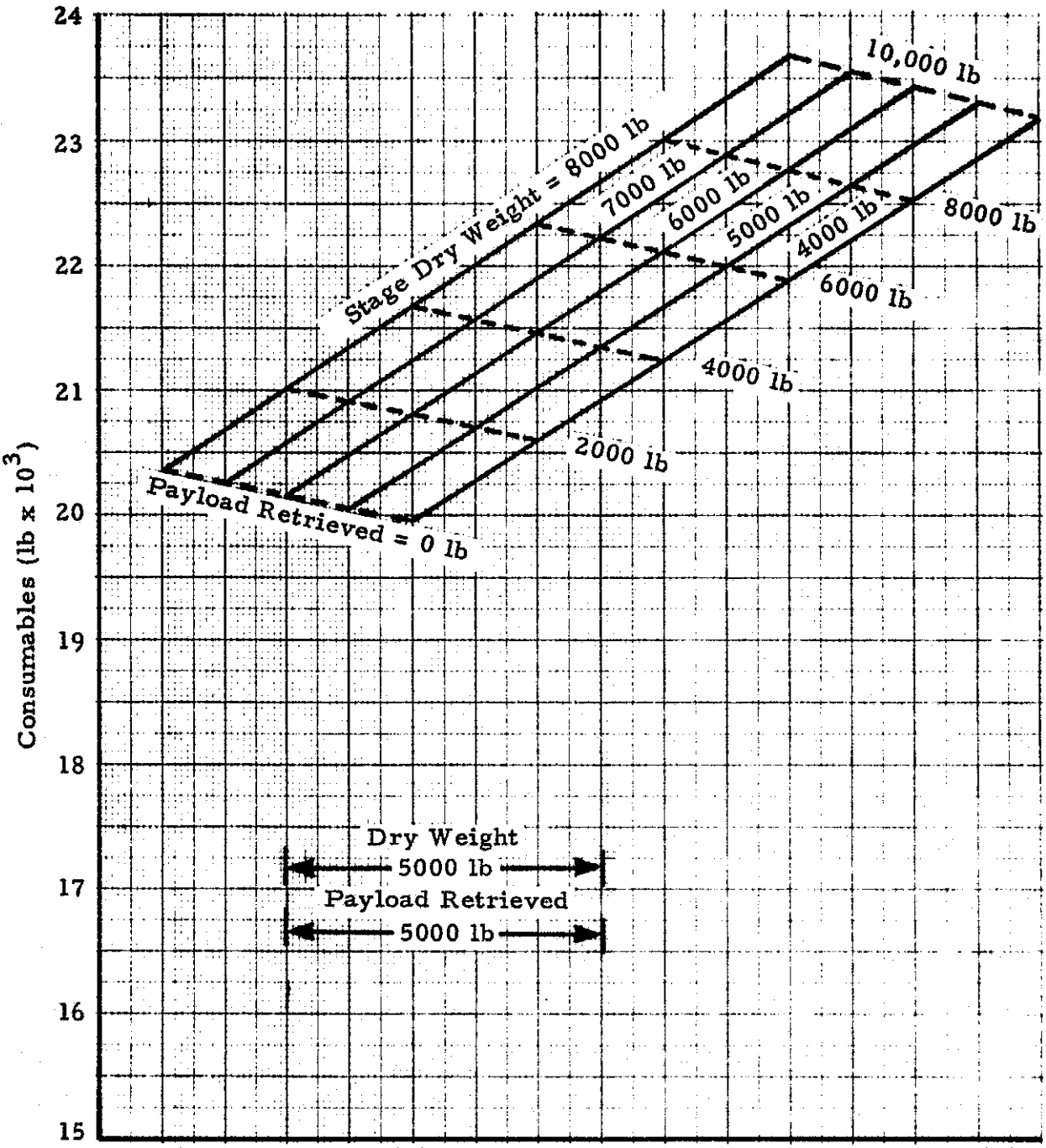

Fig. A-1c (Continued)

ii. Main Engine Consumables

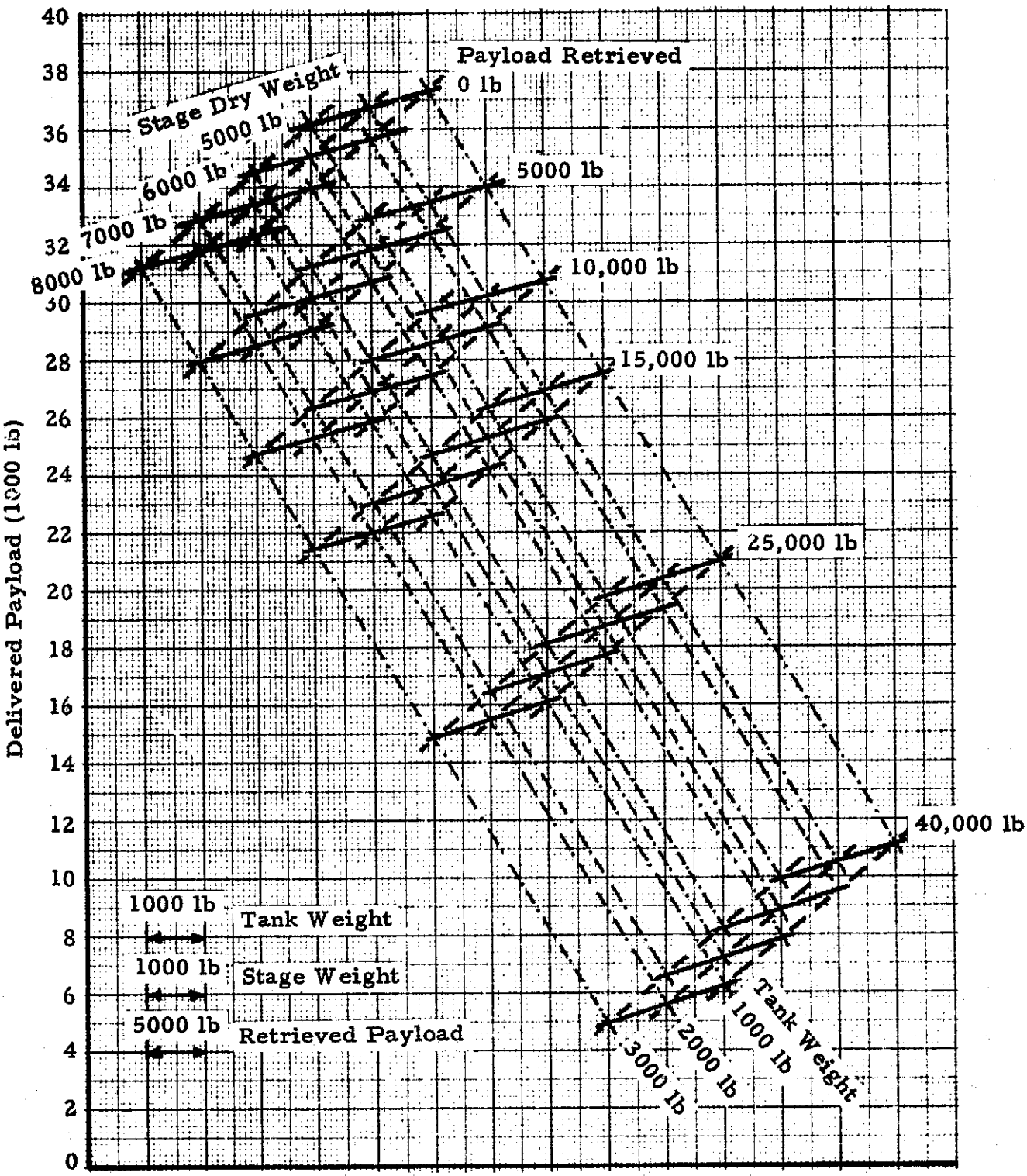

Fig. A-1 (Continued)

d. Stage and One-Half AMOOS, Two Shuttle Launches

i. Payloads

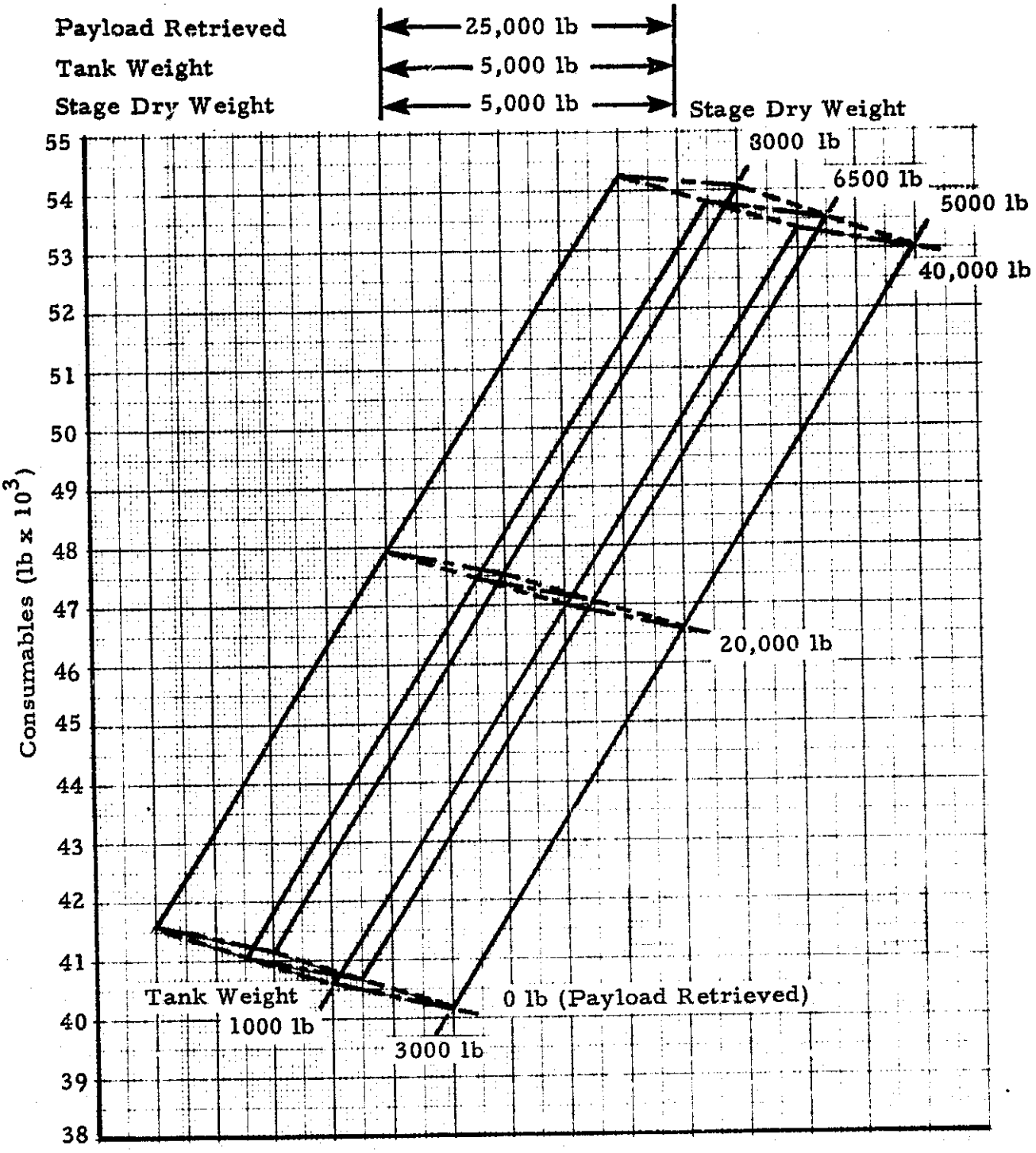

Fig. A-1d (Continued)

ii. Consumables

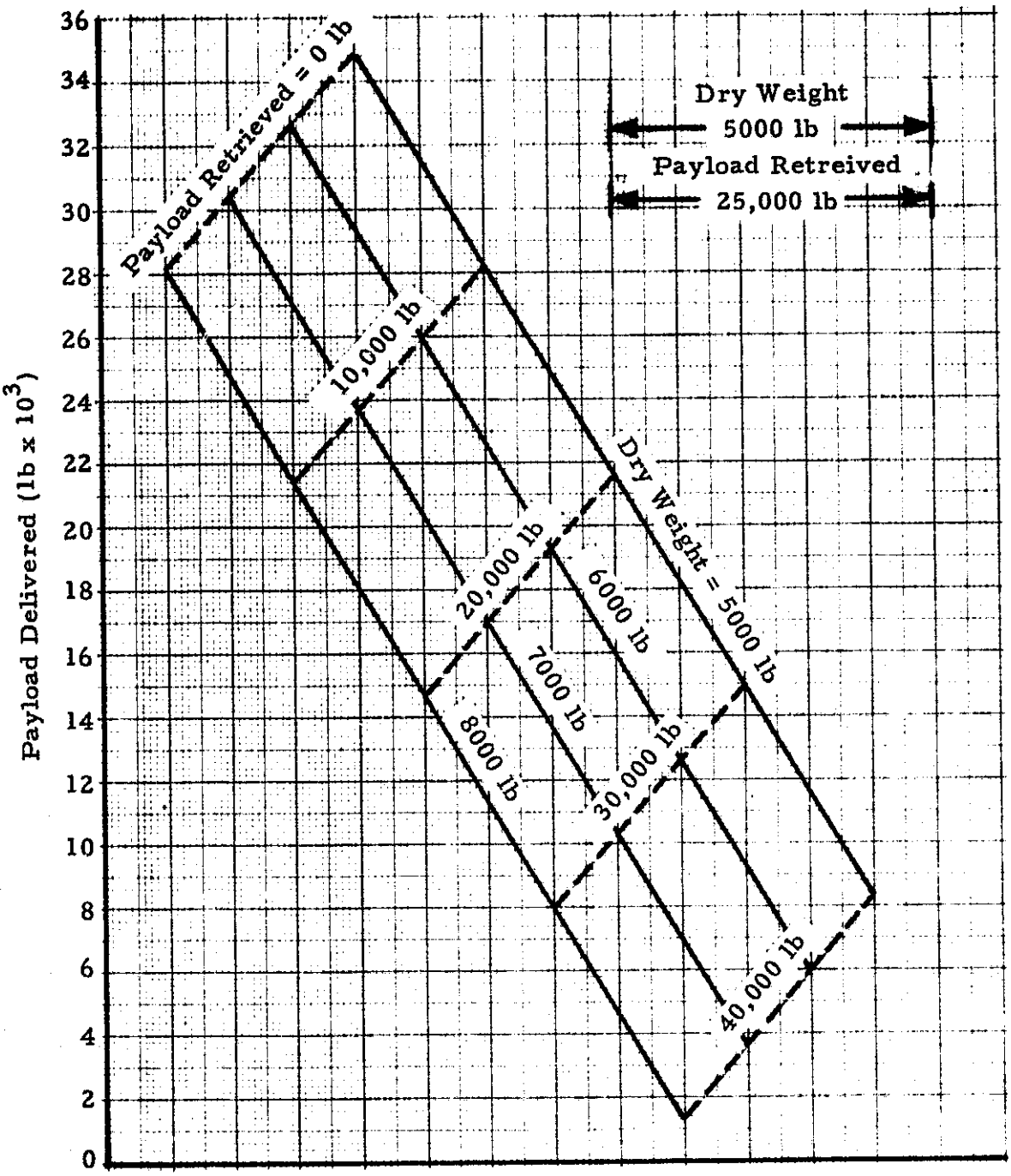

Fig. A-1 (Continued)

e. Two-Stage AMOOS,
Two Shuttle Launches

i. Payloads

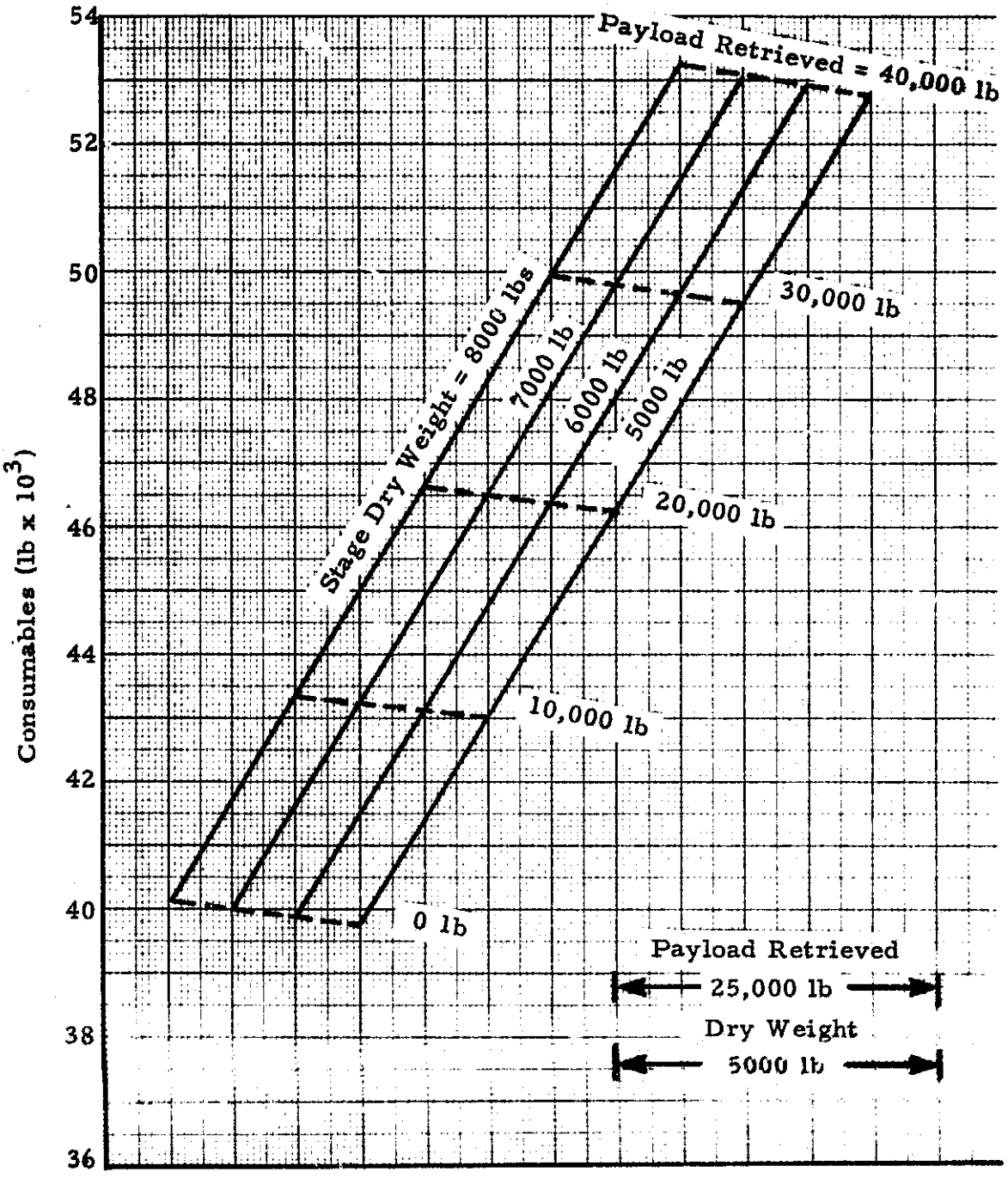

Fig. A-1e (Continued)

ii. Main Engine Consumables

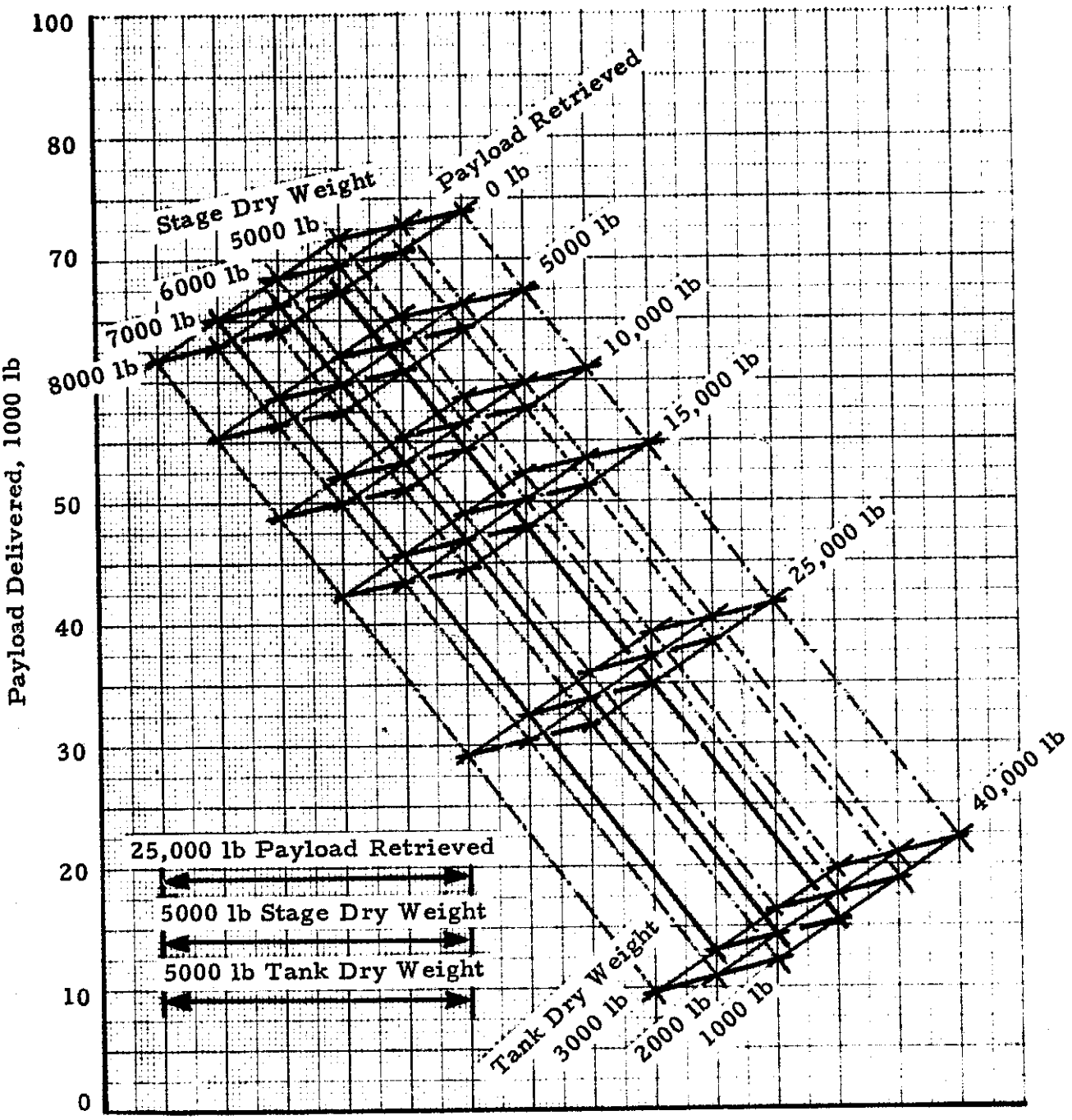

Fig. A-1 (Continued)

f. Stage and One-Half AMOOS, Three Shuttle Launches

i. Payloads

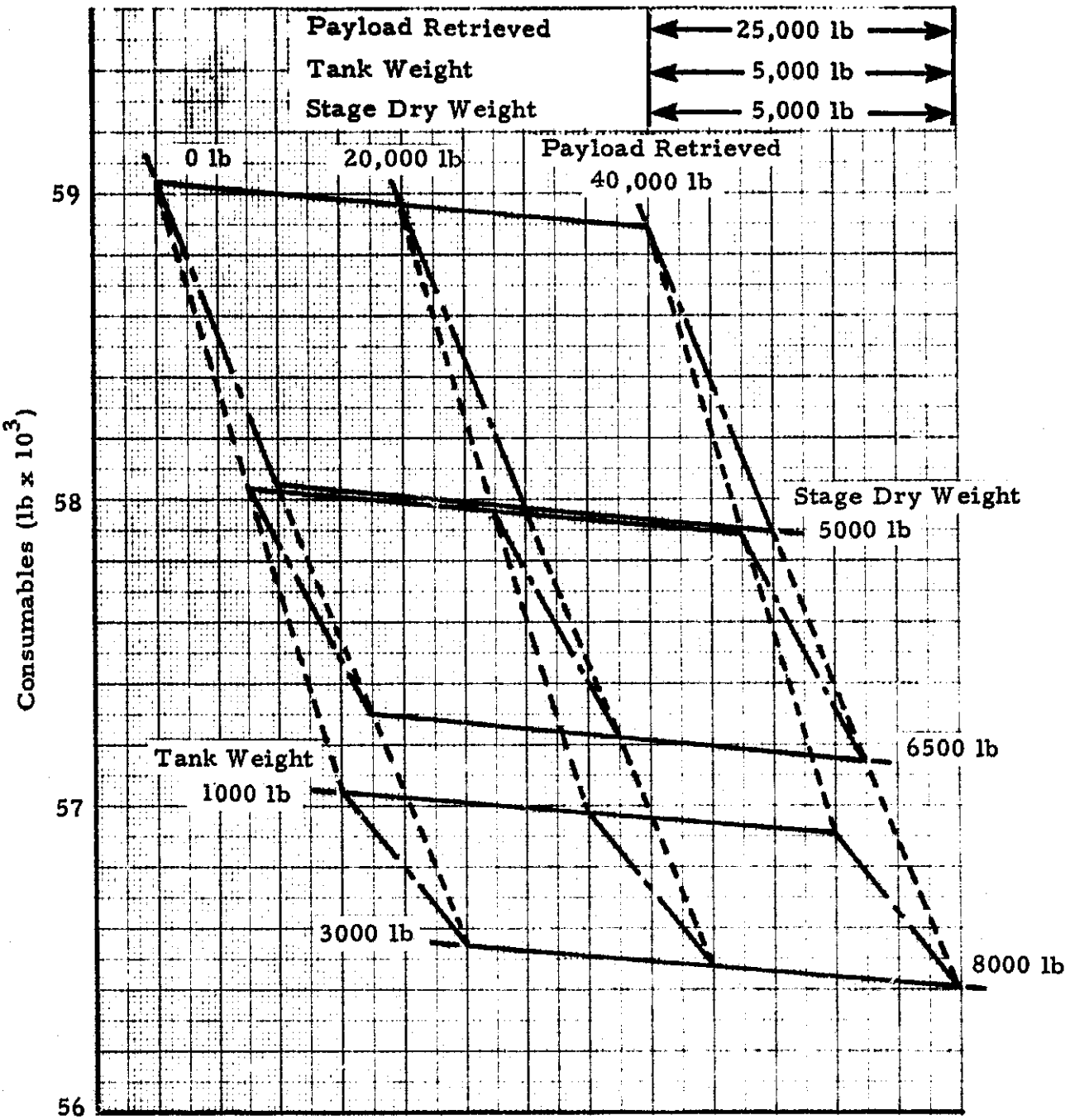

Fig. A-1f (Continued)

ii. Main Engine Consumables

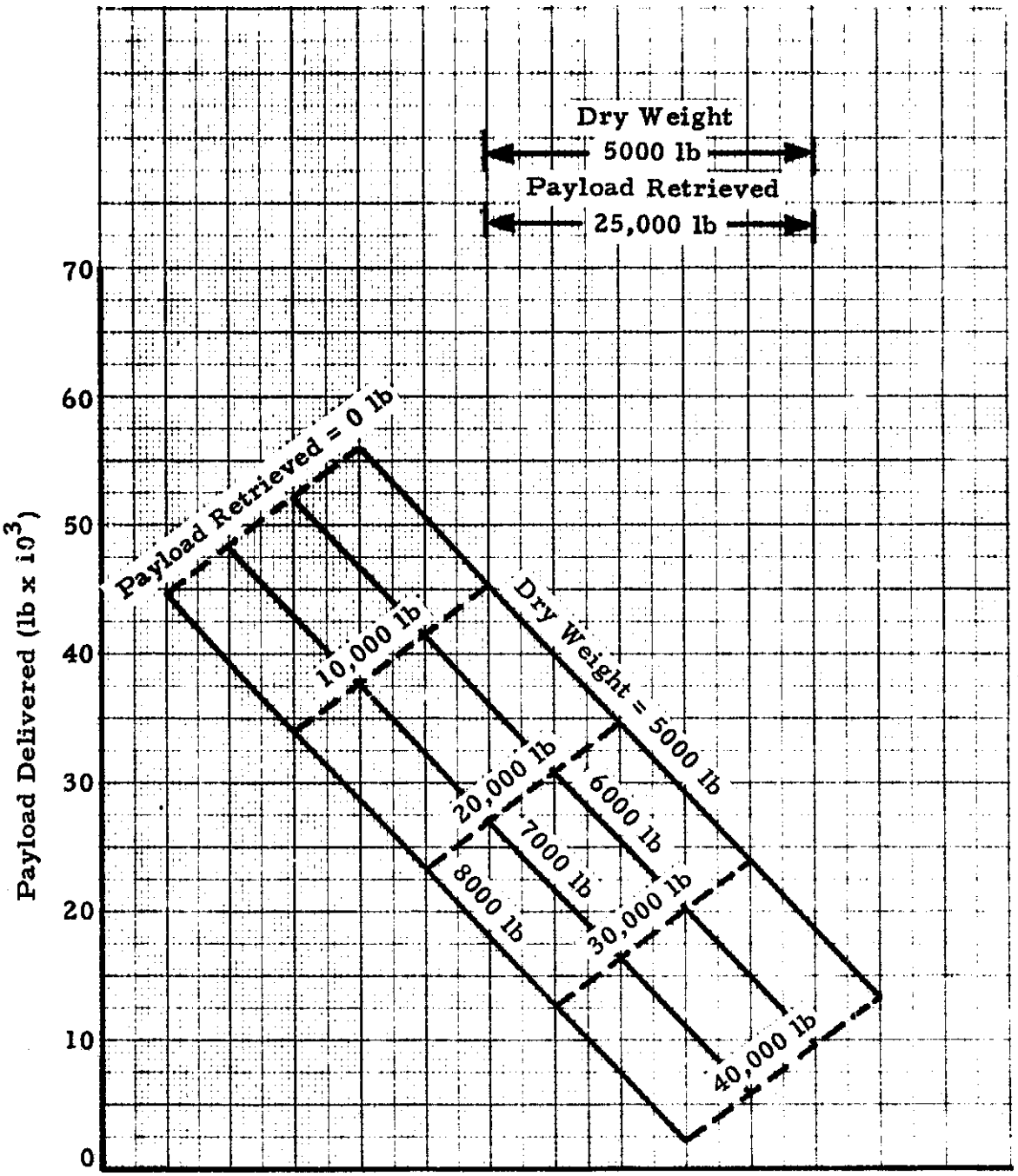

Fig. A-1 (Continued)

g. Two-Stage AMOOS, Three Shuttle Launches

i. Payloads

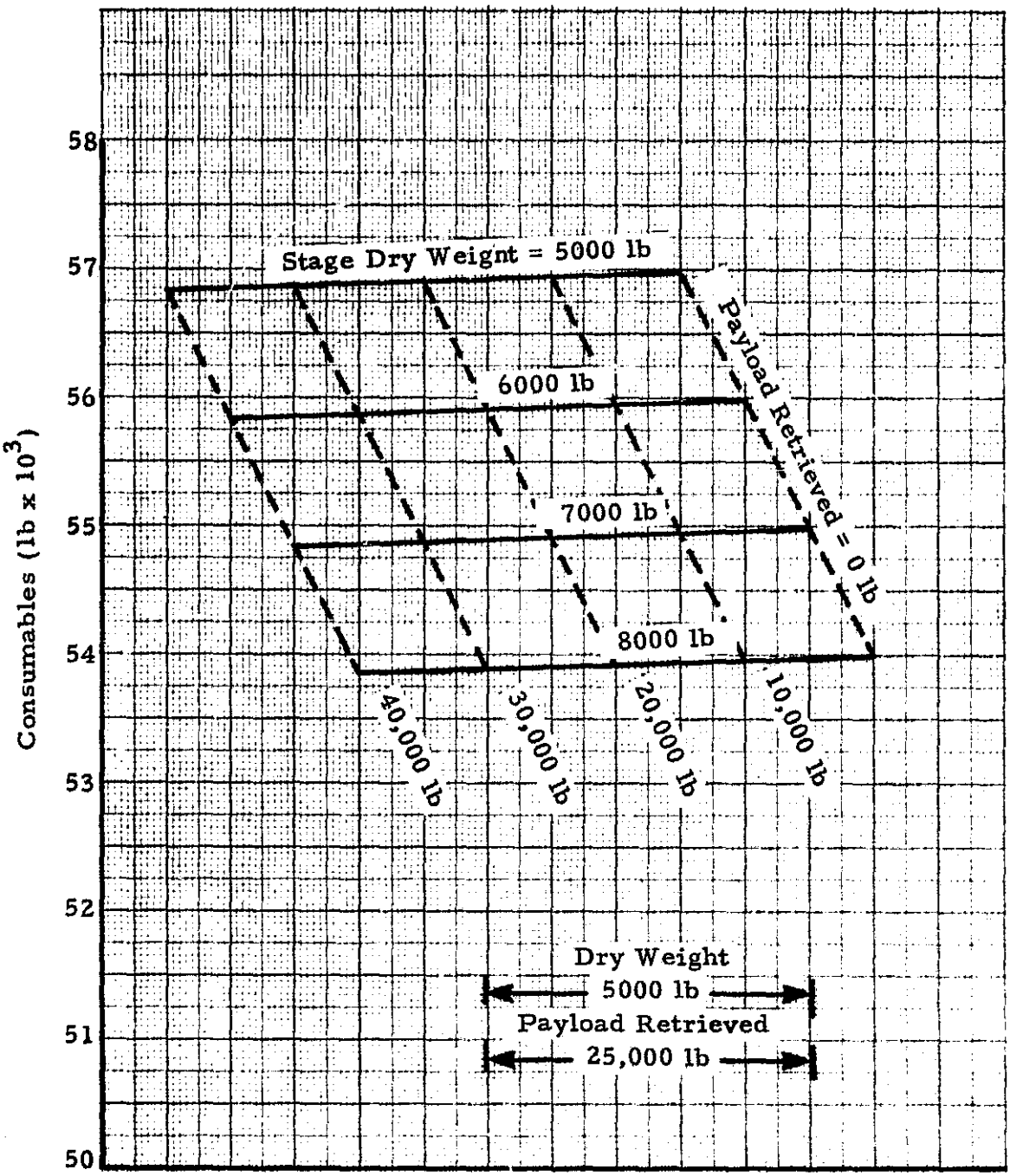

Fig. A-1g (Concluded)

ii. Main Engine Consumables

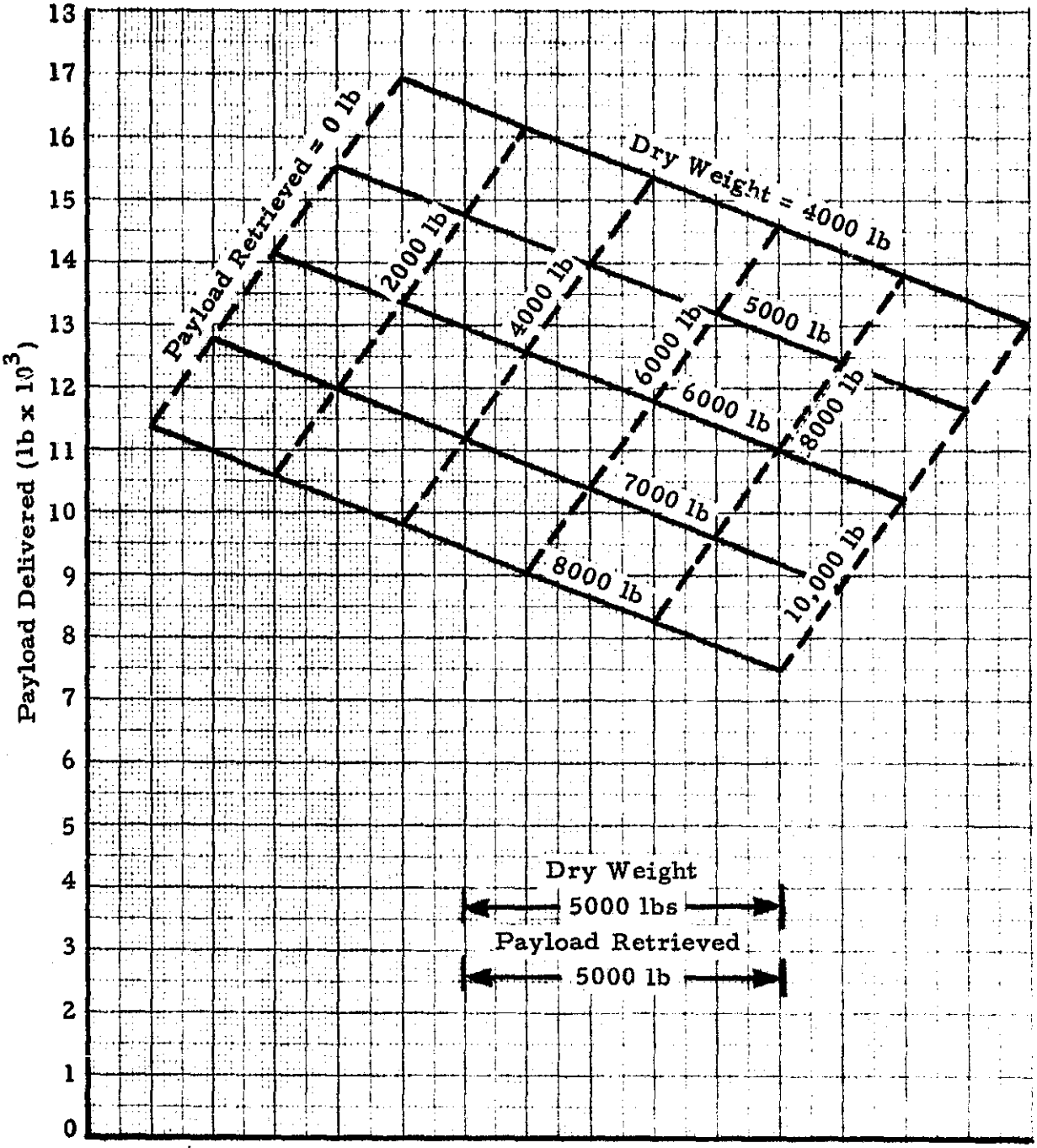

Fig. A-2 - AMOOS Payload and Main Engine Consumables for a Lunar Mission, I_{sp} = 456.5 sec and 65,000 lb Shuttle Payload

a. Single Stage AMOOS, One Shuttle Launch

i. Payloads

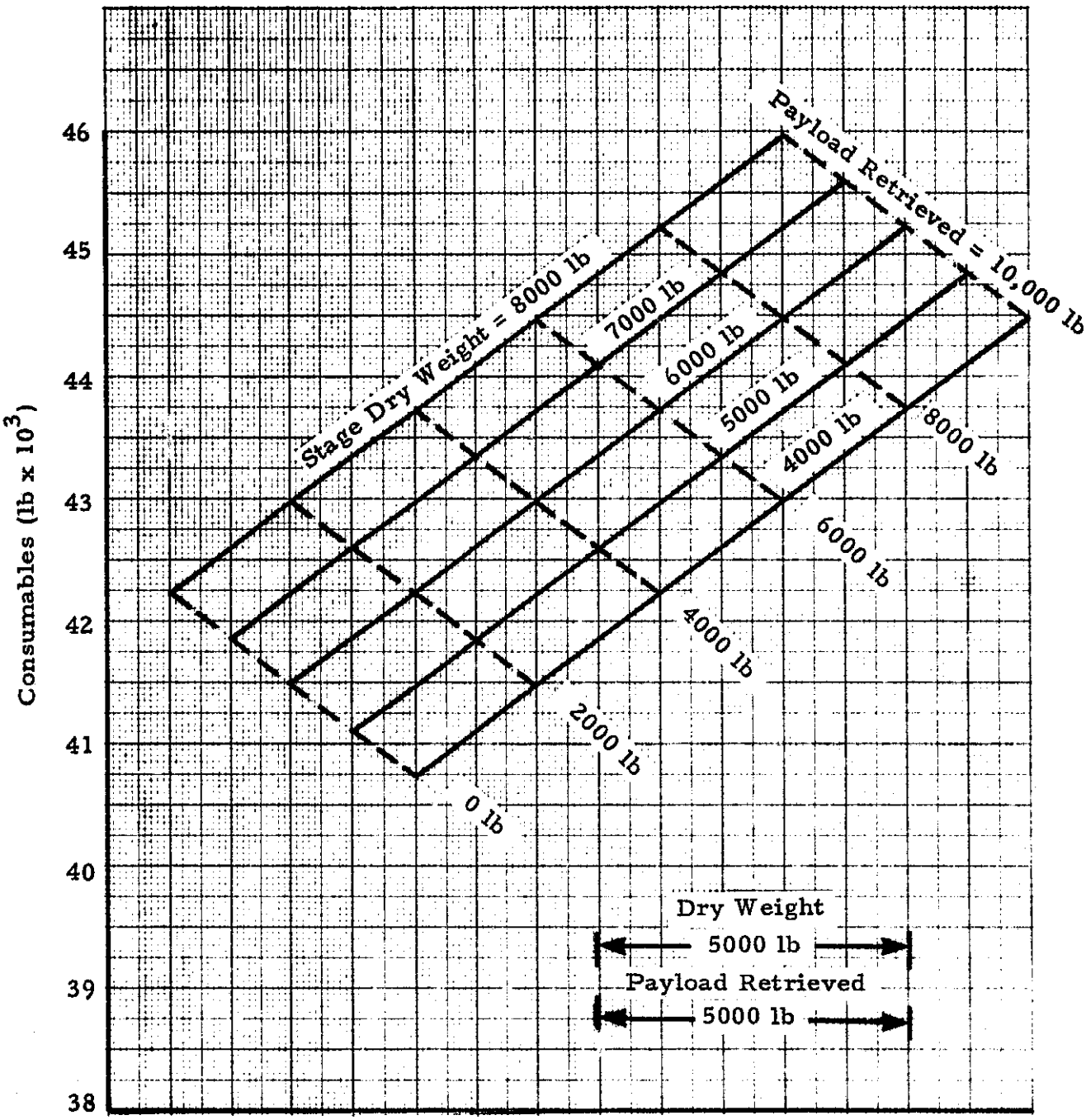

Fig. A-2a (Continued)

ii. Main Engine Consumables

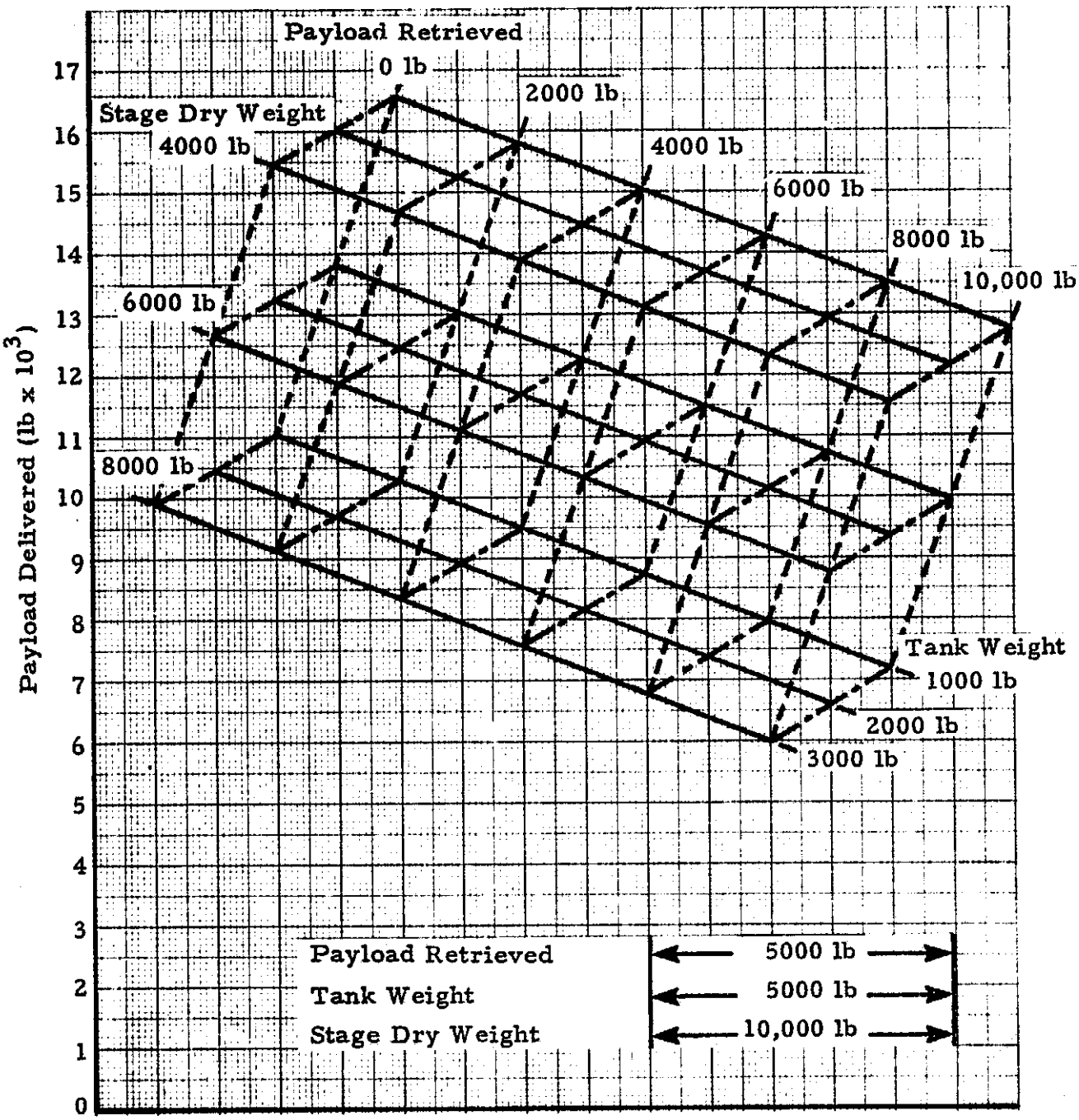

Fig. A-2 (Continued)

b. Stage and One-Half AMOOS, One Shuttle Launch

i. Payloads

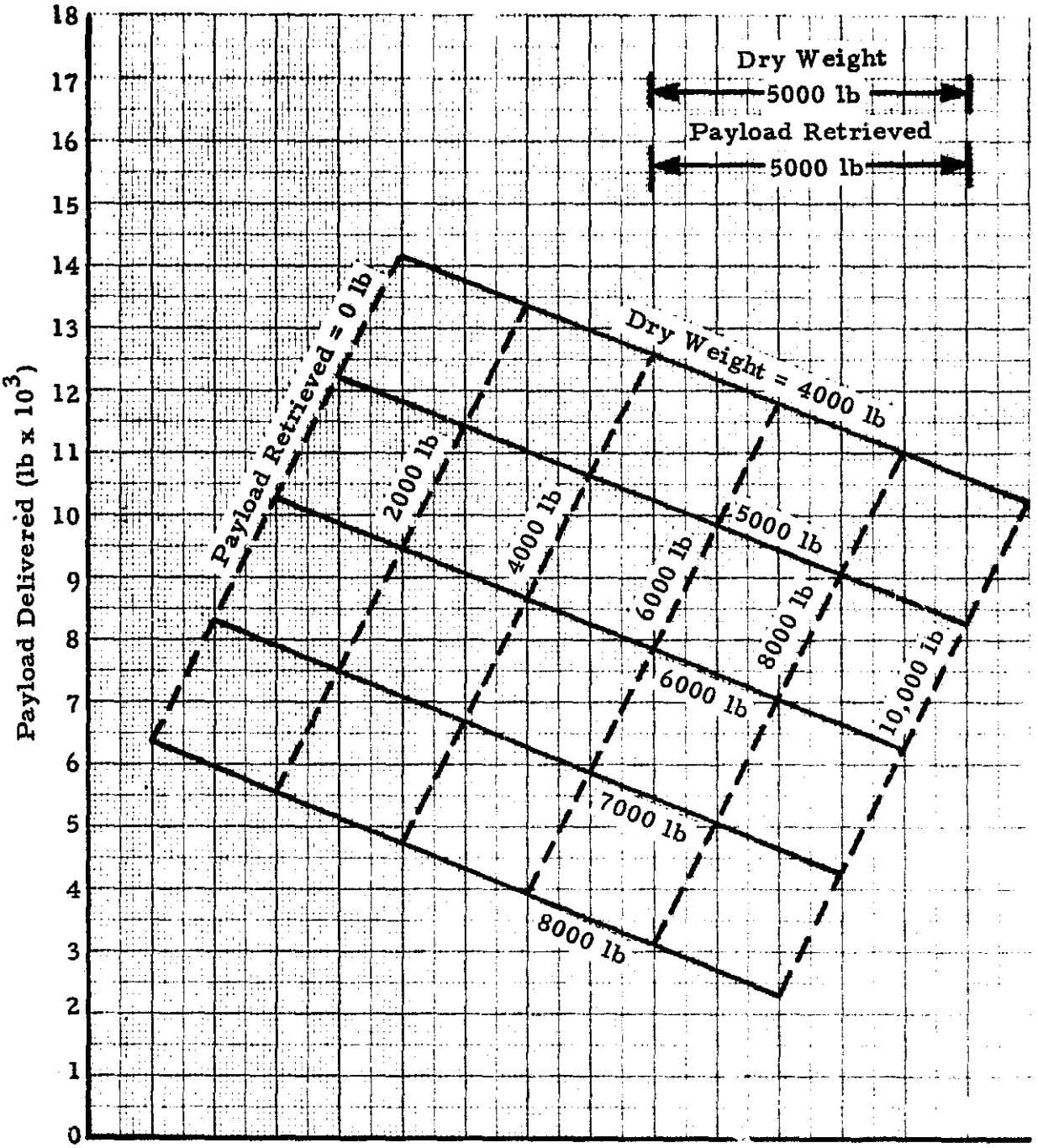

Fig. A-2 (Continued)

c. Two-Stage AMOOS,
One Shuttle Launch

i. Payloads

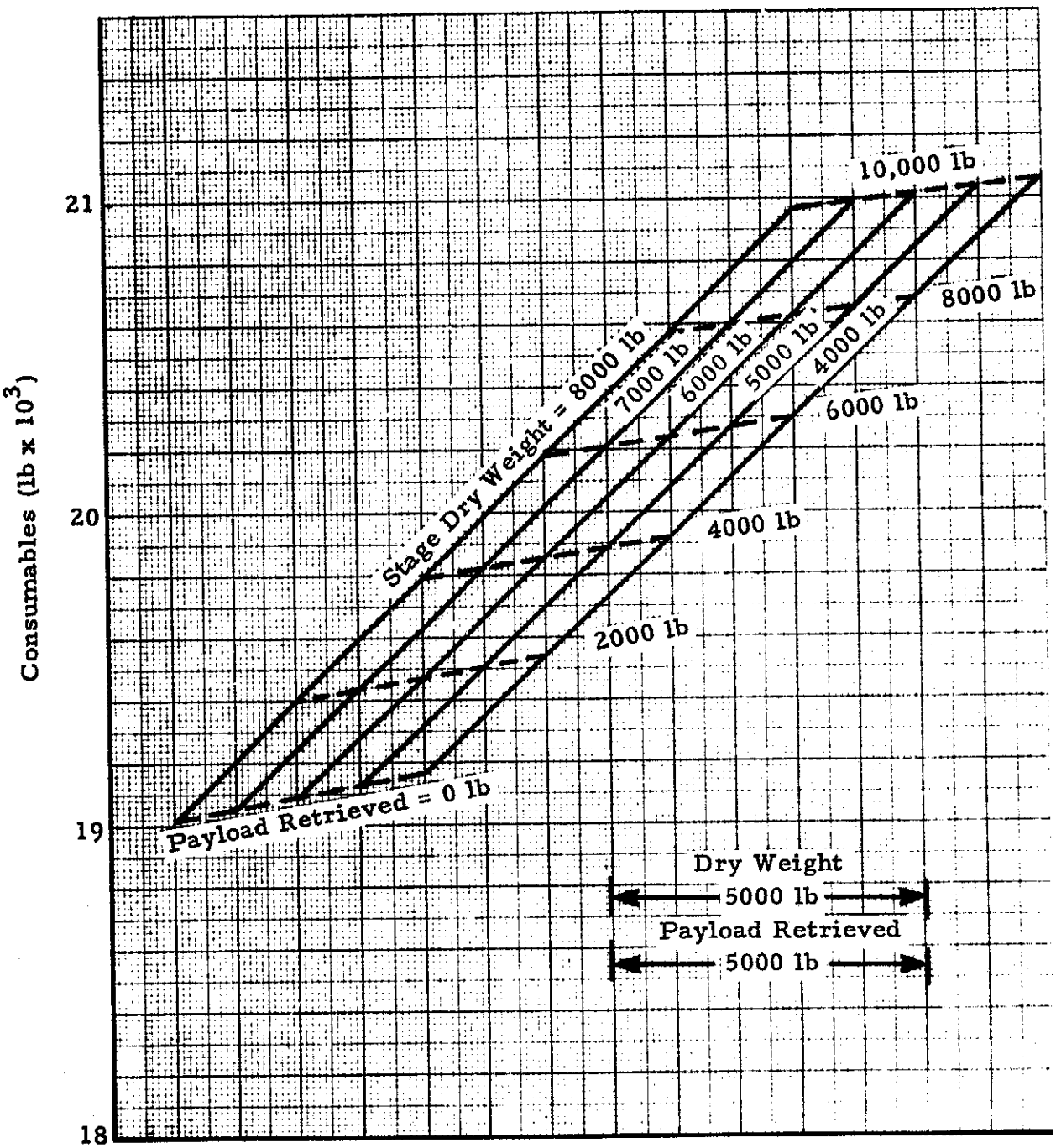

Fig. A-2c (Continued)

ii. Main Engine Consumables

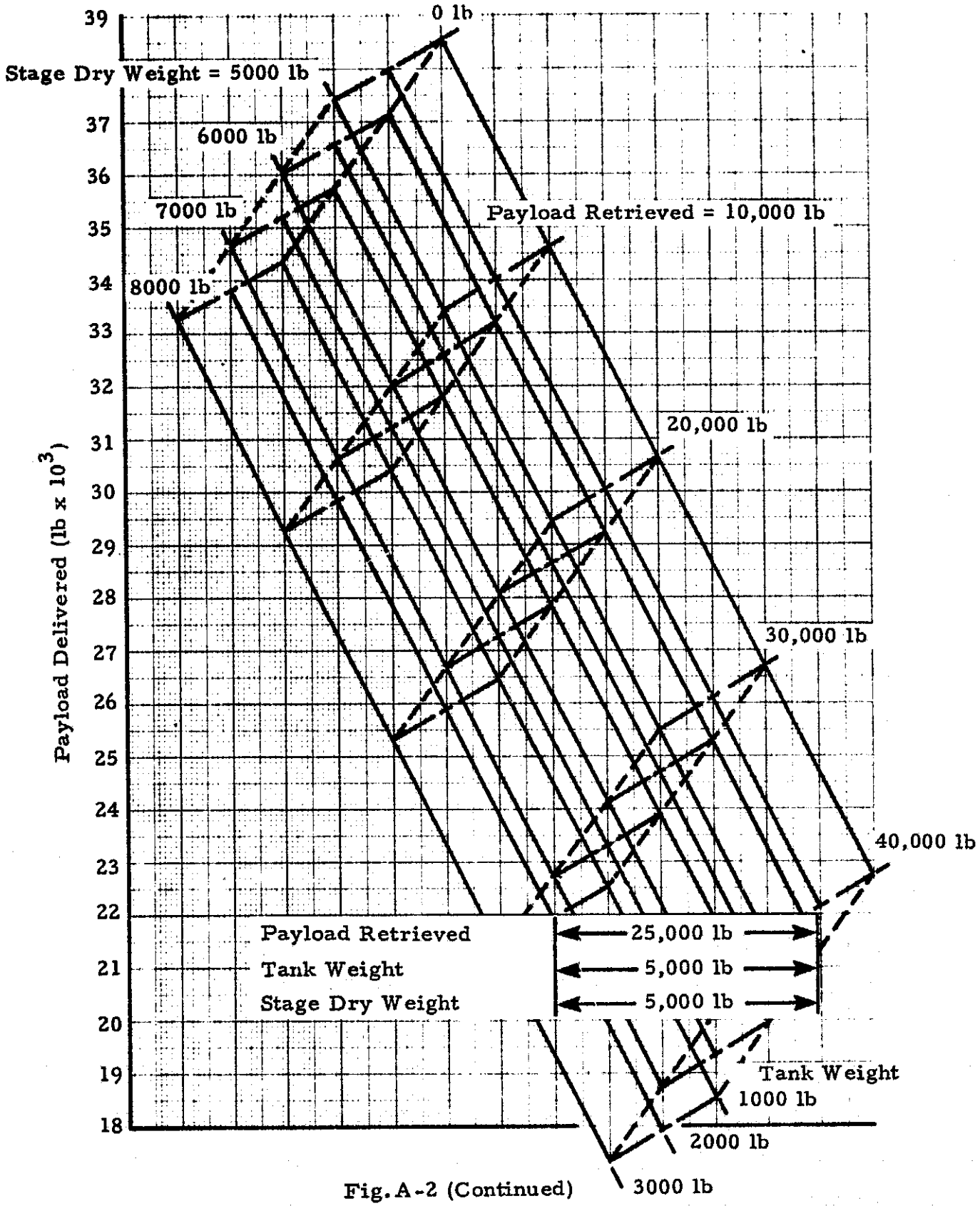

Fig. A-2 (Continued)

d. Stage and One-Half AMOOS, Two Shuttle Launches

i. Payloads

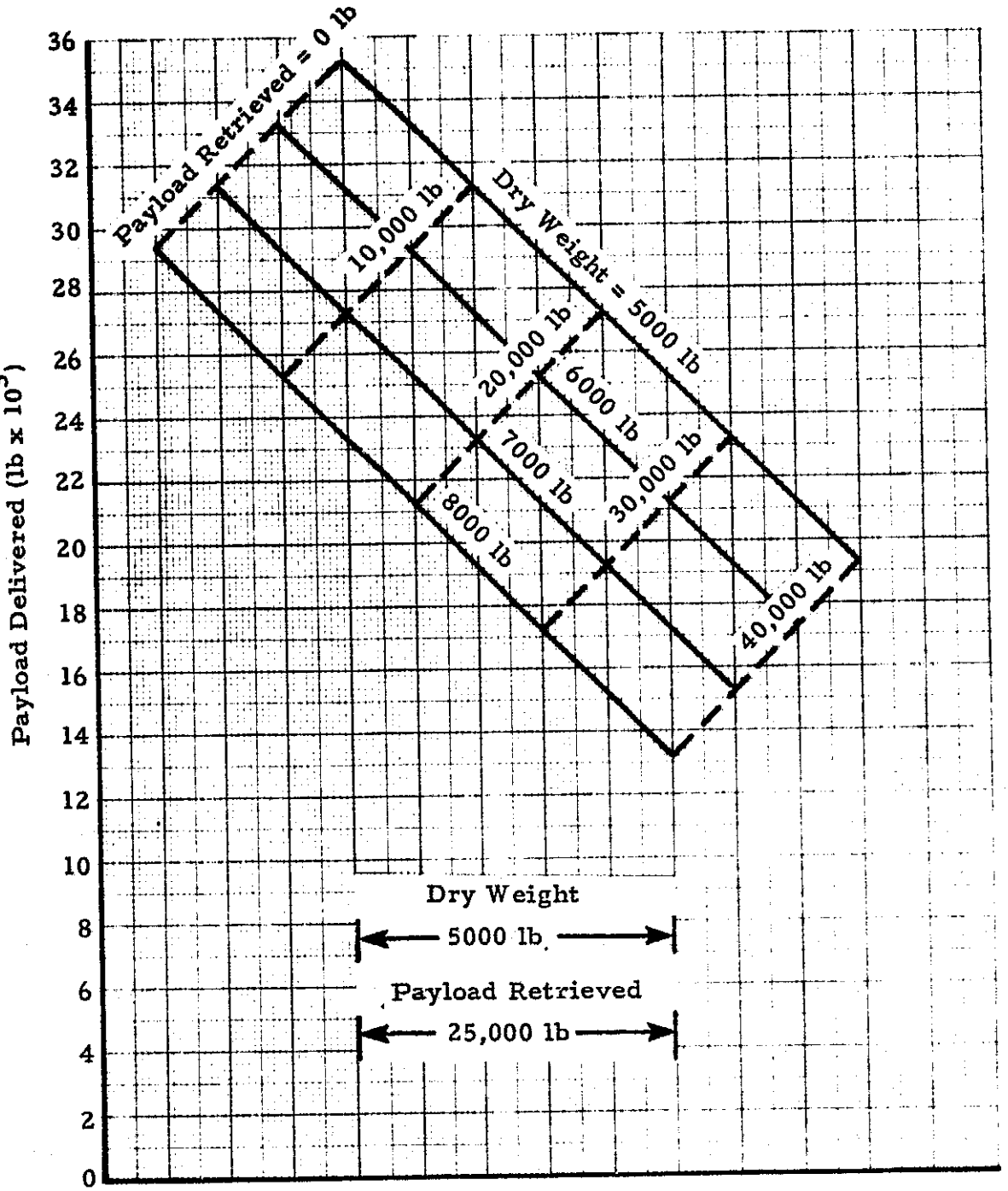

Fig. A-2 (Continued)

e. Two-Stage AMOOS,
Two Shuttle Launches

i. Payloads

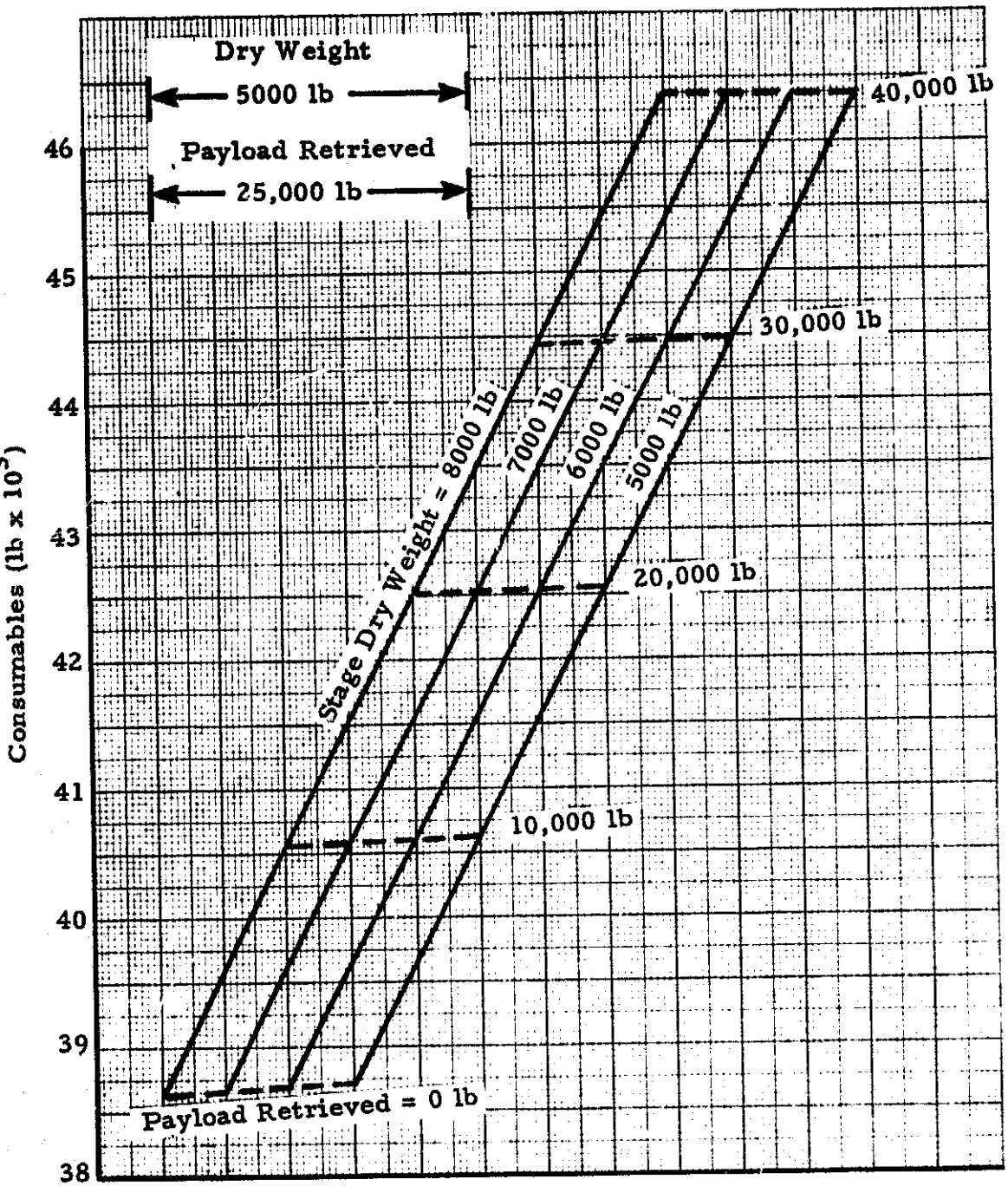

Fig. A-2e (Continued)

ii. Main Engine Consumables

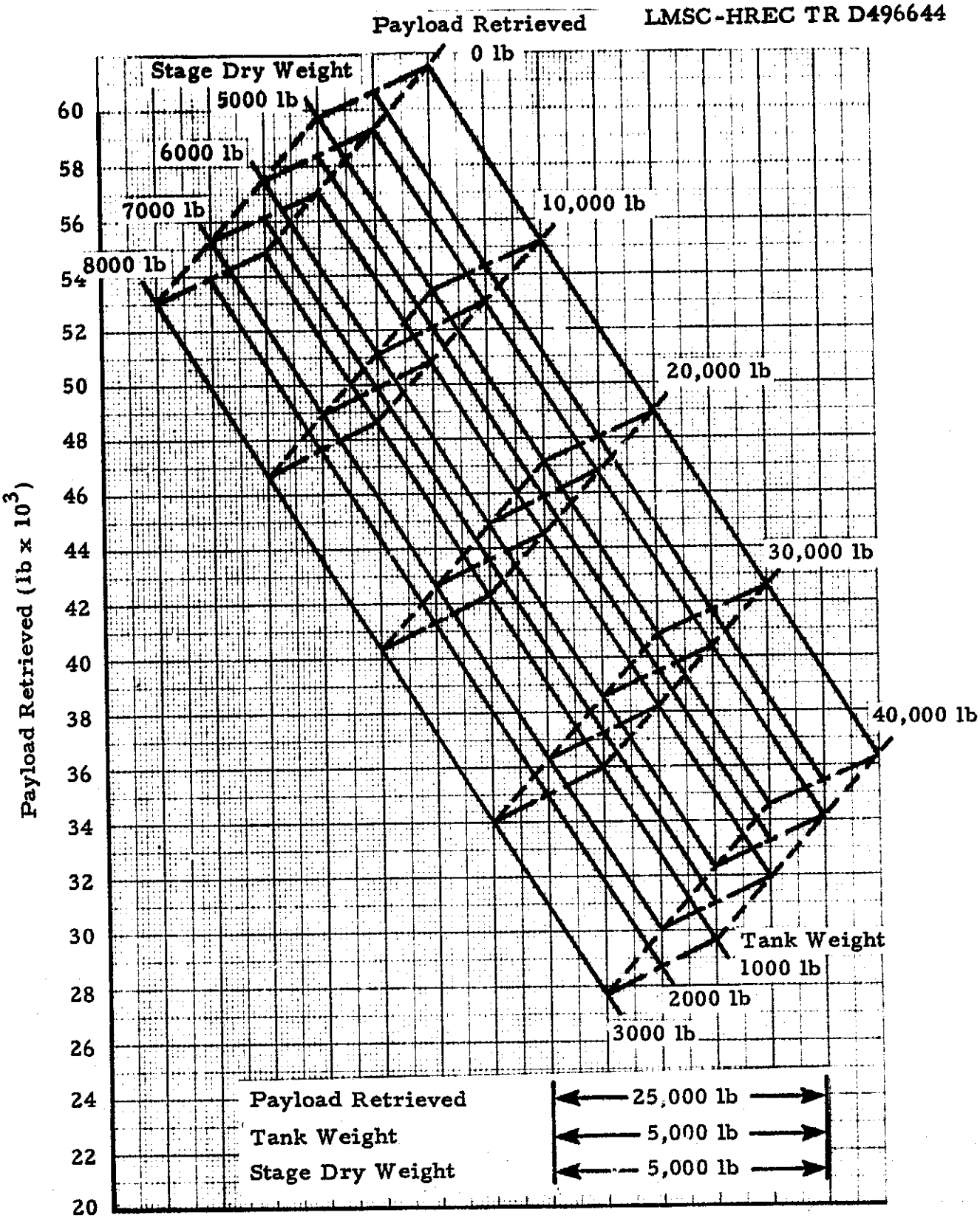

Fig. A-2 (Continued)

f. Stage and One-Half AMOOS, Three Shuttle Launches

i. Payloads

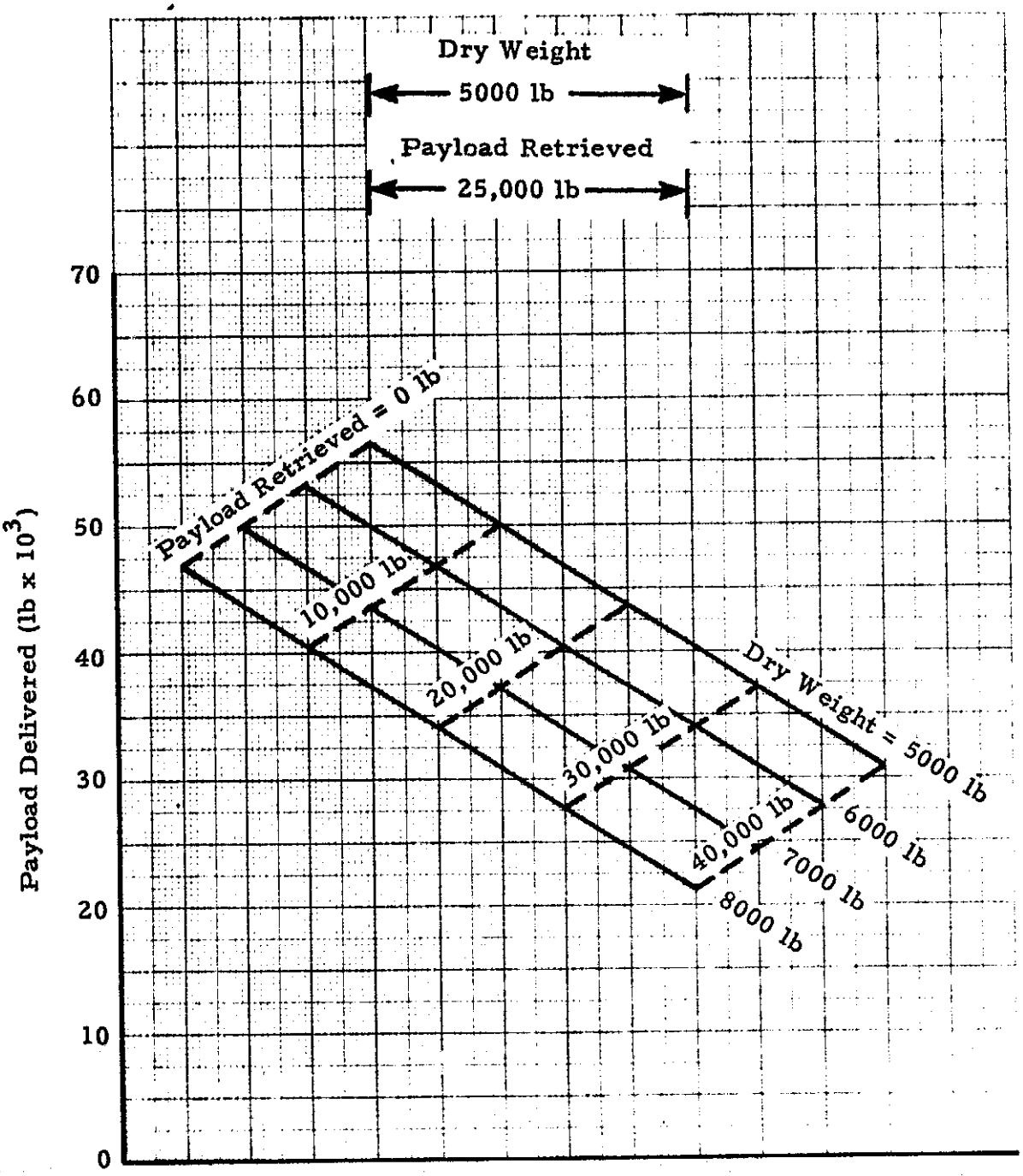

Fig. A-2 (Continued)

g. Two-Stage AMOOS, Three Shuttle Launches

i. Payloads

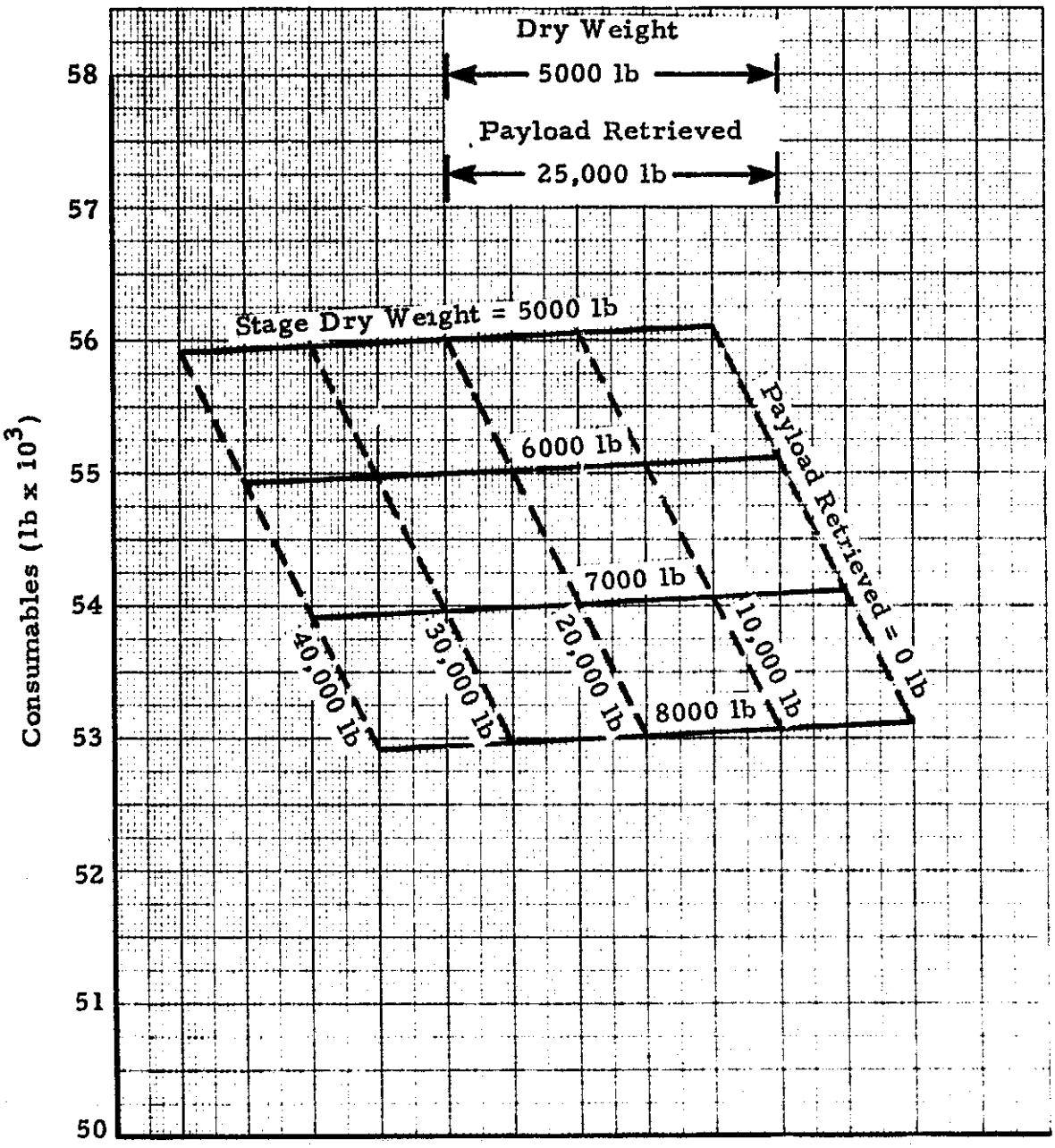

Fig. A-2g (Concluded)

ii. Main Engine Consumables

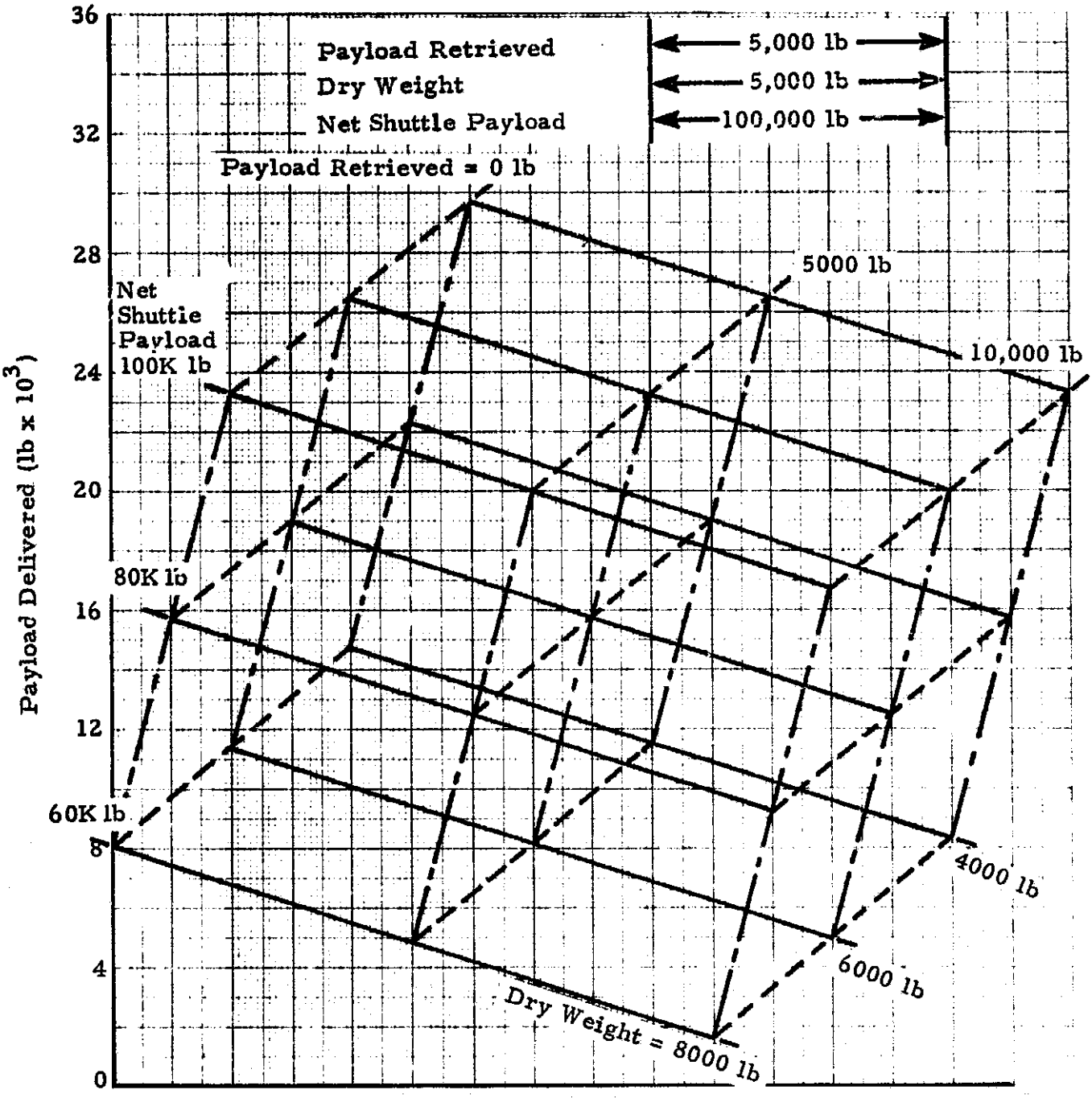

Fig. A-3 - AMOOS Payloads and Main Engine Consumables to a Geosynchronous Orbit, I_{sp} = 456.5 sec

a. Single Stage AMOOS, One Shuttle Launch

i. Payloads

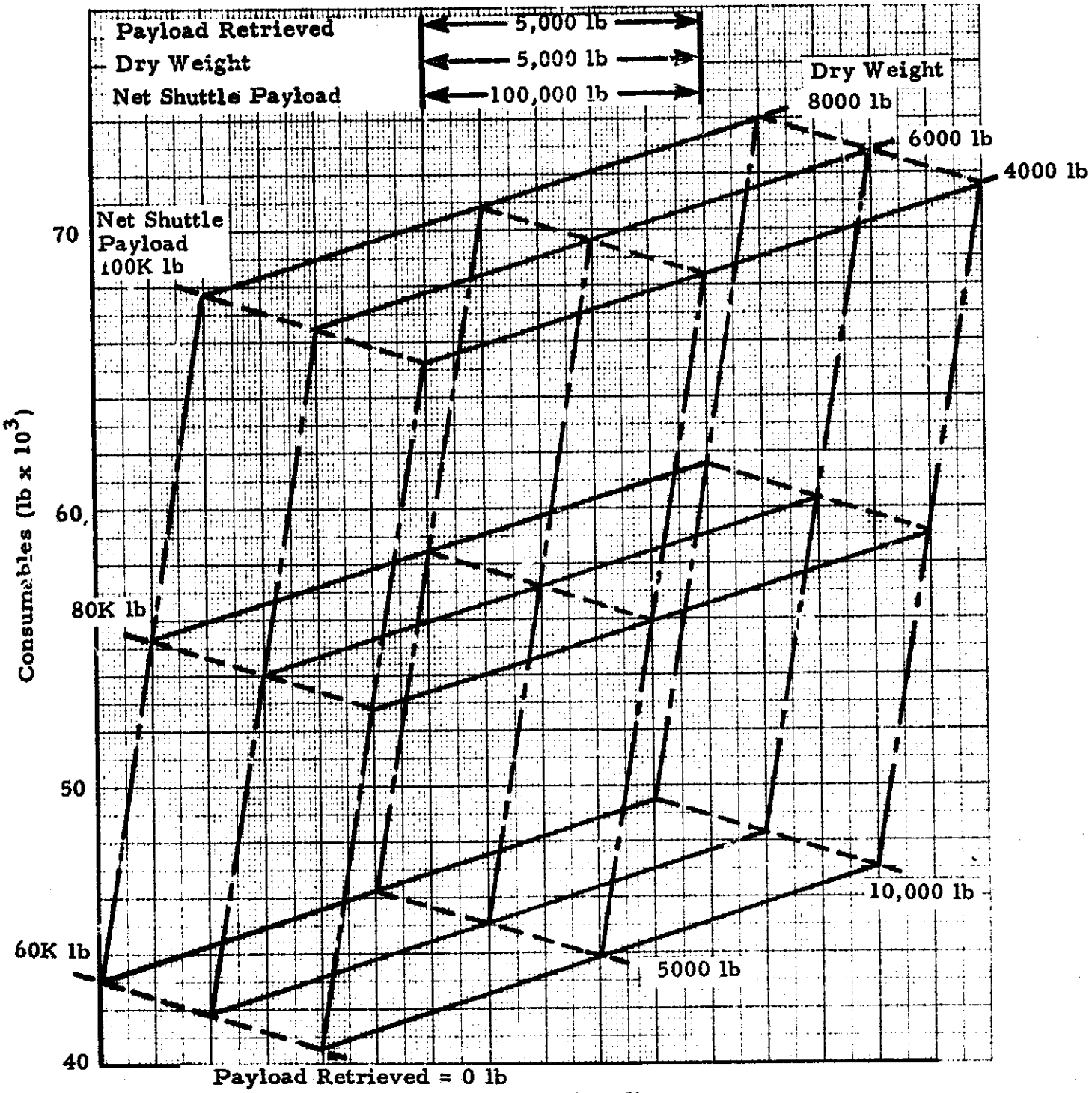

Fig. A-3a (Continued)

ii. Main Engine Consumables

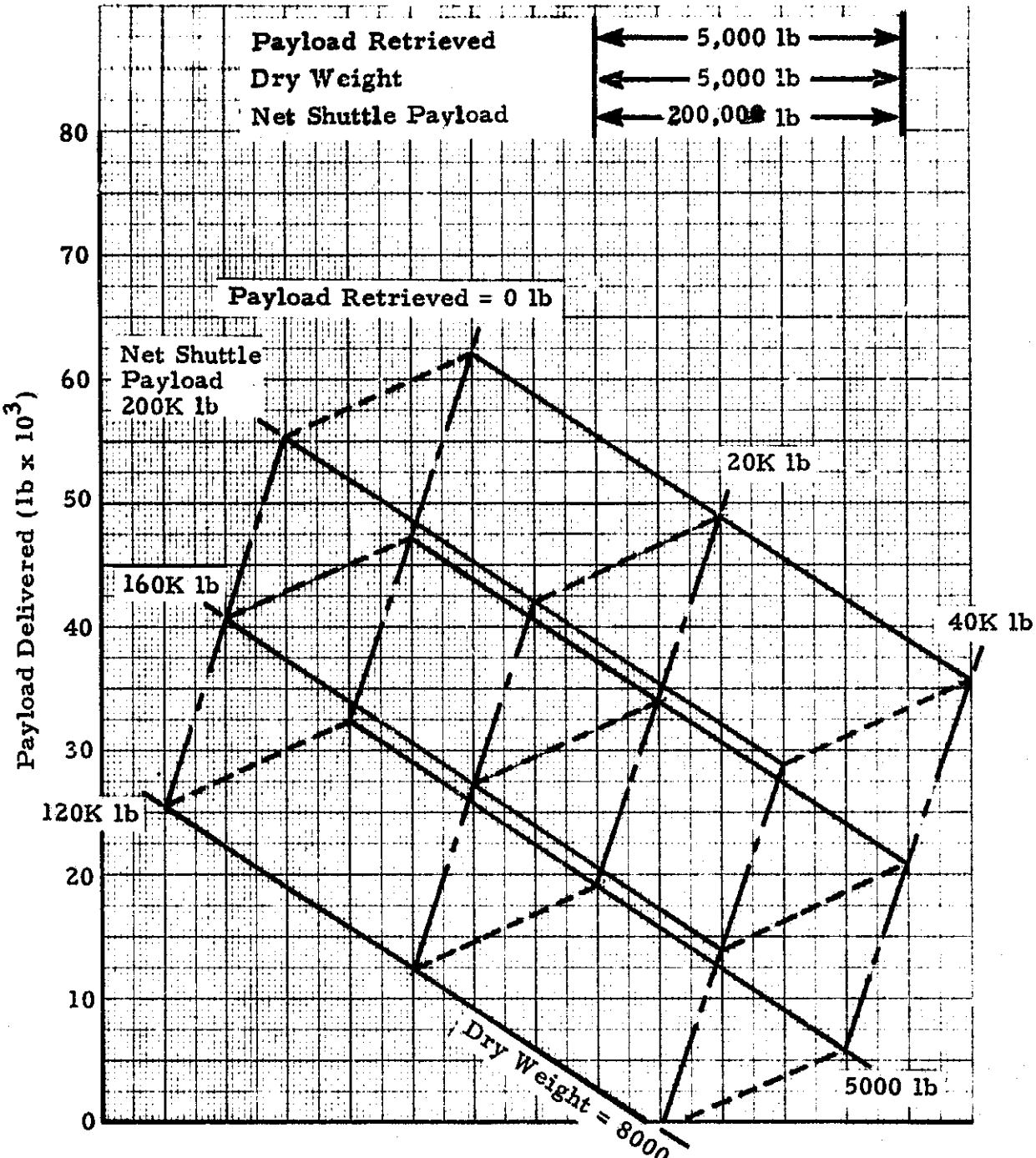

Fig. A-3 (Continued)

b. Two-Stage AMOOS, Two Shuttle Launches

i. Payloads

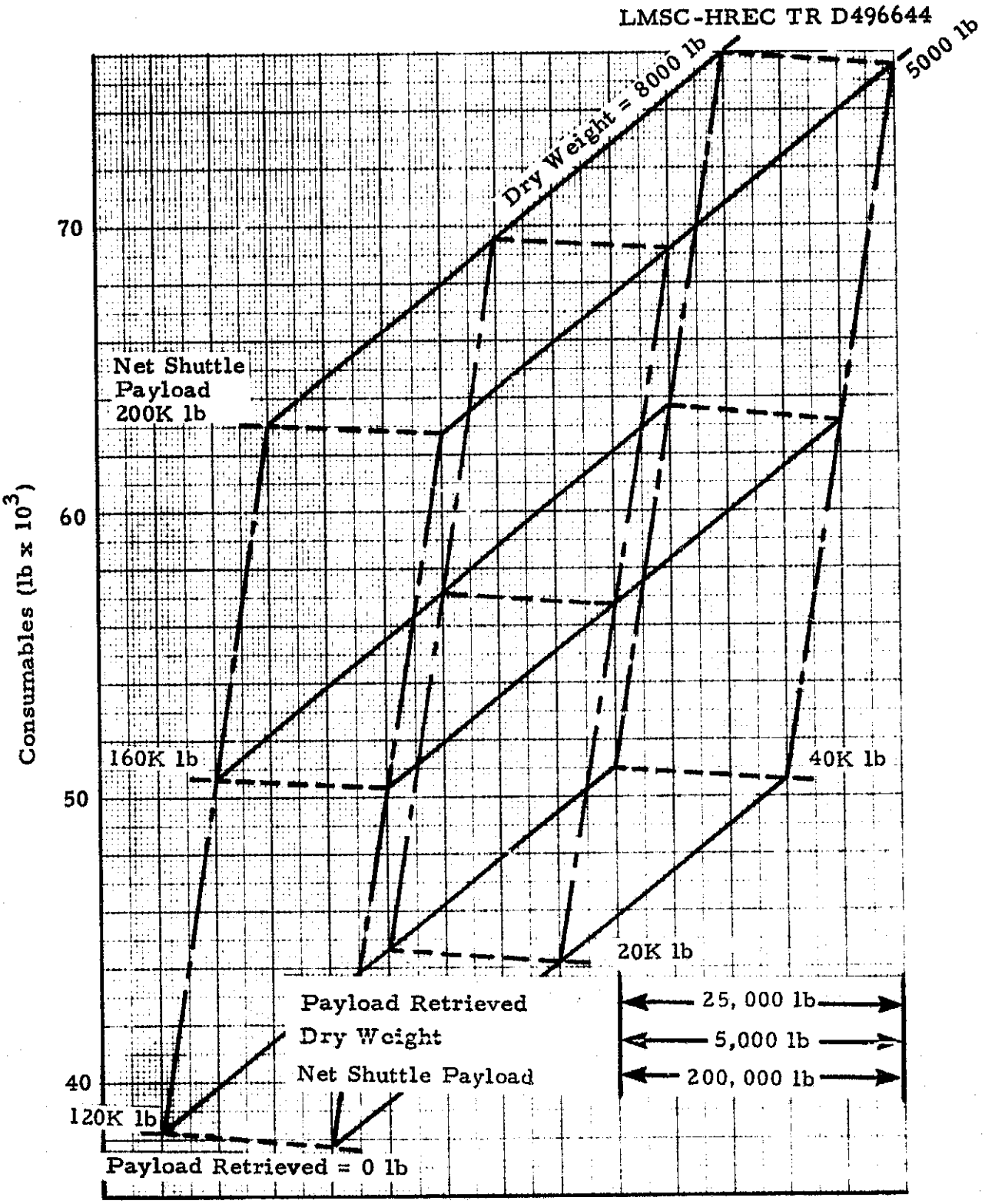

Fig. A-3b (Continued)

ii. Main Engine Consumables

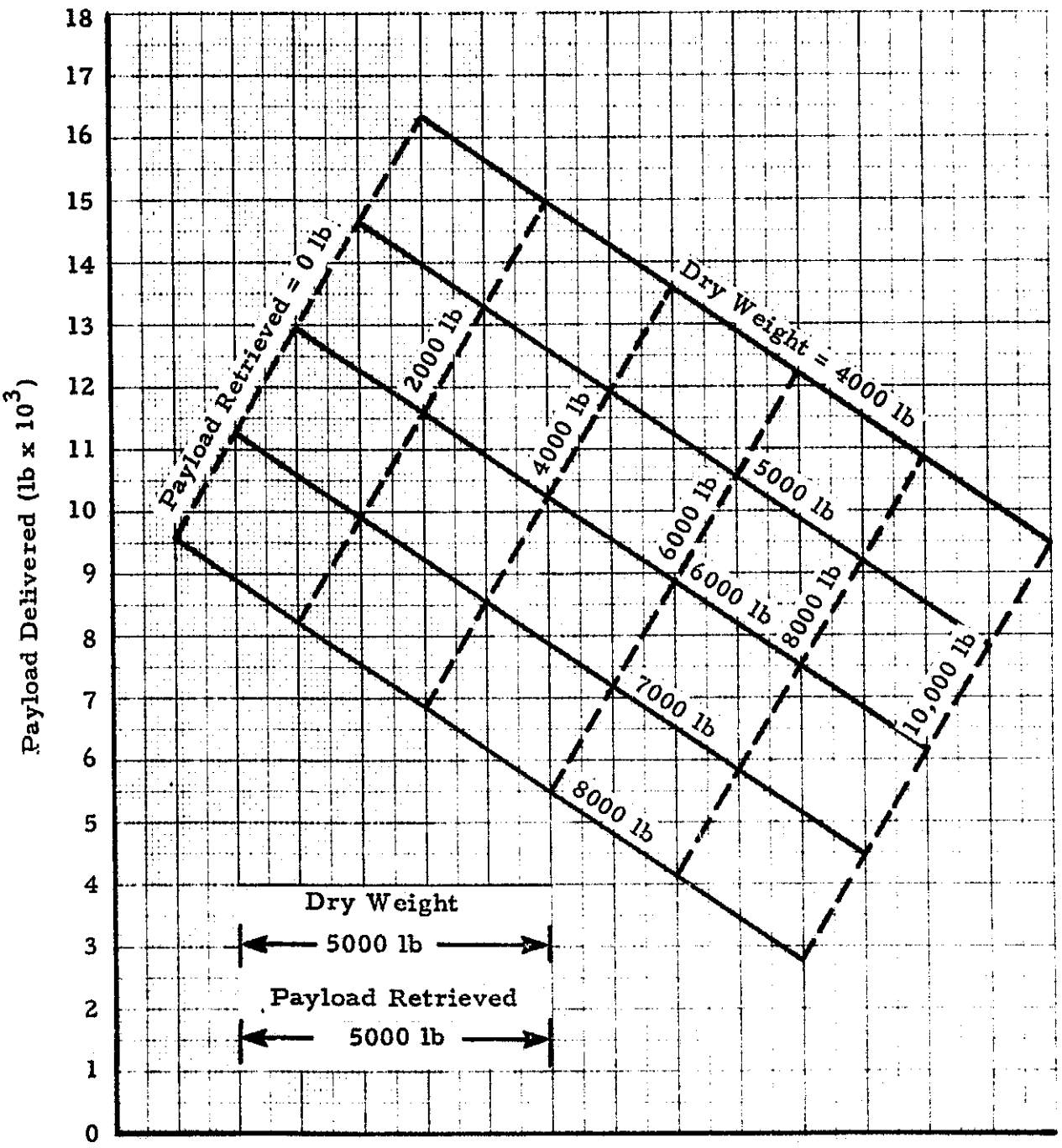

Fig. A-4 - AMOOS Payloads to a 15,000 n.mi. Circular Equatorial Orbit, I_{sp} = 456.5 sec and 65,000 lb Payload Shuttle

a. Single Stage AMOOS, One-Shuttle Launch

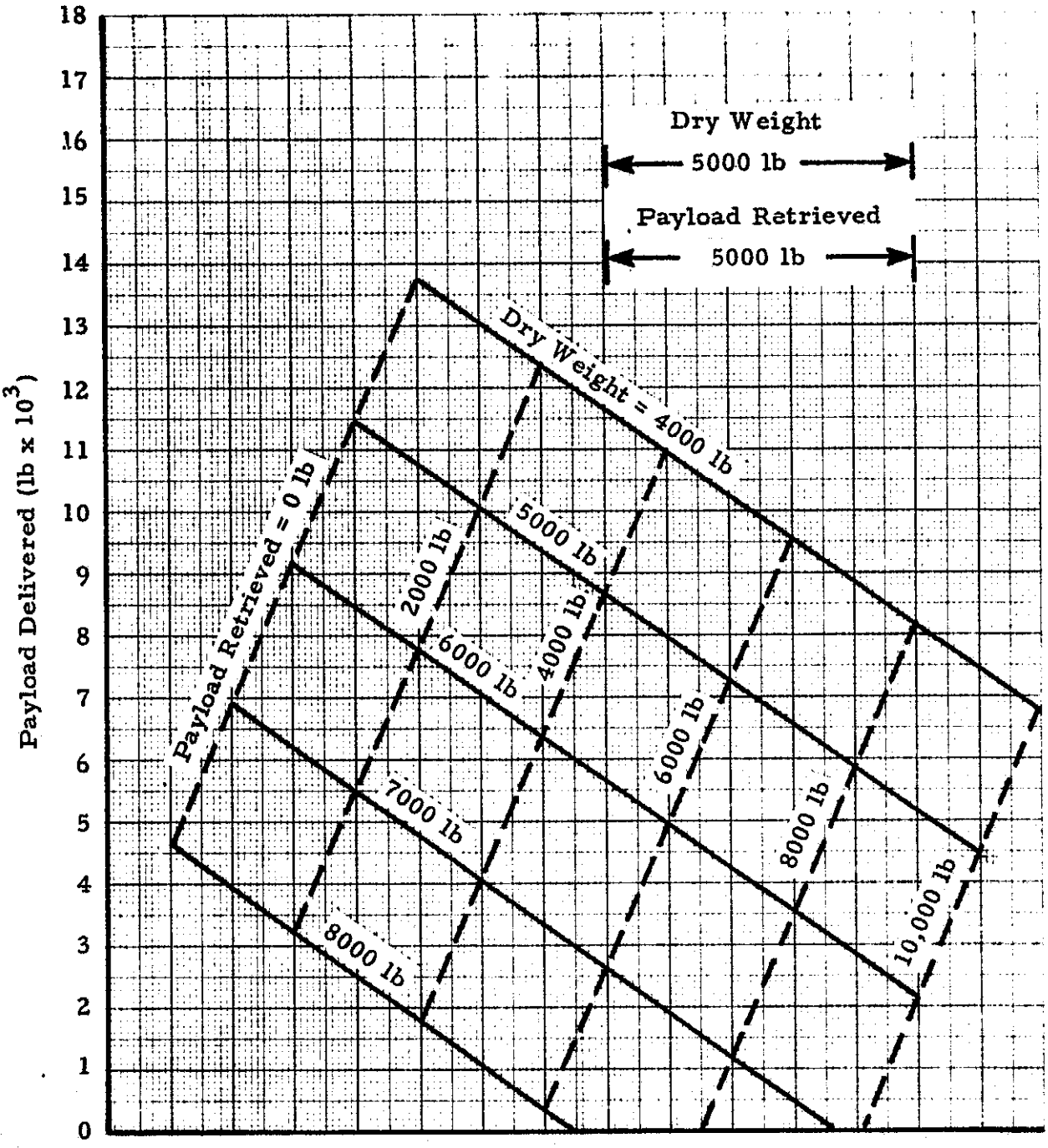

Fig. A-4 (Continued)

b. Two Stage AMOOS,
One Shuttle Launch

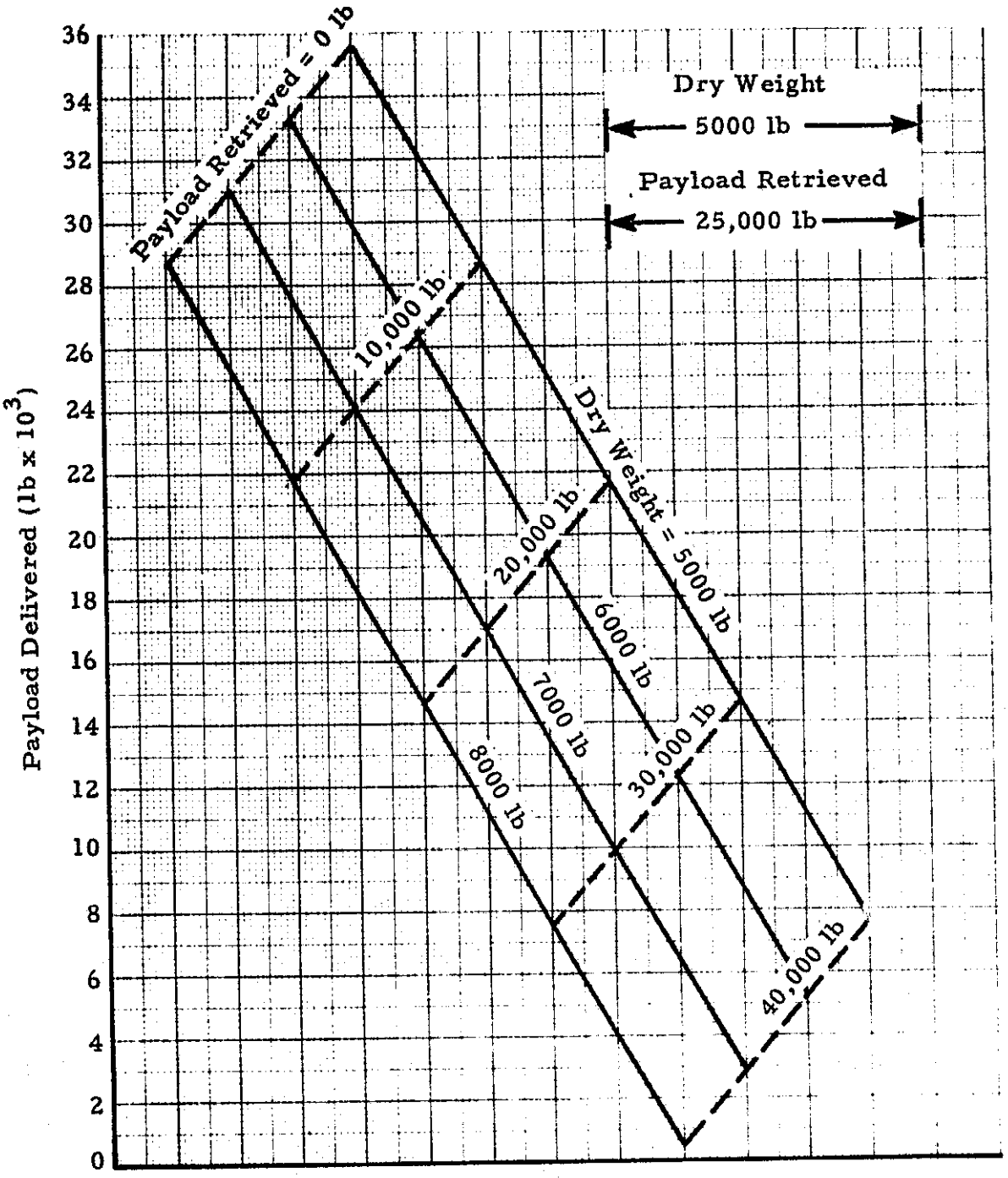

Fig. A-4 (Continued)

c. Two-Stage AMOOS,
Two Shuttle Launches

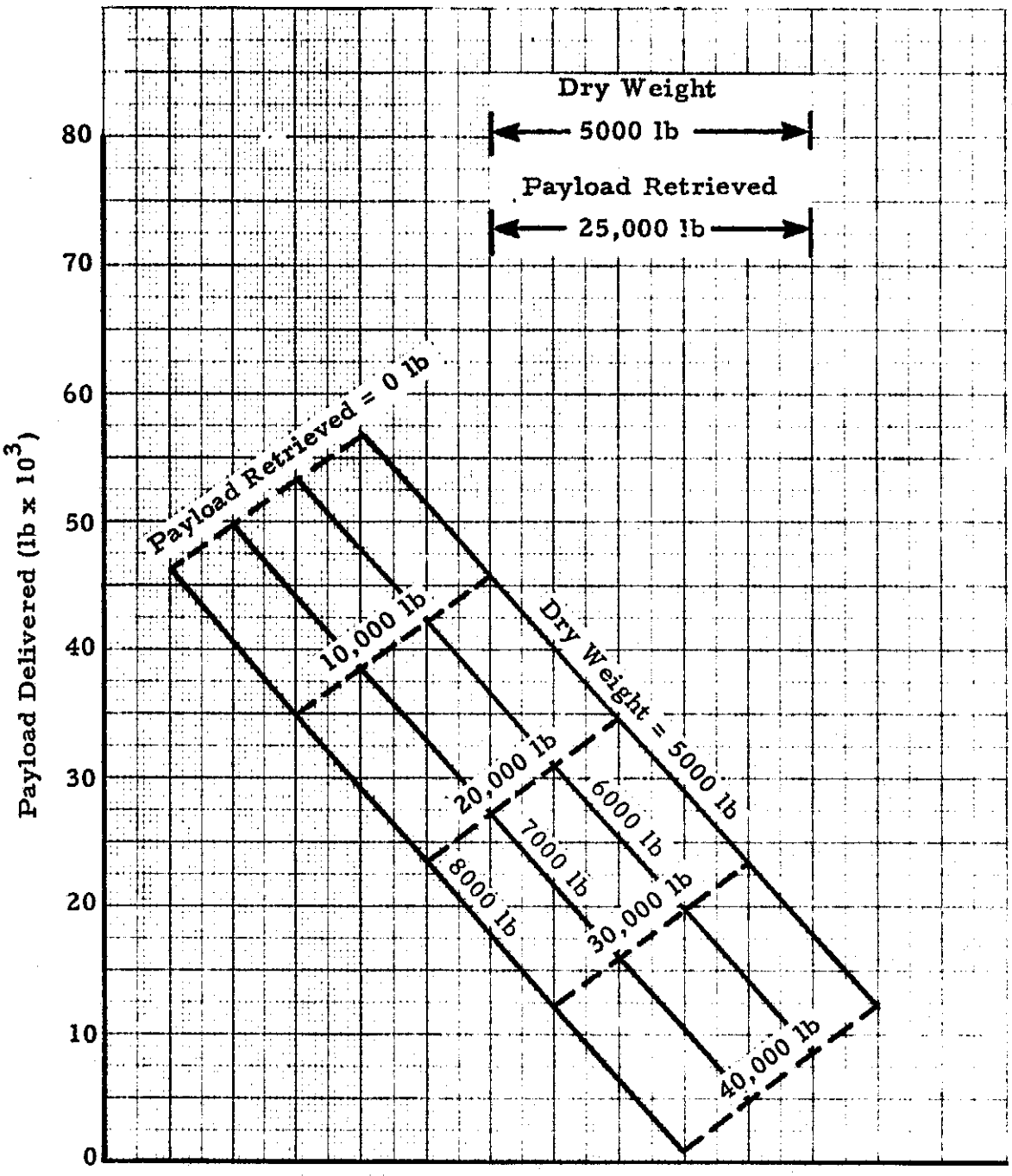

Fig. A-4 (Concluded)

d. Two-Stage AMOOS,
Three Shuttle Launches

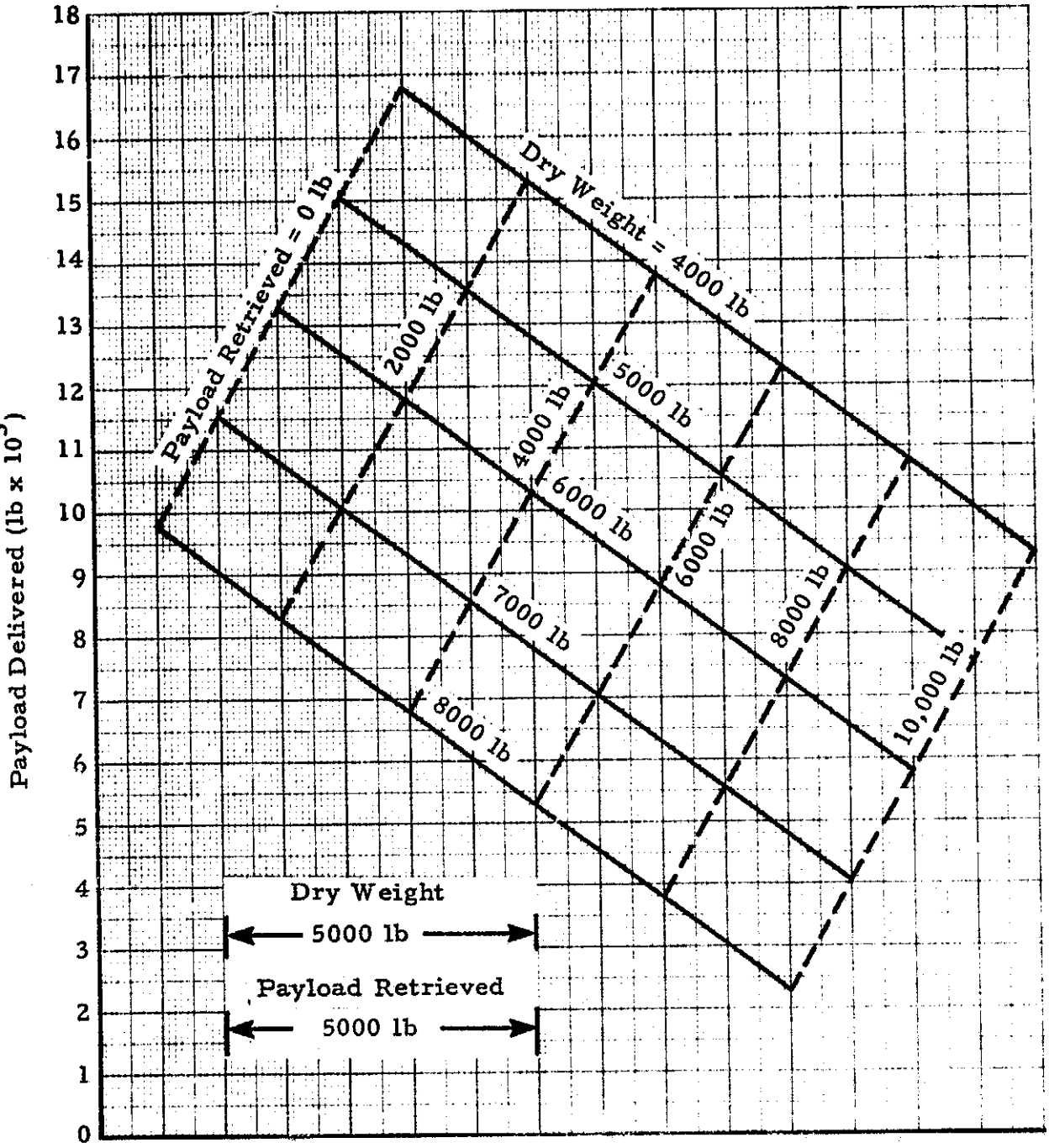

Fig. A-5 - AMOOS Payloads to a 10,000 n.mi. Circular Equatorial Orbit, I_{sp} = 456.5 sec and 65,000 lb Payload Shuttle

a. Single Stage AMOOS, One Shuttle Launch

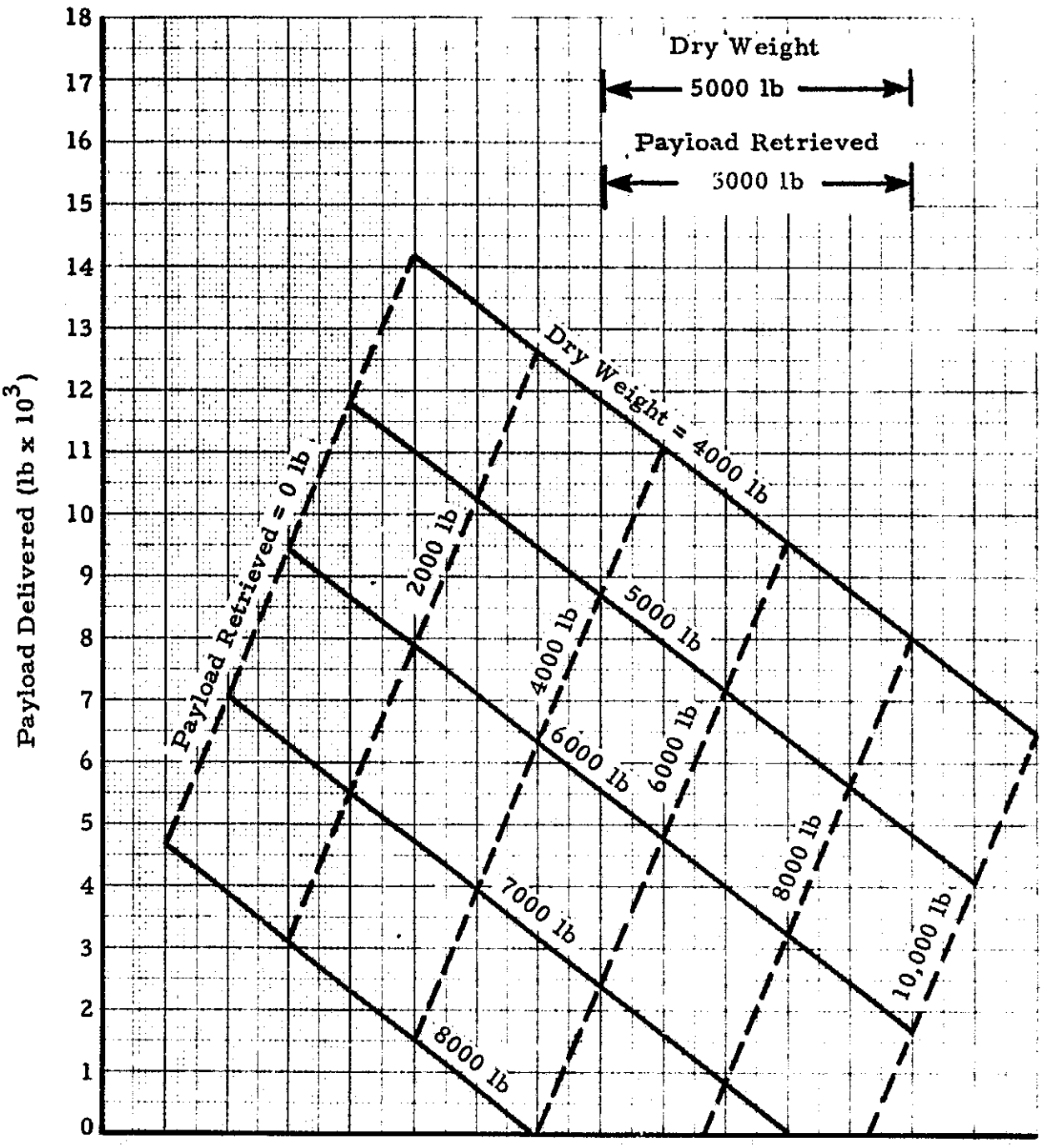

Fig. A-5 (Continued)

b. Two-Stage AMOOS,
One Shuttle Launch

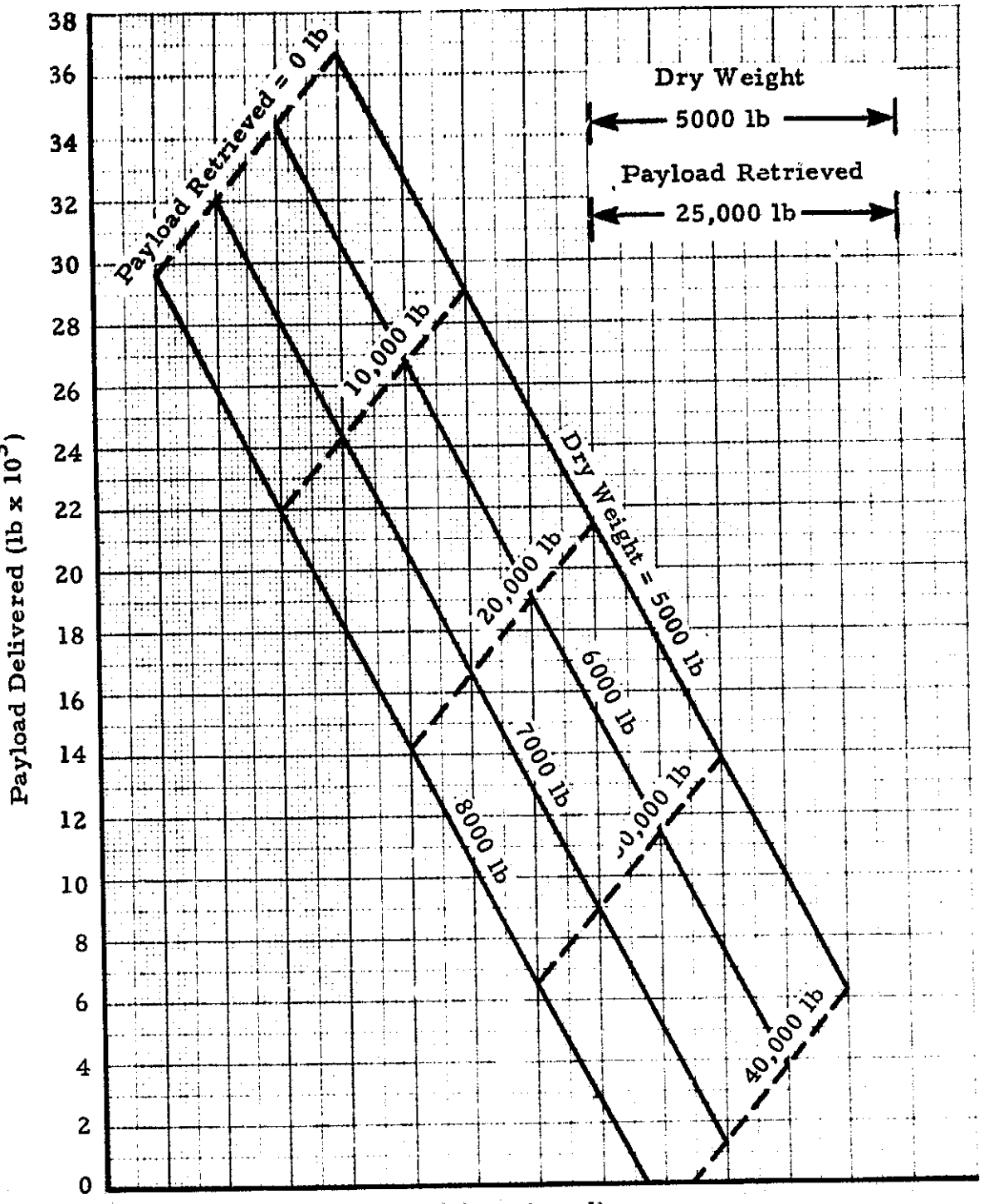

Fig. A-5 (Continued)

c. Two-Stage AMOOS,
Two Shuttle Launches

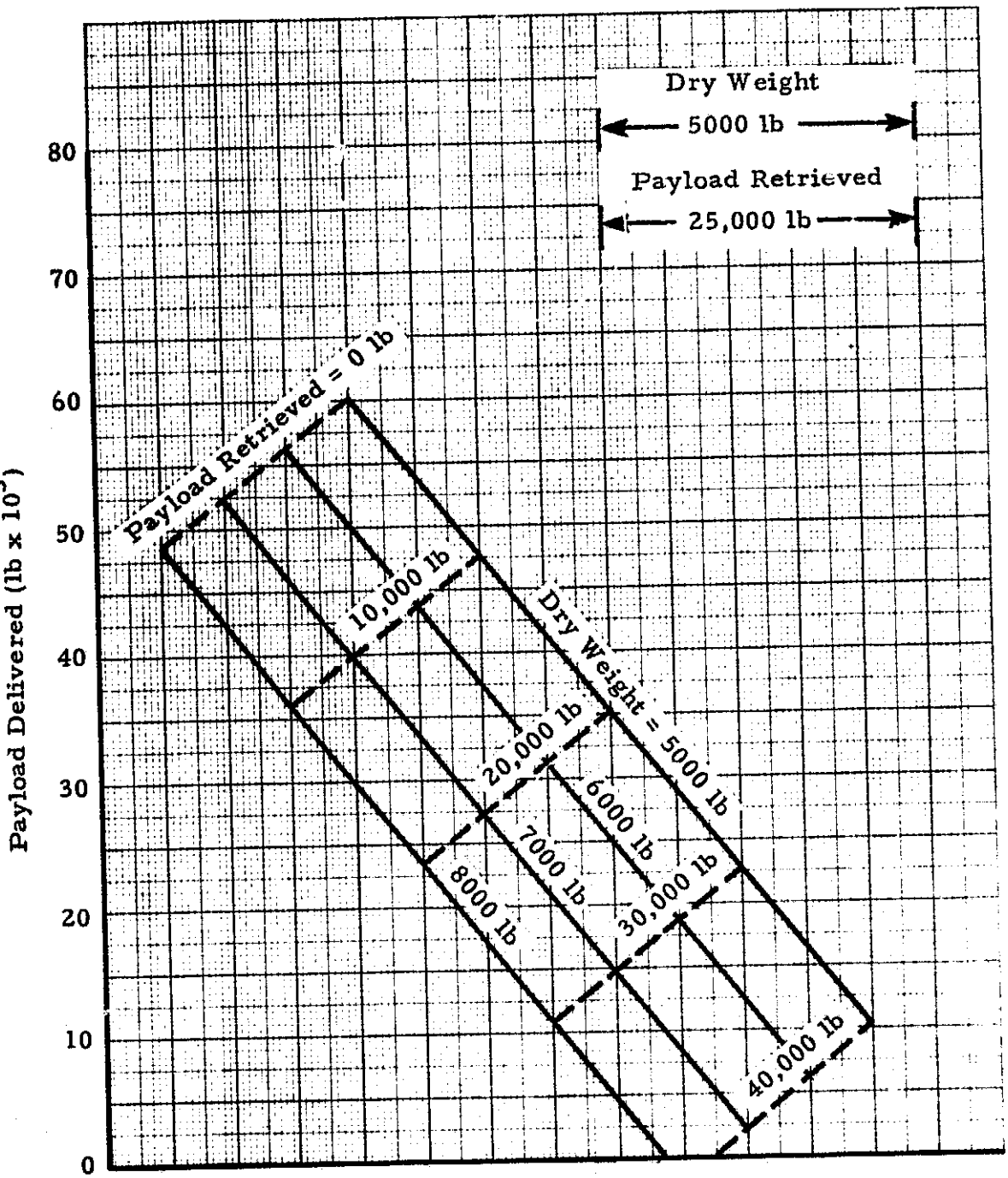

Fig. A-5 (Concluded)

d. Two-Stage AMOOS,
Three Shuttle Launches

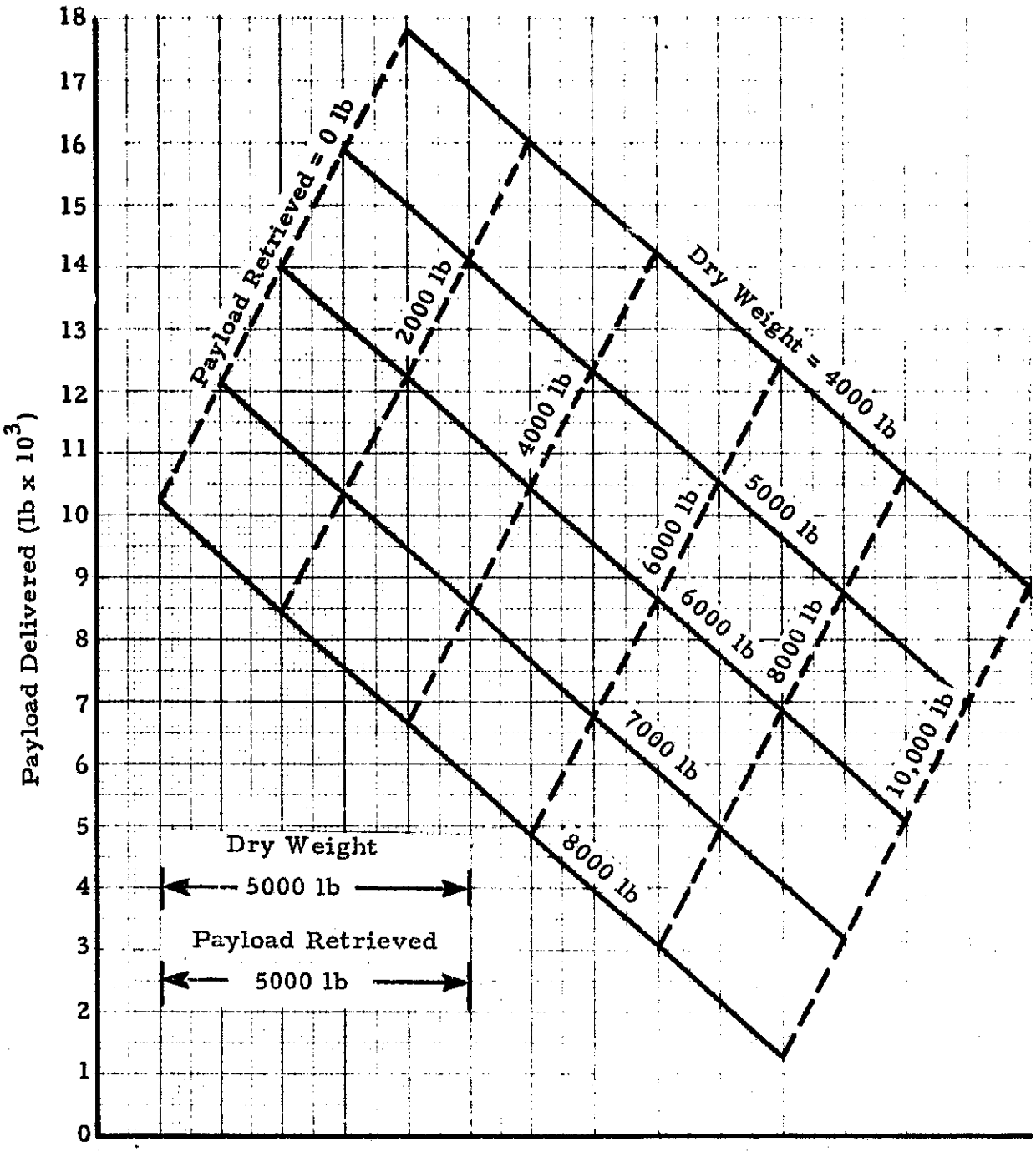

Fig. A-6 - AMOOS Payloads to a 5,000 n.mi. Circular Equatorial Orbit, I_{sp} = 456.5 sec and 65,000 lb Payload Shuttle

a. Single Stage AMOOS, One Shuttle Launch

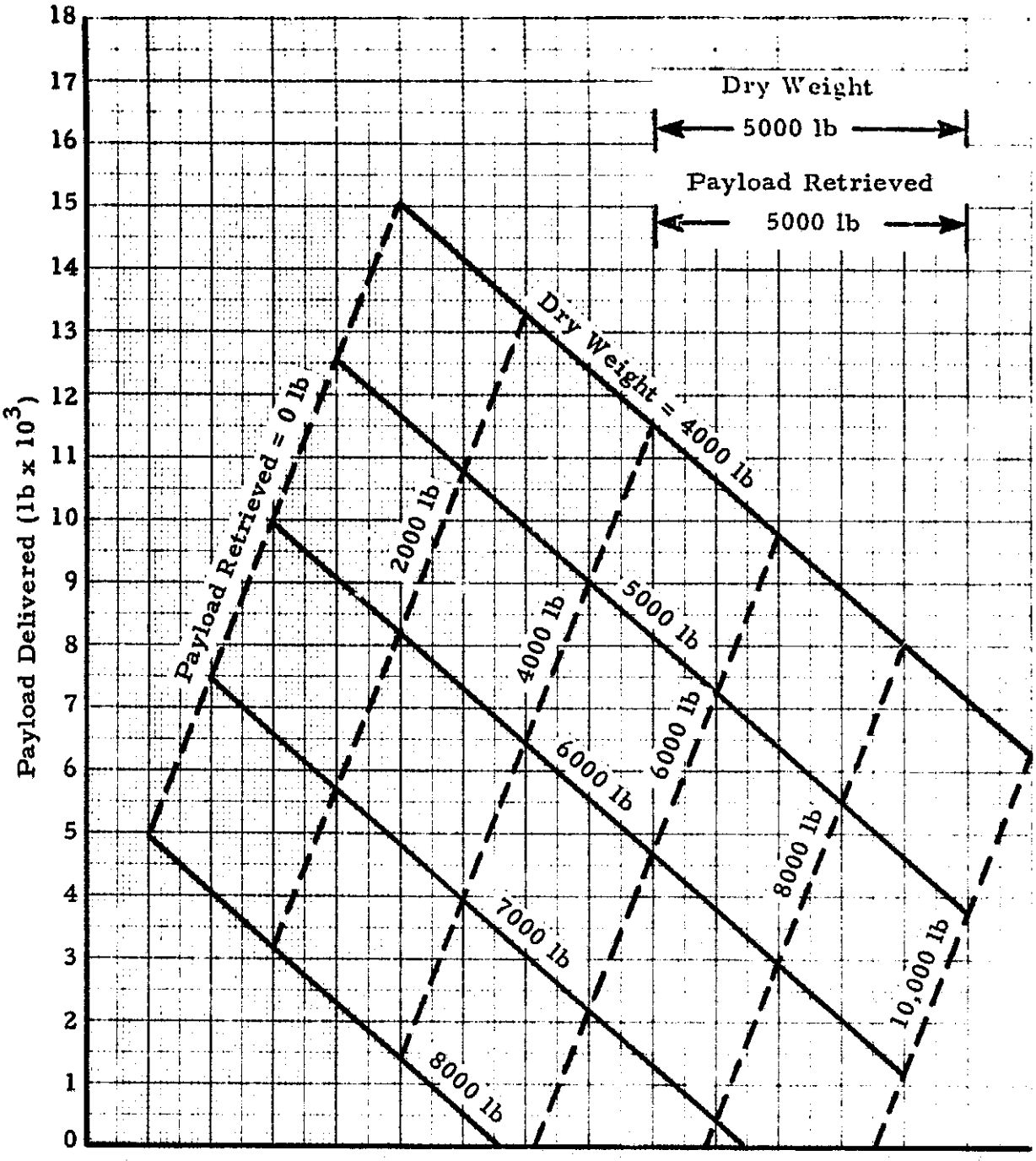

Fig. A-6 (Continued)

b. Two-Stage AMOOS,
One Shuttle Launch

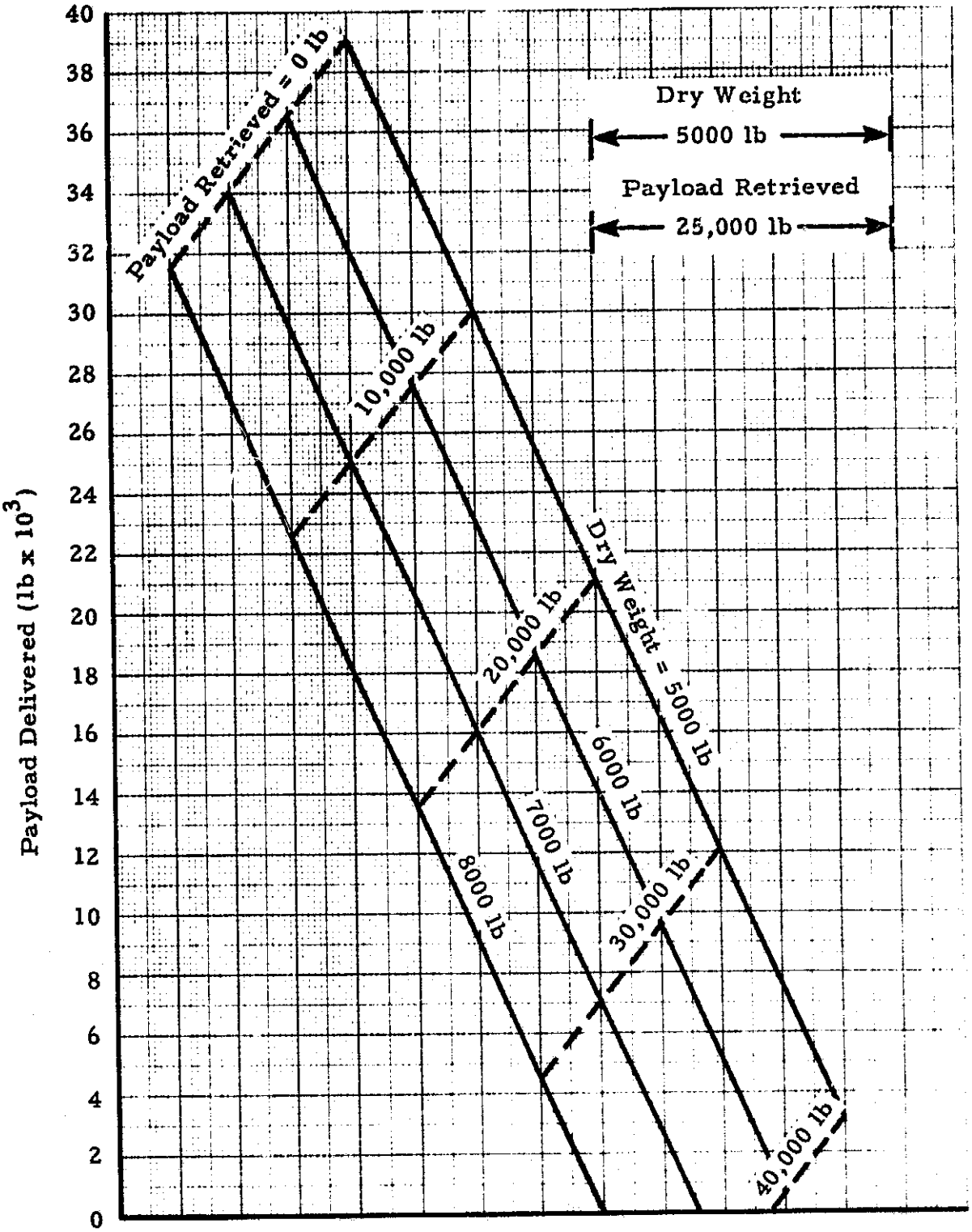

Fig. A-6 (Continued)

c. Two-Stage AMOOS,
Two Shuttle Launches

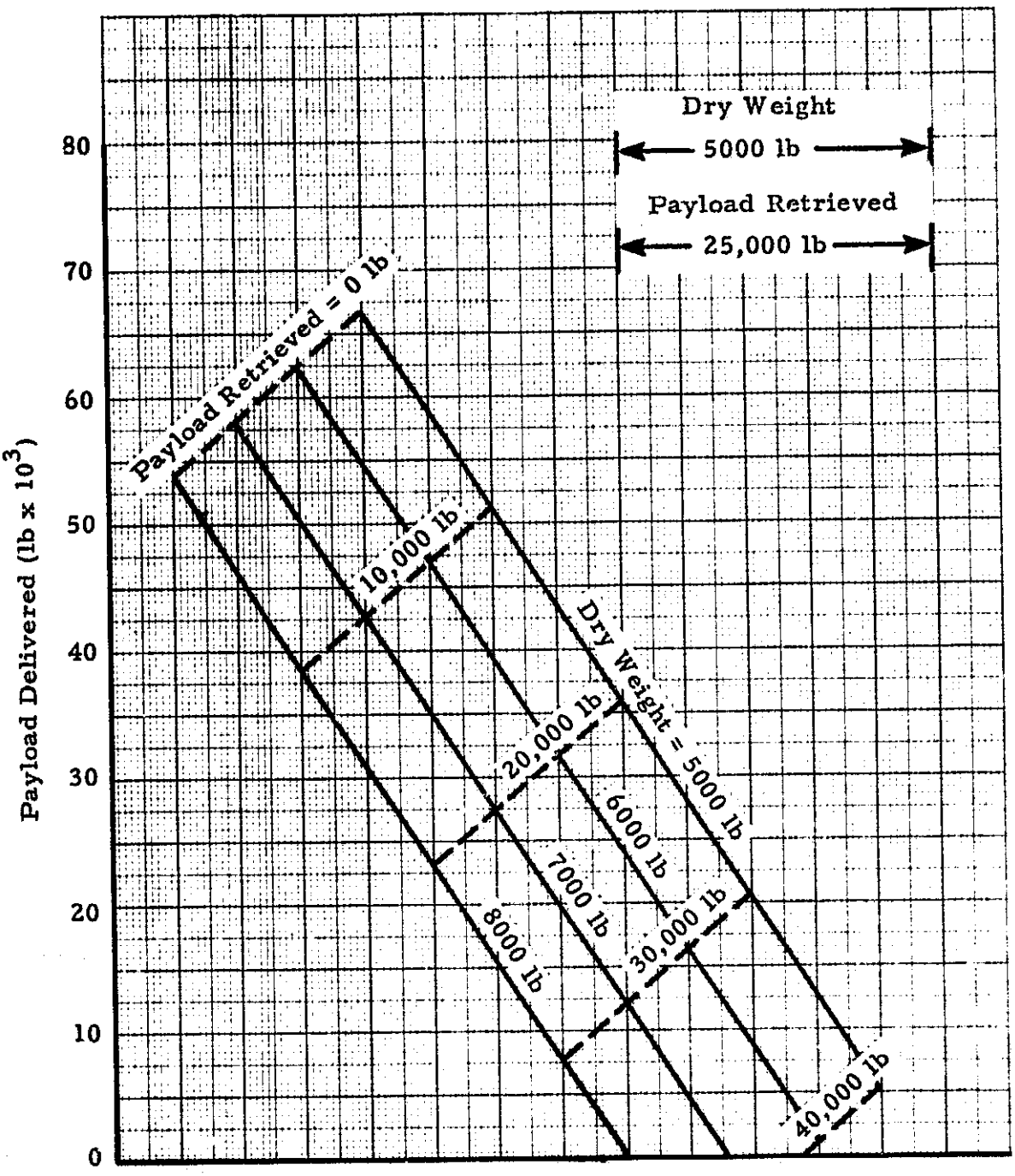

Fig. A-6 (Concluded)

d. Two-Stage AMOOS,
Three Shuttle Launches

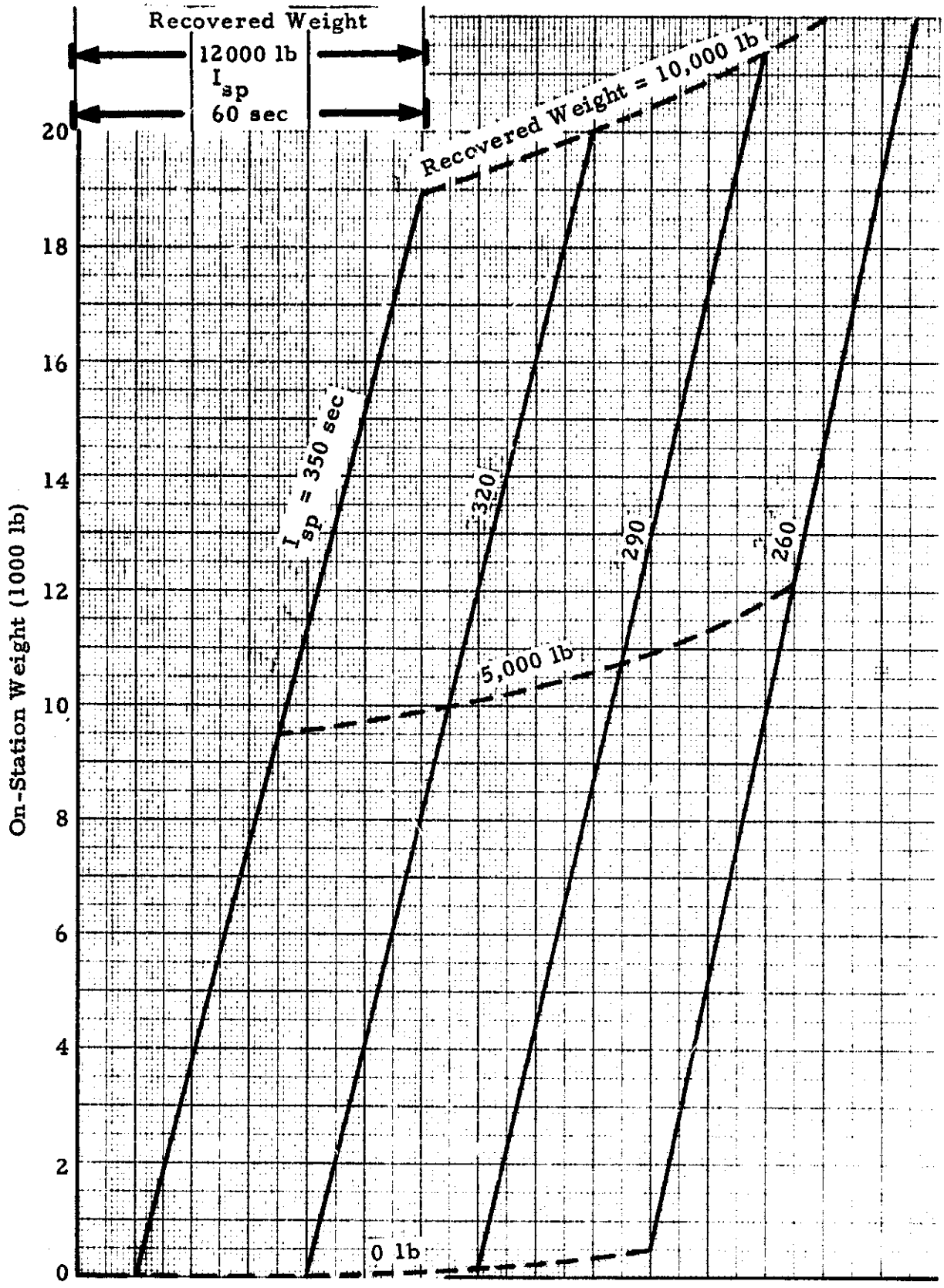

Fig. A-7 - AMRS On Station Weight and Main Engine Consumables at an Equatorial Geosynchronous Station

a. On-Station Weight

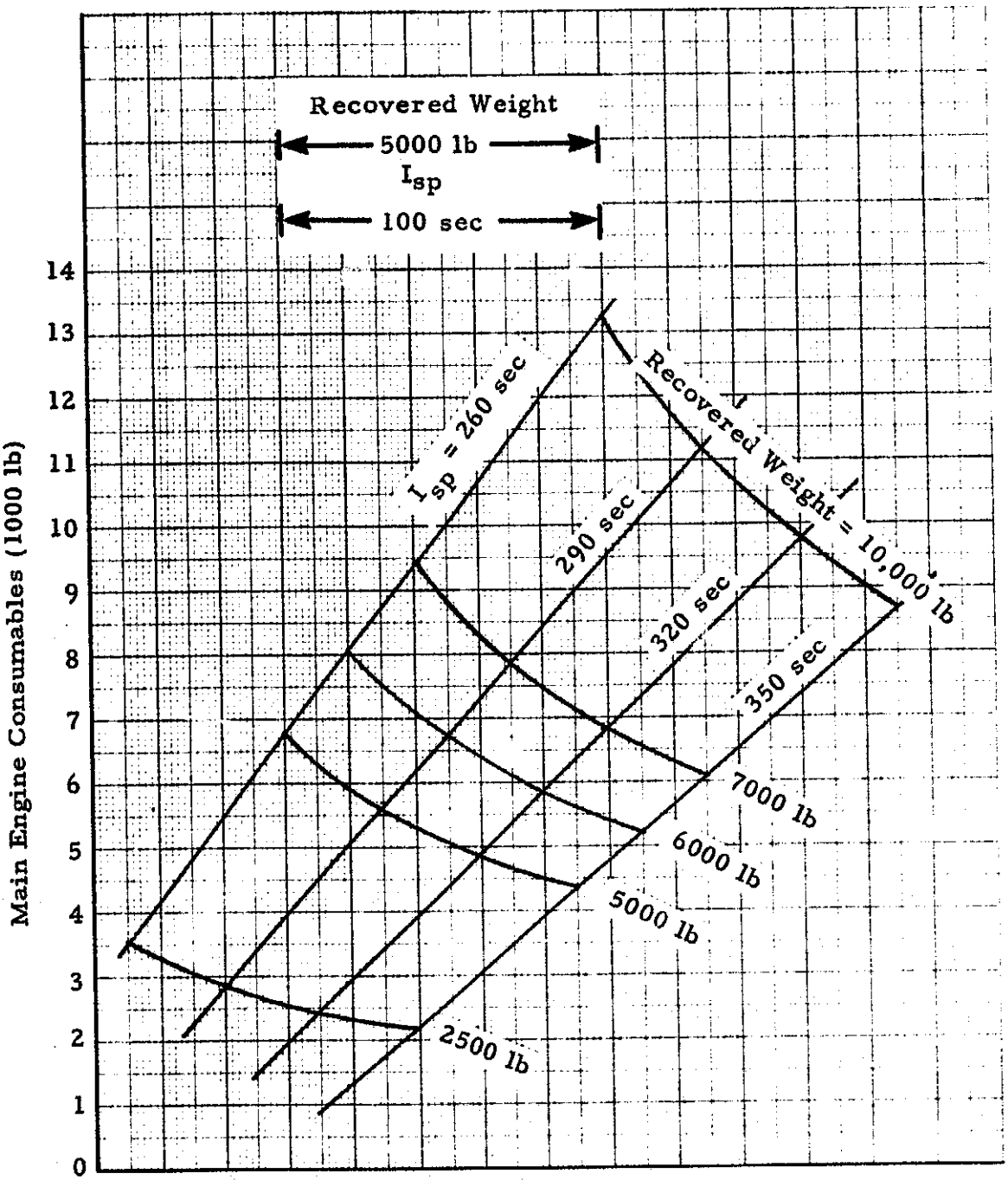

Fig. A-7 (Concluded)

b. Main Engine Consumables

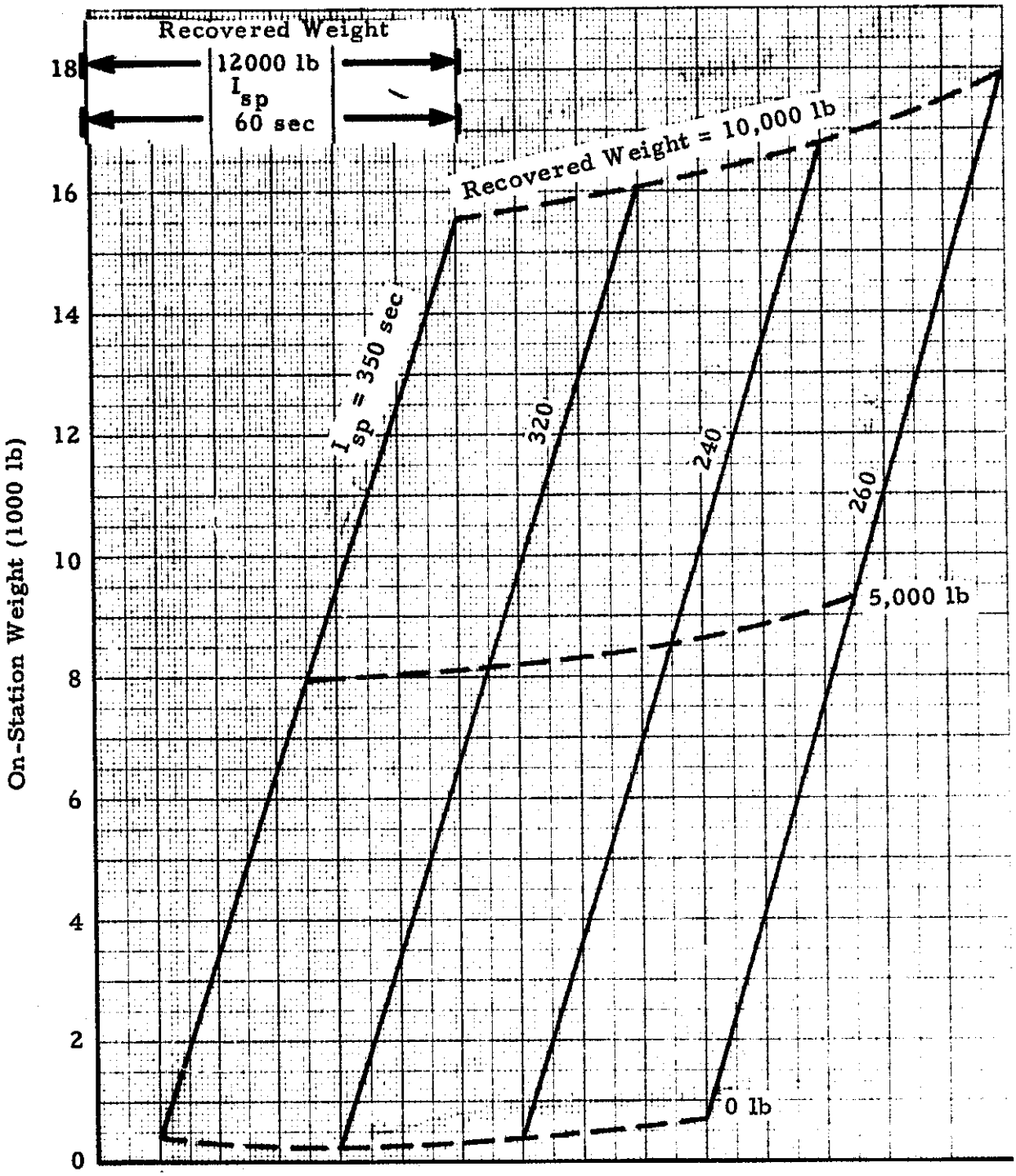

Fig. A-8 - AMRS On Station Weight and Main Engine Consumables at a Lunar Orbit Station

a. On-Station Weight

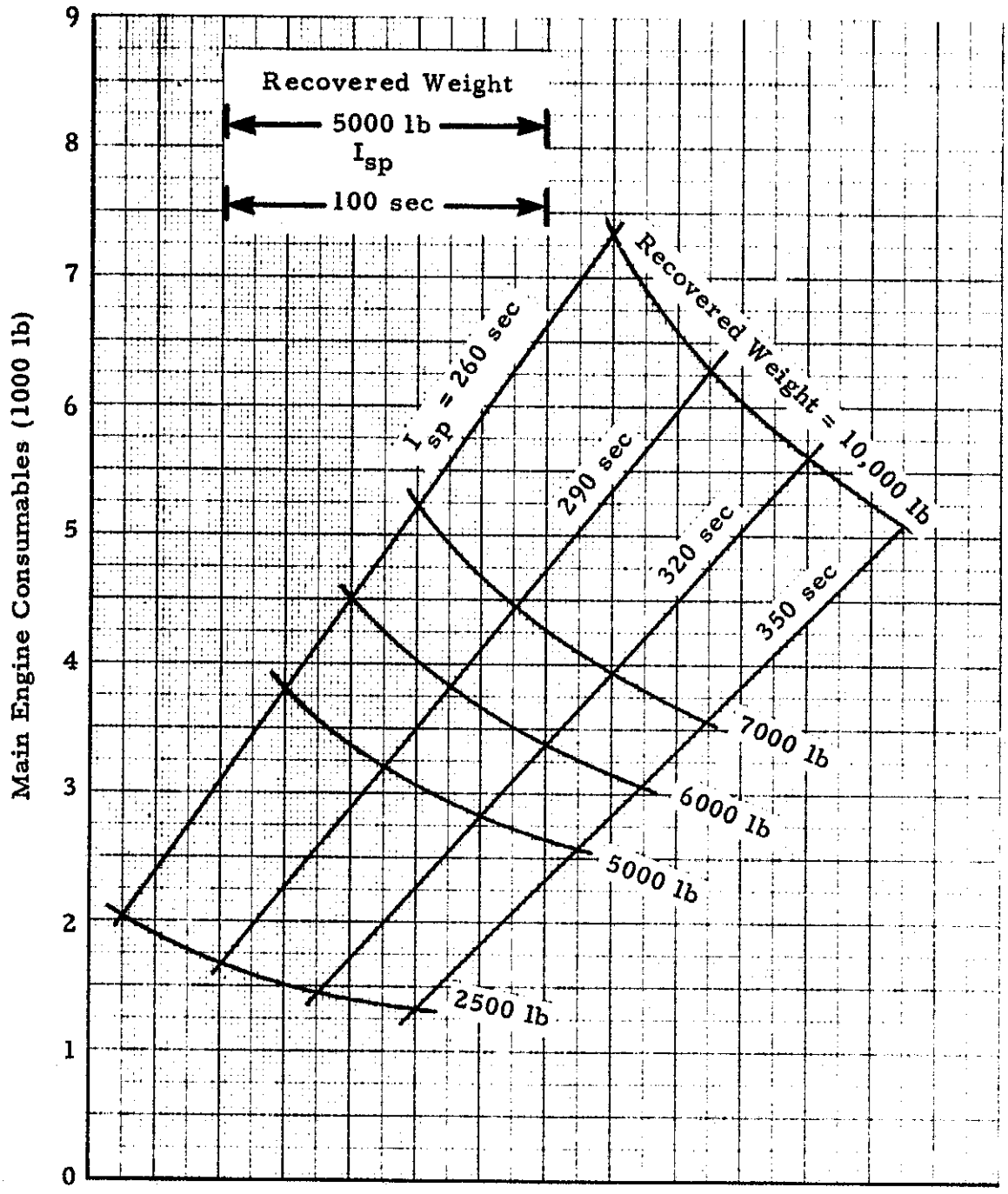

Fig. A-8 (Concluded)

b. Main Engine Consumables

Appendix B
AMOOS AND AMRS STRUCTURES

Appendix B

This appendix contains the steps in the calculation of the AMOOS propulsion module, AMRS and the AMOOS manned module primary structure design, and total weight estimate. There are four steps for each of the three vehicles:

1. Weight Distribution, in which the weight per unit length of the vehicle is determined. To do this accurately requires a knowledge of the weight of the structure to be designed. This first weight estimated was obtained from analysis of previous AMOOS vehicles and the Baseline Tug. The details are described in Section B1.
2. Loads Analysis, in which the external loads imposed on the vehicle are used to determine the internal loads. Both aerodynamic loads and loads during transportation in the Shuttle cargo bay are considered. Engine burn loads are also considered but are important only for local structure since the engine thrust is low relative to other forces imposed on the vehicle. The details of the loads analyses for each vehicle or module are discussed in Section B-2.
3. Structural Materials, in which the relative merits of the candidate materials are discussed and selections made. The details are given in Section B-3.
4. Structural Optimization, in which the size of the structural members are determined for the loads and materials of Sections B-2 and B-3, respectively. The optimization is described in Section B-4.

B.1 WEIGHT DISTRIBUTION – PROPULSION UNIT INITIAL WEIGHT ESTIMATE

The modular AMOOS concept as derived in Ref. B-1 was used as the basis for additional studies during this period of work. The mass distribution for the propulsion unit was revised based on the current configuration

requirements and data from Refs. B-2 and B-3. The tanks were sized for the required 48,5000 lb of propellant with a 6/1 ratio by weight of LOX to LH_2. This gave volume requirements of 1705 ft^3 and 634 ft^3 for the fuel and oxidizer, respectively. Since these values are close to the propellant requirements for the Baseline Tug configuration, the tank and supporting hardware weight values of Ref. B-2 were used. The supporting hardware consisted of the pumps, piping, valves, etc., required for propellant loading and measuring, hydraulics, pneumatic and pressurization, and the feed, fill and vent operations.

The RL-10 engine is common to both the AMOOS and the Baseline Tug. Since the maximum vehicle weight capability (63,100 lb) and the Shuttle launch environment is the same for both vehicles the thrust structure and other supporting hardware are assumed common. The same avionic and purge system weights were also used for the AMOOS propulsion unit.

An auxiliary propulsion system weight of 500 lb is used to account for the increased requirements during the aeromaneuvering portion of the AMOOS operations. The initial thermal protection system weight was derived by the ratio of the propulsion unit length (34 ft) to the length of the Ref. B-1 vehicle (59 ft) multiplied by its TPS weight. An additional 200 lb of TPS was added due to increases in vehicle performance during the reentry phase.

The propulsion unit shell weight was taken from the values for the modular vehicle in Ref. B-1. The vehicle weights in Ref. B-1 were approximately the same for either Be-38% Al or magnesium as the structural material; hence, this preliminary weight was essentially independent of the final selection of these two candidate materials. Two methods of weight approximation were used. The weight of the individual section of the vehicle, (nose, foward section, etc.) were obtained for the Ref. B-1 vehicle and used for the corresponding propulsion unit sections. Second, the Ref. B-1 weight was factored by the ratio of the lengths. Both values were within a few percentage points so the ratioed value of 1227 lb was used. This was the lighter weight of the two.

A weight breakdown for the propulsion unit is given in Table B-1. The distribution for the propulsion unit is shown in Fig. B-1 for the dry weight, fully fueled and aero reentry conditions.

Manned Unit Initial Weight Estimate

The manned unit is 11.6 ft in length and is a self-sustained system for 4 men for a 30-day mission. The volume and weight requirements for the system plus necessary food and supplies were derived from the data in Ref. B-3. The data in Ref. B-4 are applicable to an orbiting station and has volume requirements greatly exceeding those in Ref. B-3. The AMOOS manned configuration would be mated in orbit with another vehicle which would provide working space for the crew. Transportation and minimal activities such as sleeping, eating, personal hygene, etc., would be provided by the manned unit. Hence, in the calculations for the food and life support systems provisions were made for a 30-day mission.

The required weight for the capsule structure was obtained by determining a bulk density from Ref. B-3 data and multiplying by the required volume calculations for this configuration. A value of 2.37 lb/ft^3 and required volume of 516 ft^3 resulted in a capsule weight of 1225 lb. Table B-2 gives the volume and weight requirements for the manned unit. The structural shell and TPS weights were obtained by the ratio of the lengths times the respective weight values in Ref. B-1. The weight distribution for the manned module is also shown in Fig. B-1. The center-of-gravity locations for the propulsion unit plus manned unit are also shown in Fig. B-1. Figure B-2 shows the position of the center of gravity in the Shuttle payload bay envelope. The AMOOS vehicle is mounted backward in the payload bay.

AMRS Initial Weight Estimate

The AMRS configuration is a transportation only, minimum volume concept for four or six men for a one-day mission. The length-to-diameter

Table B-1

PROPULSION UNIT WEIGHT BREAKDOWN
(Initial Estimate)

	Weight (lb)
Gimbal	30
Fuel Tank and Supports	417
Oxidizer Tank and Support	238
Thrust Structure	29
Mounting Structure	100
Nose Actuator	100
Engine	442
Feed, Fill, Drain and Vent	256
Pneumatic and Pressure	234
Hydraulic	63
Propellant Loading and Measuring	50
APS	500
Tank Insulation	130
Purge and Thermal Control System	311
Navigation Guidance and Control	154
Data Management	158
Communications	72
Measuring System	92
Electrical Power and Distribution	410
Rendezvous and Docking	35
Aft Ring Interface	30
	3851
Thermal Protection System	1036
Shell Structure	1227
Contingency 10%	611
Total Dry Weight	6725

	Fuel-Launch Condition	Reentry Condition
LOX	41,743	4,150
LH_2	6,957	690
	48,700	4,840
	6,725	6,725
	55,425 lb	11,565 lb

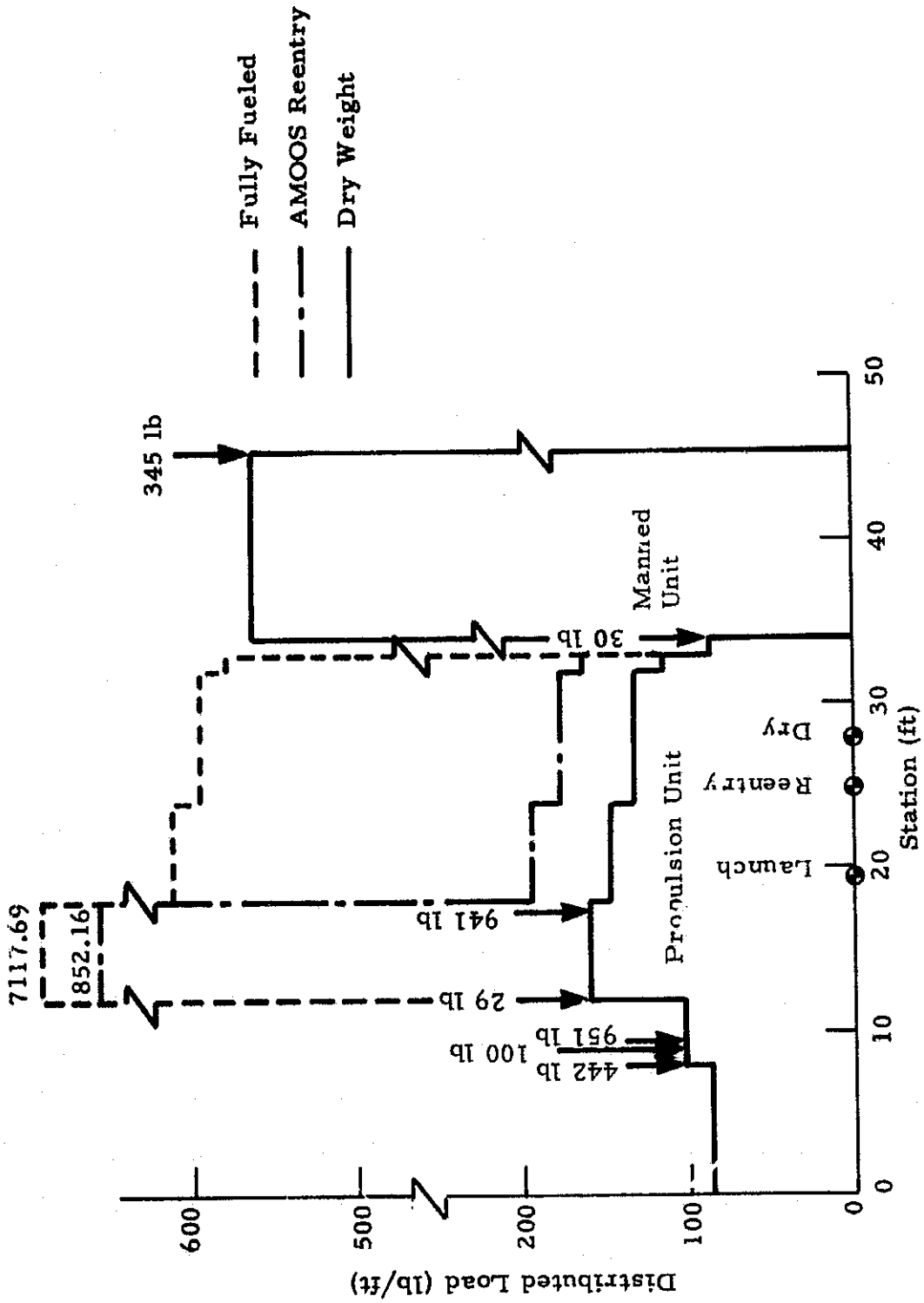

Fig. B-1 - AMOOS Weight Distribution

Table B-2

MANNED UNIT WEIGHT AND VOLUME BREAKDOWN
(Initial Estimate)

	Volume (ft^3)	Weight (lb)
Crew		
Two @ 75 ft^3/man	150	748
Two @ 56 ft^3/man	112	
Food 8 lb/ft^3	6	50
Furnishing	93	185
Bunks 3 @ 15 lb		
Seats 4 @ 20 lb		
Misc. 4 @ 15 lb		
Medical 5.5 lb/man	2	22
Personal Effects	11	213
Clothing 4 @ 45 lb		
Hygiene 28 lb		
Personal 10 lb/man		
EVA	25	372
Suits 2 @ 62 lb		
PLSS 2 @ 62 lb		
Equip. 2 @ 62 lb		
Interior Space Suit 4 @ 31 lb	8	124
EC/LSS	21	1531
Cabin Pressurization 55 lb		
O_2/N_2 Leak (5 lb/day + 100%) 300 lb		
O_2 Consumpt. (2 lb/day + 100%) 120 lb		
Water (6.2 lb/man/day) 152 lb (reclamation)		
Hardware 904 lb		
Electrical Power	4	130
Communication and Data System	10	327
Instrumentation	16	188
Miscellaneous	10	80
Maintenance Equipment		40
Flap		225
Docking Mechanism		120
Capsule		1225
TPS		335
Shell Structure		339
Contingency 10%	48	625
Total	516	6879

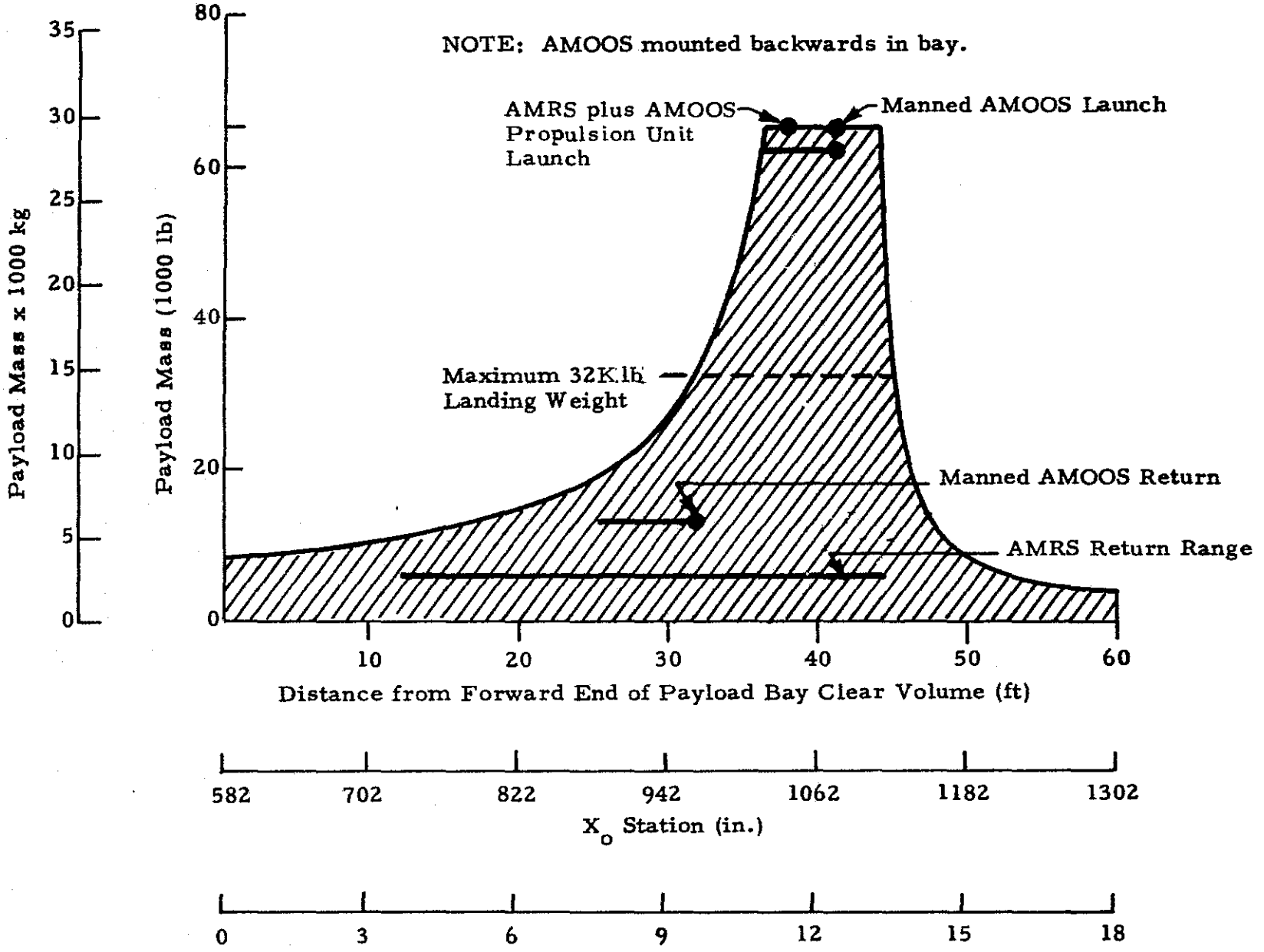

Fig. B-2 - Shuttle Payload Longitudinal Center-of-Gravity Envelope

ratio and exterior configuration were maintained to match the AMOOS vehicle. The structural shell and TPS weights were determined by factoring the AMOOS weights (Ref. B-1) by the ratio of the surface areas. This gave structure and TPS weights of 660 and 393 lb, respectively, for a magnesium structure. The tanks, engine, astrionics, etc., weights were determined using the data and formulas of Ref. B-5. The crew capsule weight and volume requirements were derived from the data in Ref. B-3. These values are given in Table B-3. A total propellant weight of 6500 lb is budgeted for AMRS with 2145 lb fuel and 4355 lb oxidizer. At aerodynamic reentry a total propellant weight of 500 lb is assumed. The weight distribution is given in Fig. B-3.

B.2 LOADS ANALYSIS

Loads analyses were performed to determine the critical bending moments and axial loads during AMOOS and AMRS flight and transportation by the Space Shuttle. Aerodynamic normal and axial force distribution for a one-pass mission were obtained for the critical dynamic pressure and angle of attack. The aerodynamic force distribution for a dynamic pressure of 105.22 lb/ft^2 is shown in Fig. B-4. The modular AMOOS configuration was analyzed for 105.22 lb/ft^2 and 156.64 lb/ft^2 dynamic pressures Digital computer programs were used to determine the net axial and shear forces and bending moment distributions for the aerodynamic and mass distributions. These results are shown in Fig. B-5 for the 156.64 lb/ft^2 loading. The AMRS vehicle was analyzed for a dynamic pressure of 146.20 lb/ft^2. The AMOOS aerodynamic loads were factored by the following relation to obtain the AMRS values.

$$F_{AMRS} = \frac{F_{AMOOS}}{q_{AMOOS} S_{ref_{AMOOS}}} \; q_{AMRS} S_{ref_{AMRS}}$$

where F = air load (lb/in)

q = dynamic pressure (psi), and S_{ref} = reference area (in^2)

The AMRS force and bending moment distributions are shown in Fig. B-6.

Table B-3

AMRS-WEIGHT AND VOLUME BREAKDOWN
(Initial Estimate)

	Volume (ft^3)	Wt (lb)
Crew		
Four @ 56 ft^3	224	748
Food 8 lb/ft^3	2	16
Furnishings 2 lb/ft^3	43	86
Medical 10 lb/ft^3	2	20
Personal Effects	10	56
EC/LSS		738
Atmosphere	2	
Water 62 lb/ft^3	1	
Waste Management	4	
Hardware	10	
Electronics	4	130
Communications and Data System	10	327
Instrumentation	16	188
Miscellaneous Equipment	10	20
Expendables	3	
Crew Capsule		507
Engine and Thrust Structure		185
Tanks and Support Structures		375
Astronics		400
Plumbing Weight		132
Flap		50
TPS		395
APS and Structure		500
Shell Structure		660
Contigency 10%	34	477
Total Dry	375	6010

	Fuel Launch Condition	Reentry Condition
Fuel	2,145 lb	165 lb
Oxidizer	4,355 lb	335 lb
	6,500 lb	500 lb
Dry	6,010 lb	6,010 lb
	12,510 lb	6,510 lb

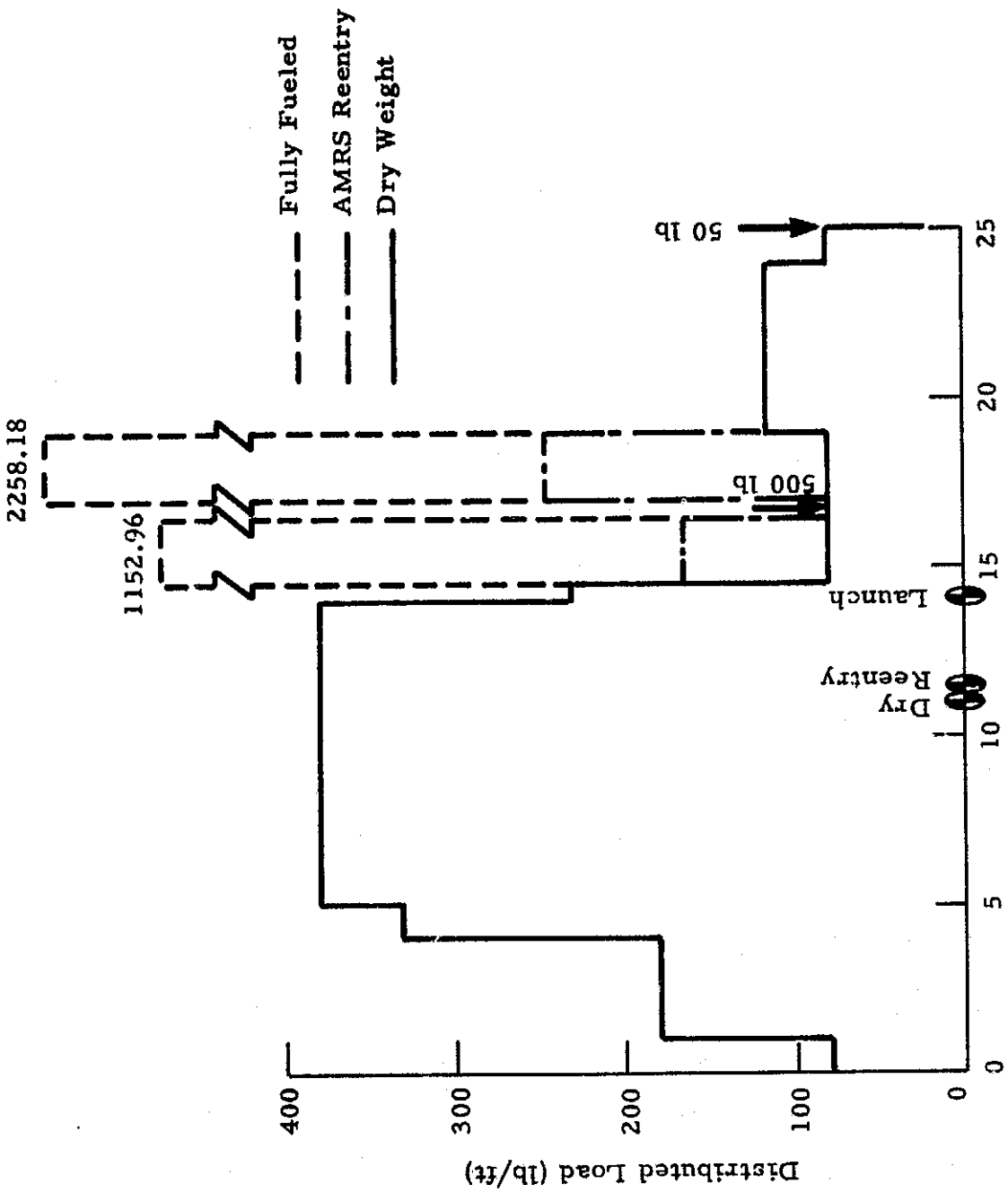

Fig. B-3 - AMRS Weight Distribution

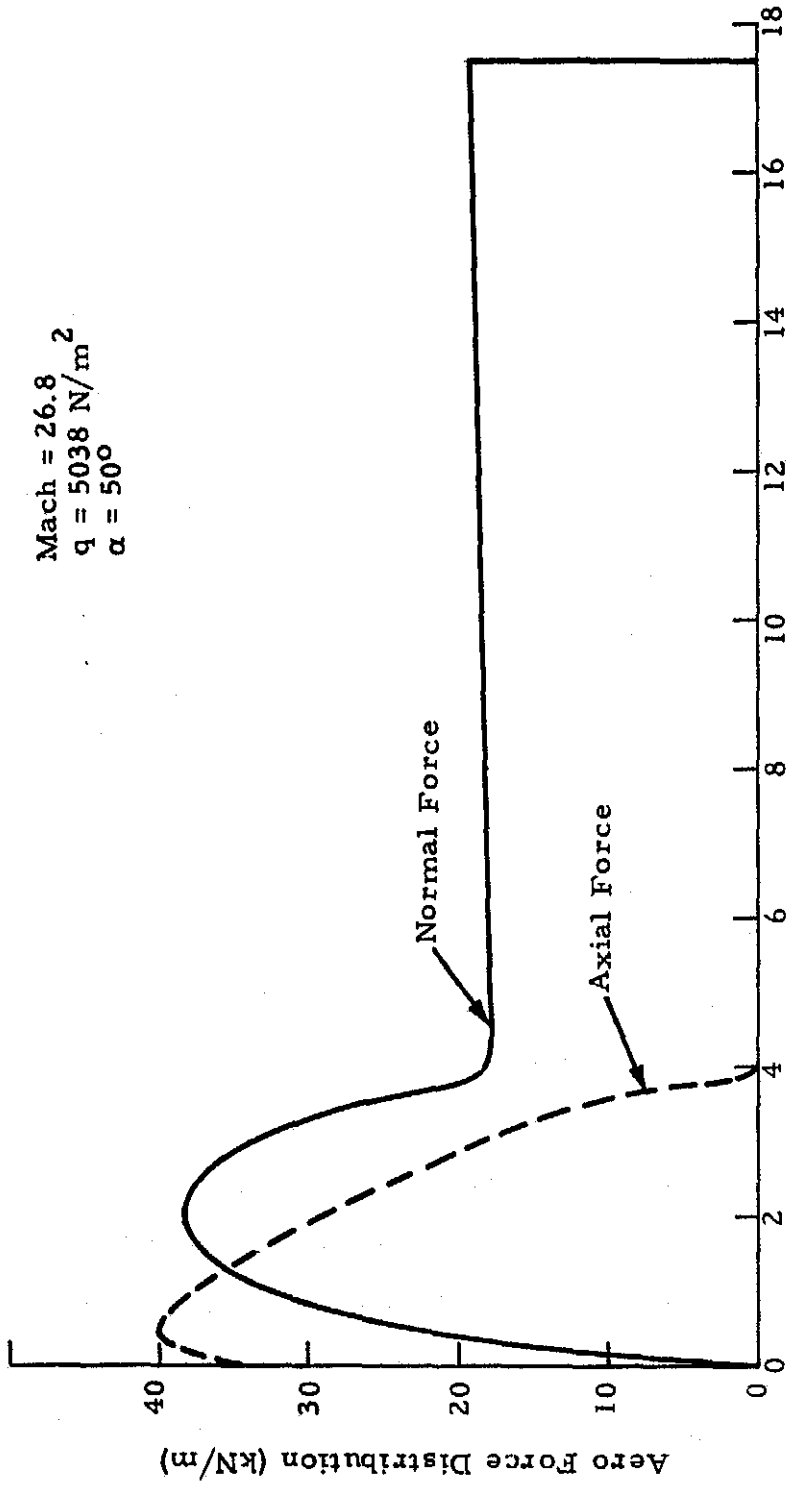

Fig. B-4 - Aerodynamic Force Distribution for AMOOS and AMRS

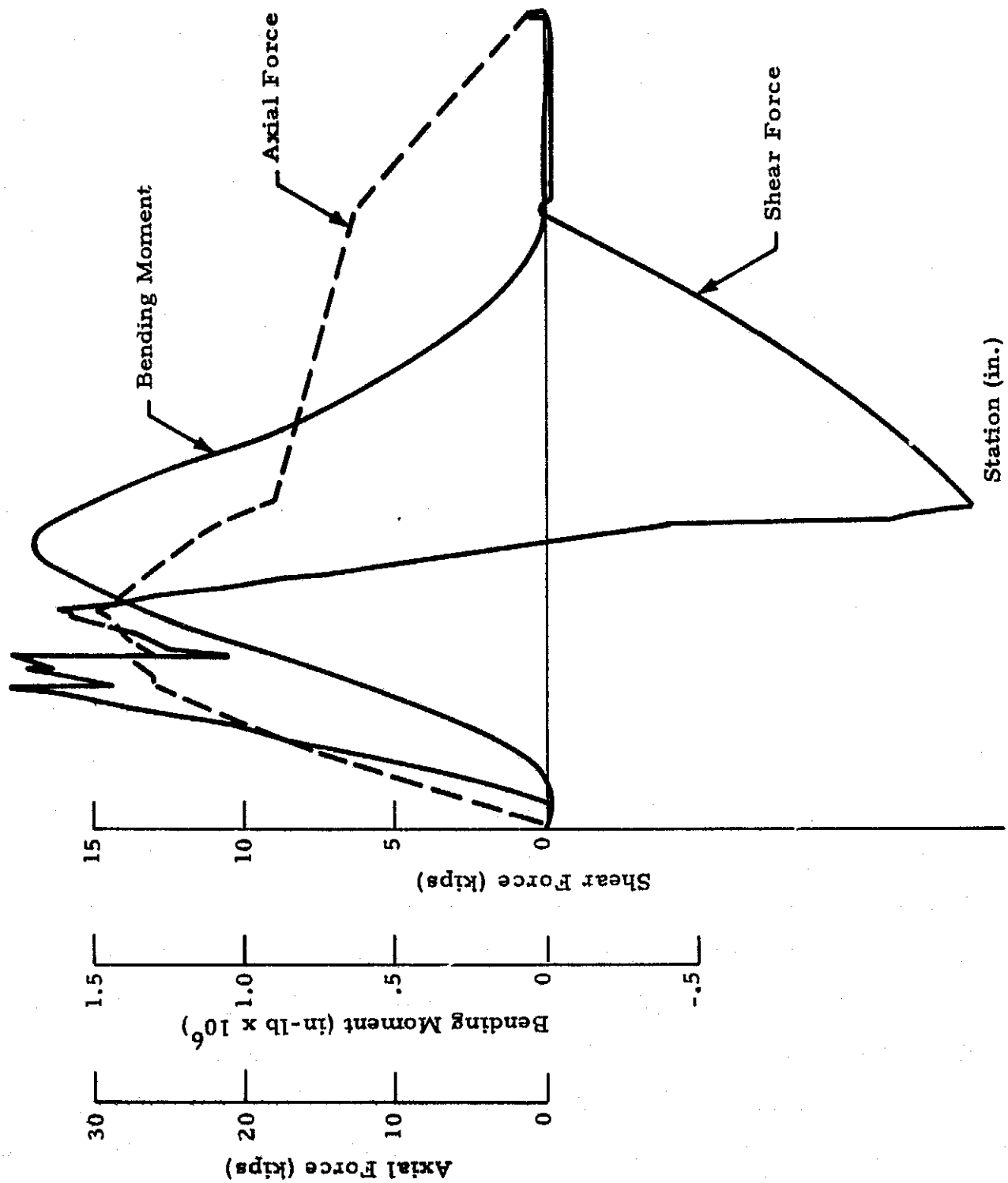

Fig. B-5 - AMOOS Force and Moment Distribution (7500 n/m^2)

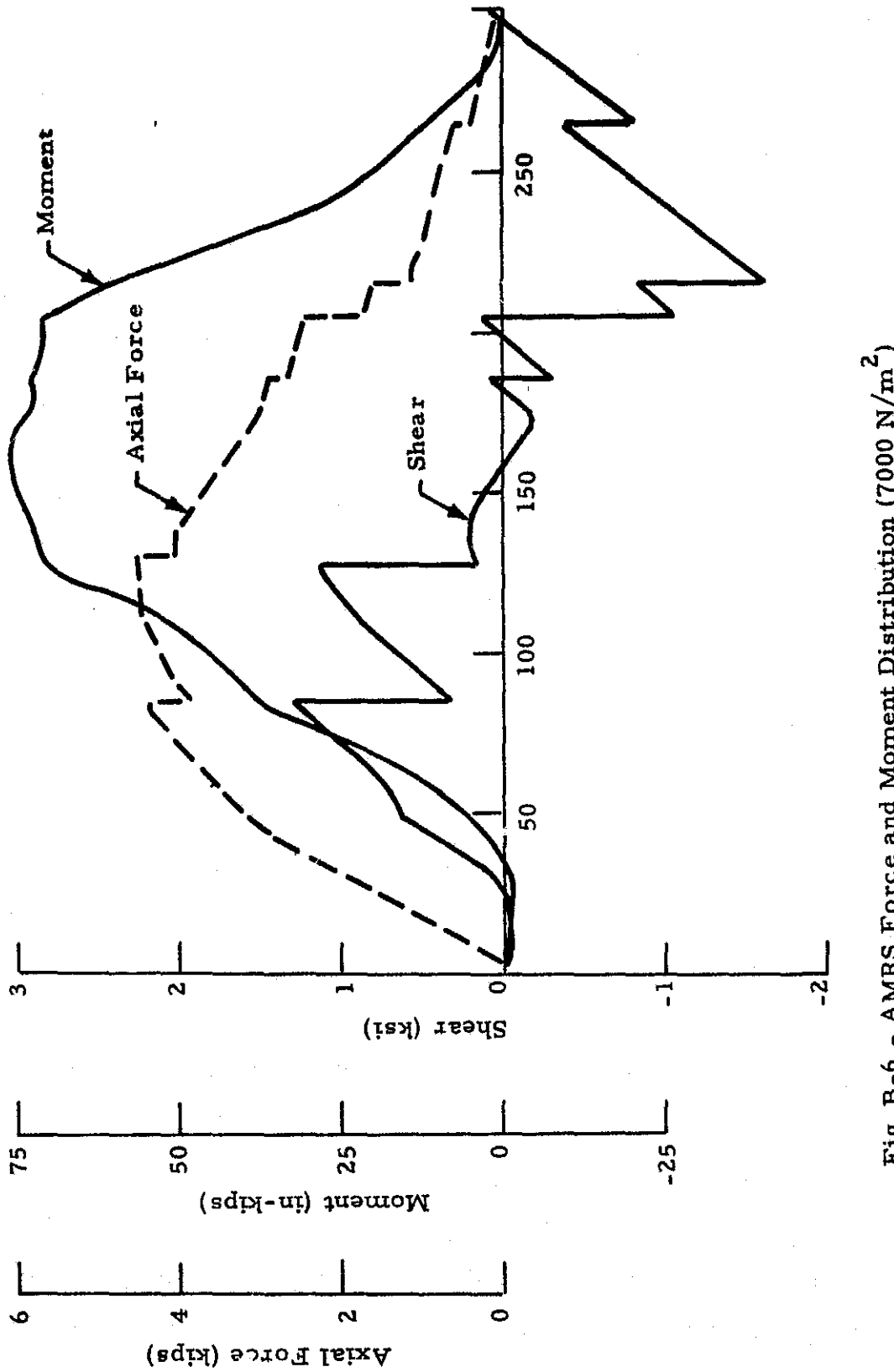

Fig. B-6 - AMRS Force and Moment Distribution (7000 N/m^2)

A beam model was used to determine the loads for the EOS flight environment. The chosen interface points in the Shuttle cargo bay and corresponding mass distribution were analyzed for the EOS payload g factors. These factors are given in Table B-4. The location of the Shuttle cargo bay attachment points and the load factors were taken from Ref. B-6. The maximum load combination occurs during lift off for the g factors of -2.9, -1.0 and -1.5 in the x, y and z directions, respectively. The beam models and resulting unit load distributions are shown in Figs. B-7 and B-8 for both AMOOS and AMRS.

The maximum compressive limit load, N, in the shell body structure was determined,

$$N = \frac{P_{AX}}{2\pi R_{avg}} + \frac{M}{\pi R_{avg}^2}$$

where

$$R_{avg} = \left(R_{major} + R_{minor}\right) / 2$$

$$M = \sqrt{M_{major}^2 + M_{minor}^2}$$

Major and minor denote the major and minor axes of the elliptical cross section.

The design load, N_D, equals $f \cdot N$ when the factor of safety $f = 1.4$. The factor of 1.4 is used since AMOOS and AMRS are manned vehicles.

The AMOOS vehicle was subdivided into a nose section, forward body, intermediate body and manned unit. The design axial line loads for the aero reentry and the EOS environment conditions for each body section are given in Table B-5. The shell structure is assumed to be at 600°F for the reentry loading. Table B-6 gives the similar design line loads for the AMRS structure.

Table B-4

SHUTTLE PAYLOAD BAY LIMIT LOAD FACTORS

Condition*	Linear - g		
	X	Y	Z
Lift-Off	-0.1 -2.9	+1.0 -1.0	+1.5 -1.5
High-Q Boost	-1.6 -2.0	+0.5 -0.5	+0.6 -0.6
Boost-Max. LP (Stack)	-2.7 -3.3	+0.2 -0.2	-0.3 -0.3
Boost-Max. LP (Orb Alone)	-2.7 -3.3	+0.2 -0.2	-0.75 -0.75
Entry and Descent Pitch Up	+1.06 -0.02	0 0	+2.5 -1.0
Entry and Descent Yaw	+0.75 +0.75	+1.25 -1.25	+1.0 +1.0
Landing	+1.0 -0.8	+0.5 -0.5	+2.8 +2.2
Crash**	+9.00 -1.5	+1.50 -1.50	+4.5 -2.0
Crash (Crew Compartment Interior)	+20.0 -3.3	+3.3 -3.3	+10.0 -4.4

*Positive X, Y, Z directions equal aft, right and up. Load factor carries the sign of the externally applied load.

**Crash load factors are ultimate and only used to design payload support fittings and payload attachment fasteners. Crash load factors for the nominal payload of 65,000 lb (29,485 kg). Longitudinal load factors are directed in the forward azimuth within 20 deg of the orbiter longitudinal axis. The specified load factors shall operate separately.

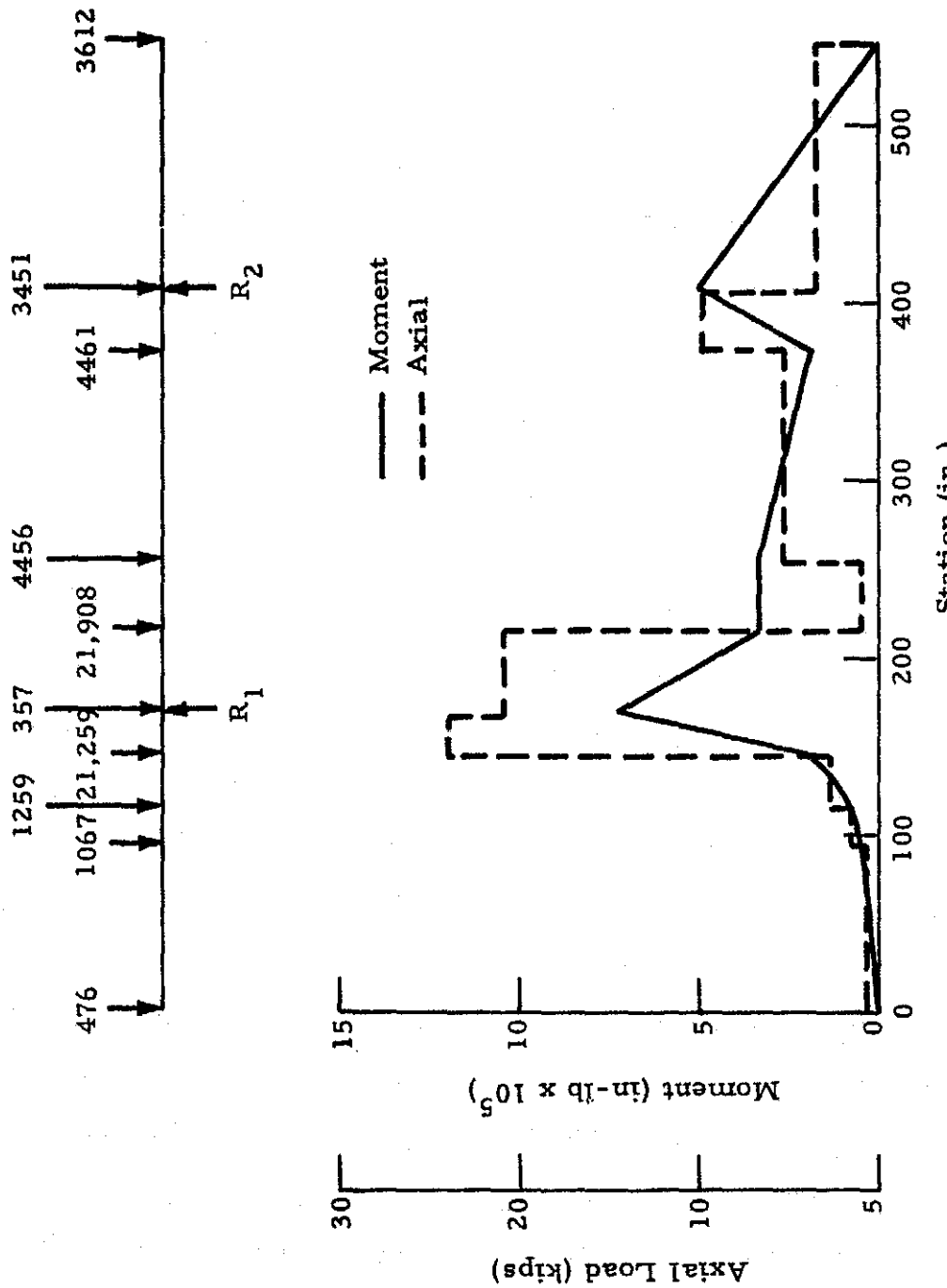

Fig. B-7 - AMOOS Beam Model, 1-g Launch Load

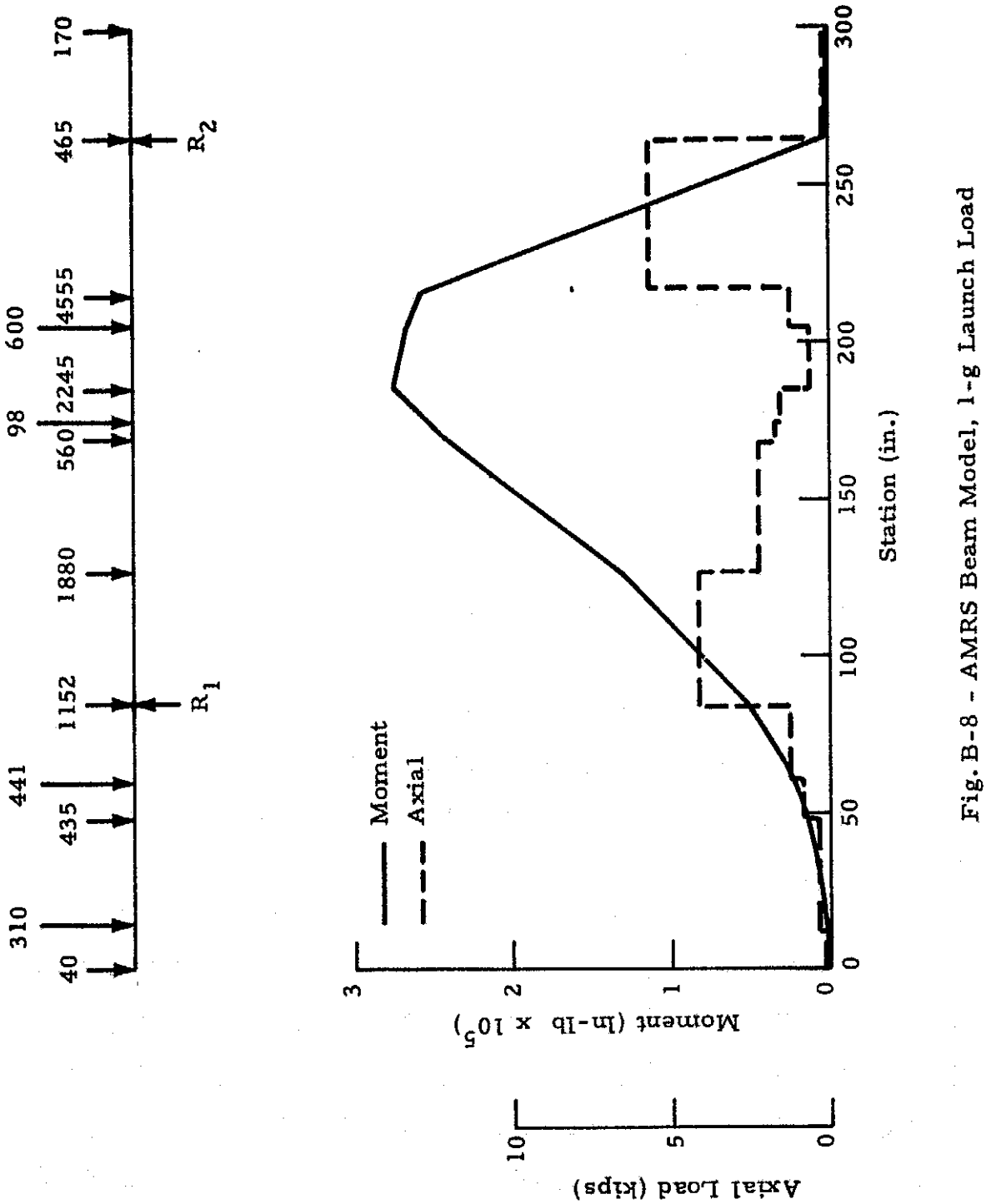

Fig. B-8 - AMRS Beam Model, 1-g Launch Load

Table B-5

AMOOS VEHICLE DESIGN LOADS

Section	Station (in.)	Load Condition	Design Line Load (lb/in)
Nose	0 – 114	59 ft Vehicle Shuttle Launch	300.28
Fwd Body	114-240	Shuttle Launch	300.28
Intermediate	240-408	AMOOS Vehicle Reentry*	126.08
Manned Unit	408-547.2	AMOOS Vehicle Shuttle Launch	134.2

*156.64 lb/ft^2

Table B-6

AMRS VEHICLE DESIGN LOADS

Section	Station (in.)	Load Condition	Design Line Load (lb/in)
Nose	0-72	Shuttle Launch	120.35
Fwd Body	72-174	Shuttle Launch	120.35
Aft Body	174-300	Shuttle Launch	169.62

B.3 STRUCTURAL MATERIALS

Two candidate materials from the results of Ref. B-1 were used for this study initially: beryllium-38% aluminum and magnesium HM21A-T8. Both of these materials are low density and both meet the 600°F temperature requirement for the body shell during reentry. Magnesium is not a high strength nor high modulus material when compared to Be-38Al or certain other materials, but, since the AMOOS vehicle is a lightly loaded shell structure and cross sections are determined by instability rather than material strength, magnesium is competitive.

Magnesium was selected and used for the analyses due to the major difference in material cost. Be-38Al cost approximately $43/lb and magnesium approximately $3/lb (Ref. B-7). Both are state-of-the-art materials and have been utilized in space hardware. The material properties for the two materials for 70°F and 600°F are given in Table B-7, (Refs. B-8 and B-9).

B.4 STRUCTURAL OPTIMIZATION

A Lockheed computer program (Ref. B-10) for the optimization of cylinders with integral ring and stringers of rectangular cross section was used to determine a minimum weight design. Each major section of the shell was analyzed for the design loads in Table B-5. Elevated temperature material properties were used for the aero load analyses. Data input consisted of line load, skin thickness, cylinder length, material properties, maximum ring and stringer height, maximum stiffener height to thickness ratio, values of ring spacing, maximum stress allowed and internal or external location of rings and stringers. External location of stiffeners is the optimum configuration, but due to the bonding of the TPS on the outside skin surface the stiffeners must be located in the interior.

The structure is optimized based on the following modes of instability:

1. Local instability of the cylinder wall and stringers

Table B-7

MATERIAL PROPERTIES

Mechanical Properties Basis	Beryllium-Aluminum Be-38 Aℓ (Sheet, Annealed) A	Magnesium HM 21A-T8 (Sheet) A
F_{tu}, ksi(MN/m^2):		
70°F (294°K)	44 (303)	33 (228)
600°F (589°K)	26 (179)	11 (76)
F_{ty}, ksi(MN/m^2):		
70°F (294°K)	31 (214)	18 (124)
600°F (589°K)	22 (152)	8 (55)
F_{cy}, ksi(MN/m^2):		
70°F (294°K)	28 (193)	15 (103)
600°F (589°K)	18 (124)	10 (69)
F_{su}, ksi(MN/m^2):		
70°F (294°K)	23 (159)	21 (145)
600°F (589°K)	14 (97)	7 (48)
E, 10^3 ksi (GN/m^2):		
70°F (294°K)	28 (193)	6.5 (45)
600°F (589°K)	25 (172)	5.2 (36)
μ	.14	.35
Physical Properties		
ρ, (lb/in^3) kg/m^3	.075 (2080)	.064 (1770)

Ref: Be-38Aℓ, LMSC Report 679606, Oct. 17, 1967
HM 21A, MIL-HDBK-5, Sept. 1971

2. General instability involving the composite structure. Two variations are considered: (a) panel instability involving the cylinder wall and stringers, and (b) overall instability involving the cylinder wall, stringers and rings.

The cylinder wall is not allowed to buckle locally below the design load. Buckling of the cylinder wall will cause failure in the TPS bond. A minimum skin gage of 0.025 inch was set based on the requirement of having to scrape the structure to replace the TPS.

Table B-8 presents the results of the AMOOS optimization study. The cross-sectional dimensions for each section and the critical load case are given. Table B-9 presents the corresponding data for the AMRS vehicle. Solid circumferential rings 4 inches wide and 0.5 inch thick were added to the structure in appropriate places. This addition provided for section interfaces and skin splices, and for the attachment of major vehicle components such as tanks, manned capsule, and rings, etc. Nine of these rings were added to the AMOOS and seven to the AMRS vehicle. The resultant optimized weights for the AMOOS and AMRS structural shells are given in Tables B-10 and B-11. These values are for magnesium HM21A-T8 material. The optimized shell weights were 252 lb and 154 lb lighter than the original estimates for the AMOOS and AMRS vehicles given in Tables B-1, B-2 and B-3, respectively.

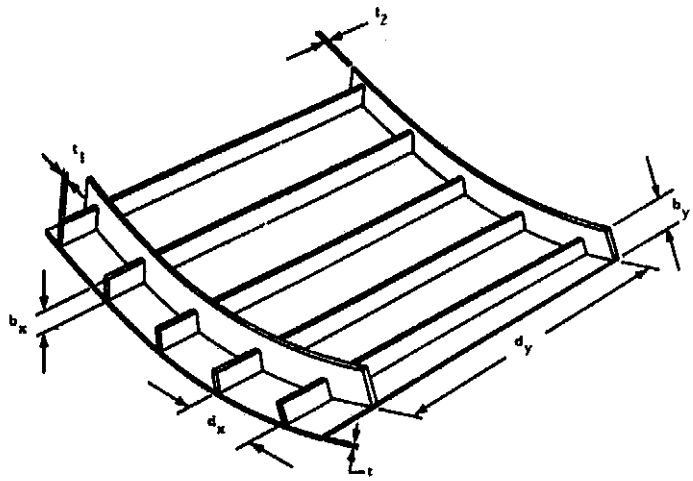

Typical Stiffened Cylindrical Cross Section

Table B-8

TYPICAL OPTIMIZED CROSS SECTION OF AMOOS VEHICLE
(All Dimensions in Inches)

	Nose	Fwd Body	Intermediate Body	Manned Unit
t	.032	.032	.025	.025
ℓ	114	126	168	139.2
d_x	1.87	1.87	1.72	1.94
b_x	.614	.614	.379	.492
t_1	.031	.031	.025	.032
d_y	16.29	15.75	10.50	17.40
b_y	.95	.95	.917	.788
t_2	.095	.095	.062	.052
$\bar{t}$	.0478	.0478	.0359	.036
Weight (lb)	173	193.18	199.2	166.2

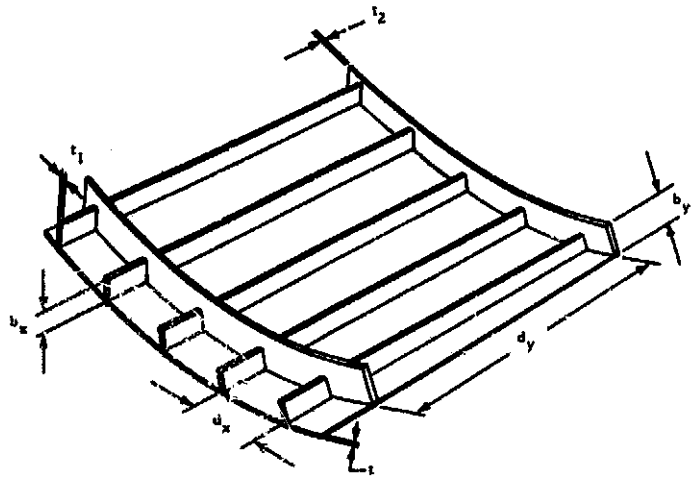

Typical Stiffened Cylindrical Cross Section

Table B-9

TYPICAL OPTIMIZED CROSS SECTION OF AMRS VEHICLE
(All Dimensions in Inches)

	Nose	Fwd Body	Aft Body
t	.026	.025	.025
ℓ	72	102	126
d_x	1.94	1.94	1.73
b_x	.379	.379	.477
t_1	.025	.025	.0315
d_y	12.00	12.75	15.75
b_y	.474	.474	.525
t_2	.031	.031	.035
$\bar{t}$	.031	.031	.035
Weight (lb)	43	60	84

Table B-10

OPTIMIZED AMOOS STRUCTURAL WEIGHT

Section	Station (in.)	Weight (lb)
Nose	0-114	301
Fwd Body	114-240	321
Intermediate Body	240-408	391
Manned Unit	408-547.2	326
Contingency 10%		134
Total		1471 lb

Table B-11

OPTIMIZED AMRS STRUCTURAL WEIGHT

Section	Station (in.)	Weight (lb)
Nose	0-72	118
Fwd Body	72-174	154
Aft Body	174-300	197
Contigency 10%		47
Total		516 lb

APPENDIX B REFERENCES

B-1. White, J., "Feasibility and Tradeoff Study of an Aeromaneuvering Orbit-to-Orbit Shuttle (AMOOS)," LMSC-HREC TR D390272, Lockheed Missiles & Space Company, Huntsville, Ala., August 1974.

B-2. "Baseline Space Tug System Requirements and Guidelines," MSFC 68-M00039-1, 15 July 1974.

B-3. Boeing Company, "Space Tug, Vol. 1 of 11, Book 2 of 4 — Final Report," NASA CR-103004, Huntsville, Ala., February 1971.

B-4. McDonnell Douglas Corp., "Manned Orbital Systems Concepts — Final Formal Review, Book 2," MDC G5955, May 1975.

B-5. Corning, G., "Weight Prediction Method for the Space Tug," IDA Log No. HQ 74-16219, Institute for Defense Analyses, Arlington, Va., June 1974.

B-6. "Space Shuttle System Payload Accommodations," JSC 07700, Vol. XIV, Rev. C, NASA-Johnson Space Center, Houston, Texas, 3 July 1974.

B-7. Materials Selector 76, Vol. 82, No. 4, Materials Engineering, Reinhold Publishing Co., Inc., Stanford, Conn., Mid-September, 1975.

B-8. "Metallic Materials and Elements for Aerospace Vehicle Structures," MIL-HDBK-5B Change Notice 2, Department of Defense, Washington, D.C., 31 August 1973.

B-9. "Strength, Efficiency and Design Data for Beryllium Alloy Structures," LMSC 679606, Lockheed Missiles & Space Company, Sunnyvale, Calif., 17 October 1967.

B-10. Hill, Julia, "Computer Programs for the Structural Optimization and Analysis of Axially Compressed Stiffened Cylinders," LMSC 6-65-65-13, Lockheed Missiles & Space Company, Sunnyvale, California, May 1965.

Appendix C
THERMAL PROTECTION SYSTEM DESIGN

Appendix C

C.1 INTRODUCTION

Prior to the design of the Thermal Protection System (TPS) for the AMOOS and AMRS vehicles a brief study was performed on the effects of bondline temperature and angle of attack on ablator weight. The method used in these studies follows the method of ablative TPS design used for AMOOS and AMRS. This method has the following steps:

1. The design trajectory is received as an input to the TPS design.
2. The stagnation point heating rates are then computed using the design trajectory to obtain the appropriate parameters. Heating rates, assuming free molecular, transitional and continuum flow, are computed together with $M/\sqrt{Re}$, which is used to determine the regime.
3. The heating rates are used to compute ablation rate and temperature within the ablator. These data are then used to determine the thickness of the ablator required at the various locations.

The procedure will now be discussed in more detail.

C.2 HEATING RATE CALCULATION METHODS

The equations for evaluating the free molecular and transitional heating rates on a stagnation point of a sphere were obtained from Ref. C-1. These were incorporated in a computer program to determine the non-continuum and continuum heating rates from the vehicle trajectory based on the effective spherical nose radius of 18.4 ft for the AMOOS configuration and 11.4 ft for the AMRS. The effective nose radii were determined from the bluntness parameter as shown in Ref. C-2. The heating rate profiles determined for the two vehicles for their respective trajectories are shown in Fig. C-1 and Fig. C-2.

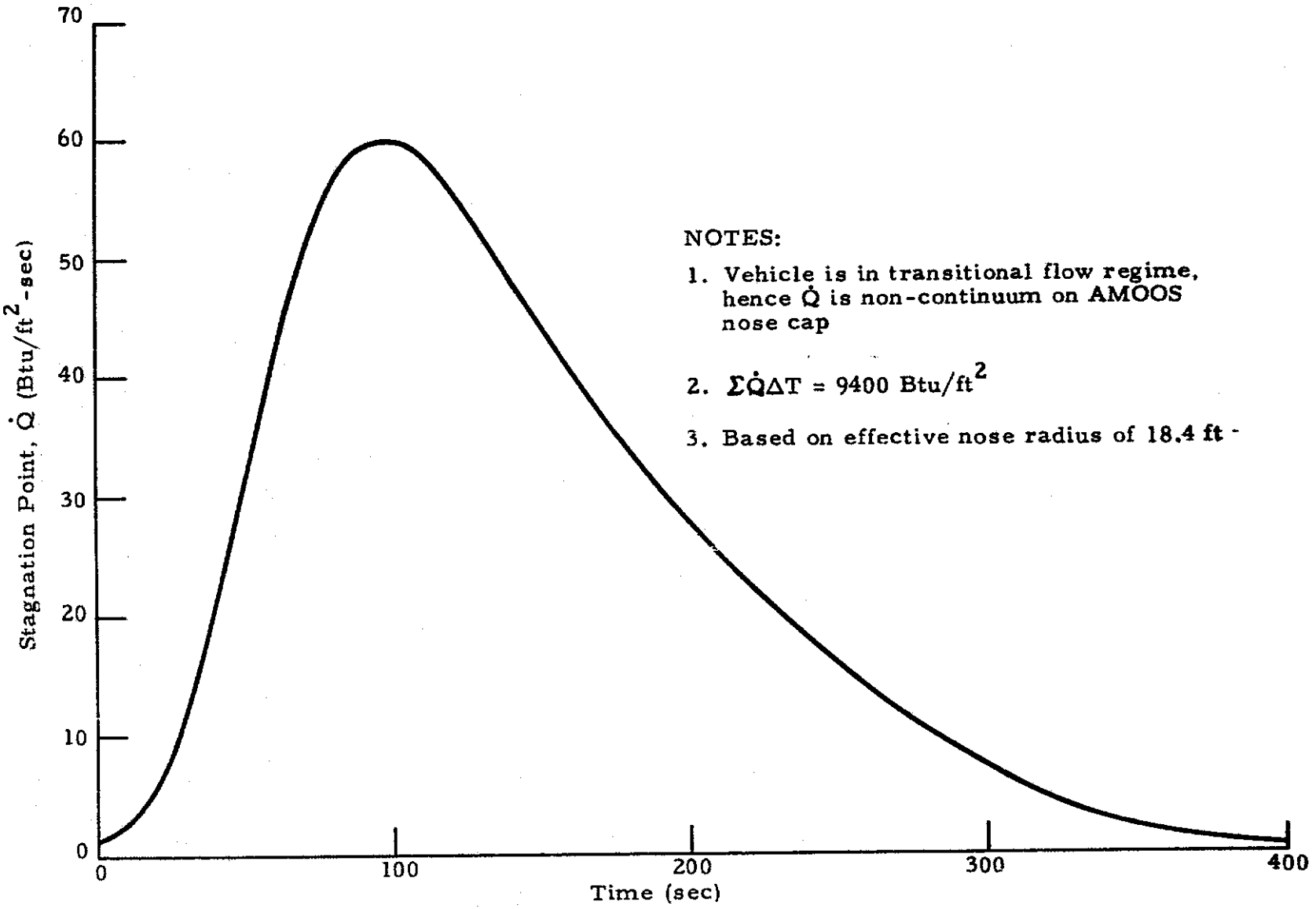

Fig. C-1 - Heating Rate vs Time Profile Obtained from AMOOS Design Trajectory

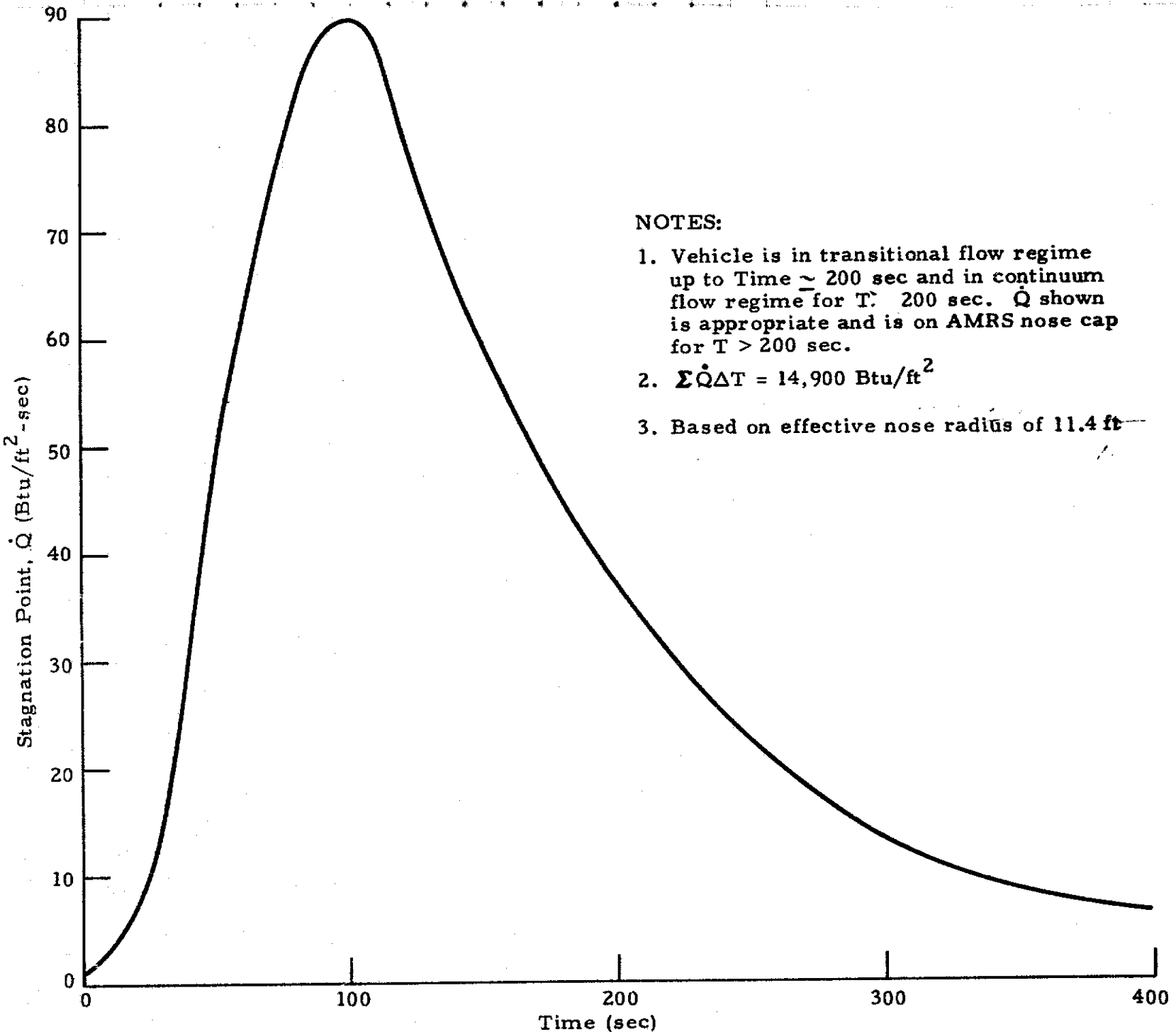

Fig. C-2 - Heating Rate vs Time Profile Obtained from AMRS Design Trajectory

C.3 DETERMINATION OF ABLATOR THICKNESS FOR GIVEN HEAT LOAD AT DESIRED BONDLINE TEMPERATURE

A standard ablation program of Ref. C-3 was used to determine maximum bondline temperature for various thicknesses of the Martin SLA-561 low density ablator. Properties of this ablative material were obtained from its principal developer, Dr. Eric Strauss, and are referenced in a letter of Ref. C-4. The heating environment used in the program was that of Fig. C-1. Radiative heating rates, which were found to have an insignificant contribution, were not included. The backup structure was modeled with 3 in. of Micro-Quartz insulation. The total heat load was varied in the program and maximum bondline temperatures determined for various thicknesses. Typical results are shown in Fig. C-3 and C-4. From these figures, ablator thicknesses for the desired bondline temperature were read off. For a bondline temperature of 600°F, a thickness versus heat load curve was obtained and is shown in Fig. C-5. This curve is subsequently used to obtain the thicknesses at various body points having different heat loads for the final ablator weight determination.

C.4 DETERMINATION OF HEAT TRANSFER DISTRIBUTION AT VARIOUS BODY LOCATIONS

The AMOOS and the ARMS consist of basically two geometrical shapes the fro. complexly curved nose cap and the rear ellipsoid part which can be approximated as a cylindrical section with an effective radius, R. The two sections were first divided into nodes. The nose section had ring-like nodes with the central node at the stagnation point and the rear cylindrical position had nodes located at different angular location, θ degrees, around the body (Fig. C-6).

For the rear cylindrical part, the heating rate with respect to the reference heating rate at the stagnation point on the vehicle nose (effective radius R = 18.4 ft for the AMOOS configuration and R = 11.4 for the AMRS) is determined as follows:

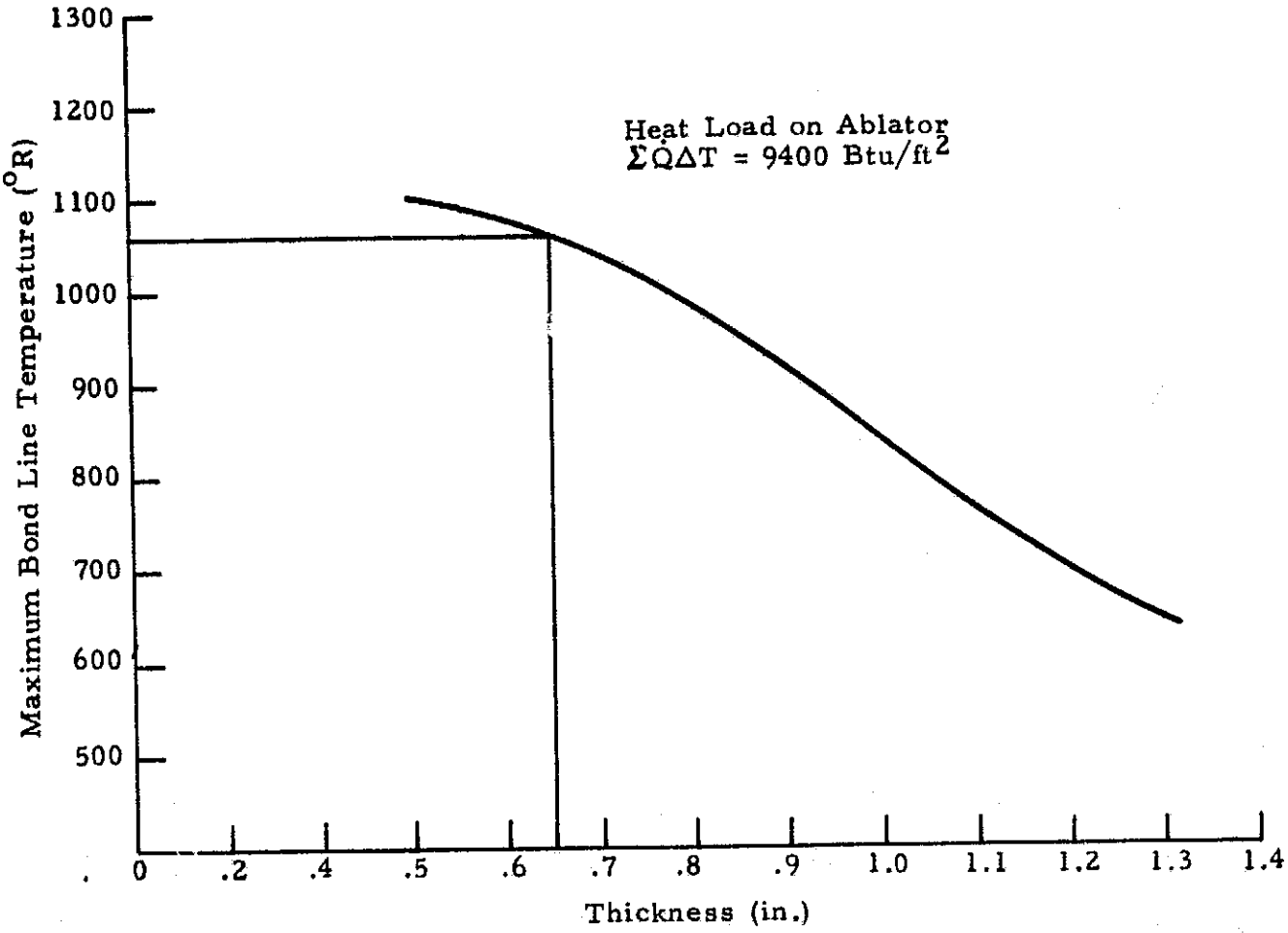

Fig. C-3 - Maximum Bond Line Temperature vs SLA-561 Ablator Thickness

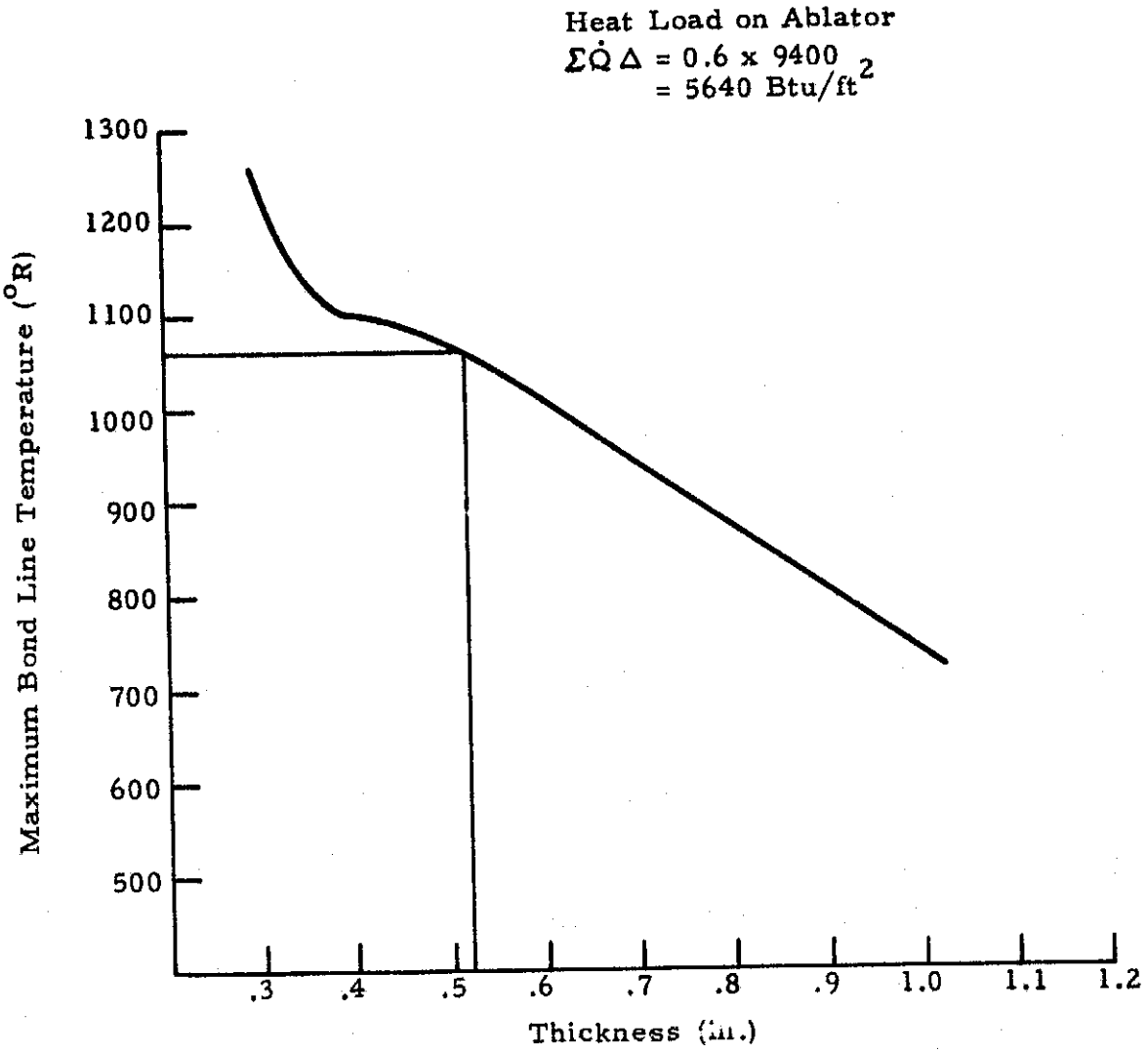

Fig. C-4 - Maximum Bond Line Temperature vs SLA-561 Ablator Thickness

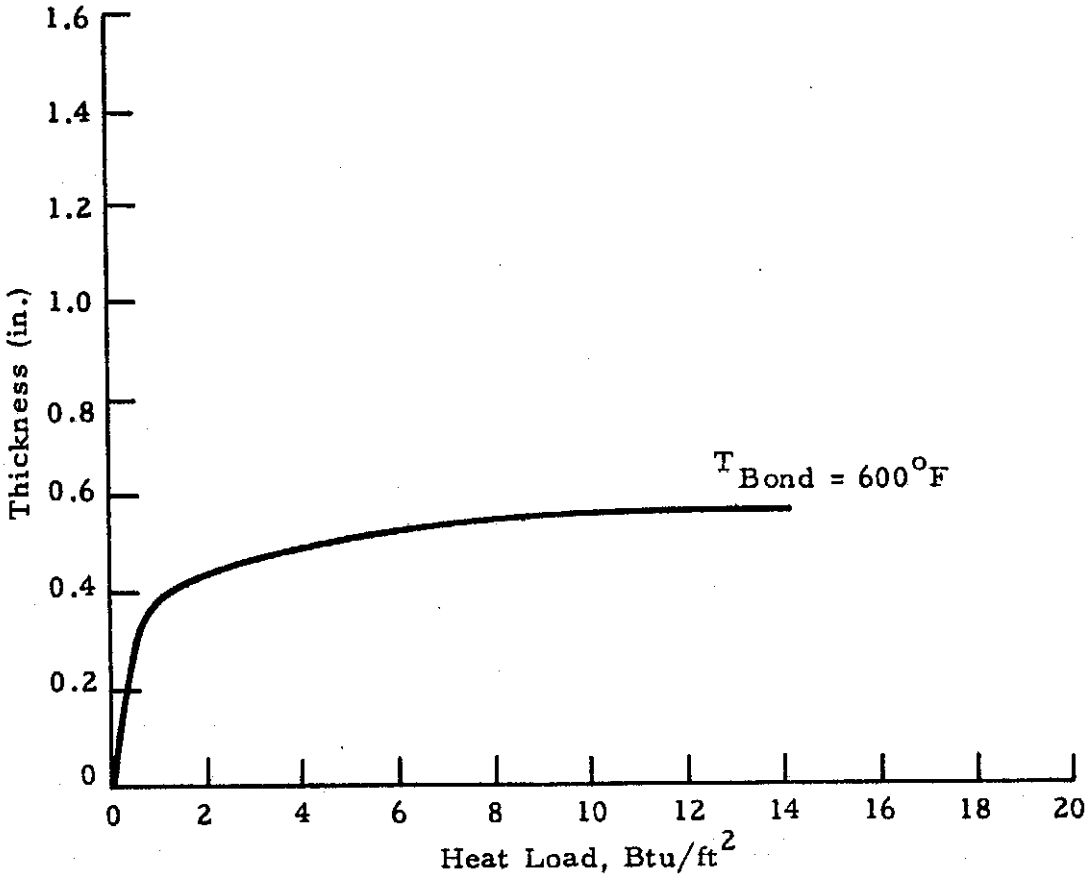

Fig. C-5 - Thickness vs Heat Load for Martin SLA-561 Ablator for Maximum Bond Line Temperature of 600°F

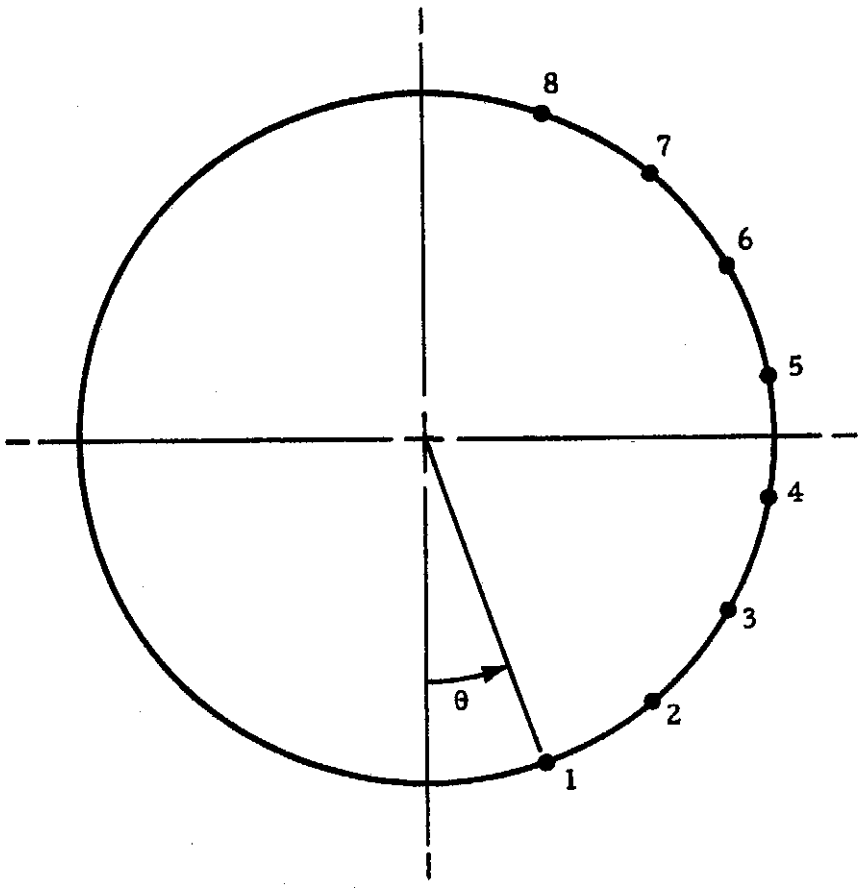

Fig. C-6 - Peripheral Location of the Nodes for the TPS Thickness Calculations on the Section of AMOOS and AMRS aft of Nose

$$\frac{\dot{q}_{\text{cylinder, radius = r at } \theta}}{\dot{q}_{\text{sphere, radius = R at stag pt.}}} = \left[\frac{\dot{q}_{\text{cyl, rad = r,}\theta}}{\dot{q}_{\text{cyl, rad = 1,}\theta}} \times \frac{\dot{q}_{\text{cyl, rad = 1,}\theta}}{\dot{q}_{\text{sph, rad = 1, stag}}} \times \frac{\dot{q}_{\text{sph, rad = 1, stag}}}{\dot{q}_{\text{sph, rad = R, stag}}}\right] = \sqrt{R} \times \frac{\dot{q}_{\text{cyl, rad = 1,}\theta}}{\dot{q}_{\text{sph, rad = 1, stag}}}$$

where θ = the angular position of any local point measured away from the windward streamline.

The heating rate ratio on the right-hand side of the last term of the equation is obtained from the swept infinite cylinder laminar heating distribution of Fig. C-7 (Ref. C-5) for the windward side of the vehicle at any desired angle of attack. For the lee-side, the peripheral laminar heat transfer distribution was deduced similarly from an experimental design curve shown in Fig. C-8 (Ref. C-6).

The heat transfer distribution around the spherical nose section of the vehicle was determined from Fig. C-9 obtained from Ref. C-5.

C.5 ANGLE OF ATTACK AND BONDLINE TEMPERATURE STUDIES

These studies were performed with the AMOOS configuration given in Ref. C-6. The ablator used was the Langley low density ablator, with properties also given in Ref. C-7. The ablator thickness was computed for angles of attack of 15, 25 and 45 degrees. For each angle of attack, the ablator weight was computed for bondline temperatures of 200, 300 and 600°F. The results of the study are shown in Fig. C-10. As can be seen, the windward side TPS weight varies slowly with angle of attack, increasing with increasing angle of attack over the range. The lee-side TPS weight is not given but is a small fraction of the total TPS weight. The variations in this small fraction with angle of attack would be expected to be small. From these studies it was concluded that the angle of attack could be chosen in the range of 25 to 45 degrees without a significant effect on TPS weight. Hence the desired value of 35 degrees from trajectory and guidance considerations was acceptable.

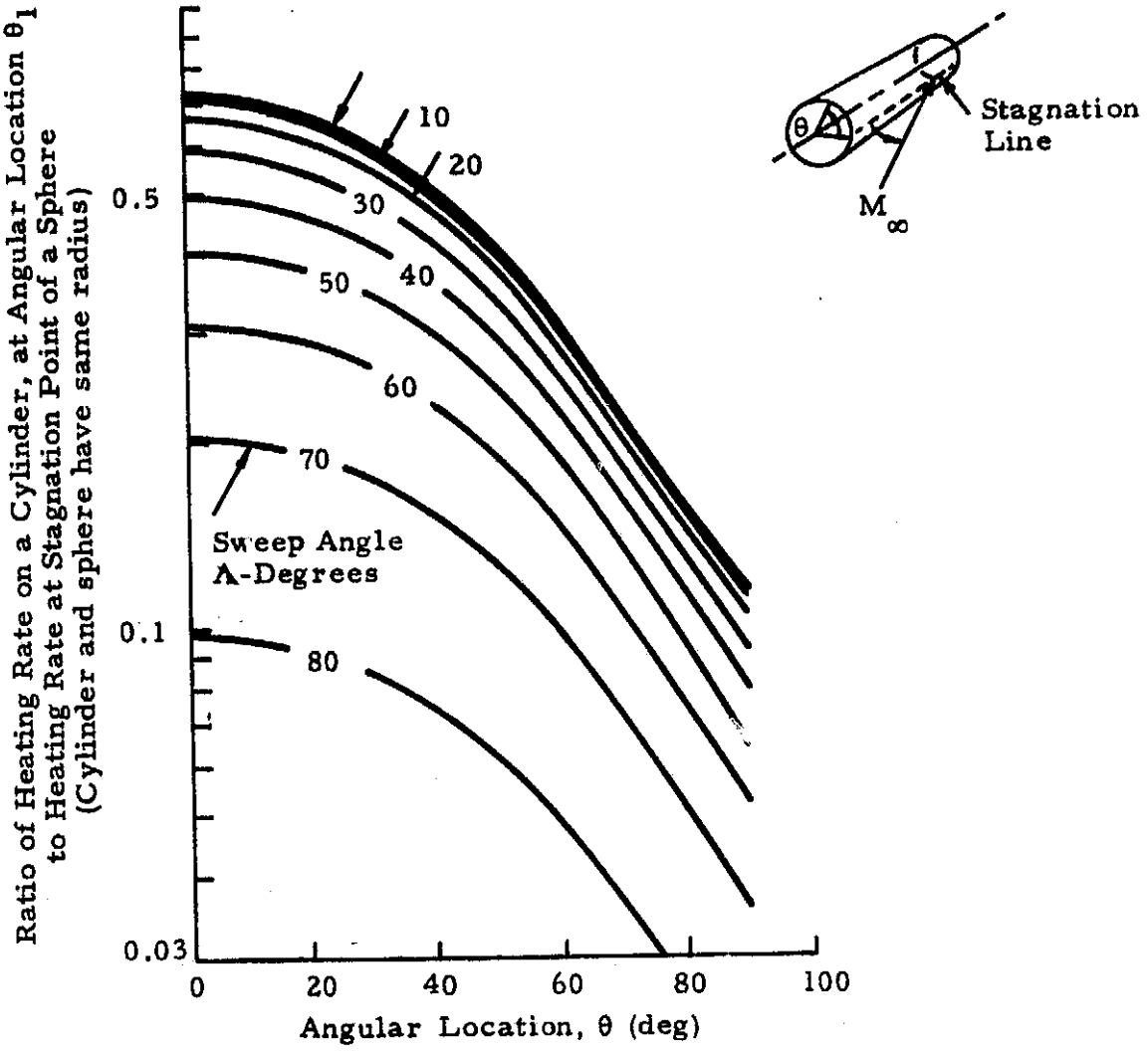

Fig. C-7 - Swept Infinite Cylinder Laminar Heating Distribution (Fig. 6-17 of Ref. C-5)

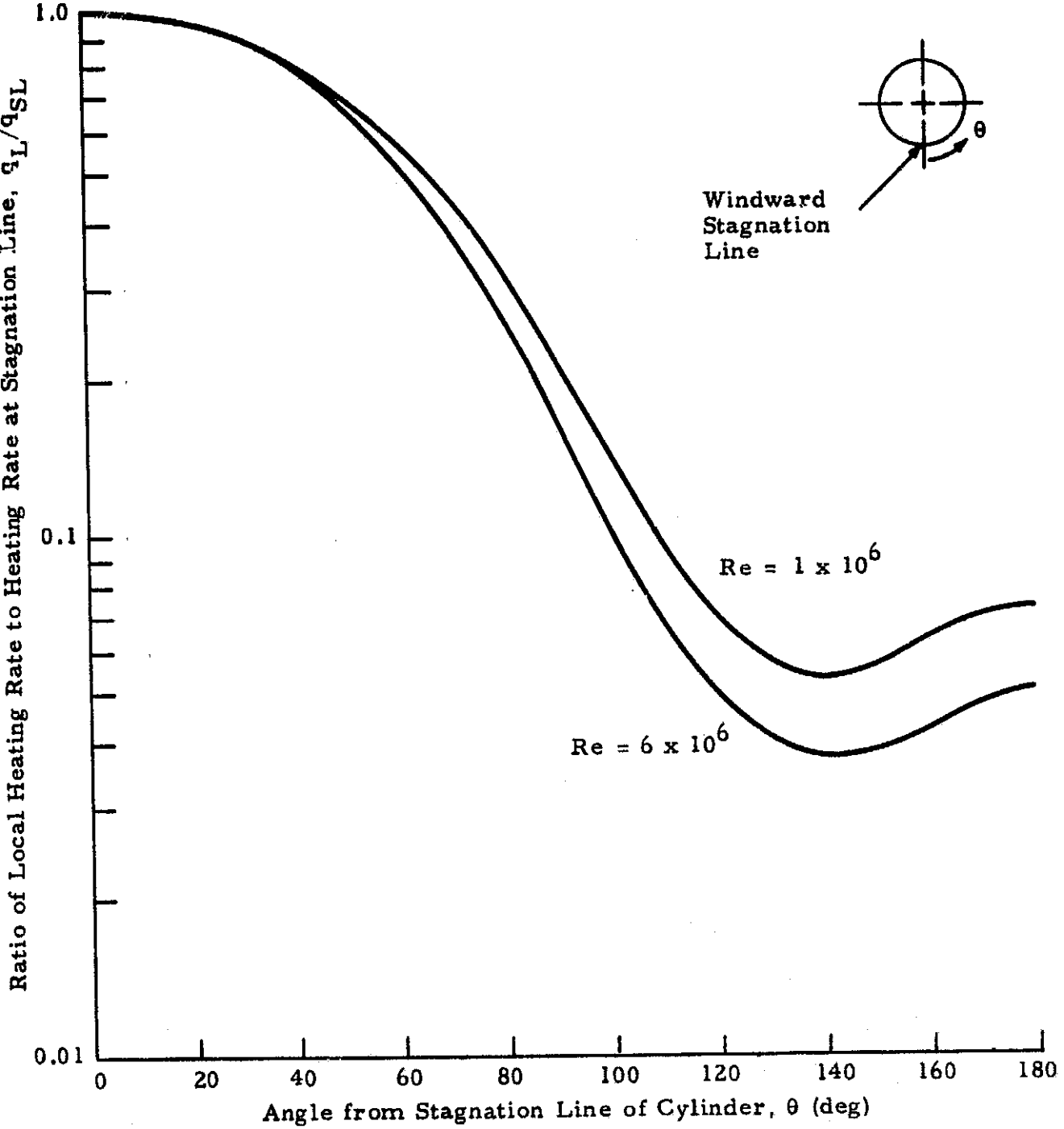

Fig. C-8 - Heating Rate Distribution Around Vehicle at 45 deg Angle of Attack (From Ref. C-6)

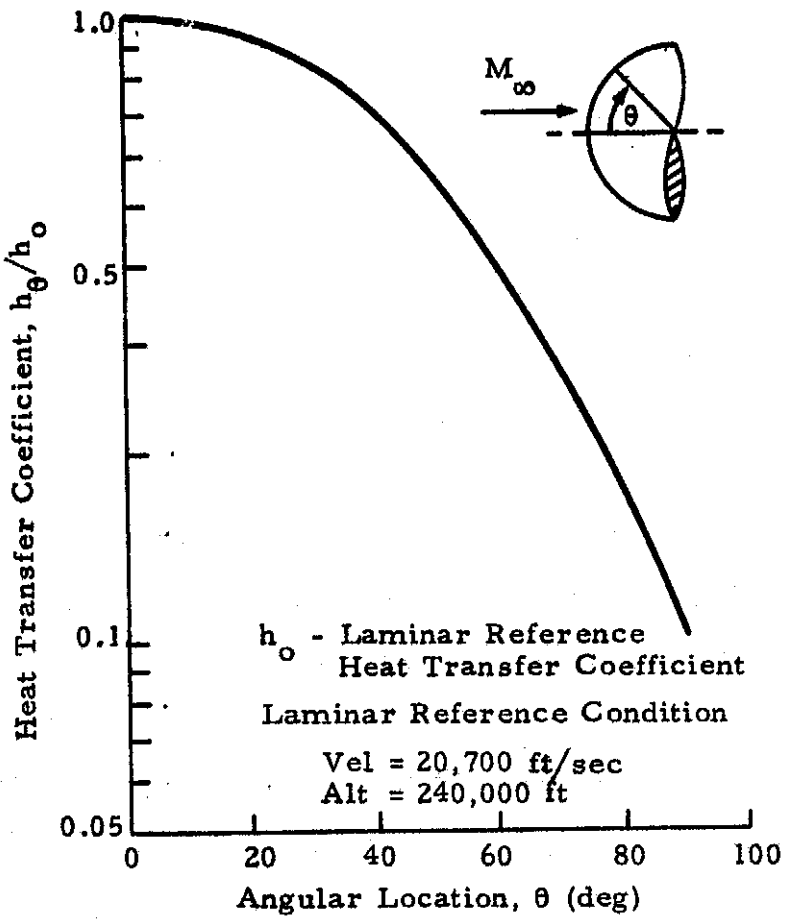

Fig. C-9 - Hemisphere Laminar Heating Distribution (Fig. 6-9 of Ref. C-5)

C.3

NOTE:

Total ablator weight includes sealer and bonding agent weight (.153 lbm/ft^2) and 10% allowed for close-outs around doors, hatches, etc.

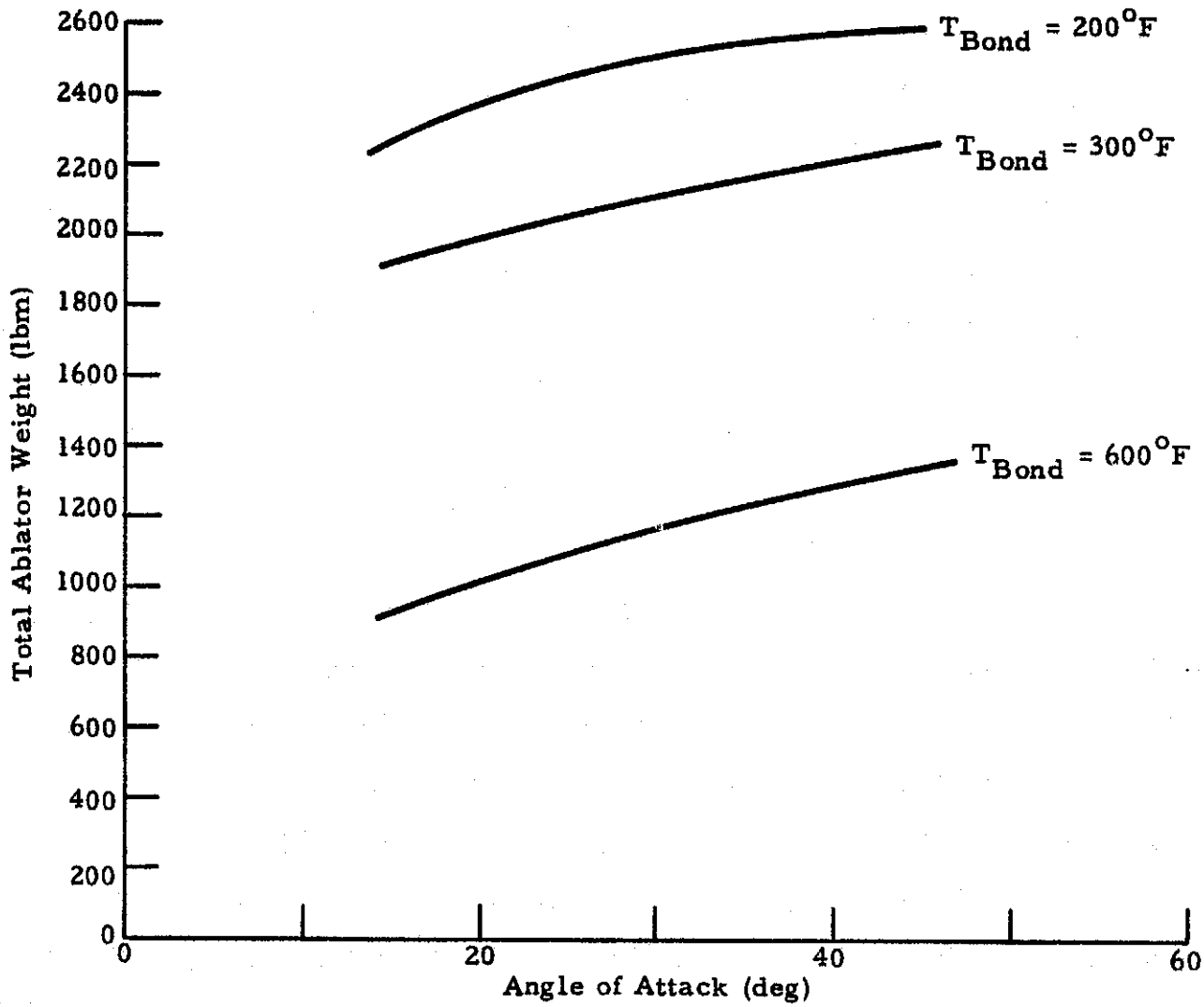

Fig. C-10 - Effect of Variation of Angle of Attack and Bond Line Temperature on Windward Side Ablator Weight on AMOOS

The effect of the bondline temperature on ablator weight is significant as can be seen in Fig. C-10. TPS weight decreases rapidly with increasing bondline temperature. Upon considerations of materials useable and the design conditions, the 600°F, bondline temperature was chosen for structural design.

A study was also performed to determine the ablator weight for various lengths of the AMOOS vehicle at the three different angles of attack and 600°F bondline temperature. This is summarized in Table C-1. The weight summary for AMRS is shown in Table C-2.

Table C-1

AMOOS SLA-561 TPS WINDWARD SIDE WEIGHT SUMMARY
(MAXIMUM BONDLINE TEMPERATURE OF 600°F)

Vehicle Length (ft)	Angle of Attack (deg)	Surface Area (ft^2)	Sealer + Bond Wt.* (lbm)	Ablator Wt. (lbm)	Ablator Wt. + 10%** (lbm)	Total Ablator Wt. (lbm)
59.0	45	1337.0	205.2	837.8	921.6	1127.0
	25	1337.0	205.2	781.0	859.1	1064.0
	15	1337.0	205.2	749.0	823.1	1029.0
45.6	45	1040.8	159.2	656.2	721.8	881.0
	25	1040.8	159.2	614.6	676.0	835.0
	15	1040.8	159.2	595.0	654.5	814.0
34.0	45	785.8	120.2	499.8	549.8	670.0
	25	785.8	120.2	470.8	517.9	638.0
	15	785.8	120.2	463.0	509.3	630.0

*Sealer plus bonding agent weight = 0.153 lbm/ft^2

**10% allowed for closeouts around doors, hatches, access areas, etc.

Table C-2

AMRS SLA-561 TPS WINDWARD SIDE WEIGHT SUMMARY
(MAXIMUM BONDLINE TEMPERATURE OF 600°F)

Angle of Attack (deg)	Surface Area (ft^2)	Sealer + Bond Wt.* (lbm)	Ablator Wt. (lbm)	Ablator Wt. + 10%** (lbm)	Total Ablator Wt. (lbm)
45	360.0	55.1	241.4	265.5	320.6
25	360.0	55.1	226.5	249.2	304.3
15	360.0	55.1	212.9	234.2	289.3

*Sealer plus bonding agent weight = 0.153 lbm/ft^2

**10% allowed for closeouts around doors, hatches, access areas, etc.

REFERENCES

C-1. Engel, C. D., "Aeroheating Correlations for Non-Continuum Hypersonic Flight," RTR-008-2, REMTECH, Inc., Huntsville, Ala., December 1972.

C-2. Boison and Curtiss, "An Experimental Investigation of Blunt Body Stagnation Point Velocity Gradient," ARS J., February 1959, p. 130.

C-3. Curry, D. M., "An Analysis of a Charring Ablation Thermal Protection System," NASA TN D-3150, December 1965.

C-4. Strauss, E. L., Letter to Z. Karu, Lockheed Missiles & Space Company, Huntsville, Ala., 35807, Martin Marietta Aerospace, Structures and Materials Dept. (Mail 0431), P. O. Box 179, Denver, Colo., 80201, 30 October 1975.

C-5. Thomas, A. C. et al., "Advanced Reentry Systems Heat Transfer Manual for Hypersonic Flight," AFFDL-TR-65-195, Wright-Patterson AFB, Ohio, October 1966.

C-6. Stevens, R. A. et al., "Re-entry Heat Transfer to a Delta Wing Space Shuttle Booster at High Angles of Attack," FZA-452, General Dynamics, Convair Division, Fort Worth, Texas, March 1971.

C-7. White, J., "Feasibility and Tradeoff Study of an Aeromaneuvering Orbit-to-Orbit Shuttle (AMOOS)," LMSC-HREC TR D390272, Lockheed Missiles & Space Company, Huntsville, Ala., August 1974.

Appendix D
ATMOSPHERIC FLIGHT GUIDANCE

LIST OF VARIABLES

A	system matrix
A_R	aerodynamic reference area
B	system matrix
$\underline{C}$	feedback gain vector
C_D	aerodynamic drag coefficient
C_L	aerodynamic lift coefficient
C_{LY}	component of C_L along the Y_R axis (Fig. D-2)
D	aerodynamic drag in direction of V
H	weighting matrix
h	altitude
h_a	apogee altitude
h_o	atmospheric scale height
h_{nom}	nominal altitude
K	gain matrix
L	aerodynamic lift perpendicular to V
m	vehicle mass
Q	weighting matrix
R	weighting matrix
r	radius from center of the earth to vehicle center of gravity
r_{nom}	nominal radius

t	time
t_f	final time (atmospheric exit)
t_o	initial time (atmospheric entry)
u	control variable
V	inertial velocity
V_E	inertial velocity of the air mass
V_R	velocity relative to surrounding air mass
V_{nom}	nominal velocity

Greek

β	bank angle (see Fig. D-2)
β_c	commanded bank angle
β_o	nominal bank angle
γ	inertial flight path angle
γ_{nom}	nominal flight path angle
δr	$r - r_{nom}$
δV	$V - V_{nom}$
$\delta \underline{X}$	state vector
$\delta\gamma$	$\gamma - \gamma_{nom}$
μ	earth gravitational constant
ρ	atmospheric density
ρ_o	reference atmospheric density
ρ_{nom}	nominal density
τ	time constant

1. GUIDANCE METHOD I: OPTIMAL LINEAR REGULATOR APPROACH

1.1 INTRODUCTION

The equations of motion for the atmospheric flight of an AMOOS or AMRS type vehicle are highly nonlinear and the "exact" optimal solution is not expected to be in a form simple enough to be implemented in the onboard computer. The more promising approach is therefore to minimize the deviations from a nominal trajectory. An optimum guidance problem can then be formulated based on the perturbation equations and a quadratic performance functional which results in a linear feedback solution.

1.2 EQUATIONS OF MOTION

The objective of the atmospheric flight guidance was to achieve a certain apogee altitude after the pass through the atmosphere. Only the motion in the orbital plane affects that parameter significantly. The equations of motion were therefore represented in terms of inertial velocity, V, inertial flight path angle, γ, and radius, r, for the purpose of the guidance problem formulation. The equations of motion are derived as follows:

$$\frac{d\underline{V}}{dt} = \underline{u}_{1\vec{V}} \frac{dV}{dt} + \underline{u}_{\perp\vec{V}} V \frac{d\theta}{dt} \qquad (D.1)$$

where

$\underline{u}_{1\vec{V}}$ = unit vector in direction of $\underline{V}$

$\underline{u}_{\perp\vec{V}}$ = unit vector perpendicular to $\underline{V}$

From the components in the direction of $\underline{V}$ results the equation for $\dot{V}$.

$$\sum \text{Forces in direction of } \underline{V} =$$

$$-D - \frac{\mu}{r^2} m \sin\gamma = m\dot{V} \qquad \text{(D.2)}$$

$$\dot{V} = -\frac{D}{m} - \frac{\mu}{r^2} \sin\gamma \qquad \text{(D.3)}$$

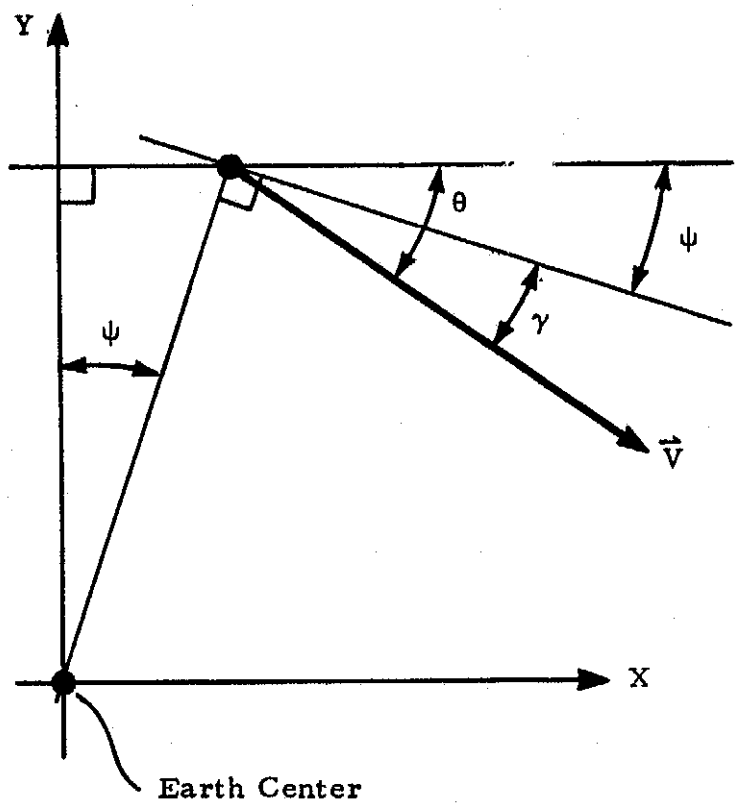

x-y Coordinates Represent an Inertial Frame

Fig. D-1 - Derivation of Equations of Motion

From the components perpendicular to $\underline{V}$ results the equation for $\dot{\gamma}$.

$$\sum \text{Forces perpendicular to } \underline{V} =$$

$$L - \frac{\mu}{r^2} m \cos\gamma = mV\dot{\theta} \tag{D.4}$$

From Fig. D-1

$$\dot{\theta} = \dot{\psi} + \dot{\gamma} \tag{D.5}$$

$$\dot{\psi} = \frac{-V\cos\gamma}{r} \tag{D.6}$$

$$\dot{\theta} = \dot{\gamma} - \frac{V}{r}\cos\gamma \tag{D.7}$$

Substituting Eq. (D.7) into Eq. (D.4) and solving for $\dot{\gamma}$ yields

$$\dot{\gamma} = \frac{L}{mV} - \frac{1}{V}\left[\frac{\mu}{r^2} - \frac{V^2}{r}\right]\cos\gamma \tag{D.8}$$

The equation for $\dot{r}$ is

$$\dot{r} = V\sin\gamma \tag{D.9}$$

Equations (D.3), (D.8) and (D.9) represent the equations of motion in the orbital plane. The aerodynamic forces L and D are here defined with respect to the inertial velocity. Since the inertial and relative velocity vectors are almost parallel over the velocity range under consideration the aerodynamic lift and drag with respect to the relative velocity will be substituted for L and D, i.e.,

$$D \approx \frac{1}{2}\rho V_R^2 A_R C_D \tag{D.10}$$

$$L \approx \frac{1}{2}\rho V_R^2 A_R C_L \cos\beta \tag{D.11}$$

$$V_R \approx V - V_E \tag{D.12}$$

The bank angle β is defined in Fig. D-2.

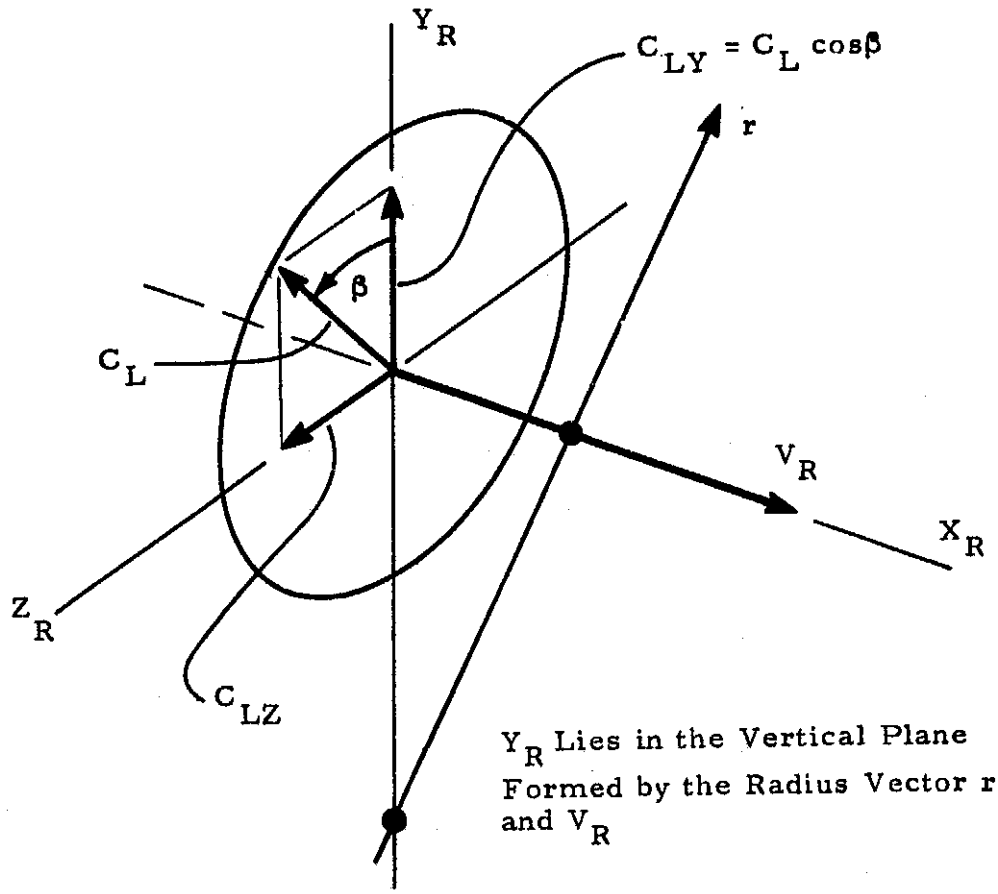

Fig. D-2 - Definition of Bank Angle, β

Trajectory control is effected by rotating the vehicle around the vector V_R (i.e., changing the bank angle). This changes the component of C_L along the Y_R-axis, C_{LY}, in Fig. D-2. The control variable, u, was defined as the deviation of the commanded value of C_{LY} from some nominal value.

$$u = C_{LY} - C_{LYo} = C_L (\cos\beta_c - \cos\beta_o) \qquad (D.13)$$

For the purpose of deriving the guidance law it was assumed that the vehicle can be rotated instantaneously from the present bank angle β to the commanded angle β_c, thus

$$\beta = \beta_c \quad . \tag{D.14}$$

However, the vehicle rotation was not ignored in the computer simulation of the guidance scheme. There, the vehicle rotation was simulated as a minimum time maneuver with a constant angular acceleration of 1 deg/sec^2.

Substituting Eqs. (D.10), (D.11), (D.12), (D.13) and (D.14) into (D.3) and (D.8) results in the final form for the equations of motion.

$$\dot{V} = -1 \frac{1}{2m} \rho (V - V_E)^2 C_D A_R - \frac{\mu}{r^2} \sin\gamma \tag{D.15}$$

$$\dot{\gamma} = \frac{1}{2mV} \rho (V - V_E)^2 A_R \left[C_L \cos\beta_o + u \right] - \left[\frac{\mu}{Vr^2} - \frac{V}{r} \right] \cos\gamma \tag{D.16}$$

$$\dot{r} = V \sin\gamma \tag{D.17}$$

The linearization of the equations of motion sought is of the form

$$\begin{bmatrix} \delta\dot{V} \\ \delta\dot{\gamma} \\ \delta\dot{r} \end{bmatrix} = [A] \begin{bmatrix} \delta V \\ \delta\gamma \\ \delta r \end{bmatrix} + [B] u \tag{D.18}$$

where

$$[A] = \begin{bmatrix} \frac{\partial\dot{V}}{\partial V} & \frac{\partial\dot{V}}{\partial\gamma} & \frac{\partial\dot{V}}{\partial r} \\ \frac{\partial\dot{\gamma}}{\partial V} & \frac{\partial\dot{\gamma}}{\partial\gamma} & \frac{\partial\dot{\gamma}}{\partial r} \\ \frac{\partial\dot{r}}{\partial V} & \frac{\partial\dot{r}}{\partial\gamma} & \frac{\partial\dot{r}}{\partial r} \end{bmatrix} \quad \text{and} \tag{D.19}$$

$$[B] = \begin{bmatrix} \frac{\partial \dot{V}}{\partial u} \\ \frac{\partial \dot{\gamma}}{\partial u} \\ \frac{\partial \dot{r}}{\partial u} \end{bmatrix} \tag{D.20}$$

The partial derivatives are obtained from Eqs. (D.15), (D.16) and (D.17) as follows.

$$\frac{\partial \dot{V}}{\partial V} = \frac{-1}{m} \rho \, V_R \, C_D \, A_R \tag{D.21}$$

$$\frac{\partial \dot{V}}{\partial \gamma} = - \frac{\mu}{r^2} \cos\gamma \tag{D.22}$$

$$\frac{\partial \dot{V}}{\partial r} = - \frac{1}{2m} V_R^2 \, C_D \, A_R \frac{\partial \rho}{\partial r} + \frac{2\mu}{r^3} \sin\gamma \tag{D.23}$$

$$\frac{\partial \dot{\gamma}}{\partial V} = \frac{1}{mV} \left[V_R - \frac{V_R^2}{2V} \right] \rho A_R \left[C_L \cos\beta_o + u \right] + \left[\frac{\mu}{V^2 r^2} + \frac{1}{r} \right] \cos\gamma \tag{D.24}$$

$$\frac{\partial \dot{\gamma}}{\partial \gamma} = \left[\frac{\mu}{Vr^2} - \frac{V}{r} \right] \sin\gamma \tag{D.25}$$

$$\frac{\partial \dot{\gamma}}{\partial r} = \frac{1}{2mV} V_R^2 \, A_R \left[C_L \cos\beta_o + u \right] \frac{\partial \rho}{\partial r} - \left[- \frac{2\mu}{Vr^3} + \frac{V}{r^2} \right] \cos\gamma \tag{D.26}$$

$$\frac{\partial \dot{r}}{\partial V} = \sin\dot{\gamma} \tag{D.27}$$

$$\frac{\partial \dot{r}}{\partial \gamma} = V \cos\gamma \tag{D.28}$$

$$\frac{\partial \dot{r}}{\partial r} = 0 \tag{D.29}$$

$$\frac{\partial \dot{V}}{\partial u} = 0 \tag{D.30}$$

$$\frac{\partial \dot{\gamma}}{\partial u} = \frac{1}{2mV} \rho V_R^2 A_R \tag{D.31}$$

$$\frac{\partial \dot{r}}{\partial u} = 0 \tag{D.32}$$

$$\frac{\partial \rho}{\partial r} = -\frac{\rho}{h_o} \quad \text{(based on exponential atmosphere)} \tag{D.33}$$

1.3 FORMULATION OF THE OPTIMUM GUIDANCE PROBLEM

The selected performance functional is quadratic in state and control. It is of the following form

$$J = \frac{1}{2} \delta \underline{x}^T (t_f) H \delta \underline{x} (t_f) + \frac{1}{2} \int_{t_o}^{t_f} \left[\delta \underline{x}^T Q \delta \underline{x} + u^2 R \right] dt \tag{D.34}$$

where

$$\delta \underline{x} = \begin{bmatrix} \delta V \\ \delta \gamma \\ \delta r \end{bmatrix}$$

H, Q and R are weighting matrices.

The differential equation constraint is given by Eq. (D.18) as

$$\delta \dot{\underline{x}} = A \delta \underline{x} + Bu \tag{D.35}$$

The solution to this optimization problem is derived in numerous textbooks on optimal control theory (see e.g., Ref. D-1*, pp. 209-212).

The solution is

$$u = - R^{-1} B^T K \, \delta \underline{x} = \underline{C}^T \, \delta \underline{x} \tag{D.36}$$

The matrix K is given by the Riccati differential equation

$$\dot{K} = - A^T K - KA - Q + KBR^{-1} B^T K \tag{D.37}$$

The Riccati equation must therefore by integrated backwards in time.

From examining the equations of motion it is evident that the altitude variation during the atmospheric flight (70 to 100 km) has an insignificant effect on the gravitational terms but has a dominating effect on the atmospheric density. The altitude error

$$\delta r = r - r_{nom} = h - h_{nom} \tag{D.38}$$

was therefore related to the atmospheric density encountered which in turn was obtained from the vehicle acceleration. Solving the equation (valid for small flight path angles),

$$\dot{V}m = - \frac{1}{2} \rho \, V_R^2 \, C_D \, A_R , \tag{D.39}$$

for ρ yields

$$\rho = \frac{- 2 \dot{V} m}{V_R^2 \, C_D \, A_R} \tag{D.40}$$

*D-1. Kirk, Donald E., Optimal Control Theory, Prentice Hall, Englewood Cliffs, N. J., 1970.

This density, ρ, can be converted to an equivalent altitude assuming an exponential atmosphere.

$$h = -h_o \ln(\rho/\rho_o) \tag{D.41}$$

The nominal altitude profile must then be computed by the same relationship from the nominal density

$$h_{nom} = -h_o \ln(\rho_{nom}/\rho_o) \quad . \tag{D.42}$$

1.3.1 Selection of the Weighting Matrices for AMOOS Guidance

The objective of the atmospheric flight guidance for the AMOOS vehicle is to achieve a specified apogee altitude (720 km) after the atmospheric pass. The apogee altitude is fully determined by V, γ and r at the time of exit from the atmosphere. The matrix H was chosen to minimize the effect of the final state $\delta\underline{x}(t_f)$ (at atmospheric exit) on apogee altitude, h_a. For small variations δh_a can be related to the final state by

$$\delta h_a = \left[\frac{\partial h_a}{\partial V}\,\delta V + \frac{\partial h_a}{\partial \gamma}\,\delta\gamma + \frac{\partial h_a}{\partial r}\,\delta r\right]_{t=t_f} \tag{D.43}$$

The matrix H was then determined from

$$\delta h_a^2 = \delta\underline{x}^T(t_f)\, H\, \delta\underline{x}(t_f) \tag{D.44}$$

which yields the elements h_{ij} of H as follows:

$$h_{11} = \left(\frac{\partial h_a}{\partial V}\right)^2 \tag{D.45}$$

$$h_{22} = \left(\frac{\partial h_a}{\partial \gamma}\right)^2 \tag{D.46}$$

$$h_{33} = \left(\frac{\partial h_a}{\partial r}\right)^2$$

$$h_{12} = h_{21} = \frac{\partial h_a}{\partial V} \frac{\partial h_a}{\partial \gamma} \tag{D.48}$$

$$h_{13} = h_{31} = \frac{\partial h_a}{\partial V} \frac{\partial h_a}{\partial r} \tag{D.49}$$

$$h_{23} = h_{32} = \frac{\partial h_a}{\partial \gamma} \frac{\partial h_a}{\partial r} \tag{D.50}$$

The partial derivatives were computed for the final state V = 7980 m/sec, γ = 1.75 deg and r = 6,498, 153 m. The numerical values are:

$$\frac{\partial h_a}{\partial V} = 3.32 \frac{\text{km}}{\text{m/sec}}$$

$$\frac{\partial h_a}{\partial \gamma} = 74.73 \text{ km/deg}$$

$$\frac{\partial h_a}{\partial r} = 3.116 \text{ m/m}$$

The weighting matrix Q accounts for the deviations from the nominal trajectory during the atmospheric flight. These deviations are significant only if they result in an excessive increase in heating rate, heating load or dynamic pressure. The simulation results have shown that this is not the case. The matrix Q was therefore set equal to zero.

The weighting function R(t) was selected based on the consideration that the control variable u should not exceed the maximum allowed value for the range of $\delta \underline{x}$ associated with the particular guidance problem.

Several functions, R(t) were investigated in order to reduce the peaking of the gains at perigee. The function selected is shown in Fig. D-3.

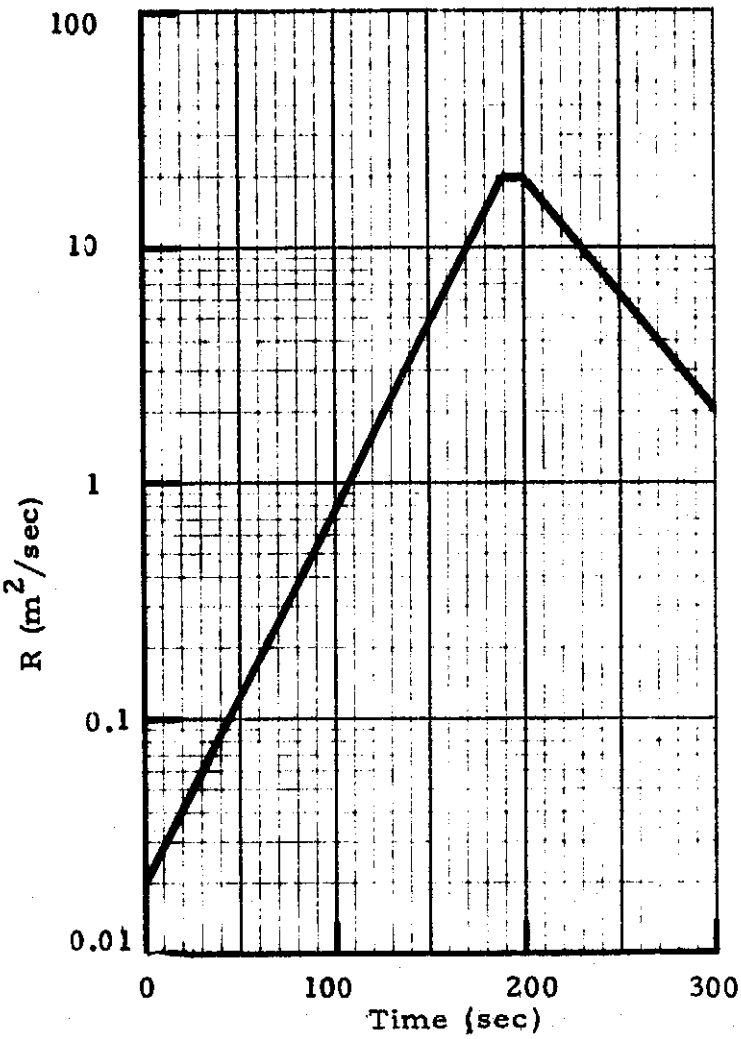

Fig. D-3 - Weighting Coefficient R vs Time

Figure D-4 shows the feedback gain vector $\underline{C}$ (see Eq. (D.36)) for the selected weighting matrices and for a nominal trajectory based on the following vehicle and orbital parameters:

Vehicle mass, m	6804 kg
Drag coefficient, C_D	2.5125
Lift coefficient, C_L	1.3457
Aerodynamic reference area, A_R	15.69 m^2

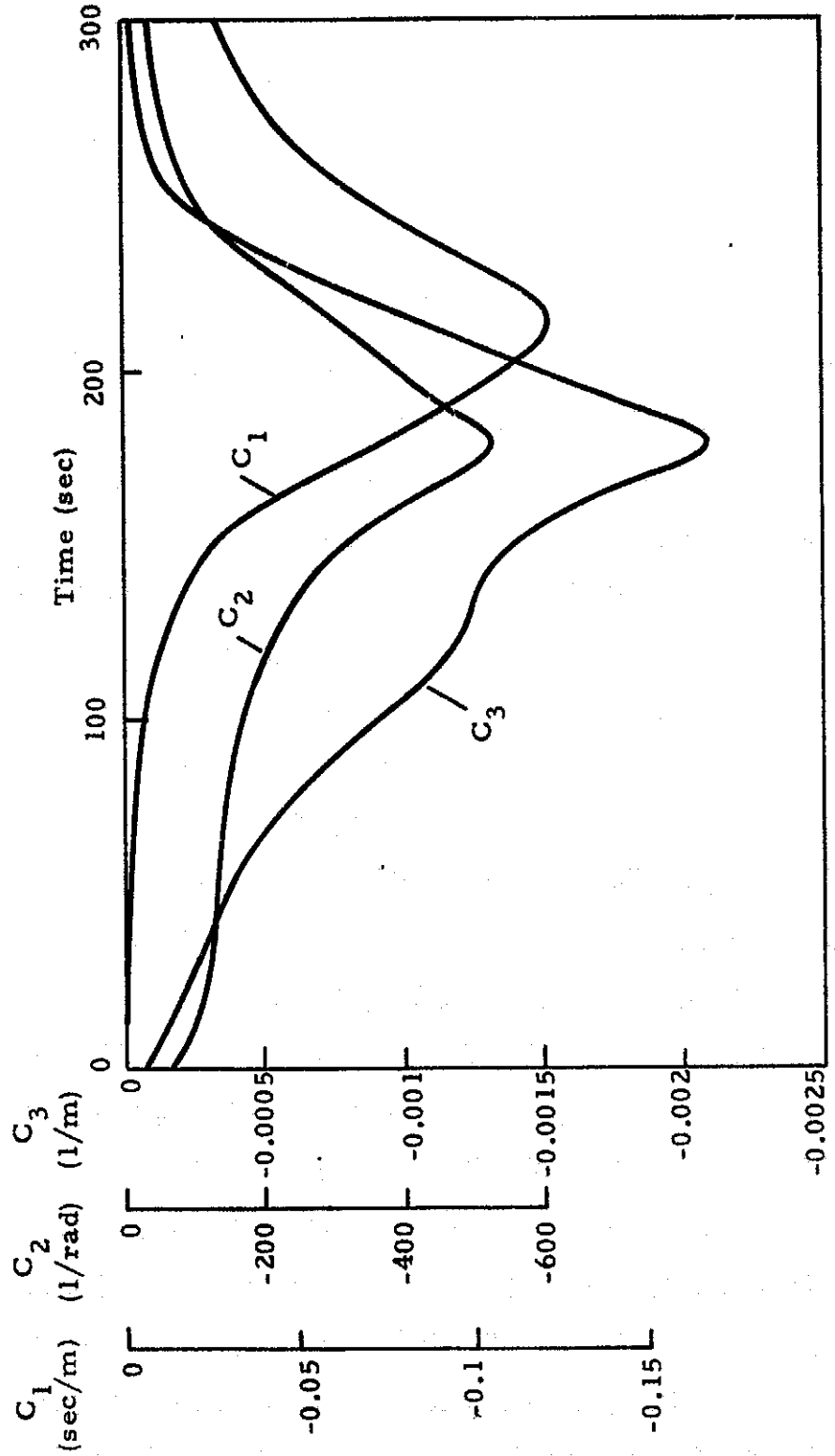

Fig. D-4 - Feedback Gain Vector $\underline{C}$ for AMOOS Guidance

Bank angle, β_o 90 deg

Atmospheric model: 1962 Standard Atmosphere

Trajectory: Transfer ellipse from equatorial geosynchronous orbit with 70.579 km target perigee altitude and 21.4 deg inclination

The time point t = 0 in Figs. D-3 and D-4 corresponds to the time when the nominal trajectory passes through 95.4 km altitude at atmospheric entry.

1.3.2 Selection of the Weighting Matrices for AMRS Reentry Guidance

The optimal linear regulator guidance approach is also applicable to the initial portion of a reentry trajectory like the direct reentry of an AMRS vehicle since a similar flight environment is encountered. However, during the later portion of the atmospheric flight when the vehicle environment becomes less severe other trajectory control methods become permissible (e.g., positive and negative angle of attack) which lead to alternate guidance methods. The present investigation covers therefore only the initial portion of the reentry trajectory.

For reentry guidance the objective is to keep the vehicle close to the nominal trajectory. A choice of the weighting matrices which often turns out to be a reasonable one for this type of problems is

$$H^{-1} = \text{maximum acceptable value of diag. } \delta\underline{x}(t_f)\,\delta\underline{x}^T(t_f) \tag{D.51}$$

$$Q^{-1} = (t_f - t_o) \times \text{maximum acceptable value of diag. } \delta\underline{x}(t)\,\delta\underline{x}^T(t) \tag{D.52}$$

$$R^{-1} = m/n\,(t_f - t_o) \times \text{maximum acceptable value of diag. } u(t)\,u^T(t) \tag{D.53}$$

where

m = number of control variables

n = number of states

The guided flight lasted 280 sec from atmospheric entry until the velocity had dropped to 4800 m/sec. The maximum acceptable errors at the end of the guided flight were somewhat arbitrarily chosen as

$$\delta V(t_f) = 100 \text{ m/sec}$$
$$\delta \gamma(t_f) = 3 \text{ deg} = 0.052 \text{ rad}$$
$$\delta h(t_f) = 2 \text{ km}$$

The matrix H becomes then

$$H = \begin{bmatrix} 10^{-4} & 0 & 0 \\ 0 & 370 & 0 \\ 0 & 0 & 2.5 \times 10^{-7} \end{bmatrix}$$

The matrix Q at final time is

$$Q(t_f) = \frac{1}{280} H = \begin{bmatrix} 3.6 \times 10^{-7} & 0 & 0 \\ 0 & 1.3 & 0 \\ 0 & 0 & 0.9 \times 10^{-9} \end{bmatrix}$$

The errors during the early portion of the atmospheric flight can be considerably larger than the values toward the end of the flight. In order not to require an excessive amount of control during that portion of the flight $Q(t_o)$ was chosen to be zero. The values between t_o and t_f were obtained by linear interpolation between $Q(t_o)$ and $Q(t_f)$.

The maximum value for u is based on the maximum deviation of β from its nominal value, β_o.

$$\left|\beta - \beta_o\right|_{max} = 30 \text{ deg}$$

From Eq. (D.13)

$$u_{max} = C_L (\cos\beta - \cos\beta_o) = 0.658$$

where

$C_L = 1.35$

$\beta_o = 90$ deg

This results in a value for R = 0.025. The actual value used was R = 0.01 since this resulted in somewhat higher gains (and therefore lower errors) without exceeding the maximum allowable value of the control variable.

The feedback gain vector $\underline{C}$ (see Eq. (D.36)) for the selected weighting matrices is shown in Fig. D-5. The nominal trajectory is based on the following vehicle and orbital parameters:

Vehicle mass, m	3170 kg
Drag coefficient, C_D	2.5125
Lift coefficient, C_L	1.3457
Aerodynamic reference area, A_R	5.37 m^2
Bank angle, β_o	(see Fig. D-6)

Atmospheric model: 1962 Standard Atmosphere

Trajectory: Transfer ellipse from equatorial geosynchronous orbit with 68.291 km target perigee altitude and 28.5 deg inclination

The nominal bank angle time history shown in Fig. D-6 was selected to keep the dynamic pressure approximately constant and below 4800 N/m^2 during the early portion of the flight.

The time point t = 0 in Figs. D-5 and D-6 corresponds to the time when the nominal trajectory passes through 92.4 km altitude at atmospheric entry.

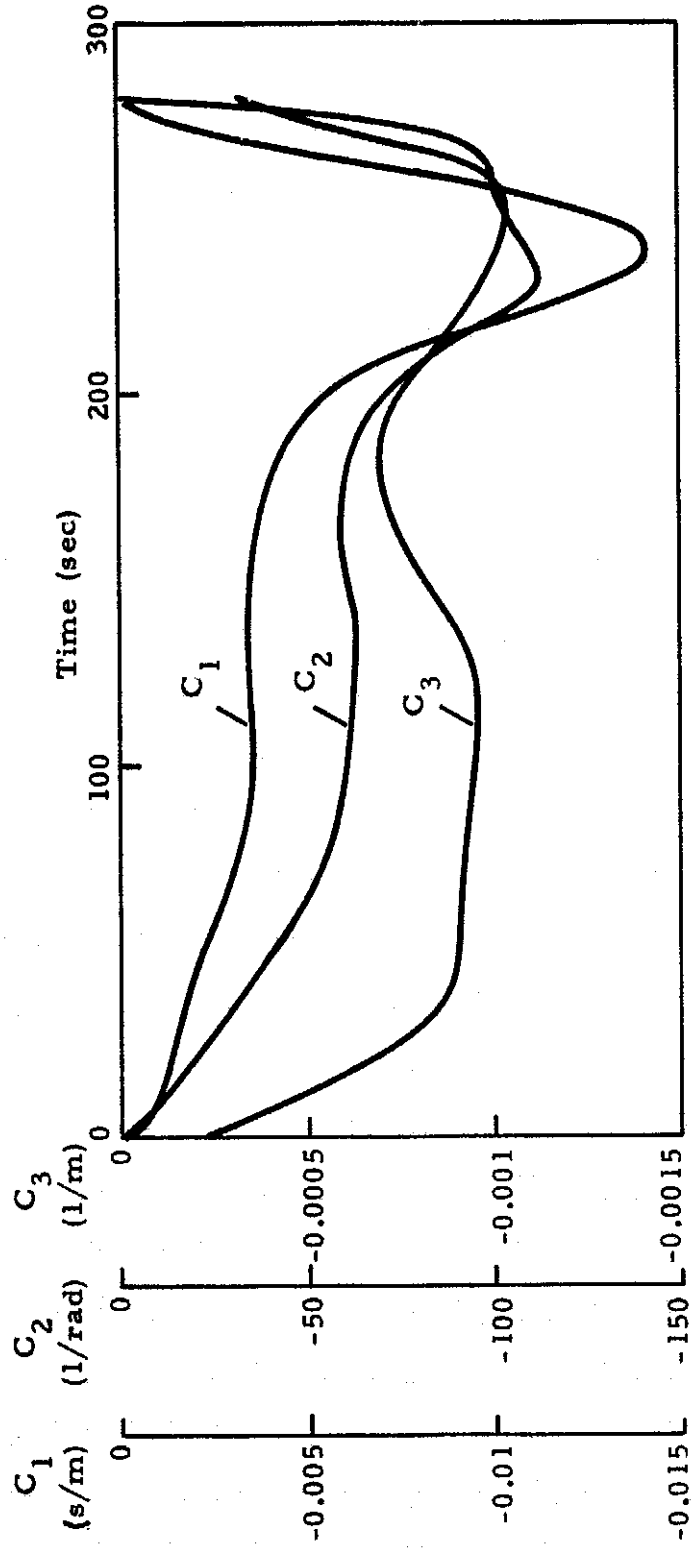

Fig. D-5 - Feedback Gain Vector $\underline{C}$ for Reentry Guidance

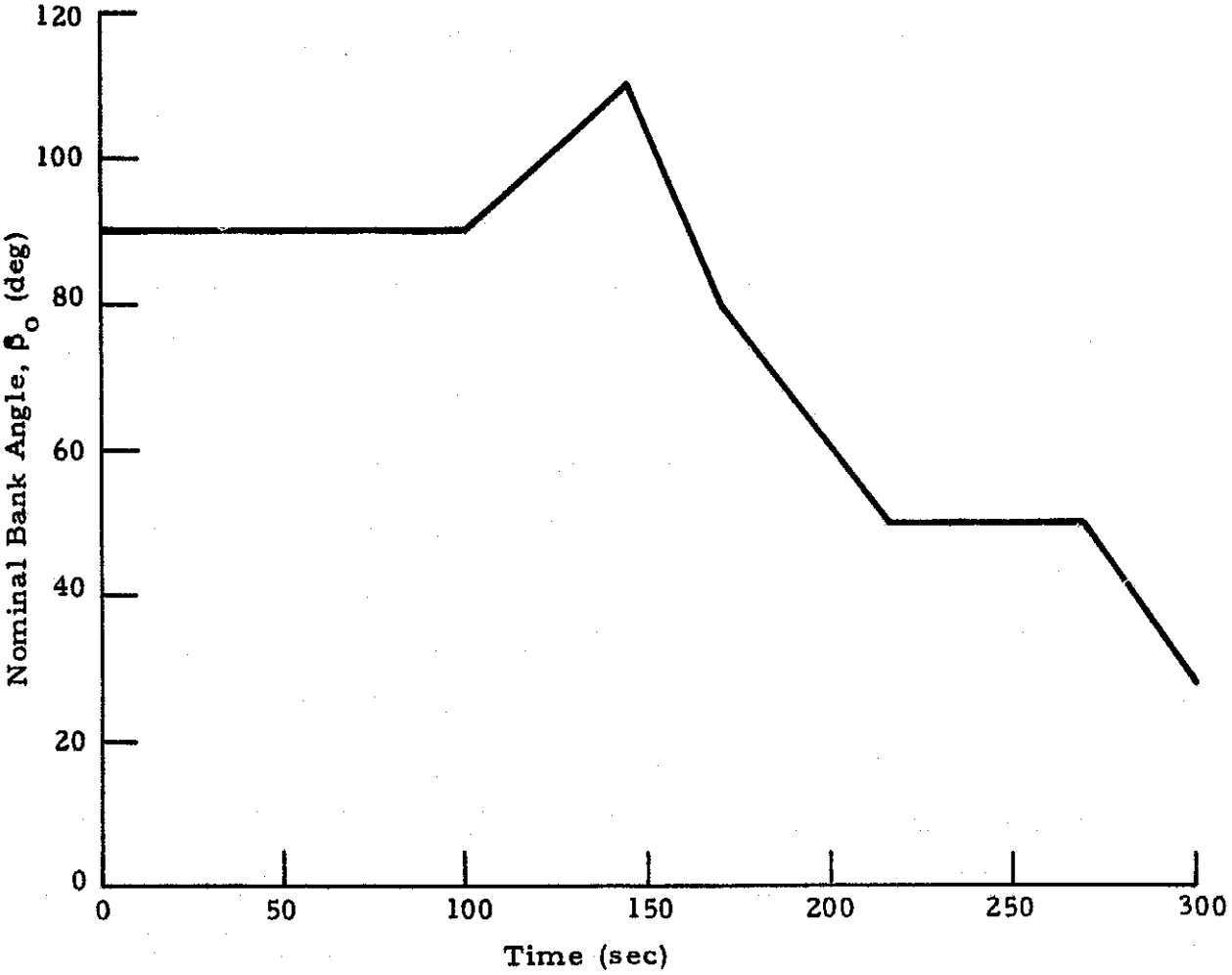

Fig. D-6 - Nominal Bank Angle, β_o

1.4 IMPLEMENTATION OF THE GUIDANCE SCHEME

The guidance scheme was implemented in a three-degree-of-freedom trajectory simulation. The implementation consists of programming the following equations.

$$\delta V = V - V_{nom} \tag{D.54}$$

$$\delta\gamma = \gamma - \gamma_{nom} \tag{D.55}$$

$$\delta h = h - h_{nom} \tag{D.56}$$

$$u = C_1\,\delta V + C_2\,\delta\gamma + C_3\,\delta h \tag{D.57}$$

The time histories for V_{nom}, γ_{nom}, h_{nom}, C_1, C_2 and C_3 were stored in the computer program. V and γ are directly available from the simulation (or from the spacecraft navigation system). The altitude h was computed from Eqs. (D.40) and (D.41). Only spacecraft parameters and measurables ($\dot{V}$ and V_R) enter those equations.

A new value of the control variable, u was computed in periodic intervals (guidance cycle) of 5 to 10 sec. The commanded bank angle, β_c was computed from equation (D.13).

$$\beta_c = \cos^{-1}\left[\frac{u}{C_L} + \cos\beta_o\right] \tag{D.58}$$

The vehicle rotation around the V_R vector by the angle $(\beta_c - \beta)$ was simulated as a minimum time maneuver with a constant angular acceleration $|\dot{\beta}| = 1\ \text{deg/sec}^2$.

2. GUIDANCE METHOD II: CLASSICAL LINEAR SYSTEMS APPROACH

2.1 FORMULATION OF THE GUIDANCE LAW

The objective of the atmospheric flight guidance is to achieve a specified apogee altitude after the pass through the atmosphere. The apogee altitude is fully determined by the velocity and the flight path angle at a given altitude (e.g., 120 km) after the exit from the atmosphere. However, the velocity is the dominating parameter. The flight path angle is only slightly dependent on the particular trajectory through the atmosphere. These considerations lead to the concept of guiding the vehicle along a nominal velocity profile. Trajectory control is effected by varying the bank angle and the control variable is defined as in Eq. (D.13).

The guidance law is based on classical linear control theory and consists of feeding back a linear combination of the variable to be controlled (V) and its derivatives. It is of the form

$$u = K_1 \delta V + K_2 \dot{\delta V} + K_3 \ddot{\delta V} \qquad \text{(D.59)}$$

The optimum set of gain constants was determined by a systematic search over the space $\{K_1, K_2, K_3\}$.

2.2 IMPLEMENTATION OF GUIDANCE SCHEME

The guidance scheme was incorporated in the three-degree-of-freedom trajectory simulation. A block diagram is shown in Fig. D-7.

Nominal time histories for V_{nom} and $\dot{V}_{nom}$ were stored in the computer program. They were used to compute δV and $\dot{\delta V}$. The variable $\ddot{\delta V}$ was obtained from a differentiating network with a high frequency roll-off as shown in Fig. D-7.

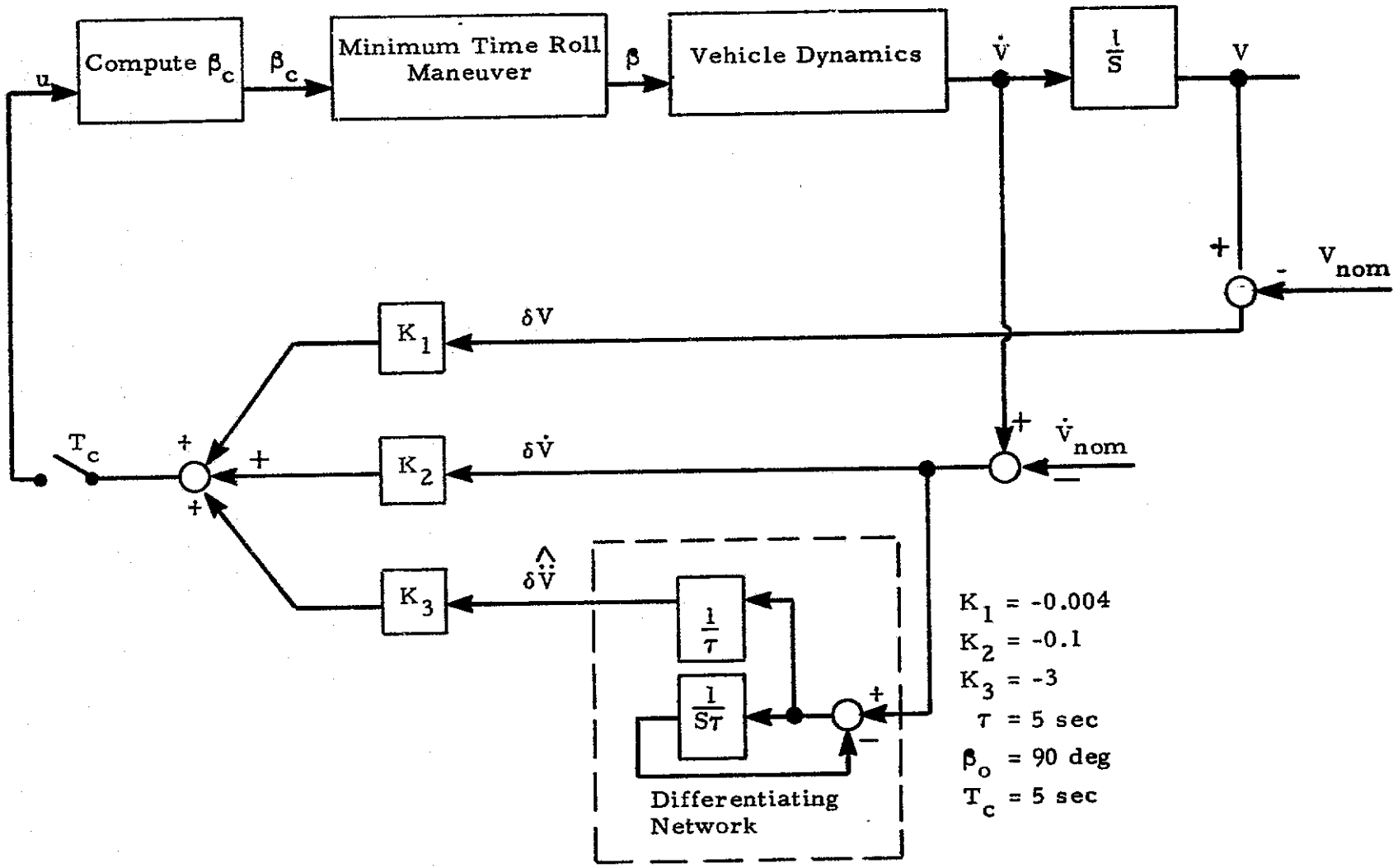

Fig. D-7 - Implementation of "Classical Linear Systems Approach"

A new value of the control variable, u, was computed periodically with a guidance cycle time, T_c = 5 sec.

The commanded bank angle is obtained from the control variable u (see Eq. D-13))

$$\beta_c = \cos^{-1}\left[\frac{u}{C_L} + \cos\beta_o\right] \qquad \text{(D.60)}$$

The roll maneuver to rotate the vehicle to the commanded bank angle, β_c was simulated as a minimum time maneuver with an angular acceleration of 1 deg/sec^2.